TECHNISCHE UNIVERSITÄT MÜNCHEN

Fakultät für Chemie

Investigations of Physical Properties of Metal-Organic Frameworks with Functional Ligands

João Guilherme Machado de Carvalho

Vollständiger Abdruck der von der Fakultät für Chemie der Technischen Universität München zur Erlangung des akademischen Grades eines

Doktors der Naturwissenschaften (Dr. rer. nat)

genehmigten Dissertation.

Vorsitzende(r): Prof. Dr. Jürgen Hauer

Prüfer der Dissertation: 1. Prof. Dr. Dr. h.c. Roland A. Fischer

2. Prof. Dr. Angela Casini

Die Dissertation wurde am 07.03.2022 bei der Technischen Universität München eingereicht und durch die Fakultät für Chemie am 12.05.2022 angenommen.

“Everybody’s journey is individual.

If you fall in love with a boy, you fall in love with a boy.”

James Baldwin

AGRADECIMENTOS

Primeiramente, eu gostaria de agradecer aos meus queridos pais, **Marilia** e **Jaimilton**, por, acima de tudo, acreditarem em mim e no meu potencial, até mesmo quando eu duvidei que conseguiria. Obrigado por nunca terem medido esforços para proporcionar a melhor educação a mim e aos meus irmãos. Se hoje esta tese está sendo escrita e este objetivo realizado, é porque eu tive vocês ao meu lado. Mãe, obrigado por me escutar quando eu liguei, mesmo que somente para contar coisas superficiais do meu dia. Esses momentos fizeram parecer que a distância não era tanta e ajudaram a amenizar a saudade que eu sinto de casa. Em breve, eu me juntarei ao grupo dos doutores da família! Eu admiro vocês. Eu amo vocês.

Aos meus amados irmãos, **Clarissa** e **Luiz Gustavo**, eu agradeço por sempre estarem presentes, apesar da distância, e por me amarem por quem sou. Eu jamais conseguiria imaginar minha vida sem vocês. Eu espero que nós possamos nos ver muito em breve. Eu sinto muita saudade. Eu amo vocês.

Ao meu orientador, **Prof. Dr. Roland Fischer**, os meus sinceros agradecimentos pela liberdade intelectual durante a confecção desta tese, pelo apoio financeiro e pela compreensão perante os meus momentos de dificuldade. Eu sempre serei grato por esta oportunidade.

Ao meu coorientador, **Dr. Alexander Pöthig**, agradeço pelos ensinamentos em cristalografia, pelas discussões, pela paciência, e por nunca ter me subestimado. Eu quereria ainda agradecer pelos ouvidos e pela porta sempre aberta durante todo o meu doutorado, especialmente nos momentos em que eu achei que estava esgotado. Eu te desejo imenso sucesso e felicidade e espero que nós possamos nos encontrar para uma “helles” mesmo após o fim deste doutorado.

Aos secretários **Martin Schellerer** e **Dr. Dana Weiß**, o meu obrigado por sempre estarem dispostos a ajudar, especialmente com a burocracia alemã. Ao técnico **Jürgen Kudermann**, agradeço profundamente pela paciência e pela realização das medições de cromatografica gasosa apresentadas nesta tese. Agradeço ainda ao **Dr. Christian Jandl** pela coleta de dados cristalográficos durante a fase mais severa da pandemia. À minha companheira de laboratório, **Zhyhing Fan**, agradeço pela atmosfera amigável, pelas conversas durante os nossos experimentos e por ter tornado estes anos mais suportáveis. Eu te desejo sempre muito sucesso.

Ao meu aluno **Korbinian Geißer**, meus agradecimentos pelo tempo investido no laboratório, pelo compromisso e por sempre escutar os meus ensinamentos. Eu tenho certeza de que você será um excelente químico. Aos meus demais alunos **Aida Art**, **Hicran Güngör** and **Than Thran**, o meu obrigado por suas contribuições. Os meus agradecimentos a todos os outros que, de alguma forma, contribuíram para a existência deste trabalho.

Ao meu amigo de infância, o terceiro irmão que a vida me deu, **Pedro Henrique**, os meus agradecimentos de coração por festejar os meus momentos de alegria, por me dar puxões de orelha quando eu saí dos trilhos e por disponibilizar um ombro quando eu precisei chorar. À minha melhor amiga, **Mayume**, eu gostaria de agradecer principalmente pelo suporte emocional, mesmo estando tão distante. Obrigado por escutar os desabafos e por estar sempre ao meu lado. Ao meu melhor amigo de Munique, **Bruno**, eu agradeço não só pelos momentos de descontração, pelas cervejas e pelas “techneiras”, mas também por ter me ajudado durante todo este doutorado. À minha amiga e terapeuta, **Mariana**, eu agradeço pelos ouvidos e por ter me assistido durante a produção desta tese. Sem você este processo teria sido muito mais difícil. A todos os meus outros amigos, o meu obrigado por fazer minha vida mais feliz.

ACKNOWLEDGMENTS

First, I am forever grateful to my dear parents, **Marilia** and **Jaimilton**, for believing in me and my potential, even when I doubted, I could make it. Thank you for always doing everything within your reach to provide the best education for me and my siblings. If this thesis is being written and this goal accomplished, it is because I had you both by my side. Mom, thank you for listening to my calls, even if just to tell you silly things about my day. Such moments made the distance between us feel virtually shorter and assisted me when I missed home the most. Soon I will join the doctors of the family! I admire you. I love you.

I would like to thank my beloved siblings, **Clarissa** and **Luiz Gustavo**, for always being there for me, despite the distance, and for loving me for the person I am. I could never imagine my life without you. I am looking forward to spending time with you again. I miss you very much. I love you.

To my supervisor, **Prof. Dr. Roland Fischer**, I am extremely thankful for the scientific freedom during this thesis, for the financial support, and for being understanding when I had challenging times. I will always be grateful for this opportunity.

To my mentor, **Dr. Alexander Pöthig**, I heartfully want to express my gratitude for the crystallography knowledge, for all the fruitful discussions, for his patience, and for never underestimating me. I would also like to thank you for being a listener and having your door always open, especially when I thought I could not go any further. I truly wish you immense success and happiness. And I hope we can still meet for a “helles” after this doctorate.

I would like to thank the secretaries **Martin Schellerer** and **Dr. Dana Weiß** for being always helpful, especially with German bureaucracy. I am also deeply thankful to the technician **Jürgen Kudermann** for performing gas chromatography measurements presented in this thesis. I would also like to thank **Dr. Christian Jandl** for collecting crystallographic data during the most severe times of the pandemic. To my lab partner, **Zhyhing Fan**, my heartful appreciation for always being kind to me, for the amusing conversations, and for making these years more tolerable. I wish you all the best. I thank any other person who by any means contributed to this thesis.

To my childhood friend, the third sibling life gave me, **Pedro Henrique**, my sincere gratitude for celebrating joyful moments with me, for calling me out when required, and for lending me a shoulder to cry on when I needed it. I would like to heartfully thank my best girlfriend, **Mayume**, for the emotional support, for listening when I had to get something off my chest, and for always being by my side. To my best friend in Munich, **Bruno**, I am grateful not

only for the entertaining conversations, beers, and techno parties but for being around all these years and for helping me throughout this doctorate too. I would like to express my deep gratitude to my old friend and therapist, **Mariana**, for listening to my issues and for assisting me during this challenging time of my life. Without you, this process would have been much harder. To all my other friends, thank you for making this life happier.

ABSTRACT

This work comprises contributions to the coordination and solid-state chemistry of quinone-based systems. The incorporation of various ligands into metal-organic frameworks is presented. Structural characterization, physicochemical properties, and potential application are discussed. In the first section, a redox-active dipyridyl-substituted anthraquinone ligand and its reduced form are introduced and structurally characterized. The physicochemical properties and redox behavior are investigated in both solution and solid states. Additionally, three novel metal-organic frameworks are presented and structurally juxtaposed. Synthetic approaches for selective incorporation of distinct oxidation states are discussed. Furthermore, studies on molecular oxygen activation and the switchable behavior of a Zn-based coordination polymer are presented. In the second part, a novel bis(diphenylamino)anthraquinone tetratopic linker is presented and its photochemical properties evaluated. Studies on the ligand coordinative behavior towards alkaline earth metals are shown together with the structural characterization of four new metal-organic frameworks. Sequentially, the physicochemical and emissive features of the inorganic materials are exposed and compared to those of the free ligand. Lastly, the catalytic behavior of the ligand and the materials on the photooxidation of sulfides is evaluated. In the last part, the quinone center is expanded to a six-condensed aromatic core. The structural characterization of the bis(diphenylamino)anthranthrone tetratopic linker and one novel Zn-based metal-organic framework is presented. Finally, an appraisal of the incorporation of quinizarin into crystalline networks is described.

TABLE OF ABBREVIATIONS

OAc acetate

AcOH acetic acid

acn acetonitrile

pK_a acid ionization constant

Aq anthraquinone

H_2AqDC anthraquinone dicarboxylic acid

AqDS anthraquinone disulfonate

a.u. arbitrary units

BDC benzene dicarboxylate

p-Bzq *p*-benzoquinone

4,4-bpy 4,4-bipyridine

BINAP 2,2'-bis(diphenylphosphino)-1,1'-binaphtyl

dppf 1,1'-bis(diphenylphosphino)ferrocene

CBP 4,4'-bis(N-carbazolyl)-1,1'-biphenyl

Et-bpy 1,2-bis(4'-pyridyl)ethane

BET Brunauer-Emmett-Teller

BuOH *n*-butanol

tBuOH *t*-butanol

^{t}BUONO *t*-butyl nitrite

Cat catechol/catecholate

CT charge transfer

H_2Cl_2DHBq chloranilic acid, 2,5-dichloro-3,6-dihydroxybenzoquinone

2-Caq 2-chloroanthraquinone

COF covalent organic framework

CV cyclic voltammetry

Cp cyclopentadienyl ligand

DFT density functional theory

DAAq 2,6-diaminoanthraquinone

DCM dichloromethane

DSC differential scanning calorimetry

H_2DHBq 2,5-dihydroxybenzoquinone

DMA dimethylacetamide

DMF dimethylformamide

DMSO dimethyl sulfoxide

DPAq 2,6-di(pyridin-4-yl)-9,10-anthraquinone

DPAHq 2,6-di(pyridine-4-yl)-9,10-anthrahydroquinone

DtBHP 3,5-di-*tert*-butyl-4-hydroxyphenyl

eq. equivalents

EtOH ethanol

EtOAc ethyl acetate

e.g. *exempli gratia*

EQE external quantum efficiency

FOX ferrous oxidation-xylenol orange

FW formula weight

FT Fourier transform

$E^x_{1/2}$ half-wave potential

GC gas chromatography

HHTP or H_6THO 2,3,6,7,10,11-hexahydroxytriphenylene

HOMO highest occupied molecular orbital

IR infrared

IVCT intervalence charge transfer

LED light-emitting diode

τ lifetime decay

LUMO lowest unoccupied molecular orbital

MS mass spectrometry

MOF metal-organic framework

MON metal-organic nanosheet

MeOH methanol

M molarity

NMP N-methyl-2-pyrrolidone

NMR nuclear magnetic resonance

1D one-dimensional

OLED organic light-emitting diode

ppm parts per million

Cp* pentamethylcyclopentadienyl ligand

PIDA phenyliodine(III) diacetate

PHOLED phosphorescent light-emitting diode

PAH polycyclic aromatic hydrocarbon

PMMA poly(methyl methacrylate)

PTFE polytetrafluorethylene

pH potential of hydrogen

^{x}J proton coupling constant

PXRD powder X-ray diffraction

QY quantum yield

H_2Quinz quinizarin, 1,4-dihydroxyanthraquinone

SBU secondary building units

Sq semiquinone/semiquinonate

SCXRD single-crystal X-ray diffraction

2-SaqS sodium anthraquinone-2-sulfonate

THF tetrahydrofuran

THT tetrahydrothiophene

THB^{4-} tetrahydroxybenzene anions

TEMPO (2,2,6,6-tetramethylpiperidin-1-yl)oxyl

TADF thermally activated delayed fluorescence

TGA thermogravimetric analysis

3D three-dimensional

TFA trifluoroacetic acid

TFP 1,3,5-triformylphloroglucinol

Me_6tren tris(2-dimethylaminoethyl)amine

2D two-dimensional

UILPE ultrasound-induced liquid-phase exfoliation

UV ultraviolet

Vis visible

0D zero-dimensional

TABLE OF CONTENTS

1. THE OUVERTURE

1.1. Quinones: Redox-Active Molecular Machineries for Natural and Synthetic Systems

Nature has always found the most elegant pathways to promote life through chemical reactions. Redox activity plays a decisive role in all kinds of biological systems, taking part in fundamental processes, such as photosynthesis and cellular respiration.[1] Redox behavior may originate from organic, inorganic, or hybrid systems.[1–3] The accessible distinct oxidation states of some transition metals and the non-innocent character of organic struts such as porphyrins and quinones made them crucial pieces for small molecule activation, catalysis, electron transfer, and energy storage and transduction in living apparatuses.[1–4]

Metal-organic frameworks (MOFs) constitute an exceptional class of crystalline functional porous hybrid materials that have been extensively studied in the past decades. The organic components can be modified and tailored to generate, change, or improve desired physicochemical properties, whereas the inorganic units may carry relevant features of the metals, such as redox and catalytic behavior. Furthermore, guest molecules and nanoparticles may be encapsulated in the voids, expanding the richness of structural engineering.[5–7] The wide number of possible combinations and architectural design allowed the usage of MOFs in several fields, for instance, in gas storage, separation, and purification[8,9], catalysis[6], electrochemistry,[7,10] and optics/photophysics[11].

Redox character in metal-organic architectures can be promoted using different approaches (Figure 1). The direct incorporation of intrinsically redox-active units into the framework can be exploited in both organic linker and inorganic nodes. Guest molecules can be either attached covalently to the network or encapsulated in pore environments. Lastly, the promotion of charge transfer in the solid state has proven to be a viable option for charge mobility.[7] The non-innocence of distinct organic building blocks has been consistently reported in crystalline coordination polymers. Prominent motives are porphyrins, naphthalene diimide and tetrathiafulvalene derivatives, arylamines, and quinoid systems. The employment of metals with multiple oxidation states as inorganic subunits in MOFs constitutes a direct pathway as well towards redox activity.[7] Such redox materials have shown potential application as electrochemical[12] and luminescent sensors[13], supercapacitors[14], photochromic[15] and battery materials[16], (semi)conductors[17], and (electro)catalysts[18]. Post-synthetic modifications can likewise foster redox behavior in MOFs. Cation and ligand exchange approaches have been reported. The intrinsic porosity of MOFs may as well be used to generate hosting environments for redox-active guest molecules, which may be covalently attached to the framework or encapsulated in permanent voids.[7]

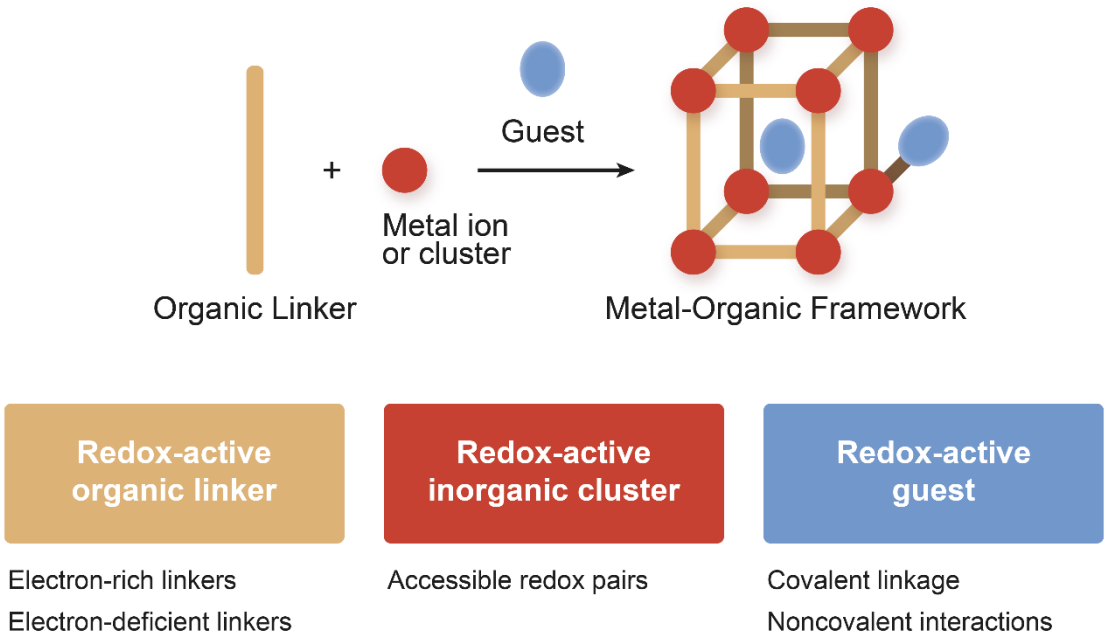

Figure 1. Illustration of different approaches for incorporation of redox-active entities into metal-organic frameworks. Figure adapted and reproduced with permission of the Royal Society of Chemistry.[7]

Although redox-active metal-organic frameworks constitute a class of materials of broad interest, only a few publications are comprising anthraquinone-based MOFs. Furthermore, there is a relevant number of quinoid systems, whose solid-state coordination chemistry remains nearly unexplored. Due to the relevant photochemical properties and interesting electrochemical behavior, these molecules show great potential towards current topics, such as energy storage and conversion. Moreover, the expansion into less exploited redox-active systems might lead to innovative functional materials. Motivated by that, this thesis comprises contributions to the implementation of quinoid-based systems into crystalline metal-organic architectures, to their solid-state structural chemistry, and related physicochemical properties.

1.2. General Aspects of Quinones and Derivatives: Physicochemical Properties and Applications

Quinones constitute a class of electron-deficient organic compounds with relevant biochemistry, electrochemistry, and dye chemistry. Such compounds are typically used as reactants or as catalysts in organic chemistry. In living systems, quinones act as charge acceptors and carriers, being part of fundamental processes, such as photosynthesis and aerobic respiration.[19–22] Their intrinsic redox behavior and photochemistry have been explored in materials chemistry, for example as redox[23] and fluorescence switches[24], cathode battery materials[25,] and organic light-emitting devices.[26]

Quinones can be monocyclic or be part of an extended conjugated system. The variable positioning of the keto groups enables the formation of different isomers. Simple quinones can usually be synthesized via the oxidation of phenols or their derivatives. For example, 1,4-benzoquinone and 1,4-naphthoquinone derivatives can be obtained via oxidation of phenol or 1-naphthol precursors by Cr(VI) reagents or hydrogen peroxide in presence of a titanium silicate catalyst. Functional groups attached to the quinone, like alcohols, do not get oxidized in these conditions. Anthraquinones may be synthesized via oxidation of anthracenes with Cr(VI) oxidants; however, Diels-Alder and Friedel-Crafts approaches are far more interesting, especially when constructing substituted derivatives. The preparative reduction of quinones to the corresponding hydroquinones may be carried out using various reducing agents, including sodium hydrosulfite, ascorbic acid, and H_2 (catalytic hydrogenation or metals in acidic aqueous solutions).[27,28]

Quinone redox cycling is an elementary process, which plays a decisive role in energy transduction and storage. In this process, the anthraquinone is reduced to semiquinone or hydroquinone. When molecular oxygen is present, the semiquinone and hydroquinone are autoxidized back to the quinone, and dioxygen is reduced to the superoxide anion radical.[29] The superoxide anion radical can then further react to hydrogen peroxide and hydroxyl radicals. The redox behavior of quinones varies according to the milieu (Scheme 2). In acidic aqueous buffer, the reduction is a single step two-electron two-proton process, whereas in alkaline buffered solutions it is solely a two-electron process. At pH values close to neutrality, the quinone might undergo either a one proton two-electron or a two-electron reduction, depending on the pK_a value of the associated hydroquinone. In nonaqueous milieux, quinone reduction follows a two-successive one-electron process.

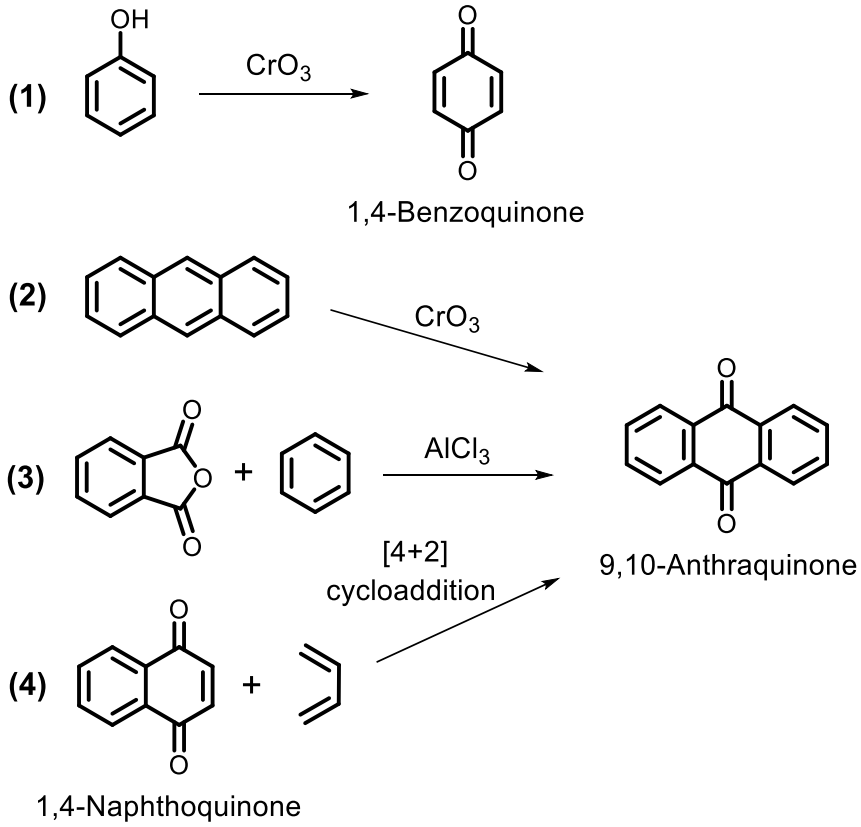

Scheme 1. Reaction schemes for the synthesis of (1) benzoquinone from phenol via oxidation with Cr(VI) oxide; (2) anthraquinone from anthracene via oxidation with Cr(VI) oxide; (3) anthraquinone from phthalic anhydride and benzene in presence of $AlCl_3$; (4) anthraquinone from naphthoquinone via [4+2] cycloaddition with butadiene.

First, the semiquinone radical is formed and then the dianion is formed. Both steps may be influenced by solvent polarity, intramolecular hydrogen bonding, and the addition of protic solvents. In presence of protic sources, the semiquinone radical and the dianion can be stabilized via hydrogen bonding. Carboxylic acids can also be used as hydrogen bonding agents in organic solvents because the dissociation is not expressive. The reduction potential of quinones can be influenced by the addition of substituents. The addition of protic groups, such as hydroxy and amino groups, next to the quinone allows the formation of hydrogen bonds with the semiquinone and quinone dianion.[30]

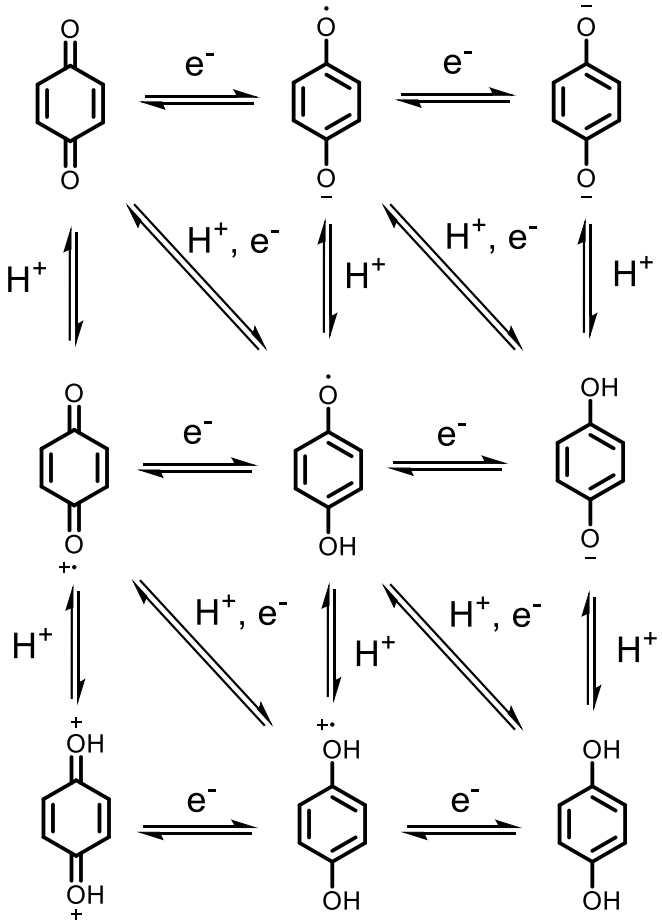

Scheme 2. Electrochemical pH-dependent equilibria of benzoquinone derivatives.

The anthraquinone process is the major industrial application of quinones and is used to generate hydrogen peroxide from molecular hydrogen and oxygen. The process consists of four steps: hydrogenation, oxidation, hydrogen peroxide extraction, treatment of the working solution. In a hydrogenator, the 2-alkyl-9,10-anthraquinone working solution is hydrogenated in the presence of a suspended, supported, or fixed-bed catalyst as Raney Nickel or palladium to the anthrahydroquinone, which is then oxidized back to the anthraquinone with dioxygen, forming hydrogen peroxide. The oxidation follows a free radical chain mechanism (Scheme 3). The hydrogen peroxide is then extracted with water and subsequently concentrated. The working solution is purified, regenerated, and returned to the hydrogenator, completing the cycle. This process has some drawbacks such as solubility issues, overoxidation, and deactivation of the anthraquinone catalyst.[31]

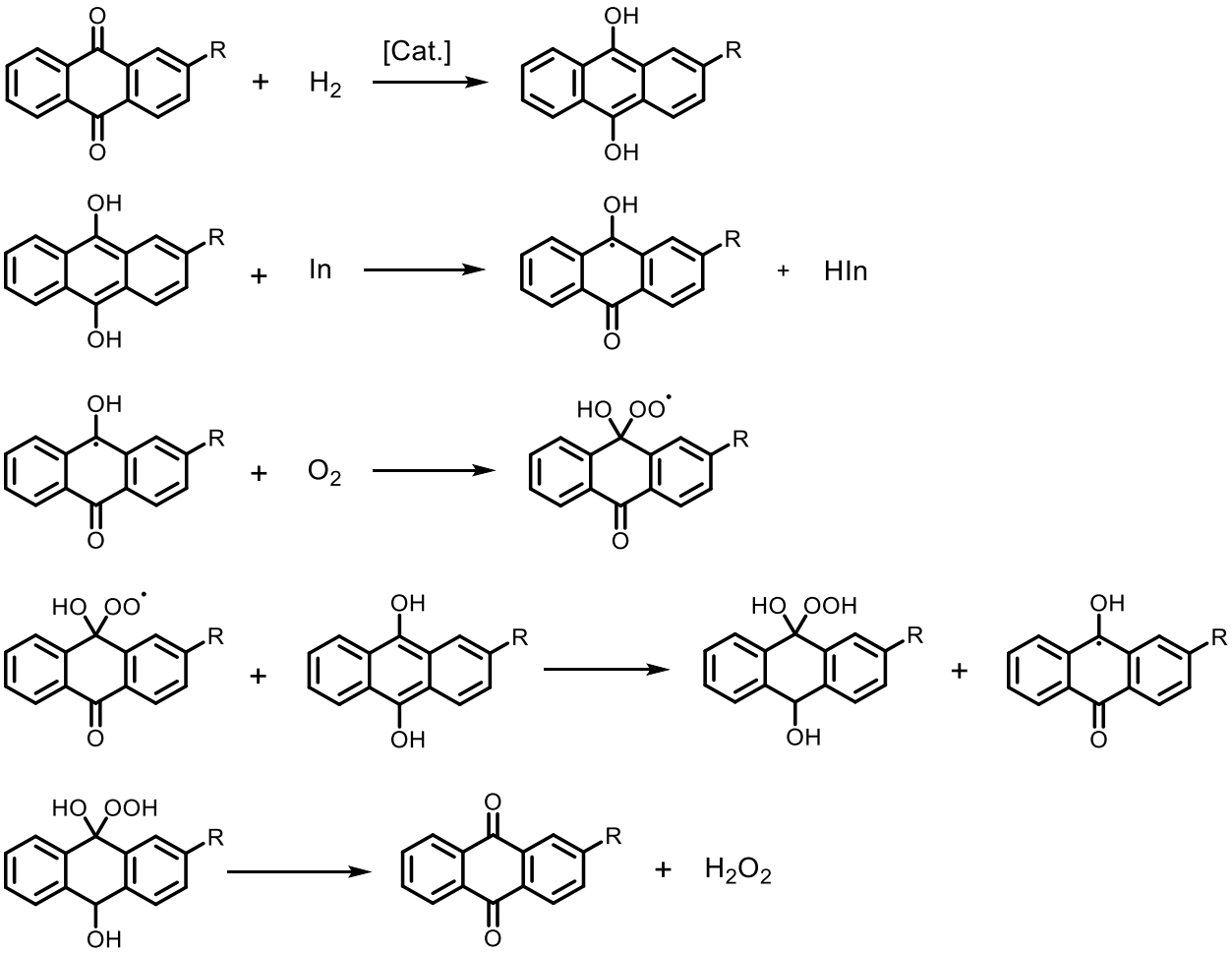

Scheme 3. Proposed mechanism for the anthraquinone-mediated catalytical synthesis of hydrogen peroxide from dioxygen.[31]

The reversible redox behavior of quinones has been explored for the development of metal-free electrocatalysts for oxygen reduction[32], metal-free redox-flow batteries[33], cathode materials[25], and stimuli-responsive molecular switches.[34] Recently, an Al-battery with an anthraquinone-based organic cathode was reported which has been claimed to overperform the state-of-the-art Al-graphite battery.[25] Although the quinones might usually be reversibly switched in solution, the redox properties do not always translate into the solid state, possibly due to the spatial confinement effect. The synthesis of porous materials might come up as a solution for such difficulties. A 3D porous covalent organic framework (COF) containing hydroquinone units, **Ia**, has been recently reported. The redox-active centers could be oxidized up to 90% using benzoquinone as an oxidant, yielding the oxidized COF, **Ib**. The re-reduction was carried out using ascorbic acid as a reducing agent. Powder diffractometry shows retention of crystallinity and the topology. Additionally, the gas sorption properties of **Ia** and **Ib** were shown to be strongly associated with the pore surface and structure, highlighting the applicability of quinones as immobilized molecular switches in stimuli-responsive materials.[34]

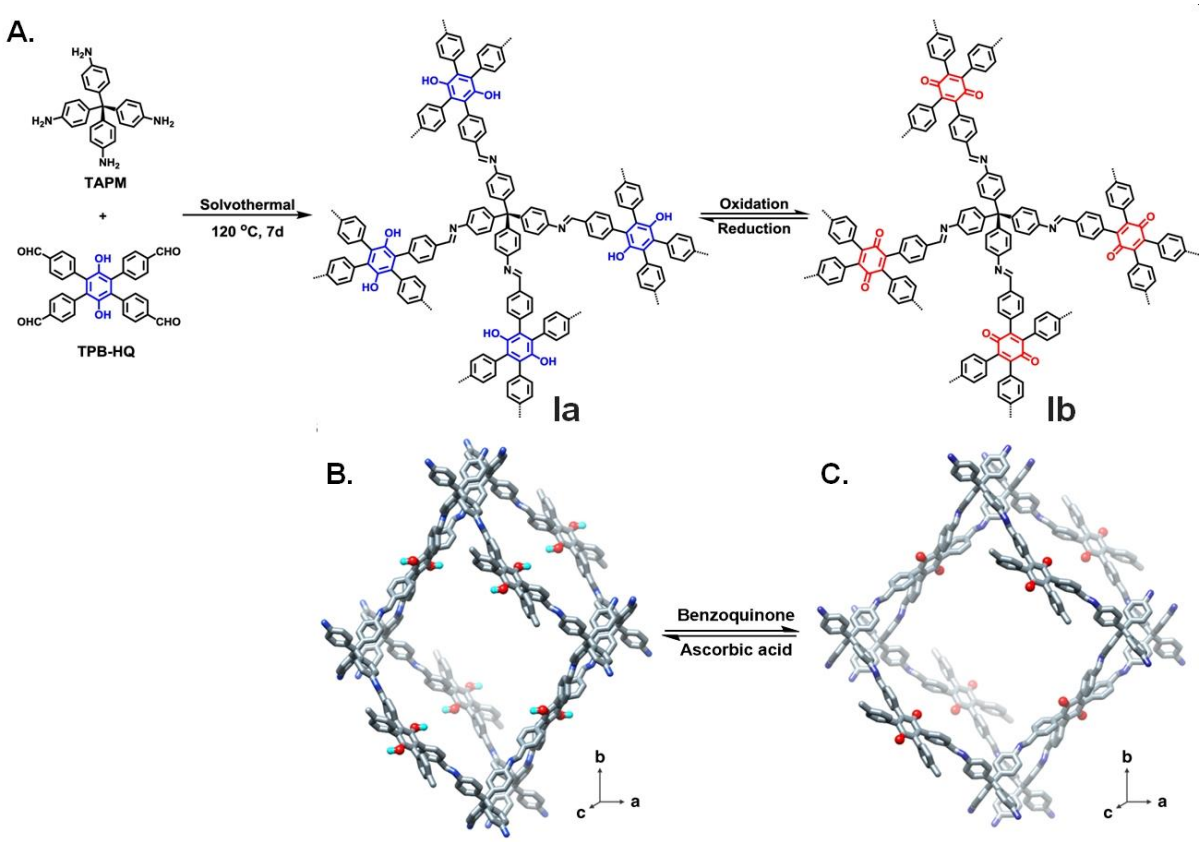

Figure 2. A. Synthetic approach towards **Ia** and **Ib**. **B.** Structural model of **Ia**. **C.** Structural model of **Ib**. Atom colors are gray (C), red (O), dark blue (N), light blue (H). Aromatic hydrogen atoms are not shown.[34] Figures adapted and reproduced with permission of Nature Research. For the open-access license see the link as follow: http://creativecommons.org/licenses/by/4.0/.

The electron-accepting properties of quinones enable the formation of charge transfer (CT) complexes. The coexistence of *p*-benzoquinone (bright yellow) and hydroquinone (colorless) in ethanolic solution leads to the formation of green crystals of a CT-complex denominated quinhydrone (Figure 3A). In this complex, the hydroquinone acts as electron-donor and the benzoquinone as electron-acceptor. Hydrogen bonding also plays a relevant role in stabilizing the CT complex.[35] A resorcinarene macrocycle with 3,5-di-*tert*-butyl-4-hydroxyphenyl (DtBHP) *meso*-substituents has shown multimodal switchable behavior based on hemiquinhydrone-type CT-complexes (Figures 3B and 3C). The macrocyclic scaffold allows spatial proximity of the *meso*-positions, enabling interactions between the substituents. DtBHP can be oxidized under mild conditions and contains the phenolic functionality needed for the generation of the hemiquinhydrone complexes. Two phenol groups of the benzylated compound (**II**) could be independently oxidized to the hemiquinones via stoichiometric oxidation with 2,3-dichloro-5,6-dicyano-1,4-benzoquinone (DDQ), yielding **[Ox$_1$]** and **[Ox$_2$]**. The first oxidation step could also be performed via irradiation at 285 nm. Generation of the quinhydrone-complexes, **CT-[Ox$_1$],** and **CT-[Ox$_2$]**, was achieved upon the addition of trifluoroacetic acid (TFA) (Figure 3D). The reaction proved to be reversible when neutralized

with pyridine or potassium carbonate. Overall, the system provided five different optical outputs based on different redox and charge transfer states, highlighting the suitability of such compounds for the development of molecular switches, chemosensors, and chemical memory elements.[36]

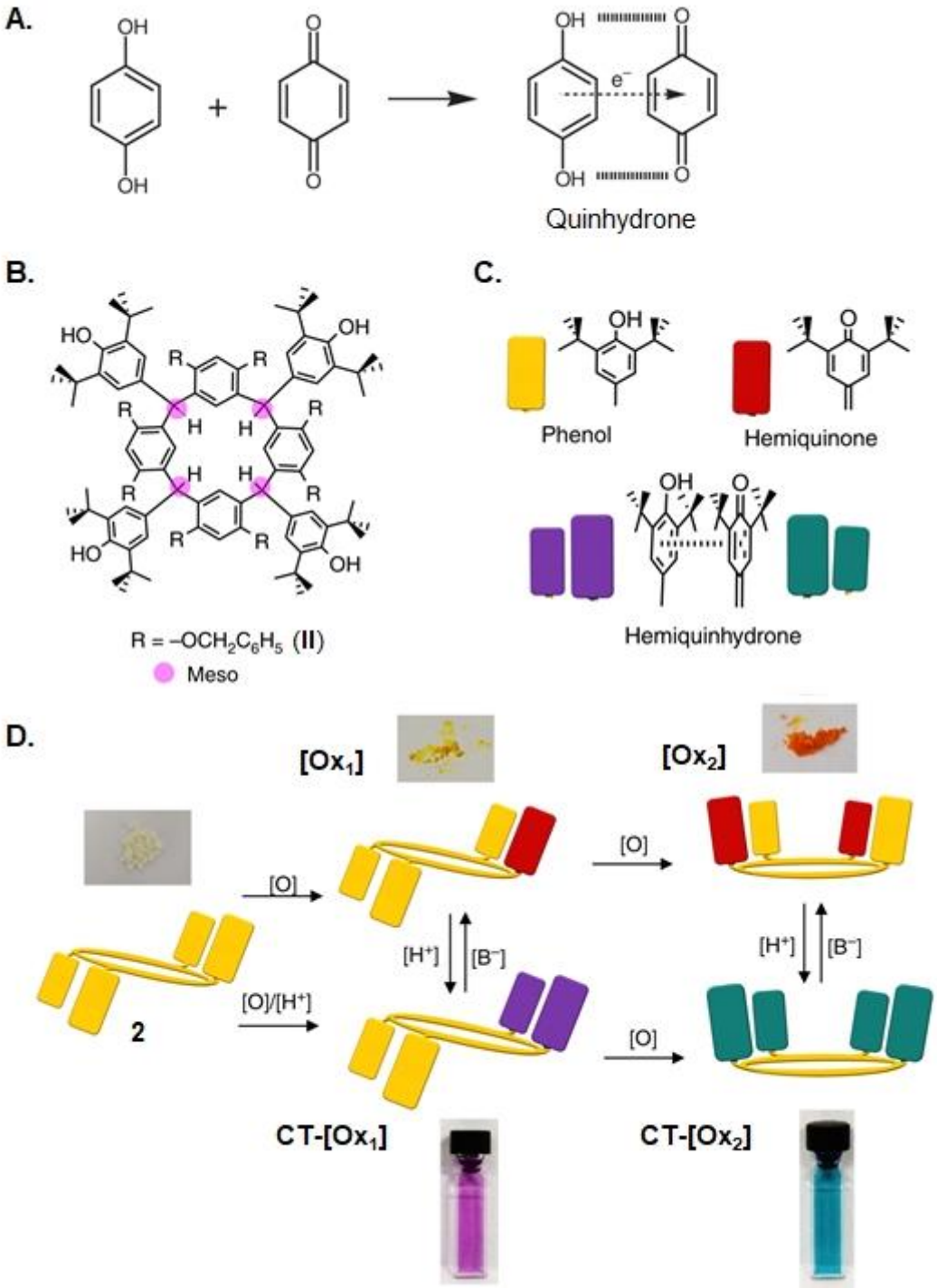

Figure 3. Depiction of the **A.** formation of quinhydrone from *p*-benzoquinone and hydroquinone **B.** resorcinarene macrocyclic scaffold in its fully reduced form **C.** color code for the different oxidation/charge transfer states **D.** transformations between all five distinct redox/charge transfer states and the corresponding observed colors outputs.[36] Figures adapted and reproduced with permission of Nature Research. For open-access license see the link as follow: http://creativecommons.org/licenses/by/4.0/.

Donor-Acceptor relationships are not solely related to quinhydrone-type complexes. The electron-accepting properties of quinones can be used to design diverse push-pull systems exhibiting nonlinear optical features, which may be potential candidates for storage devices. The highly delocalized electronic situation of quinone-tetrathiafulvalene dyads, **III**, and triads, **IV**, allowed third-order nonlinear optical properties and second-order optical hyperpolarizability (Figure 4, top).[37] When covalently attached to chromophores, quinones may quench the emissive state via intramolecular electron transfer from the chromophore to the acceptor or by excitation energy transfer to a non-emissive charge transfer state. In this kind of system, the quinone/hydroquinone redox pair acts as a control subunit for absorption and emission.[38] Such systems might be used for probing local redox properties and as biosensors.[39,40] 2-Chloro-1,4-naphthoquinone when bound to 5-dimethylamino naphthalene yields a reversible molecular switch, **V**. The quinone form is not emissive; however, upon exposure to sodium borohydride, it immediately switches to the green-fluorescent reduced form. Subjection to aerobic conditions led the system back to its non-emissive form (Figure 4, bottom).[41]

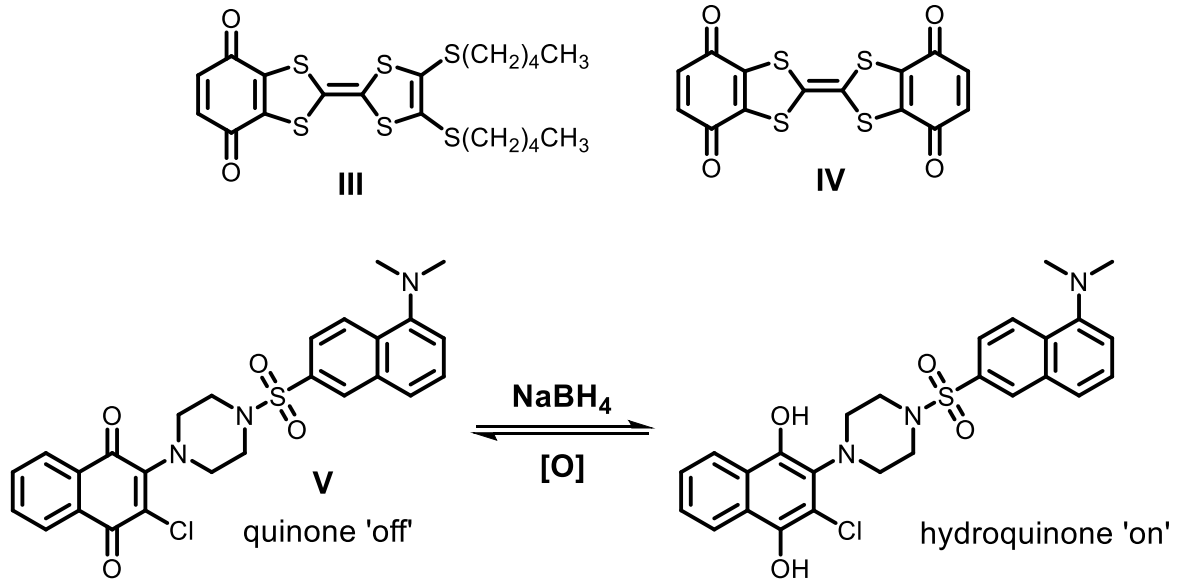

Figure 4. Illustration of donor-acceptor quinone-tetrathiafulvalene systems (top). Chloro-1,4-naphthoquinone-based molecular switch, highlighting the 'on' and 'off' states (bottom).

Anthraquinone dyes constitute the second most prominent class of synthetic organic dyes. Substitution of aromatic hydrogens by electron-rich donors, such as hydroxyl and amino functionalities, yields pigments from red to dark purple with good lightfastness. This property measures the resistance of a pigment to fading when exposed to light. Alizarin and purpurin are herbal, naturally occurring hydroxyanthraquinones. Likewise, carminic acid, the main component of the red pigment carmine, is a glycosylated polyhydroxyanthraquinone derivative found in some scale insects. The broad absorptivity in the UV-Vis range, the possibility of

structural designing, and potent excited-state reduction in an aprotic medium could enable the use of anthraquinones for visible-light-driven photoredox and photooxygenation reactions. One drawback compared to other photoactive dyes is the low molar absorptivity in the visible region.[42,43]

Quinones are known for photon-induced radical formation. A prominent example occurs in living organisms, i.e., the polymerization of 5,6-indolquinone to eumelanin (brown/red pigment) to protect the organisms from ionizing UV irradiation.[44] Recently, anthraquinones have been applied in visible-light-induced, catalytic photooxidations to generate carboxylic acids, phenols, *gem*-diols, epoxides, aromatic methyl esters, hydroxyalkyl esters, and diacylamines. Such transformations involve either hydrogen-atom or electron transfer. For example, 2-chloroanthraquinone (2-CAq) was able to oxidize in good yields (83–99 %) benzylic alcohols to carboxylic acids. The mechanism involves likely two hydrogen abstraction/oxidation steps by the anthraquinone at the benzylic position (Scheme 4, top). In contrast, the water-soluble sodium anthraquinone-2-sulfonate (2-SAqS) could be used to avoid over oxidation and selectively synthesize benzaldehyde (81 %) from toluene via aerobic photooxidation. A minor concentration of benzyl alcohol was detected (Scheme 4, bottom). Besides photooxidations, anthraquinones found use in the reductive coupling of halides, cross-dehydrogenative coupling, and halogenation of electron-rich arenes.[42-44]

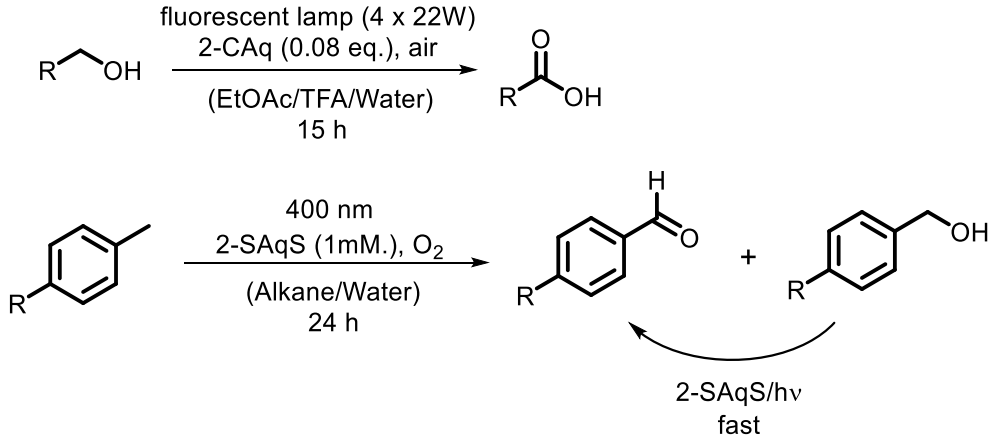

Scheme 4. Visible light-induced photooxidation reactions with anthraquinones.[42]

Very recently, the incorporation of anthraquinone in porous COFs allowed selective heterogenous photooxidation of sulfides to sulfoxides under visible light. The AQ-COF, **VI**, was synthesized via Schiff-base condensation of 1,3,5-triformylphloroglucinol (TFP) and 2,6-diaminoanthraquinone (DAAq) in a mixture of anhydrous 1,4-dioxane and mesitylene with acetic acid (Scheme 5A). Spectroscopic evidence suggests the presence of a keto-amine and enol-imine tautomeric equilibrium in the material. Powder diffractometry revealed an AB staggered structure and BET measurements show permanent porosity with a surface area of

609 m^2/g. The photocatalytic activity of **VI** was evaluated by the selective oxidation of sulfides under monochromatic irradiation at 420 nm (purple LED). The photooxidation of thioanisole in acetonitrile was achieved with 99+ % conversion and 97 % selectivity for the sulfoxide. To understand the oxidation mechanism, different conditions and various scavengers were tested (e.g., hydroquinone/$CuSO_4$ and TEMPO), which suggested the formation of $O_2^{\bullet-}$ and $^1O_2$ species, as well as electron holes, h^+ (Scheme 5B, top blue part). These radical and singlet oxygen species were generated via the reduction of molecular oxygen by the quinone moieties. Simultaneously, the generated electron holes recaptured an electron from the sulfide reagent, allowing oxidation of the sulfide and closure of the catalytic cycle (Scheme 5B, bottom pink part).[45]

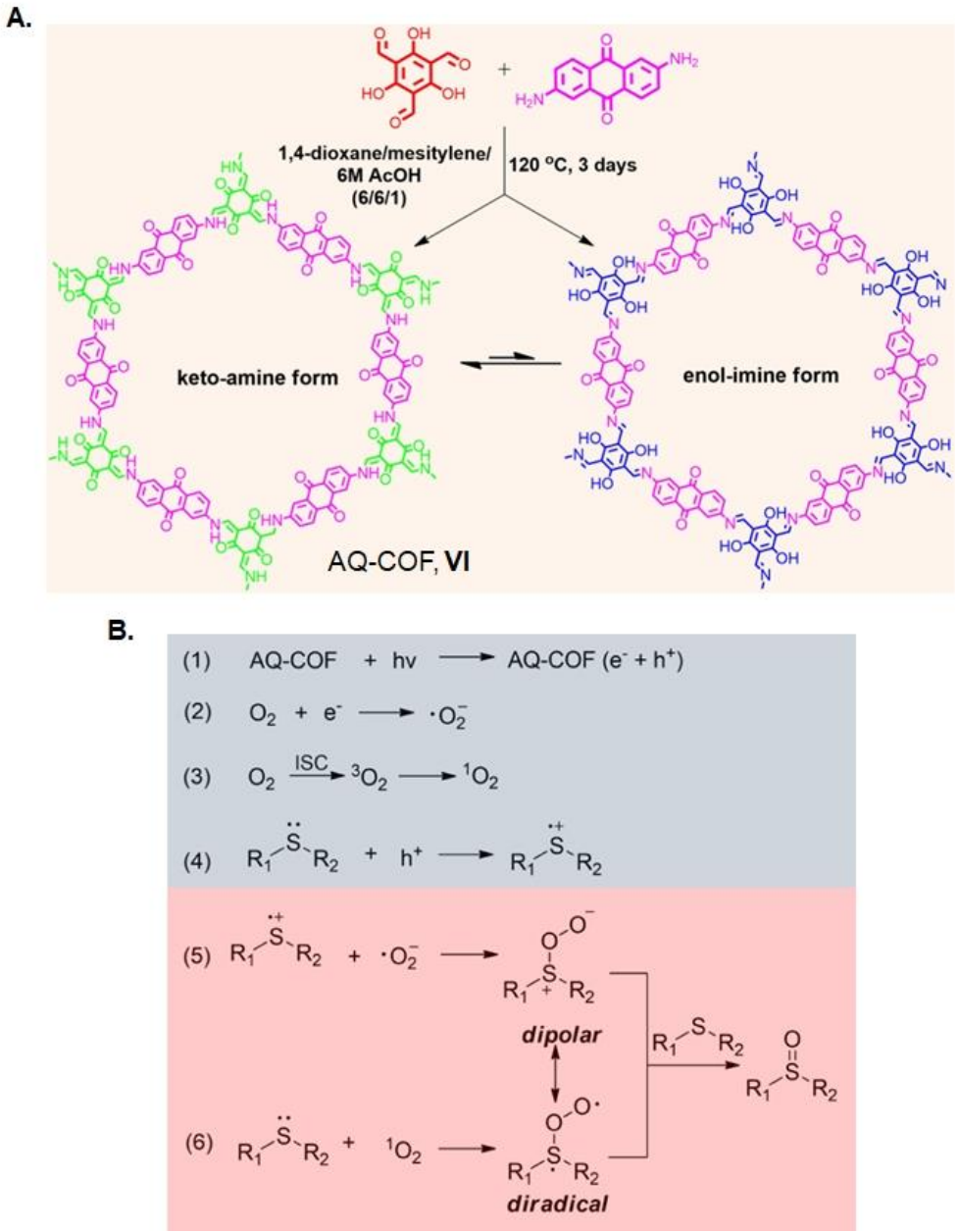

Scheme 5. A. Reaction scheme for the synthesis of AQ-COF, **VI**, highlighting the existing tautomeric equilibrium **B.** Sequence of possible reactions involved in the oxidation of sulfides to sulfoxides.[45] Figures adapted with permission of the American Chemical Society.

There is an extensive library of quinoid pigments comprising polycyclic aromatic hydrocarbons (PAHs). Many of these molecules belong to the vat dyes, which are relatively cheap because of their production for the textile coloring industry. By definition, a vat dye is an organic pigment, which can be made water-soluble upon reduction with an inorganic salt, such as sodium dithionite, for the dying process. The re-oxidation of the dye to its insoluble form grants stable coloring to the textile. Considering the low-cost production, extended conjugated π-system, thermal stability, and self-assembly behavior in the solid state, vat dyes are attractive candidates for organic electronics.[46]

Anthraquinone-based push-pull systems have been used for the construction of highly efficient red-emitting organic light-emitting diodes (OLEDs). A series of symmetric 2,6-disubstituted intramolecular charge transfer compounds was computationally and experimentally studied to evaluate their potential as thermally activated delayed fluorescence-based (TADF) red emitters. Initially, the compounds were analyzed in solution and, excepting the low emissive compound **VIId**, all showed yellow to red photoluminescence. Chromophores of the D-Ph-A-Ph-D (**VIIIa-d**) type showed higher quantum yields than the D-A-D molecules (**VIIa-d**) with a comparable singlet-triplet energy gap. The reasoning was attributed to the N–C bond twisting, which stabilized the excited state and led to more pronounced non-radiative processes. **VIIIa** exhibits orange emission at 614 nm, quantum yield as high as 55 %, and a short TADF lifetime of 120 µs in 10 wt%-doped CBP films. The constructed OLED device with the **VIIIa** film showed external quantum efficiency (EQE) of 8.1 % at a luminance of 100 cd/m^2, which is comparable to the best reported PHOLEDs.[26]

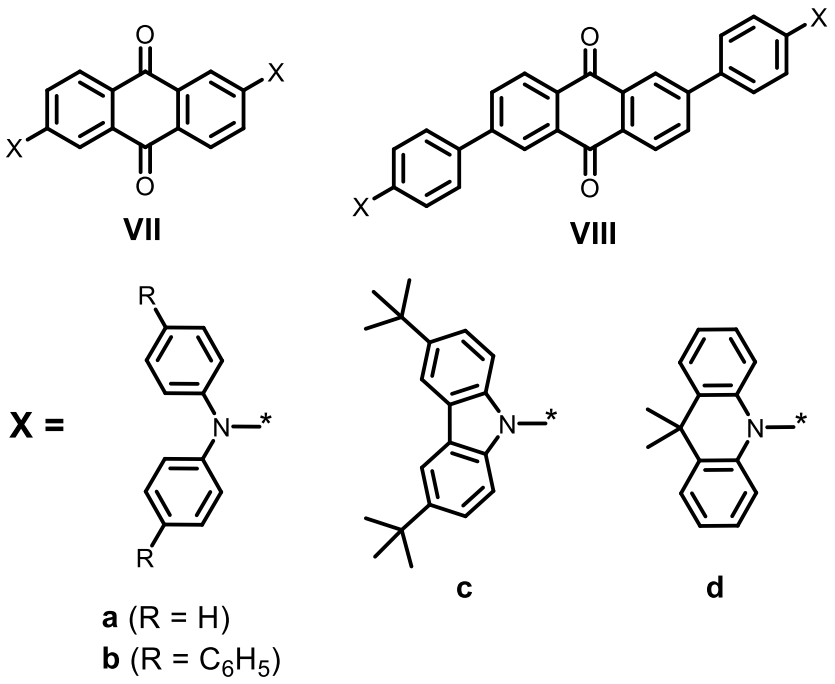

Figure 5. Illustration of the studied anthraquinone-based TADF emitters.[26]

Anthanthrone is a six-membered fused PAH, which is obtained from naphtholactam after its hydrolyzation, diazotization, and dimerization. Ring closure and cyclization lead to the six-fused ring. The 4 and 10 positions can be halogenated via exposure to molecular dihalides, yielding pigments with distinct colors. 4,10-Dibromoanthanthrone (vat orange 3) is a popular dye in the coloring industry due to its bright orange color. Although anthanthrone and 4,10-dibromoanthraquinone have been used in electronic devices, their low solubility in organic solvents makes them unsuitable for solution processing. The existence of ketones and halides provides further synthetic pathways to functionalize anthanthrone, enabling solubility enhancement and tunning of properties.[46] The synthesis of a functionalized D-A-D diphenylamine-anthanthrone compound, **IX**, and its application as dopant-free hole transporting material in perovskite solar cells have been recently reported.[47] Two other prominent dyes containing N-heterocyclic units can be obtained via dimerization 2-aminoanthraquinone under alkaline conditions at different high temperatures, namely indanthrone (vat blue 4, **X**) and flavanthrone (vat yellow 1, **XI**). There are only a limited number of publications on these dye molecules; nevertheless, the liquid crystallinity of indanthrone derivatives and their nonlinear optical features have been described.[46]

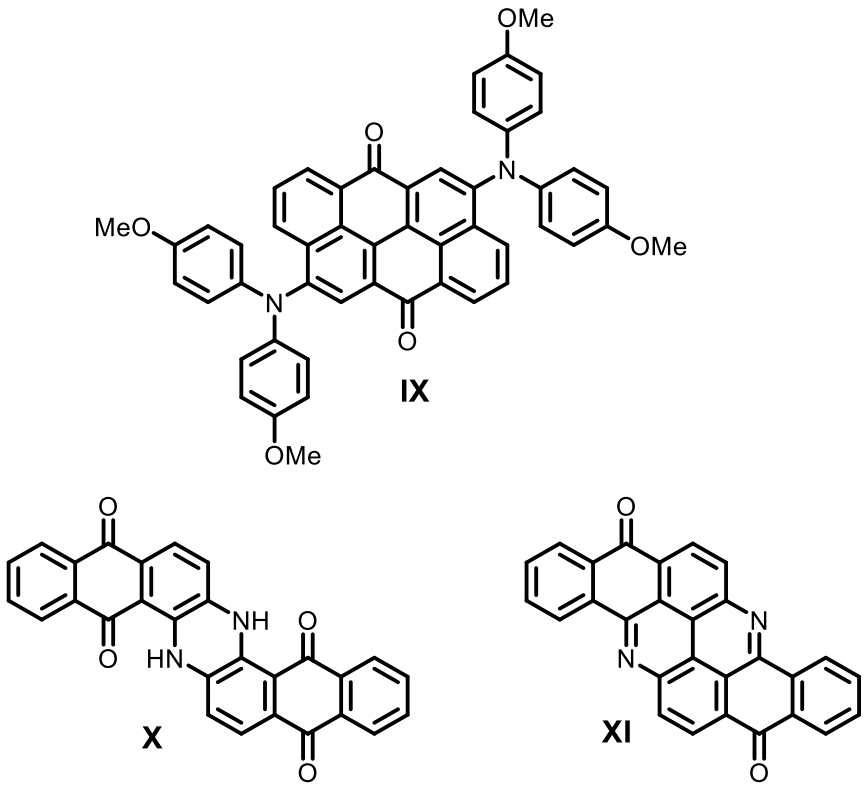

Figure 6. Illustration of an anthanthrone-diphenylamine system (top) and the vat dyes indanthrone, vat blue 4, and flavanthrone, vat yellow 1 (bottom).

Indanthrone is insoluble in most common organic solvents; however, this has been explored for the growth of high-quality nanocrystals with singular optical properties. A soluble Boc-protected precursor was used to obtain indanthrone nanocrystals via slow thermal deprotection in a coordinating solvent and the presence of an organic ligand. The indanthrone-based nanocrystals are absorbed all over the visible range, whereas the Boc-derivative, **XII**, is only in the blue-green region. Additionally, the nanocrystals exhibit emission in the near-infrared region (λ = 1020 nm), being potential candidates for biomedical applications.[46,48]

The solubility of indanthrone can be increased similarly via reduction of the quinone cores followed by O-alkylation to yield soluble derivatives with azaacene structure, **XIII**. The latter fosters high electron affinity and, therefore, n-conducting properties. Cyclic voltammetric studies of a tetraoctyloxy-substituted indanthrone revealed a smaller bandgap compared to phenazine (1.89 vs. 2.91 eV), a consequence of the D-A-D structure with dialkoxynaphtalene units as donors and the phenazine core as acceptor. The donor-acceptor character was supported by theoretical approaches and solution-state UV-vis spectroscopy. The compound displays efficient green emission (Φ = 56 %) and was used as electroluminophore in guest/host-type OLEDs with poly(9-vinylcarbazole). Reduction of the alkyl chain from C8 to C4 resulted in a higher electroluminescence efficiency (luminance of 1670 vs. 250 cd m^{-2}). A

similar study with soluble alkylated flavanthrones resulted similarly in green-emitting OLEDs when combined with poly(9-vinylcarbazole). Luminance values up to 1860 cd m^{-2}. The flavanthrone derivatives displayed a much higher quantum yield (Φ = 80 %) than the parent indanthrone compounds. Functionalization of flavanthrone with lithiated triisopropylacetylene yielded a flavanthrene derivative, **XIV**, with good charge mobility in single-crystal transistors (μ_h = 0.14 cm^2 $V^{-1}s^{-1}$). The favorable mobility was attributed to the small π-stacking distance (3.38 Å) and high overlapping surface.[46,49-53]

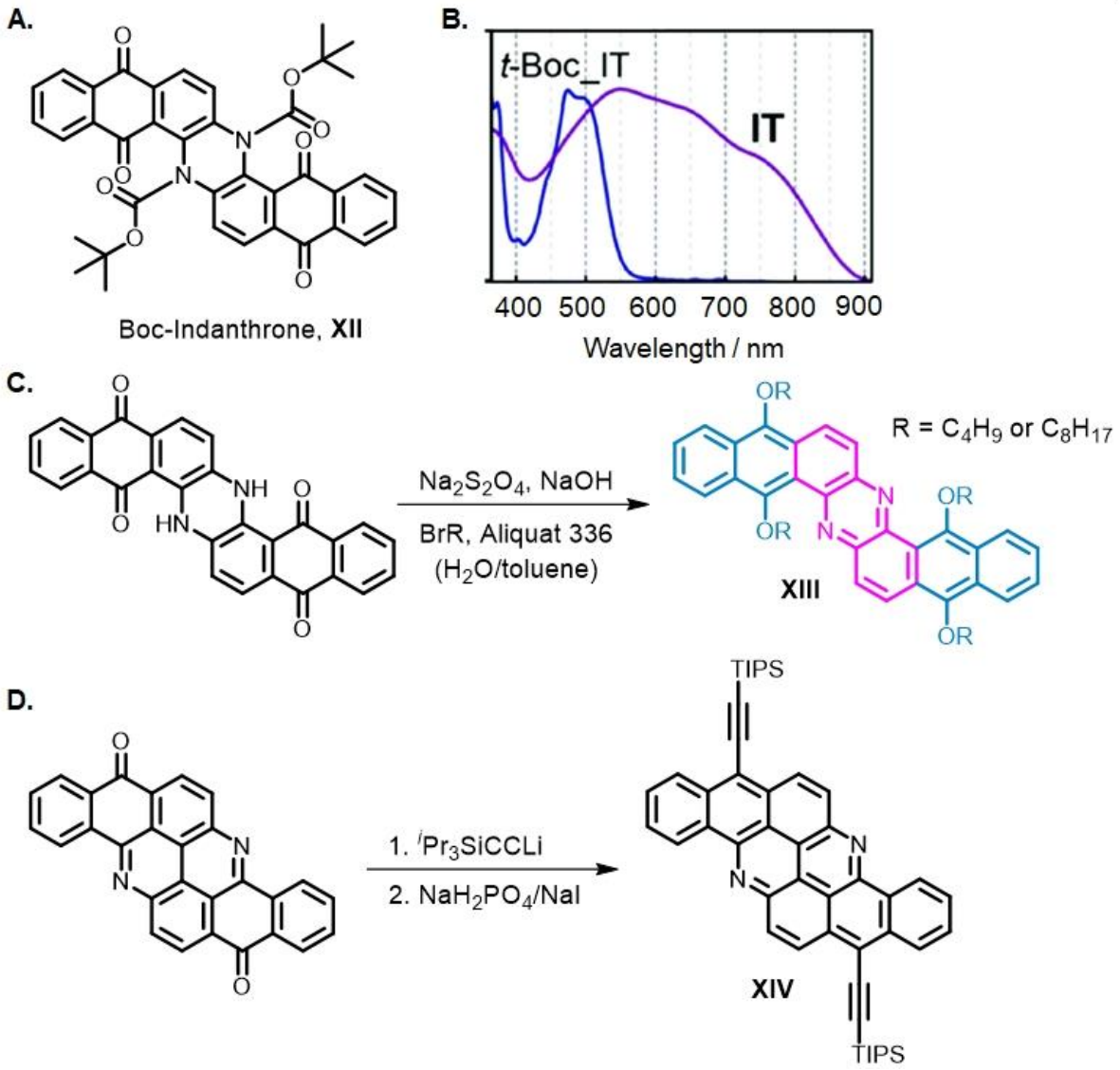

Figure 7. Depiction of **A.** a Boc-substituted indanthrone (*t*-Boc_IT) **B.** the absorption spectra of *t*-Boc_IT (blue line) and indanthrone (IT, purple line) **C.** the biphasic synthesis of tetraalkoxy-substituted indanthrone derivatives. The electron-donating dialkoxynaphtalene units and the electron-accepting phenazine core are highlighted in blue and in pink, respectively **D.** the functionalization of flavanthrone with lithiated triisopropylacetylene. Figure 7B adapted and reproduced with permission of the Royal Society of Chemistry.

1.3. Coordination Chemistry of Quinones: From Discrete Molecular Complexes to Functional Polymeric Architectures

The coordination chemistry of the small benzoquinones and their reduced forms is vastly different depending on the substitution pattern of the oxygenated groups, redox state, and ring functionalization. This class of molecules can engage in charge-transfer complexes (σ and π donation) and hydrogen bonding both as acceptors (keto groups) and donors (hydroxy groups). The catecholate/*o*-benzoquinone redox couple is possibly the most studied class of non-innocent organic ligands. The *ortho*-substitution intrinsically provides a chelating site – formation of a 5-membered ring – while the *para*-isomer may need additional functionalization for chelation.[54] The chelating properties of catecholate are exploited by some bacteria, which produce and secrete siderophores as sequestering agents for ferric ions in aqueous environments. Enterobactin is a triscatecholamide siderophore capable of binding iron(III) with high affinity. The hydroxy groups point outwards in the free siderophore, and the carbonyl group of the amide participates as an acceptor on hydrogen bonding. Upon deprotonation and coordination, the O-donors turn inward building an octahedral pocket for the ferric ion, which is stabilized via hydrogen bonding to the NH-group of the amid bridge.[55]

The ability to coordinate inorganic residues to the π-system of hydroquinone or catechol is one of the bases for the development of supramolecular metal-organometallic coordination networks.[56-58] Organometallic complexes containing η^6-hydroquinone could be, for example, stabilized on electron-rich IrCp* fragments yielding [Cp*Ir(η^6-hydroquinone)][BF_4]$_2$ (**XV**). Attachment to the metal cation facilitates deprotonation of the hydroxy groups and enables reversible redox-chemistry to the semiquinone [Cp*Ir(η^5-semiquinone)][BF_4] (**XVI**), and quinone [Cp*Ir(η^4-p-benzoquinone)] (**XVII**) via acid-base reactions (Figure 8A). The oxidation state of the iridium cation changes from +III to +I as well as the hapticity of the ligand. In the p-benzoquinone π-complex, the oxygen atoms stick out of the ring plane. Solid-state structure determination via single-crystal X-ray diffraction reveals that the semiquinone complex exists as a 1D hydrogen-bonded network (Figure 8b).[59] Similar complexes, including the catechol series, with the $Mn(CO)_3^+$ fragment showed similar acid-base reactivity; however, the semiquinone species adopts a dimeric structure in [$(CO)_3$Mn(η^5-*o*-semiquinone)] due to the *ortho*-positioning of the oxygenated groups. Exposure of the p-benzoquinone π-complex, [$(CO)_3$Mn(η^4-*p*-benzoquinone)]$^-$, to divalent metal cations which adopt commonly octahedral geometries led to σ bonding via keto oxygen atoms and formation of 1D polymeric arrays (Figure 8c). The reaction of the same complex with zinc(II) cations yielded a 3D polymer built from two interpenetrated diamondoid networks with tetrahedral inorganic nodes (Figure 8d). The addition of 4,4-bipyridine as N-donor pillars enabled the formation of a **pcu** framework structure with rectangular pores and encapsulated DMSO molecules (Figure 8e).[60,61] Despite

its *ortho*-substitution, there are reports of coordination polymers containing 1,2-benzoquinone derivatives with pyrazine as coligand.[62]

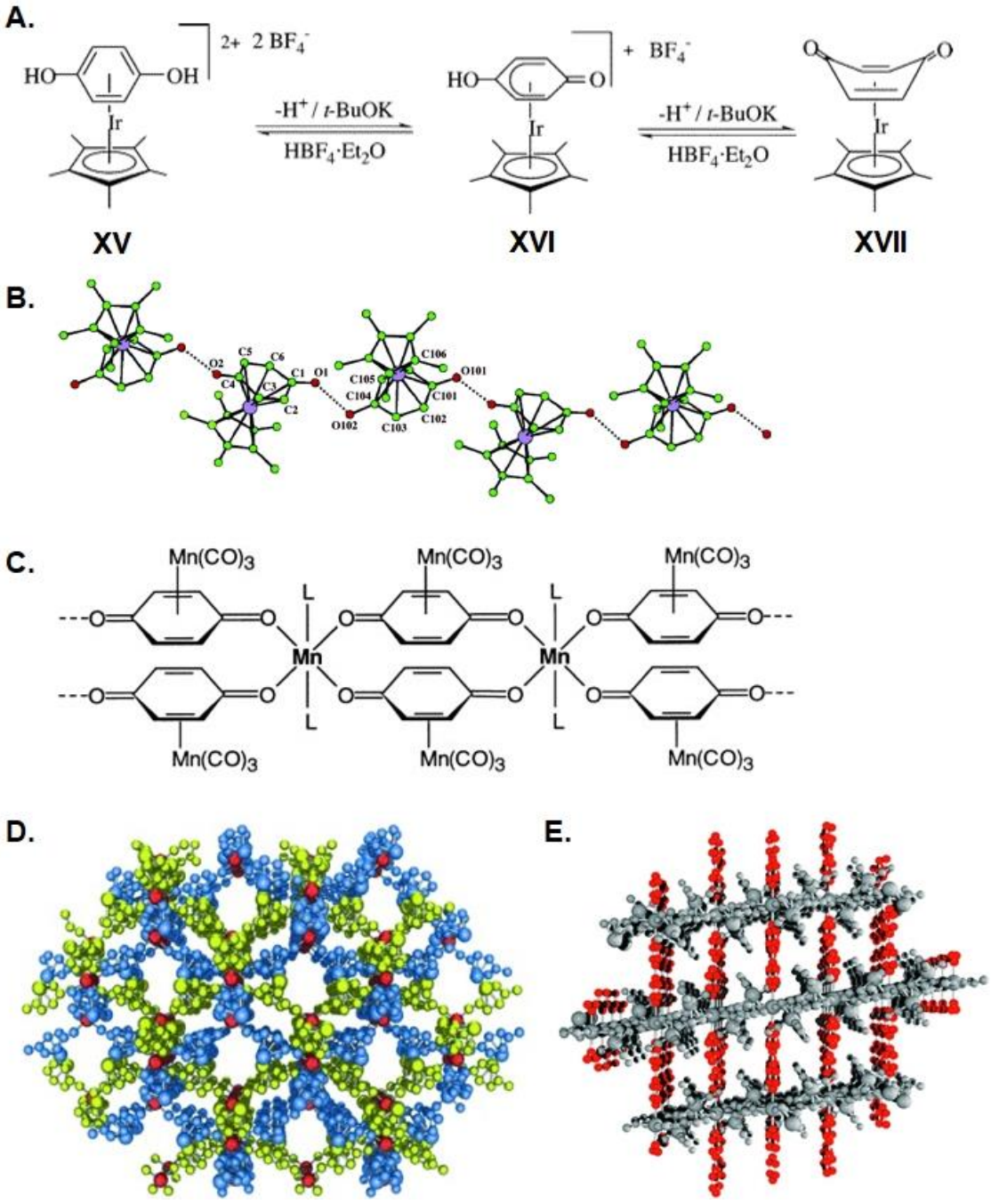

Figure 8. Illustration of **A.** the acid-base equilibria involved in the oxidation of the hydroquinone π-complex to the semiquinone and p-benzoquinone derivatives **B.** the hydrogen-bonded polymeric strands in **XVI**. **C.** the 1D polymeric structure (with L = DMSO or pyridine) **D.** the two-interpenetrated framework (highlighted individually in blue and yellow) consisting of tetrahedral Zn(II) inorganic nodes and $[(CO)_3Mn(\eta^4\text{-}p\text{-benzoquinone})]^-$ as bridging ligands **E.** the topology of the 3D coordination polymer $Mn^{II}(4,4\text{-bpy})[(CO)_3Mn(\eta^4\text{-}p\text{-benzoquinone})]_2$. The structure can be understood as "$Mn^{II}[(CO)_3Mn(\eta^4\text{-}p\text{-benzoquinone})]_2$" 2D sheet-like ensembles which are connected via 4,4-bipyridine pillars (highlighted in red). Atom colors are green (C), red (O), light blue (Ir). Hydrogen atoms were omitted for clarity.[59-61] Figures adapted and reproduced with permission of the American Chemical Society.

Alternative to the π-system, metal complexes can undeniably be obtained via O-coordination. 1,2-benzoquinoid derivatives are bidentate ligands with three accessible redox states. Reduction to the semiquinone (Sq) yields a delocalized radical with pronounced spin density on the donor atoms, which undergoes direct-exchange magnetic coupling when attached to paramagnetic metal centers. Further reduction generates the diamagnetic catecholate species (Cat) or also commonly named dioxolene. The valence tautomerism between redox-active metal centers and semiquinonates has been observed in many complexes and is allowed due to the largely covalent bond between metal and ligand. For example, the reaction of 3,5-di-tert-butyl-1,2-benzoquinone and $Co_2(CO)_8$ followed by treatment with bipyridines yielded Co(II)-semiquinonate complexes at room temperature, [Co(II)(bpy)$(Sq)_2$], as evidenced by single-crystal X-ray diffraction and effective magnetic moment measurements. Sample cooling led to changes in the molecular structure of the ligand and the effective magnetic moment of the complex, which were then compatible with a low-spin [Co(III)(bpy)(Sq)(Cat)] complex.[63,64]

1,4-Semiquinone radical has been used as bridging ligand in binuclear complexes of the formula $[(Me_6tren)_2M^{II}_2(C_6H_4O_2^{-\cdot})]^{3+}$ (Me_6tren = tris(2-dimethylaminoethyl)amine; M = Fe, Co, Ni; **XVIII**–**XX**, respectively) to foster magnetic exchange between the paramagnetic centers (Figure 9A). The complexes were obtained via one-electron oxidation of the hydroquinone precursors with $[FeCp_2][B(C_6F_5)_4]$ and were structurally characterized via SCXRD analysis. All metal ions are found in trigonal bipyramidal environments (Figure 9B), as imposed by the ligand, and are *trans* aligned to each other, which results in a parallel orientation of the M–O vectors and the local magnetic anisotropy. The geometry of the Co(II) ion is the closest to the ideal polyhedron due to its fully symmetric electronic configuration, whereas the other two complexes face Jahn-Teller distortion. Notably, the semiquinone complexes were air-stable, which might be due to steric hindrance of the $[B(C_6F_5)_4]$ counter ions. As expected, shortening of the C–O bond distances after oxidation was observed and further spectroscopic evidence arguably defined the oxidation state of the ligand. Magnetic susceptibility data revealed strong antiferromagnetic coupling between the semiquinone ligand and the metal ions and significant zero-field splitting. The Ni(II) complex, **XX**, showed temperature-independent paramagnetism and a well-isolated S=3/2 ground state even at 300 K (Figure 9C). The obtained coupling constants are considerably larger than those observed for bis(bidentate) semiquinoid complexes, which may arise from spin density concentration over solely one atom instead of two. Slow magnetic relaxation was observed in **XIX** and **XX**.[65]

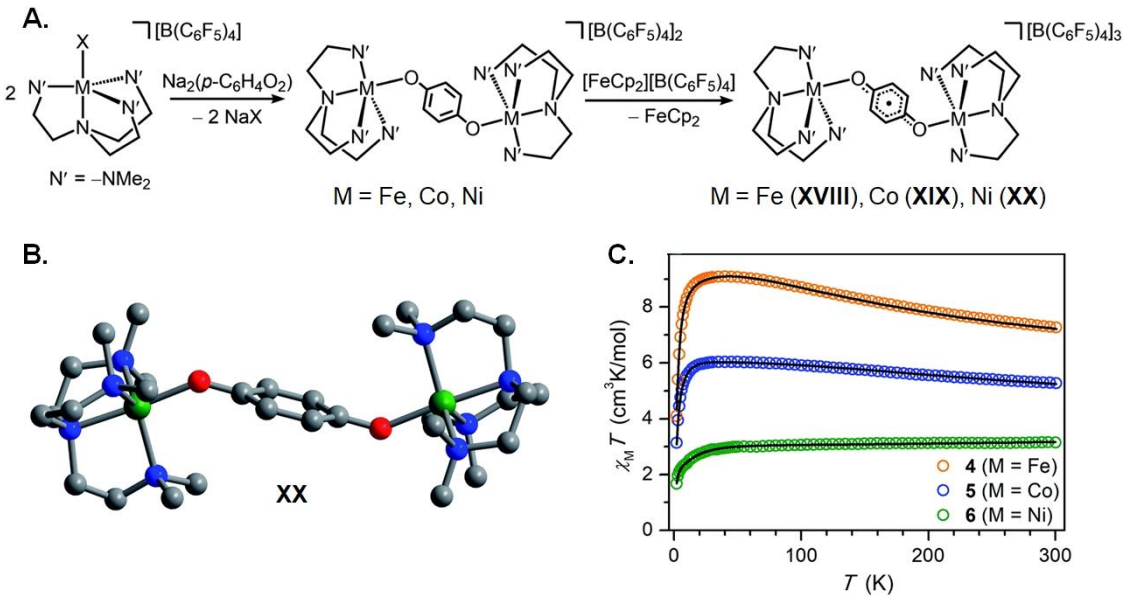

Figure 9. A. Reaction scheme for the synthesis of the binuclear semiquinone bridged complexes **XVIII**–**XX B.** Illustration of the molecular structure of **20**. **C.** Magnetic susceptibility data for the semiquinoid complexes **XVIII**–**XX**. Atom colors are gray (C), red (O), blue (N), green (Ni). Hydrogen atoms were omitted for clarity.[65] Figures adapted and reproduced with permission of the Royal Society of Chemistry.

One strategy to construct quinoid-based 3D polymeric architectures is the implementation of the bis(bidentate) hydroxylated derivatives, which contain a higher number of potential coordination sites. 2,5-dihydroxybenzoquinone (H_2DHBq) and chloranilic acid (2,5-dichloro-3,6-dihydroxybenzoquinone, H_2Cl_2DHBq) have been used to obtain conductive iron-quinoid magnets. The synthesis of $(Bu_4N)_2[Fe^{III}_2(DHBq)_3]$, **XXIa**, was achieved by heating an acidic aqueous mixture of 2,5-diaminobenzoquinone and ferrous sulfate heptahydrate in presence of Bu_4NBr at 120 °C (Figure 10B). The H_2DHBq ligand was generated via *in situ* hydrolysis and attempts starting with the hydroxylated ligand led to amorphous samples. The oxidation state of the iron cations was assigned using Mössbauer spectroscopy, which strongly indicated high-spin Fe(III) ions. Based on further spectroscopic and crystallographic evidence, the quinoid ligands were assigned as mixed $DBHq^{2-}$ (quinone dianion) and $DBHq^{\cdot 3-}$ (semiquinone radical trianion) in a 1:2 ratio. Chemical reduction of the framework with one equivalent sodium naphtalenide led to formula $Na_{0.9}(Bu_4N)_{1.8}[Fe^{III}_2(DHBq)_3]$, **XXIb**, which represents formally a 0.7 electron/mol reduction. Mössbauer spectroscopy did not evidence metal-centered reduction, suggesting thus ligand-based reduction of $DBHq^{2-}$ units to the $DBHq^{\cdot 3-}$ radical species (0.3:2.7 ratio). When using four equivalents of the reducing agent, a compound with formula $Na_{3.2}(Bu_4N)_{1.8}[Fe^{III}_2(DHBq)_3]$, **XXIc**, was obtained. The reduction was shown to be again ligand-based and to generate additionally fully reduced tetrahydroxybenzene anions (THB^{4-}). Due to the presence of radical species, the electronic conductivity of **XXIa** and **XXIb** were measured, reaching, respectively, high values of 0.16 and 0.006 S cm^{-1} at 298 K (Figure 10C). The results suggested an electron hopping mechanism

and the lower conductivity of **XXIb** was attributed to the diminished concentration of vacancies for electron mobility compared to **XXIa**.[66]

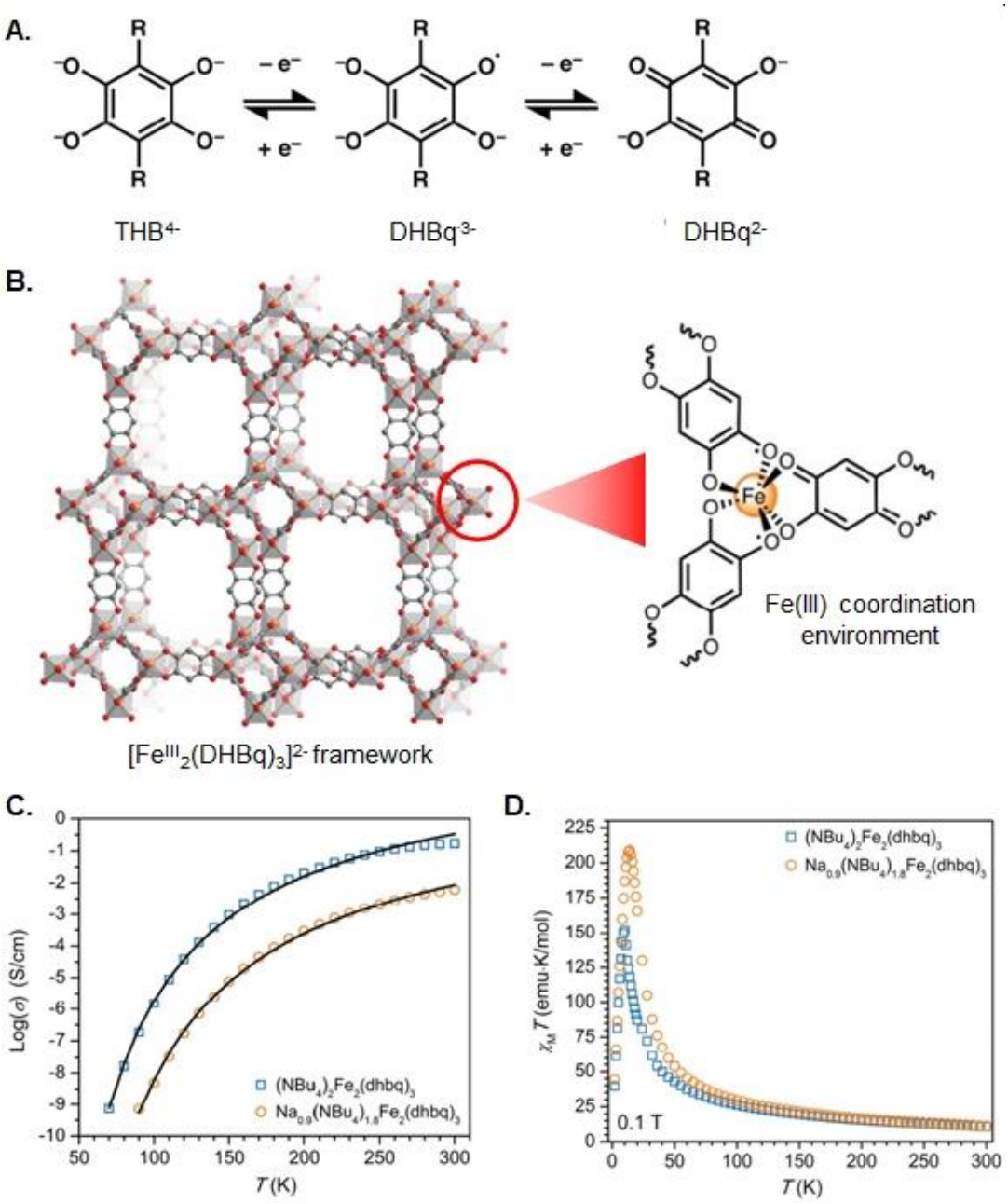

Figure 10. Illustration of **A.** the three accessible redox states of dihydroxybenzoquinone derivatives. **B.** the overall topology of the anionic framework [Fe$^{III}_2$(DHBq)$_3$]$^{2-}$ and the coordination environment of the Fe(III) ions. Tetrabutylammonium cations were omitted for clarity reasons. **C.** temperature-resolved conductivity data for **XXIa** (blue squares) and **XXIb** (orange circles). The black lines correspond to Arrhenius fits of the data. **D.** dc magnetic susceptibility data for **XXIa** (blue squares) and **XXIb** (orange circles).[66] Figures adapted and reproduced with permission of the American Chemical Society.

Concurrently, the magnetic properties of both materials were investigated. The magnetic ordering temperature for **XXIa** and **XXIb** was 8 and 12 K, respectively (Figure 10D). The unexpected low values were ascribed to a competition of ferromagnetic and ferrimagnetic

interactions, which prevented bulk three-dimensional ordering of the material.[66] When using the chlorinated parent linker, chloranilic acid (H_2Cl_2DHBq), two-dimensional networks (Figure 11A) with formula $(Me_2NH_2)_2[M_2(Cl_2DHBq)_3]\cdot 2H_2O\cdot 6DMF$, where M = Fe^{III} (**XXIIa**) or Zn^{II} (**XXIII**), were obtained. In these compounds, the oxidation state of the linker is directly influenced by the redox character of the chosen metal. The redox inert behavior of Zn(II) cations led to a framework comprising solely Cl_2DHBq^{2-} anions, whereas redox-active Fe(II) cations act *in situ* as reducing agents yielding a mixed-valence compound (1:2 quinone to semiquinone ratio) similar as in **XXIa**. Exposure of the iron-based material to cobaltocene afforded the parent framework with only semiquinone ligands, $(Cp_2Co)_{1.43}(Me_2NH_2)_{1.57}[Fe^{III}_2(Cl_2DHBq)_3]\cdot 4.9DMF$, **XXIIb**. The oxidation state assignment was supported by spectroscopic evidence and crystallographic data. The concomitant elongation of the C–O bond and shortening of the vicinal C–C bond are in good agreement with the degrees of reduction observed for the ligand (Figure 11B). Electronic conductivity measurements were also following the observed valence states. **XXIII** shows low conductivity ($\sigma = 1.5 \times 10^{-9}$ S cm^{-1}), which was addressed as a consequence of the closed-shell d^{10} valence of Zn(II) cations that possibly hinders the electron hopping mechanism. The as-synthesized **XXIIa** showed an ambient temperature conductivity of 1.5×10^{-2} S cm^{-1}, which dropped roughly one order of magnitude upon desolvation ($\sigma = 1.0 \times 10^{-3}$ S cm^{-1}) due to slight structural distortions of the honeycomb structure. Finally, the reduced MOF **XXIIb** exhibited even lower conductivity ($\sigma = 5.1 \times 10^{-4}$ S cm^{-1}) because of the removal of the mixed-valence state. Interestingly, **XXIIa** shows magnetic ordering below 80 K and the further reduced MOF, **XXIIb**, already below 105 K due to stronger magnetic interactions.[67]

Although the use of anthraquinones for the construction of metal-organic frameworks has not been extensively exploited yet, there are reports of molecular cages, which indicate the potential for the development of porous materials.[68,69] Very recently, an iron-based MOF with quinizarin (1,4-dihydroxyanthraquinone) as a ligand was obtained via the solvothermal synthesis in an $EtOH/H_2O$ mixture. Crystal structure determination revealed each organic linker coordinated to two equivalent iron cations which are found in octahedral environments. The proximity of the aromatic cores enables π-π interactions. The optical bandgap of the Fe-quinizarin MOF was determined to be between 2.3–3.3 eV and the material behaves as a semiconductor. A conductivity of 1.73×10^{-2} S cm^{-1} was measured and is attributed to electronic conduction along the π-chains.[70]

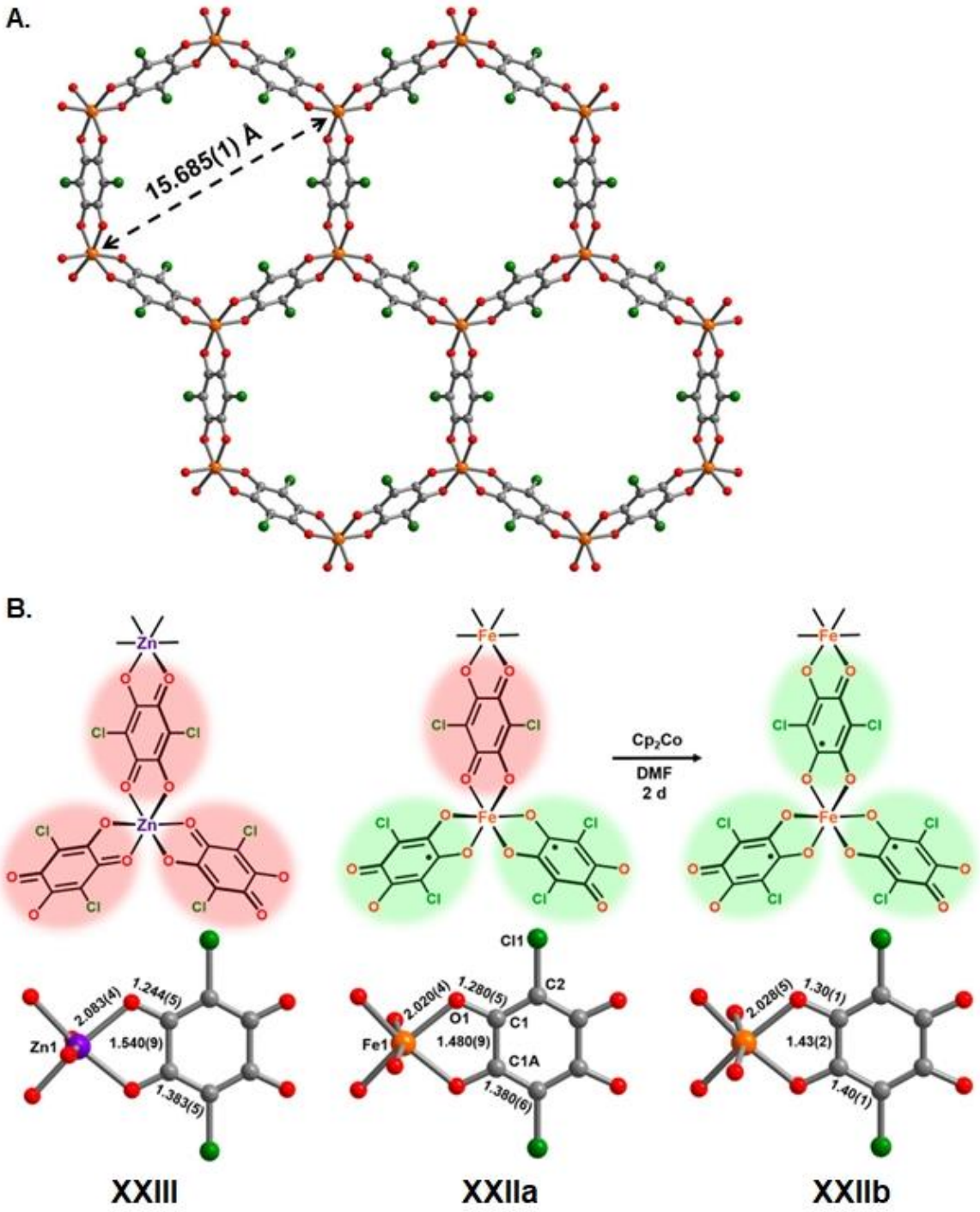

Figure 11. Illustration of the **A.** structure of **XXIIa** with the highlight of the pore size **B.** metal coordination environment and distinct oxidation states of the ligand in **XXIIa,b,** and **XXIII**. Atom colors are gray (C), red (O), green (Cl), purple (Zn), orange (Fe). Pore solvent molecules were omitted for clarity.[67] Figures adapted and reproduced with permission of the American Chemical Society.

The triscatechol molecule 2,3,6,7,10,11-hexahydroxytriphenylene (HHTP or H_6THO) and derivatives have also been used for building 2D and 3D coordination frameworks. Two-dimensional stacked sheet-like networks could be synthesized with bivalent metals (Co, Ni, Cu) which adopted square planar geometry. Such coordination polymers showed to be highly conductive via the π-interactions.[71-73] When combined with metals which rather prefer higher coordination numbers, 3D polymers can be obtained. A series of MOFs with Fe(II,III) (**XXIV**), Ti(IV) (**XXV**), and V(IV) (**XXVI**) was synthesized from DMF mixtures in presence of tetrabutylammonium salts under solvothermal conditions. Truncated octahedral-shaped single crystals of **XXIV** suitable for SCXRD were obtained. The structure was solved and refined in the cubic space group *Pa*-3 and reveals a 2-fold interpenetrated framework with **srs** topology. Each organic linker is connected to three equivalent iron centers which are coordinated in an octahedral fashion. Additionally, the two independent frameworks are connected through $Fe_2(SO_4)_2(H_2O)_2$ units comprising two octahedrally coordinated iron centers. The coordination sphere is built up from three μ_2-O atoms from the ligand, two μ_2-bridging sulfate anions, and one terminal aqua ligand. The Fe–O bond distances between the ligand and the iron cations in the bridging cluster (2.138 Å) are longer than those in the **srs** network (1.998 Å), revealing weaker bonding to these units. The structures of **XXV** and **XXVI** were solved via PXRD analysis and refinement and were determined as 2-fold interpenetrated and non-interpenetrated **srs** frameworks, respectively. **XXIV** and **XXV** showed high proton conductivity, with maximum values, respectively, of 5.0×10^{-2} and 8.2×10^{-4} S cm^{-1} at 98% relative humidity and 25 °C. The activation energy indicates a Grotthuss mechanism, in which the protons hop through a hydrogen-bonded network. The higher proton conductivity of **XXIV** was based on the greater amount of dimethylammonium cations and sulfate anions.[74]

Very recently, rare-earth metals were used to construct 3D porous conductive frameworks with **spn** topology and formula $[M_6(\mu_6\text{-}NO_3)(THO)_2]^{5+}$, whereby M = Y, Eu. The charge balance is provided by encapsulated hydroxide or nitrate anions. Color darkening of the crystals suggests partial oxidation of the ligand, which was confirmed via *in situ* diffuse reflectance spectroscopy. The absorptions related to the π-π* transitions of the aromatic core at 350 nm and the ligand-to-metal charge transfer at 800 nm decreased upon heating, whereas a broad band at 1100 nm, corresponding to the π-π* transitions in the semiquinone, rose. The presence of the semiquinone form increased the number of charge carriers and electrical conductivities on the order of 10^{-5} – 10^{-6} were measured.[75] There are also computational-structural studies on 3D MOFs with trivalent metals (Al^{3+}, Ga^{3+}) containing the radical ligand.[76]

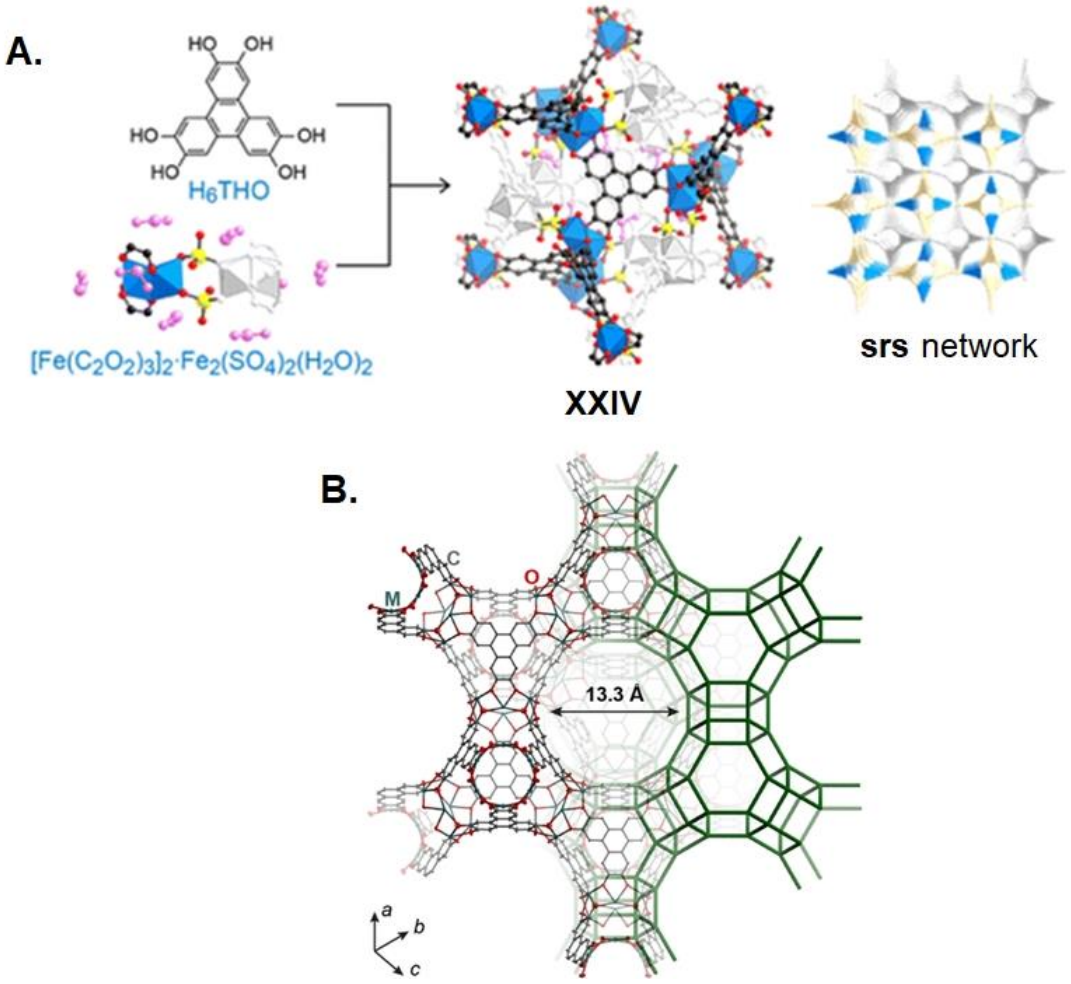

Figure 12. Illustration of the **A.** structure of the H_6THO ligand, the inorganic SBU, and the resulting framework **24.** Atom colors are black (C), red (O), yellow (S). The blue octahedra represent the geometry of individual iron centers. **B.** general structure of the 3D rare-earth metal-based MOFs of the formula $[M_6(\mu_6\text{-}NO_3)(THO)_2]^{5+}$, whereby M = Y, Eu. Atom colors are gray (C), red (O), dark green (M). Pore solvent molecules were omitted for clarity.[74,75] Figures adapted and reproduced with permission of the American Chemical Society.

Beyond polyhydroxylated systems, other functional groups can be implemented to obtain coordination polymers with quinoid systems. Carboxylic acids have been extensively used for the synthesis of metal-organic frameworks. The reproduction of the reversible solution redox chemistry of the *p*-benzoquinone/hydroquinone pair has been targeted in MOFs and MONs. The reaction of 2,5-bis(*p*-carboxyphenyl)hydroquinone with $ZrCl_4$ in DMF with benzoic as modulator yielded a UiO-66 type Zr-MOF (**XXVII**, Figure 13A). The synthesis does not yield the isomorphous phase when starting from the oxidized ligand. Nevertheless, the oxidation of the hydroquinone core was carried out post-synthetically using phenyliodine(III) diacetate (PIDA) in a single-crystal to single-crystal transformation. The re-reduction was possible via treatment with ascorbic acid. The Zr-MOF was chemically stable and retained its crystallinity for at least three cycles. The crystals suffer a color change (Figure 13B) from colorless to yellow upon oxidation as well as quenching of their luminescence.[77] Similarly, the tetratopic

parent linker, 2,3,5,6-tetrakis(*p*-carboxyphenyl)hydroquinone has been applied to the growth of switchable 2D-metal-organic nanosheets. The self-assembly of the linker in presence of Zn(II) ions led to bidimensional sheets, which stack down along the *y* axis, generating a stacked MOF. Even though the crystals of the Zn-MOF did not show chemically induced redox chemistry, the nanosheets obtained via ultrasound-induced liquid-phase exfoliation (UILPE) exhibited accessible redox behavior. In the same fashion, the oxidation of the hydroquinone core was carried via treatment with PIDA and the reduction with ascorbic acid.[78]

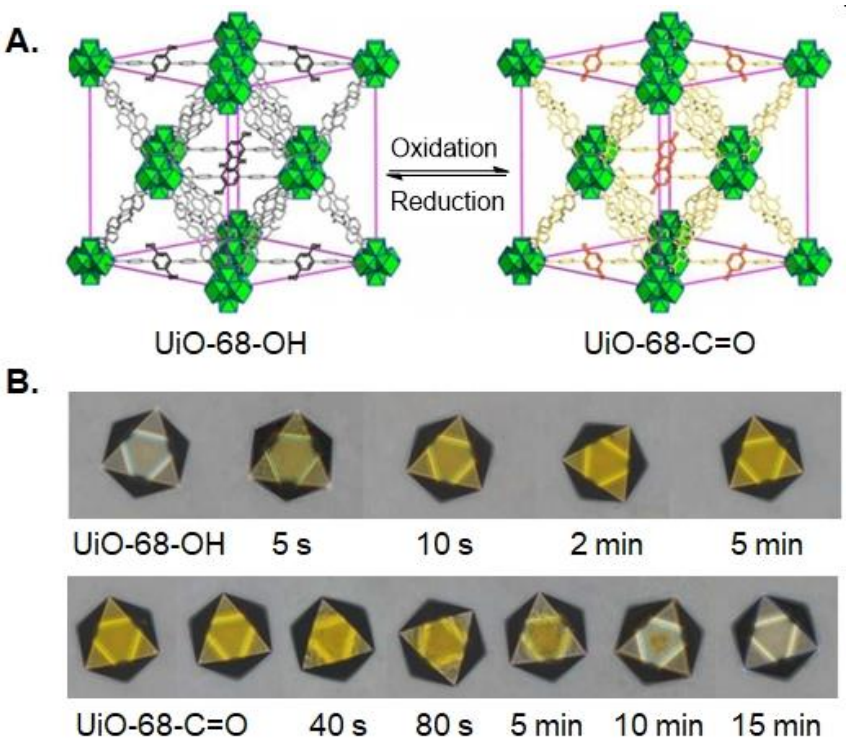

Figure 13. Illustration of **A.** the overall structure of UiO-68-OH and UiO-68-C=O. The hydroquinone and benzoquinone cores are highlighted in black and red, respectively. The Zr-nodes are depicted in green **B.** the color change of a single crystal during the oxidation and reduction processes.[77] Figures adapted and reproduced with permission of the American Chemical Society.

There are a few reports on the electrochemistry of metal-organic frameworks derived from isomers of the anthraquinone dicarboxylic acid (H_2AqDC). The *para*-substituted 1,4 and 2,6-isomers have been used to investigate the proton-coupled electron transfer processes of anthraquinone in the MOFs. Chemically robust Zr-MOFs with UiO-66 topology were synthesized, and their pH-dependent aqueous electrochemistry was characterized via cyclic voltammetry. Pourbaix diagrams of both ligands and MOFs were constructed and revealed similar electrochemical behavior of the anthraquinone cores in the solution and the solid state. The results also supported that the pH-value in the inner voids was the same as in the bulk solution, suggesting efficient proton diffusion into the coordination networks.[79]

The fabrication of batteries with anthraquinone-based MOFs as cathode materials has been performed using 2,7-dicarboxy-9,10-anthraquinone (2,7-AqDC). The reaction of the organic linker with $Cu(ClO_4)_2 \cdot 6H_2O$ in DMF led to 2D Kagomé lattice architectures comprising $Cu(OAc)_4$ paddle-wheel clusters as SBUs and overall formula $[Cu(2,7\text{-}AqDC)(DMF)]_n$ (**XXVIII**, Figure 14A). The axial positions were occupied by DMF molecules. The MOF possesses hexagonal pores, and the redox-active linkers are exposed to the internal pore surface. The charge-discharge profile showed two independent redox processes in a 1:2 ratio, a total uptake of three electrons, resulting in a theoretical specific capacity of 162 mAh g^{-1}. Solid-state cyclic voltammetry (Figure 14B) enabled the assignment of the two-electron event to the reduction of the quinone core of the ligand. The single redox step was shown to be related to the Cu(II)-cluster. An initial specific capacity of 147 mAh g^{-1} was close to the expected; however, it dropped and stabilized to 105 mAh g^{-1} within 50 cycles. The reason for the observed decrease in capacity was limited exposed surface area and low charge transfer rate.[16]

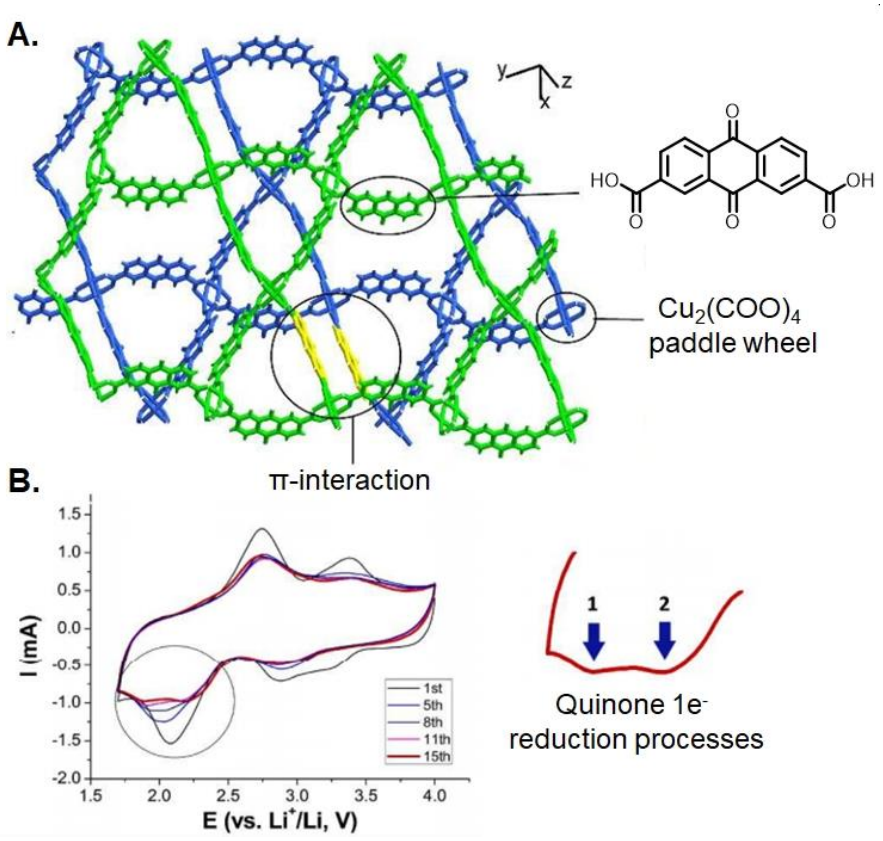

Figure 14. Illustration of **A.** the overall topology of **XXVIII**. The independent 2D coordination frameworks are highlighted in green and blue **B.** solid-state voltammogram of **XXVIII**. The one-electron reduction steps could be observed separately within a higher number of cycles.[16] Figures adapted and reproduced with permission of the American Chemical Society.

The photochemistry of anthraquinones in coordination frameworks has not been extensively investigated yet. Nevertheless, the *ortho*-isomer, 2,3-H_2AqDC, is a commercial compound and has been reacted with divalent metal cations for the synthesis of discrete

molecular complexes and coordination polymers (Figure 15A). Photoluminescence measurements were carried out at 77 K since the complexes were not emissive at room temperature. Temperature increase led to luminescence quenching due to the flexibility of the non-substituted side of the linker, which allowed non-radiative relaxation pathways (Figure 15B). The vibrational freedom of the ligand was evaluated in terms of the atomic displacement parameters obtained from the solid-state structures (Figure 15C). One of the polymers showed a large emission shift, which might have arisen from excimer formation or ligand-to-metal charge transfer. The authors, however, did not perform time-resolved measurements to clarify these assumptions.[80]

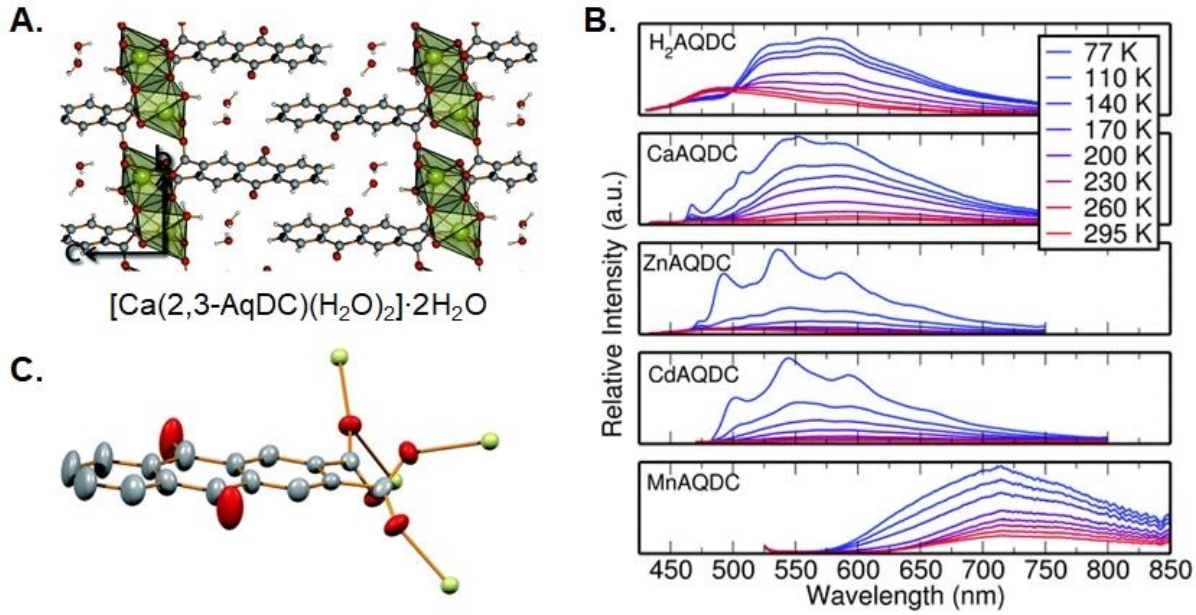

Figure 15. Illustration of **A.** the solid-state structure of one reported coordination polymer with 2,3-H_2AqDC **B.** temperature-resolved photoluminescence spectra of 2,3-H_2AqDC and derived coordination polymers. **C.** a crystallographic representation of 2,3-H_2AqDC in a crystalline network showing the increased atomic displacement parameters at the non-coordinated site.[80] Figures adapted and reproduced with permission of the American Chemical Society.

Anthraquinone disulfonates could also be incorporated in supramolecular structures despite the general weaker coordination strength of sulfonates compared to carboxylates. Usually, the sulfonates cannot displace water molecules from the first coordination sphere leading to 0D or 1D structures. In contrast, the reaction of anthraquinone-2,6-disulfonate (2,6-AqDS) with alkaline earth metals yielded 2D and 3D coordination polymers which were also catalytically active for alkene hydrogenation and ketone hydrosilylation reactions.[81] The non-innocent character of 1,5-AqDS has been observed in rare-earth metal-based MOFs. The 2D inorganic frameworks encompassed the semiquinone anion $AqDS^{3-\cdot}$ and showed high charge mobility and conductivity through the π-π interactions. The semiquinone presence was confirmed based on electrical neutrality, structural modifications, and bond length analysis.[82]

The coordination chemistry of vat dyes remains practically uncharted. Very recently, the controlled reduction of flavanthrone and a flavanthrone-vanadocene adduct, $[(Cp_2V)_2(Flavanthrone)]\cdot C_6H_4Cl_2$, **XXIX**, were reported. The semiquinone radical was obtained via reduction with sodium fluorenone ketyl in *o*-dichlorobenzene in presence of cryptand [2.2.2]. The quinone dianion could be synthesized using different organometallic reduction agents ($Na[Re(CO)_5]$, $Na[Cp_2Co(CO)_2]$); however, the metal fragments were not present in the isolated products. Interestingly, when using the electron-poor vanadocene, Cp_2V, a flavanthrone-vanadocene complex was formed. The flavanthrone dianion coordinates via the O-atoms with a short V–O bond, 1.971(1) Å, and the polyaromatic cores stack effectively with an interplanar distance of 3.38 Å. Weak antiferromagnetic coupling between the V(III) ions ($J = -2.0\ cm^{-1}$) was observed. No metal-organic networks have been reported so far with such polyaromatic vat dyes.[83]

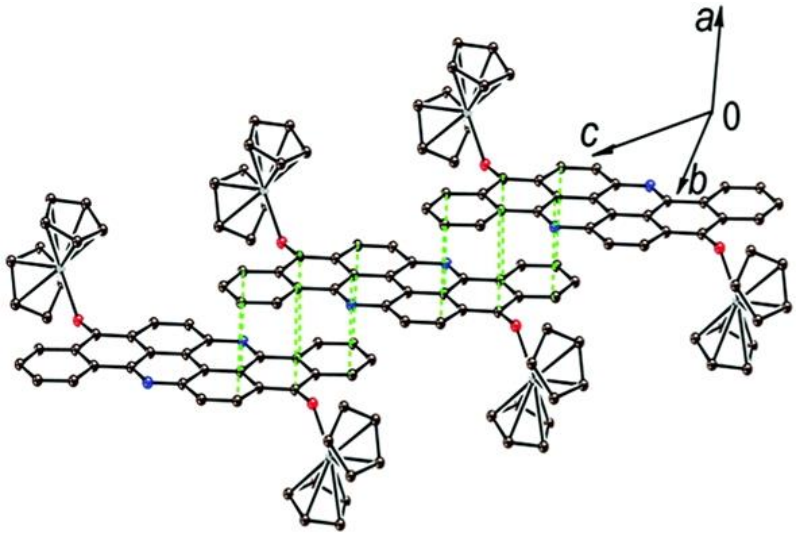

Figure 16. Depiction of the solid-state structure of $[(Cp_2V)_2(Flavanthrone)]\cdot C_6H_4Cl_2$. The π-interactions are highlighted in green. The *o*-dichlorobenzene solvent molecules were omitted for clarity. Atom colors are black (C), blue (N), red (O), light blue (V).[82] Figure adapted and reproduced with permission of the Royal Society of Chemistry.

2. RESULTS AND DISCUSSION

2.1. Exploiting the Anthraquinone/Anthrahydroquinone Chemistry in Metal-Organic Frameworks: Immobilized Redox Switches for Molecular Oxygen Activation

The manuscript “Molecular Oxygen Activation by Redox-Switchable Anthraquinone-Based Metal-Organic Frameworks” was based on this chapter.

de Carvalho, J.G.M., Fischer, R.A., Pöthig A., *Inorg. Chem.*, **2021**, 60, 7, 4676–4682

2.1.1. Design of anthraquinone-based linkers for redox-active architectures

To incorporate anthraquinone moieties into crystalline frameworks for studies on solid-state reversibility and solid-gas molecular oxygen activation, the choice of the linker is crucial. The linker should resemble alkyl-substituted anthraquinones, which are utilized in the anthraquinone process. Considering the typical building blocks for MOFs, carboxylic acids or pyridine derivatives of anthraquinone rise as possible candidates. Carboxylic acids, however, become negatively charged upon coordination, which could affect the quinone electron-accepting properties. Pyridines, on the other hand, remain neutral after coordination and might be more appropriate as a model for anthraquinone itself. In this chapter, 2,6-di(pyridin-4-yl)-9,10-anthraquinone (DPAq) is presented as a structural motive for the construction of redox-active pillar-layered architectures together with benzene dicarboxylate (BDC) as co-linker.

COUDRET C. has previously reported the synthesis of DPAq on his work on *Suzuki* cross-coupling reactions with anthraquinone-triflate.[84] The reduction of the quinone core to generate 2,6-di(pyridine-4-yl)-9,10-anthrahydroquinone (DPAHq) was not yet described. Both the oxidized and the reduced linker molecules were synthetically accessible within a three-step procedure. First, 2,6-diaminonanthraquinone underwent a *Sandmeyer* reaction in acetonitrile with *tert*-butylnitrite and cupric bromide to 2,6-dibromoanthraquinone (**1**). The second step involved a *Suzuki* coupling reaction between 4-pyridinylboronic acid and the aryl dibromide, yielding DPAq (**2**). Finally, reduction of the quinone moiety of the linker under solvothermal conditions in a DMF/H_2O mixture in presence of Al^{3+} or Fe^{3+} ions yielded the corresponding hydroquinone, DPAHq (**3**) (Scheme 6). The reduction could not be carried out when using softer metal cations such as Cd^{2+}, suggesting a *Lewis*-acid catalyzed reaction.

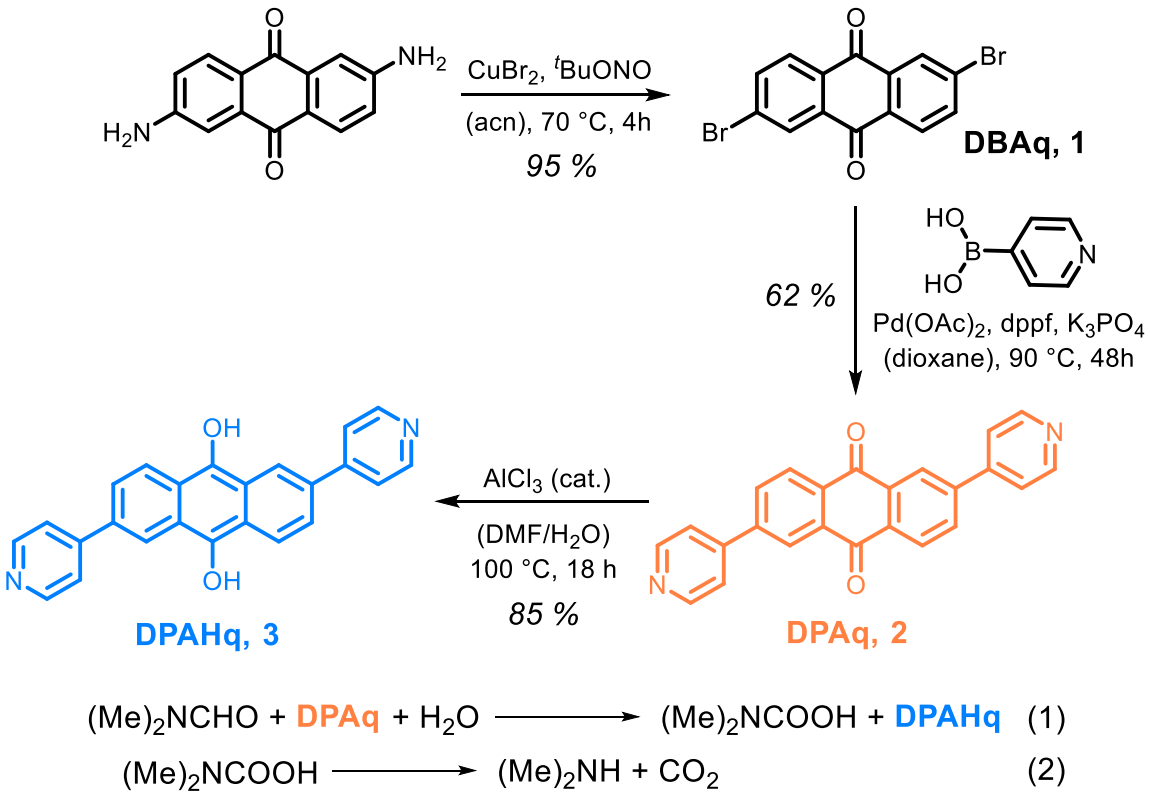

$$(Me)_2NCHO + DPAq + H_2O \longrightarrow (Me)_2NCOOH + DPAHq \quad (1)$$

$$(Me)_2NCOOH \longrightarrow (Me)_2NH + CO_2 \quad (2)$$

Scheme 6. Synthetic approach towards the DPAq and DPAHq linkers.

The synthesis of 2,6-dibromoanthraquinone (DBAq, **1**) was carried out according to a literature procedure.[85] Suitable crystals for SCXRD were obtained by slow evaporation of a solution in $CHCl_3$. The structure was solved and refined in the monoclinic space group *P* $2_1/c$ and the asymmetric unit comprises half a molecule. The C=O bond length is 1.22 Å and the adjacent C–C bonds are 1.49 Å long, compatible with an anthraquinone core. The remaining C–C bonds are shorter, 1.39 Å, as expected for fully delocalized aromatic rings. The C–Br bond length is in the expected range (Figure S1). π-Stacking is observed along the b-axis with a ligand-to-ligand distance of 3.84 Å.

The solid-state structure of DPAq could be determined via single-crystal X-ray analysis of colorless plates obtained from DMF. The crystal structure of DPAq was solved and refined in the monoclinic space group *P n*. The asymmetric unit comprises two crystallographic non-equivalent DPAq molecules. The average C=O bond length of approximately 1.23 Å is in good accordance with the observed value for anthraquinone.[86] The vicinal C–C bonds to the carbonyl groups are roundly 1.48 Å long and compatible with a single bond character. The remaining C–C bonds are shorter, 1.39 Å, and in agreement with aromatic character. π-Stacking is observed along the a-axis with a ligand-to-ligand distance of 3.74 Å (Figures 17A and 17B).

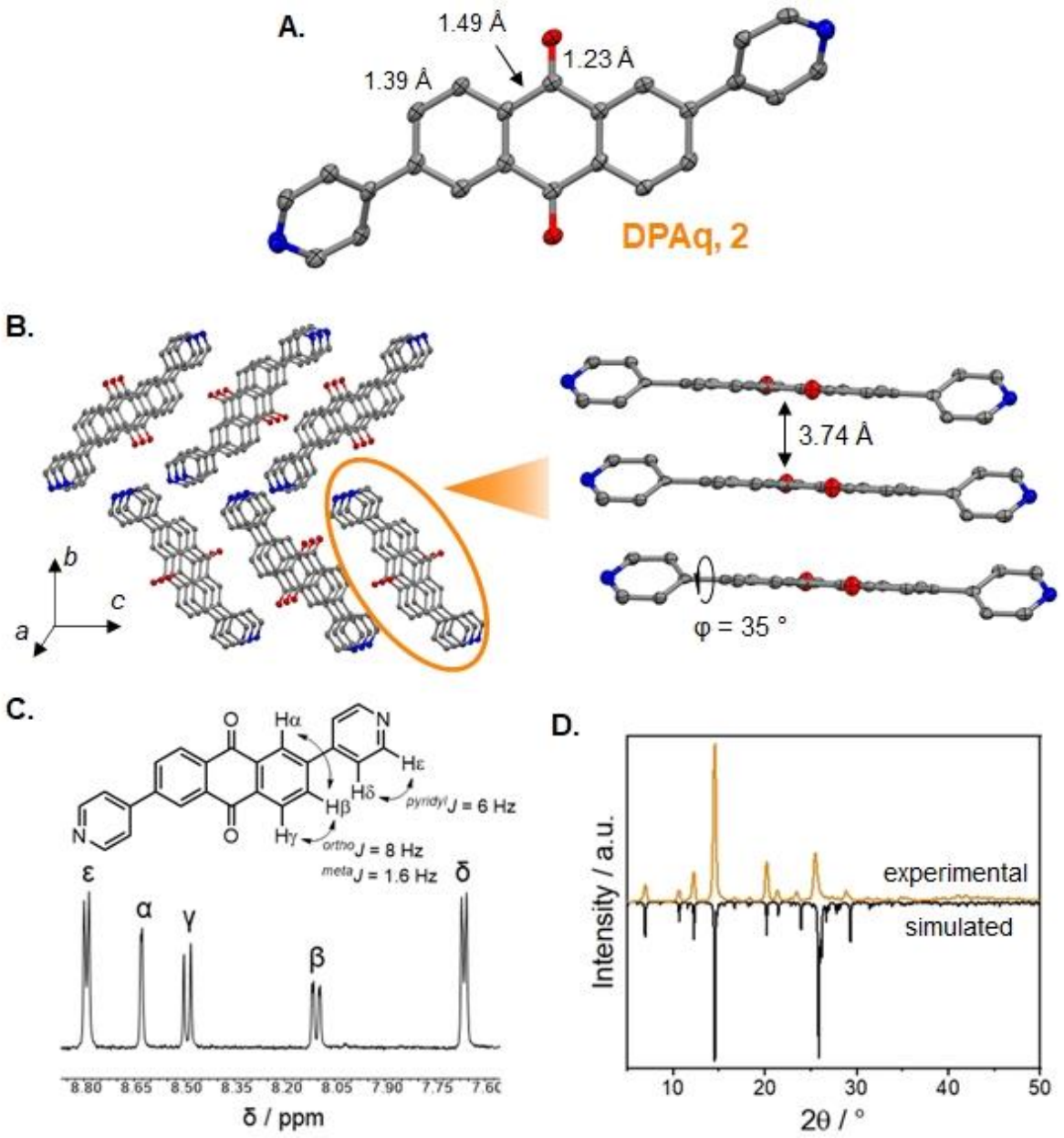

Figure 17. A. Molecular structure of DPAq, highlighting selected bond distances; **B.** solid-state structure of DPAq along the *a* axis (left) and depiction of the π-stacking between molecules (right); **C.** section of the ^{1}H NMR spectrum of DPAq in $CDCl_3$ with proton assignment (for the full spectrum see Figure S2); **D.** simulated (from SCXRD data, black line) and experimental (orange line) powder diffractograms of DPAq. Aromatic hydrogen atoms were omitted for clarity reasons. All ellipsoids are shown at the 50% probability level. Atom colors are grey (C), blue (N), red (O).

The oxidized linker was obtained as a crystalline beige powder and its purity was checked through ^{1}H NMR spectroscopy and powder XRD (Figures 17C and 17D). The proton assignment was carried out based on chemical shifts and multiplicity of the signals. The 2,6-anthraquinone core has a characteristic splitting consisting of two doublets and a doublet of doublets. The ortho protons couple with a constant $^{ortho}J$ = 8 Hz, while ^{meta}J = 1.6 Hz for the meta protons. Therefore, the H_α, H_β, and H_γ were, respectively assigned to the signals at 8.49, 8.11, and 8.63 ppm. The pyridyl protons were attributed considering the stronger deshielding

effect of the N-atom on the α and γ positions. Thus, the signals at 7.67 and 8.79 ppm are assigned to H_δ and H_ε, respectively. ^{13}C NMR spectroscopy was not viable due to the low solubility of the ligand. The powder diffractogram is in good agreement with the simulated and supports phase purity.

The reduction of the quinone moiety was achieved under solvothermal conditions in presence of a strong Lewis acid. Less acidic metal cations, such as Cd^{2+}, were used instead, no reduction of the quinone was observed over days, which points towards a Lewis-acid catalyzed reaction. DMF can act as a reducing agent under solvothermal conditions[87] and several mechanisms have been proposed for its oxidation.[88] Accordingly, the formation of the related carbamic acid and subsequent thermal decomposition (Scheme 6, bottom) can be expected to take place. The crystal structure of DPAHq, which is the first example of a crystal structure reported for an anthrahydroquinone with unsubstituted hydroxylic groups, was also achieved.[89] Red crystals suitable for single crystal X-ray diffraction measurements were obtained from the mother-liquor and the crystal structure of DPAHq was solved and refined in the monoclinic space group *P 2₁/c*. The C–O bond length is 1.36 Å which is in good agreement with those observed for hydrogen-bonded phenolic groups (Figure 18A).[90] The C–C bonds next to the phenolic groups are significantly shorter, 1.41 Å, also sustaining reduction of the central ring. Additionally, the phenolic hydrogen atoms could be located in the difference Fourier maps, unequivocally proving the reduced character (Figure S3). The crystal structure reveals an extended hydrogen-bonded organic framework, in which every DPAHq molecule exhibits contact with four neighboring molecules. (Figure 18B). The donor-acceptor distance is 2.73 Å and the O–H –N angle is 167°, characterizing moderate, mostly electrostatic hydrogen bonds.[91] As a result, the reduced ligand is stabilized by intermolecular hydrogen bonding between the phenol and the pyridine groups of the ligand in the solid state. Infrared spectroscopy suggests proton transfer and the formation of a pyridinium phenoxide salt.[92] Going along with this multifold hydrogen bonding, solid DPAHq is not prone to oxidation and can be stored under aerobic conditions, whereas it is readily oxidized to DPAq when dissolved in polar organic solvents upon addition of strong acids. The identification and phase purity were also checked using ^1H NMR spectroscopy and powder XRD (Figures 18C and 18D).

To get further insights into the electronic properties of the linkers, further spectroscopic characterization was carried out. In the IR spectrum of DPAq (Figure S5), the quinone stretch can be observed at 1672 cm^{-1}, closely related to 9,10-anthraquinone (C=O stretch at 1671 cm^{-1}).[93] This absorption band is absent in the spectrum of DPAHq (Figure S6), supporting successful reduction. Additionally, a strong broad band centered at 3000 cm^{-1} in the spectrum of DPAHq is in good agreement with the presence of hydrogen-bonded hydroxy groups. Further broad strong bands at 1207 and 1060 cm^{-1} can be seen in the spectrum of the

hydroquinone, which are tentatively attributed to the in-plane O–H bending and the C–O stretching of the phenols. The out-of-plane O–H bending rises as a strong absorption at 808 cm^{-1}.

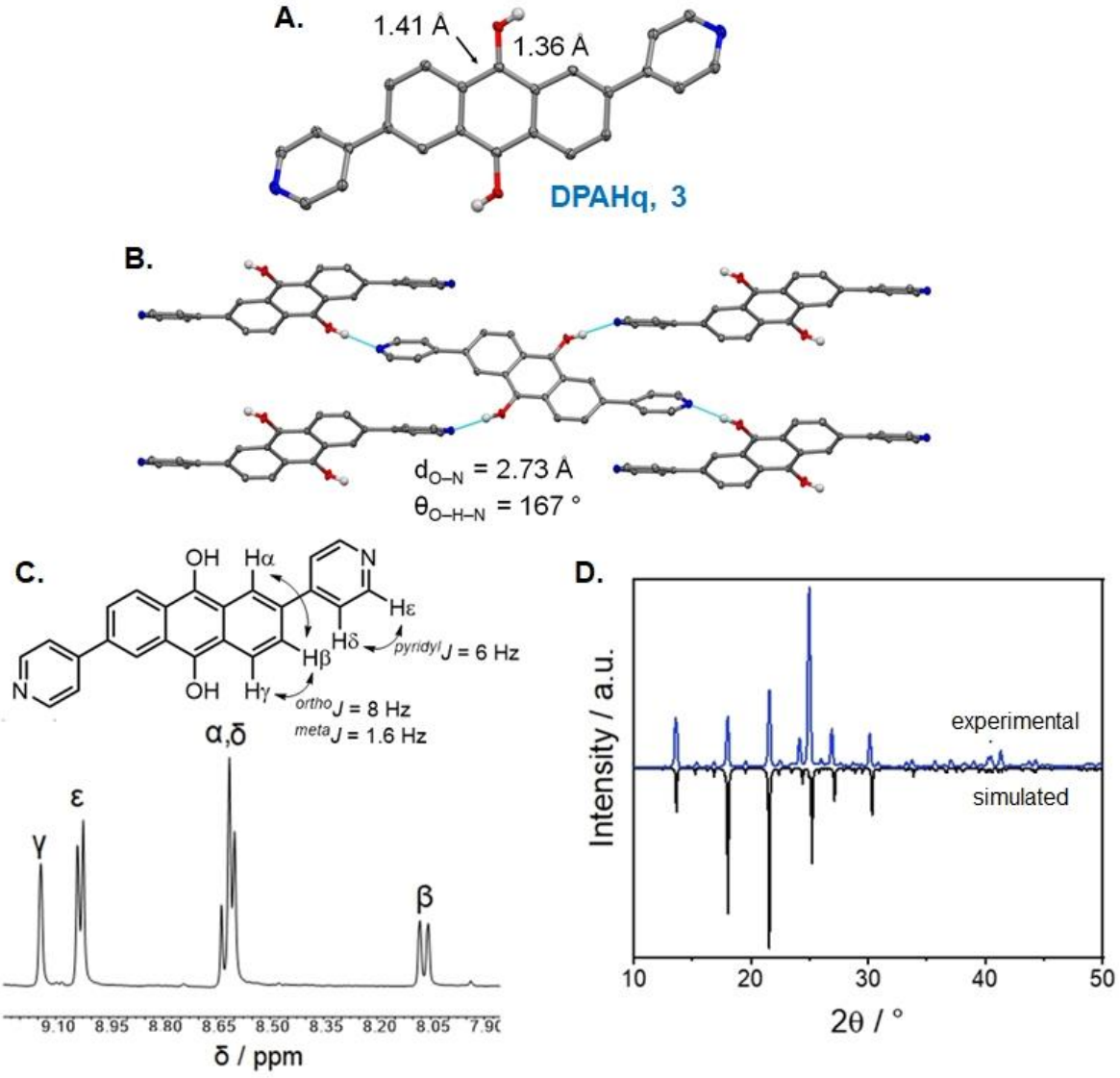

Figure 18. A. Molecular structure of DPAHq, highlighting selected bond distances; **B.** solid-state structure of DPAHq depicting the hydrogen-bonded framework connectivity; **C.** section of the ^{1}H NMR spectrum of DPAHq in degassed TFA/DMSO-d_6 with proton assignment (for the full spectrum see Figure S4); **D.** simulated (from SCXRD data, black line) and experimental (blue line) powder diffractograms of DPAHq. Aromatic hydrogen atoms were omitted for clarity reasons. All ellipsoids are shown at the 50% probability level. Atom colors are grey (C), white (H), blue (N), red (O).

A solution-state electronic spectrum of the quinone form was recorded in CH_2Cl_2. The spectrum of the hydroquinone was recorded in degassed 1% TFA in DMF solution (Figure S7). DPAq shows a strong band at 277 nm with a shoulder at 293 nm and a less intense absorption at 341 nm, which are attributed to π→π* and n→π* transitions.[94] After reduction, a bathochromic shift is observed for the signals corresponding to these transitions, which are

then found at 340 and 425 nm, due to extended cross-conjugation in the hydroquinone form. A broad absorption centered at 545 nm gives the wine-red color and is tentatively assigned to intraligand transitions. The solid-state absorption spectra are closely related to those recorded in solution (Figure S8). Cyclic voltammetry of DPAq was performed in DMF using $[NBu_4][PF_6]$ as supporting electrolyte (Figure S9). The DPAq linker underwent, as expected, two redox events, which were interpreted as the two one-electron reductions of the quinone to the hydroquinone dianion via the semiquinone radical anion.[95] The first reduction wave was found at $E^1_{1/2}(DPAq/DPAq^{\bullet-}) = -0.70$ V (vs. Ag/AgCl), being more positive than the value observed for 9,10-anthraquinone (Aq) in DMF, $E^1_{1/2}(Aq/Aq^{\bullet-}) = -0.81$ V. Similarly, the second reduction wave of DPAq is also found at a less negative potential, $E^2_{1/2}(DPAq^{\bullet-}/DPAq^{2-}) = -1.23$ V whereas $E^2_{1/2}(Aq^{\bullet-}/Aq^{2-}) = -1.35$ V. The higher tendency for reduction might be explained by the extended π-system, which allows better electron delocalization and therefore, better stabilization of both formed anionic species compared to the unsubstituted anthraquinone. Together, these results evidence a similar electronic situation between 9,10-anthraquinone and DPAq and an accessible reduced state, sustaining DPAq as an appropriate candidate for the construction of redox-active metal-organic frameworks.

2.1.2. Controlling the incorporation of distinct oxidation states into metal-organic frameworks

Having full control over the oxidation state of the dipyridine linker molecules, the synthesis of corresponding MOFs with defined oxidation states of the linker was attempted. For this, the redox-inactive metal ions Zn^{2+} and Cd^{2+} were chosen as metal nodes in combination with terephthalate (1,4-benzenedicarboxylate, BDC). In total, three new pillar-layered Zn(II) and Cd(II) MOFs, $[Zn_2(BDC)_2(DPAHq)_2]_n \cdot 4DMF$ (**4**), $[Zn_2(BDC)_2(DPAq)]_n \cdot DMA$ (**5**) and $[Cd_2(BDC)_2(DPAq)_2]_n \cdot DMA$ (**6**) were synthesized upon heating the DPAq ligand, 1,4-benzenedicarboxylic acid and the corresponding metal nitrate at 100 °C in different solvent (mixtures) as depicted in Scheme 7.

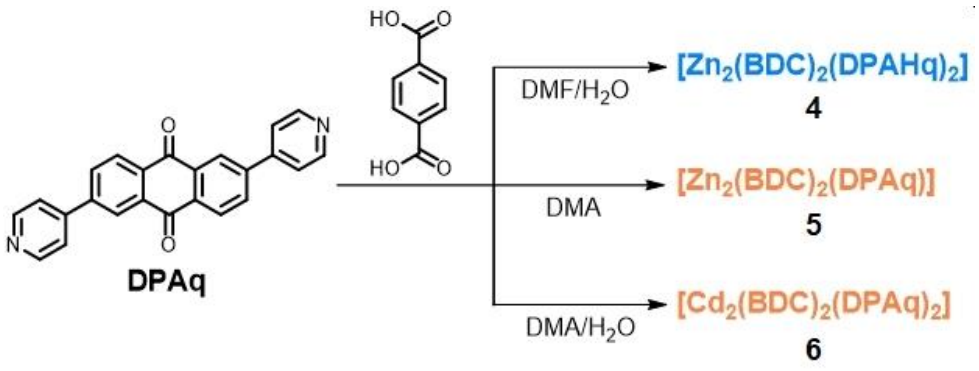

Scheme 7. The synthetic route towards the MOFs **4**–**6**.

The Zn(II) coordination polymer **4** possessing the reduced linker could not be prepared by direct application of DPAHq as the linker. However, it was accessible via the *in situ* reduction of the DPAq linker during the hydrothermal synthesis using DMF as the solvent, which synchronously acted as the reducing agent like in the case of the DPAHq synthesis. The composition was unequivocally determined through ^{1}H NMR spectroscopy digestion studies and infrared spectroscopy (Figures S10 and S11), including the structure elucidation via single-crystal X-ray diffraction. The crystal structure of **4** was solved and refined in the orthorhombic space group *P c a* 2_1. The 1,4-benzenedicarboxylate groups exhibit monodentate, bidentate, and bridging (μ^2-η^1:η^1) coordination modes and together with the metal centers build up two-dimensional networks. Those sheets are connected by DPAHq molecules overall resulting in a two-fold interpenetrated **pcu** framework (Figure 19A). In this network, two π-stacking DPAHq ligands are found in proximity with a ligand-to-ligand distance of around 3.7 Å. The average C–O bond length observed in the DPAHq moiety is 1.36 Å which corresponds to the linker in its hydroquinone form. Furthermore, like for the crystal structure of DPAHq, hydrogen bonding can be identified as a stabilization factor of the solid-state structure of the hydroquinone form. Three hydroxy groups are found close to DMF molecules and are involved in hydrogen bonding (Figure 19B). The average donor-acceptor distance is 2.67 Å and the O– H–O average angle is 155°, hence the interactions are classified as mostly electrostatic.[91] One disordered DMF molecule is located between two BDC linkers and not involved in any hydrogen bonding. **4** can be isolated under aerobic conditions while preserving the hydroquinone linker, which only gets oxidized upon longer exposure to air. Phase purity was confirmed via PXRD analysis (Figure 19C).

In the IR spectrum of **4**, a broad absorption centered at 3000 cm^{-1} is also observed and is caused by stretching of the O–H bond. Strong absorption at 1655 cm^{-1} is observed and is assigned to the C=O stretching of the encapsulated DMF molecules. A band at 1673 cm^{-1} is also observed and is thought to arise from DPAq molecules incorporated into the structure before reduction. The strong, broad band at 1588 cm^{-1} is probably caused by the overlap of ring deformation modes of the DPAHq ligand with the asymmetric stretching mode of the BDC carboxylate groups. The symmetric vibrational mode can be seen at 1386 cm^{-1}. The group of bands between 1200 – 1000 cm^{-1} is tentatively assigned to modes involving the in-plane bending of hydrogen-bonded hydroxy groups and bending of C–H bonds. The out-of-plane deformation of the O–H bond can be found at 801 cm^{-1}, being slightly shifted compared to the linker (808 cm^{-1}). The shift is probably related to the different kinds of acceptors in **4** (C=O from DMF) and DPAHq (N from pyridine).

The digestion study of **4** is in good agreement with the determined structure as well as thermogravimetric analysis (Figure S12). The “molar mass” of a $[Zn_2(BDC)_2(DPAHq)_2]\cdot 4DMF$

unit is 1480.2 g mol^{-1}. Thus, the expected solvent and ligand contents, in wt.%, are 19.8 and 71.3 %, respectively. Due to the aerobic conditions, ZnO is expected as the residual product (11 %). The recorded TGA curve shows four distinguishable events. The first two mass losses are attributed to the loss of the encapsulated solvent. The reason for the two different plateaus might be related to the different types of DMF molecules in the solid state. The solvent molecules stabilizing the hydroquinone probably leave first, concerted with the oxidation of the ligand. Then the residual pore solvent leaves. Decomposition and combustion of the framework are observed between 400 – 600 °C and correspond to 69 % of the initial mass. The final ZnO content is also in good accordance with the expected value.

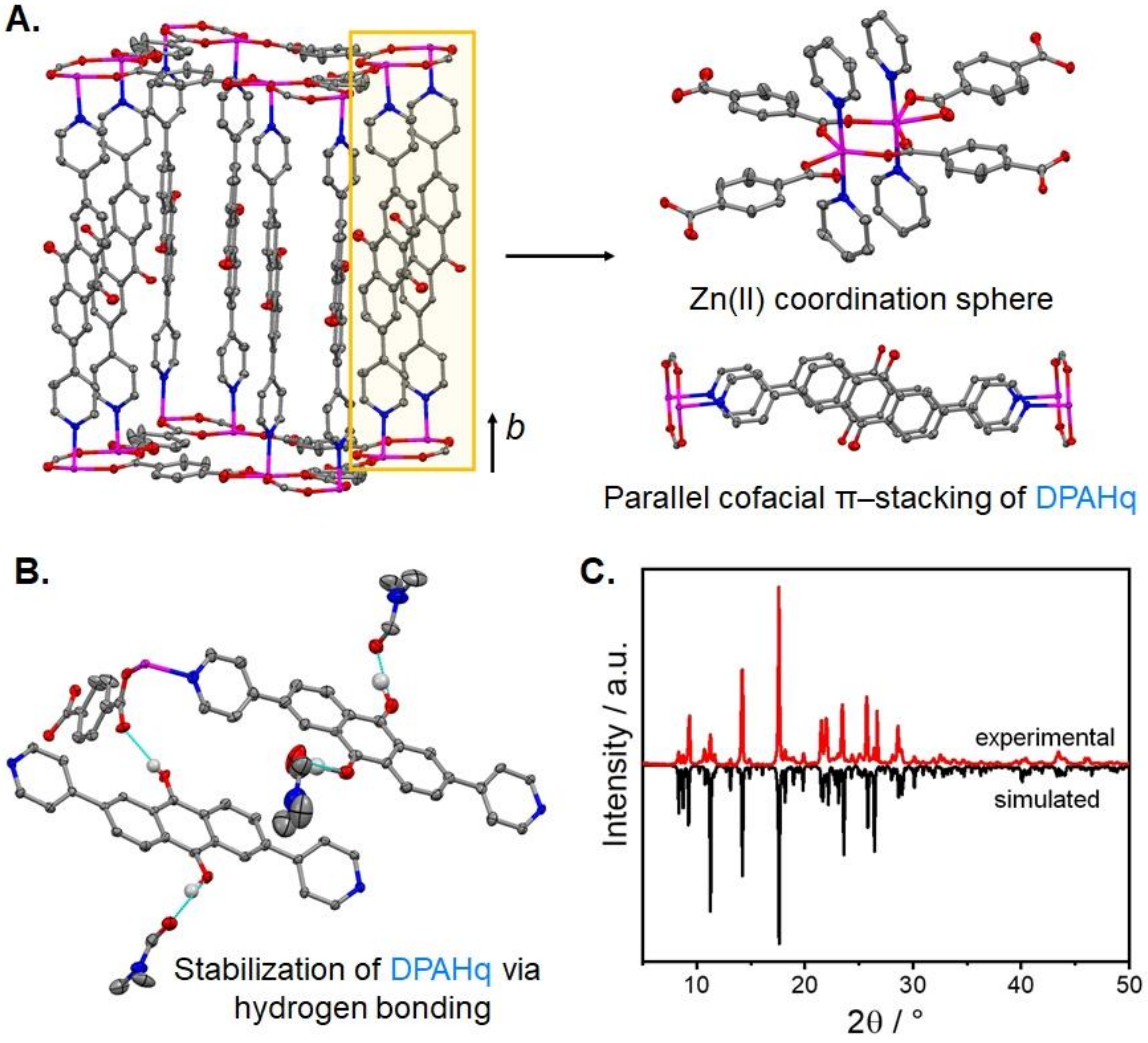

Figure 19. Representation of the crystal structure of **4** displaying **A.** the overall **pcu** framework and the highlight of the coordination of Zn(II) centers and the cofacial dimer arrangement of DPAHq molecules and; **B.** the stabilization of the hydroquinones moieties via hydrogen bonding to DMF molecules and a free carboxylate oxygen; **C.** simulated (from SCXRD data, black line) and experimental (red line) powder diffractograms of **4**. Aromatic hydrogen atoms and additional solvent molecules were omitted for clarity reasons. All ellipsoids are shown at the 50% probability level. Atom colors are grey (C), white (H), blue (N), red (O), pink (Zn).

When using DMA instead of DMF as the solvent, the oxidation state of the linker can be retained and the metal-organic framework **5** with DPAq linkers can be achieved. Single-crystals suitable for X-ray diffraction were grown, allowing a detailed structural analysis. The crystal structure of **5** was solved and refined in the triclinic space group *P* -1. The asymmetric unit comprises two Zn(II) centers, two BDC, and one DPAq linker molecule. In contrast to **5**, the zinc ions are coordinated by four BDC linkers in the "paddle-wheel" fashion. These SBUs are connected by DPAq ligands in the apical positions to build a two-fold interpenetrated **pcu** framework (Figure 20A). Additionally, no π-stacking between DPAq ligands is observed. The C–O bond length is found in the range expected for the oxidized linker, clearly showing that the oxidation state of the linker remained unchanged. Phase purity was confirmed via PXRD analysis (Figure 20C). In the IR spectrum of **5** (Figure S13), which contains the linker in its quinone form, the characteristic C=O stretching can be observed as a strong absorption at 1675 cm^{-1}. The small shift is consistent with the presented structures since the anthraquinone moiety does not take part in coordination. The carboxylate asymmetric and symmetric stretches of the BDC linkers are also observed in the expected regions. Digestion studies of **5** (Figure S14) fairly agree with the proposed structure. A thermogravimetric curve of **5** (Figure S15) was recorded to determine the amount of encapsulated solvent in the framework. The recorded TGA curve shows three distinguishable mass losses. The first event is attributed to the loss of the encapsulated DMA molecules. Decomposition and combustion of the framework are observed between 400 – 600 °C and correspond to 66 % of the initial mass. Due to the aerobic conditions, ZnO is expected as the residual product (24 %). This data suggests the following composition $[Zn_2(BDC)_2(DPAq)]_n \cdot DMA$.

A Cd(II) based coordination polymer, **6**, containing the oxidized ligand was also synthesized in a redox-inactive DMA/water mixture. The structure of **6** was solved and refined in the orthorhombic space group *I b c a*. In the crystal structure, a C–O bond length of 1.24 Å is observed, supporting that the linker retained its quinone form. However, the metal node coordination, in this case, is closer to the one observed in **4** and the BDC carboxylate groups form 2D sheets upon metal coordination. Similarly, these sheet-like networks are connected by DPAq molecules acting as pillars and resulting in a two-fold interpenetrated **pcu** topology. Likewise, two π-stacking DPAq ligands are found in proximity with a ligand-to-ligand distance of 3.65 Å, however, in a crossed cofacial arrangement (Figure 20B). Phase purity was confirmed via PXRD analysis (Figure 20D). IR spectroscopy of **6** (Figure S16) shows the C=O stretching mode at 1673 cm^{-1}, supporting the ligand in its quinone form. The carboxylate asymmetric and symmetric stretches of the BDC linkers are also observed in the expected regions. Digestion studies of **6** (Figure S17) fairly agree with the proposed structure. Thermogravimetric analysis of **6** (Figure S18) was carried out to determine the amount of encapsulated solvent in the framework. The recorded TGA curve shows three distinguishable

mass losses. The first event is attributed to the loss of the encapsulated DMA molecules. Decomposition and combustion of the framework are observed between 400 – 600 °C and correspond to 72 % of the initial mass. Due to the aerobic conditions, CdO is expected as the residual product (18.5 %). This data suggests the following composition $[Cd_2(BDC)_2(DPAq)_2]_n \cdot DMA$.

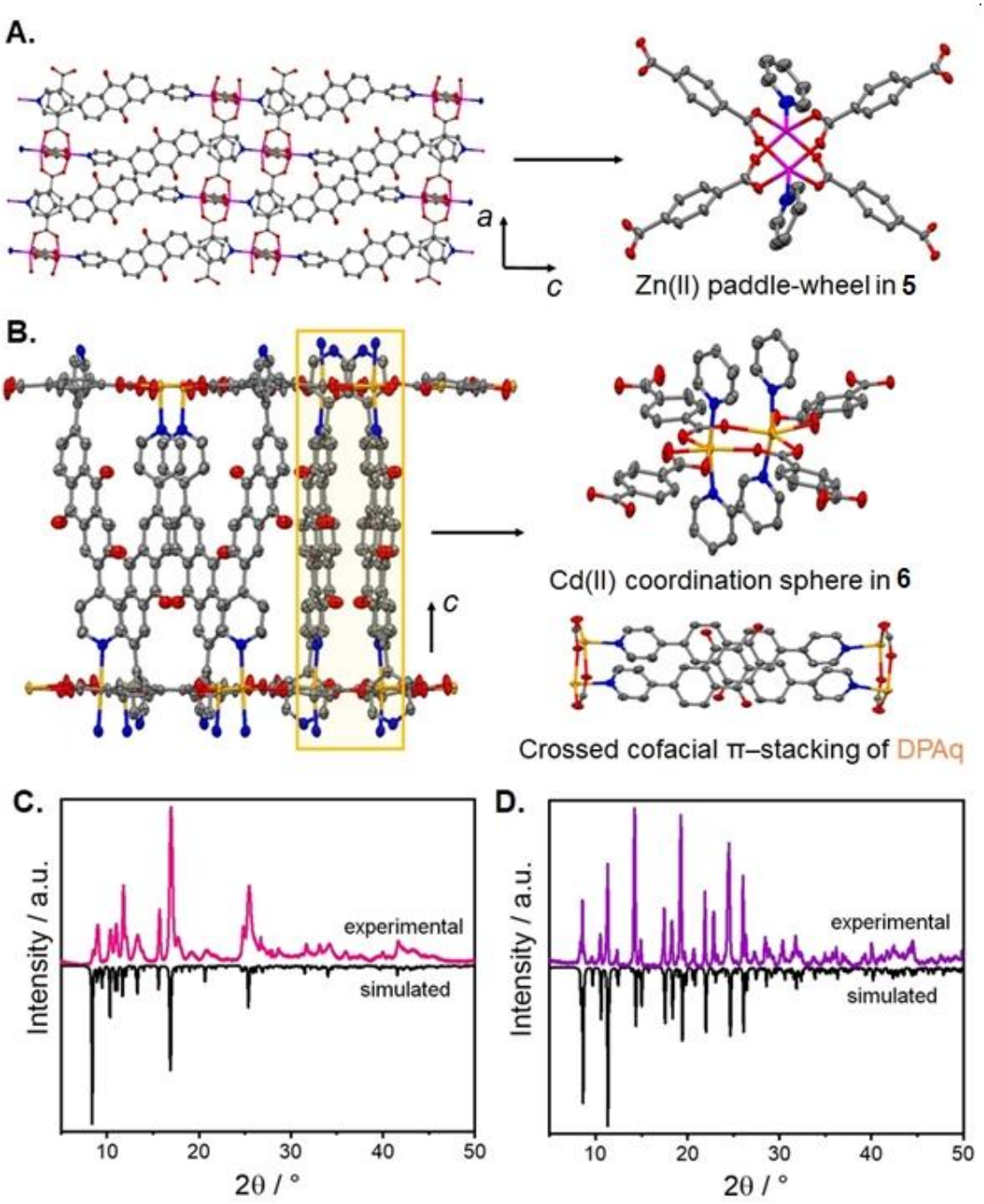

Figure 20. Representation of the crystal structure of **A. 5** and highlight of the coordination of Zn(II) centers; **B. 6** and highlight of the coordination of Cd(II) centers and the crossed dimer arrangement of DPAq molecules; **C.** simulated (from SCXRD data, black line) and experimental (pink line) powder diffractograms of **5**; **D.** simulated (from SCXRD data, black line) and experimental (purple line) powder diffractograms of **6**. Aromatic hydrogen atoms

and additional solvent molecules were omitted for clarity reasons. All ellipsoids are shown at the 50% probability level. Atom colors are grey (C), blue (N), red (O), pink (Zn), yellow (Cd).

The results demonstrate that the choice of the metal node can be used as a structural parameter independently from the linker oxidation state. Despite having the same **pcu** topology, distinct structural differences between the MOFs can be observed which are possible reasons for the hydroquinone stabilization in **4**. As previously mentioned, the ligand arrangement is unique to each MOF and, in **4** enables the hydrogen bonding. In contrast, in **5** and **6**, all BDC-carboxylate oxygens are involved in the metal coordination and thus are not available for hydrogen bonding. Moreover, the amount of pore solvent derived from SCXRD and thermogravimetric analysis in **5** and **6** is lower than in the case of **4** (referring to the as-synthesized materials), indicating that the accessible pore volume of **5** might be larger than for the two other MOFs. This might be advantageous, e. g. due to higher amounts of incorporated DMF molecules, which can serve as reduction agents and potential hydrogen bond acceptors.

2.1.3. Anthraquinone-based redox-switches: following new perspectives on heterogeneous systems for dioxygen activation and hydrogen peroxide synthesis

Based on the isolated compounds and the reactivity of anthrahydroquinones toward molecular oxygen, the synthesis of hydrogen peroxide via autoxidation was targeted. To determine qualitatively the formation of H_2O_2, low concentration peroxide stripes were used. DPAHq, **3**, cannot be oxidized via solid-gas phase reaction up to 120 °C. Thus, the organic polymer was dissolved under air exclusion in degassed TFA/DMSO to yield a dark purple solution. The addition of degassed pH = 5.0 acetate buffer followed by immersion of a peroxide stripe did not lead to any color change (negative for peroxide). In a second experiment, after the dissolution of DPAHq, air was bubbled into the solution leading to an immediate color change from purple to brown. The addition of degassed acetate buffer followed by immersion of a peroxide stripe led to a color change of the stripe to blue, supporting peroxide formation (Figure S19, left). For **4**, a solid-gas phase reaction was attempted. A small sample of **4** was oxidized at 100 °C in a sealed glass vial, extracted with water, and the solution separated by filtration. Immersion of a stripe led immediately to a color change to greenish-blue (Figure S19, right), suggesting the presence of H_2O_2. To quantify the amount of hydrogen peroxide, a modified FOX colorimetric assay was used (Figure 21).[96] The production of H_2O_2 was achieved with a 37 % yield. No oxidation side products were observed on ^{1}H NMR digestion studies and phase crystallinity was retained (Figure S20). The distinct reactivities observed for DPAHq and **4** highlight the role of hydrogen bonding and structural features in the reactivity of crystalline materials.

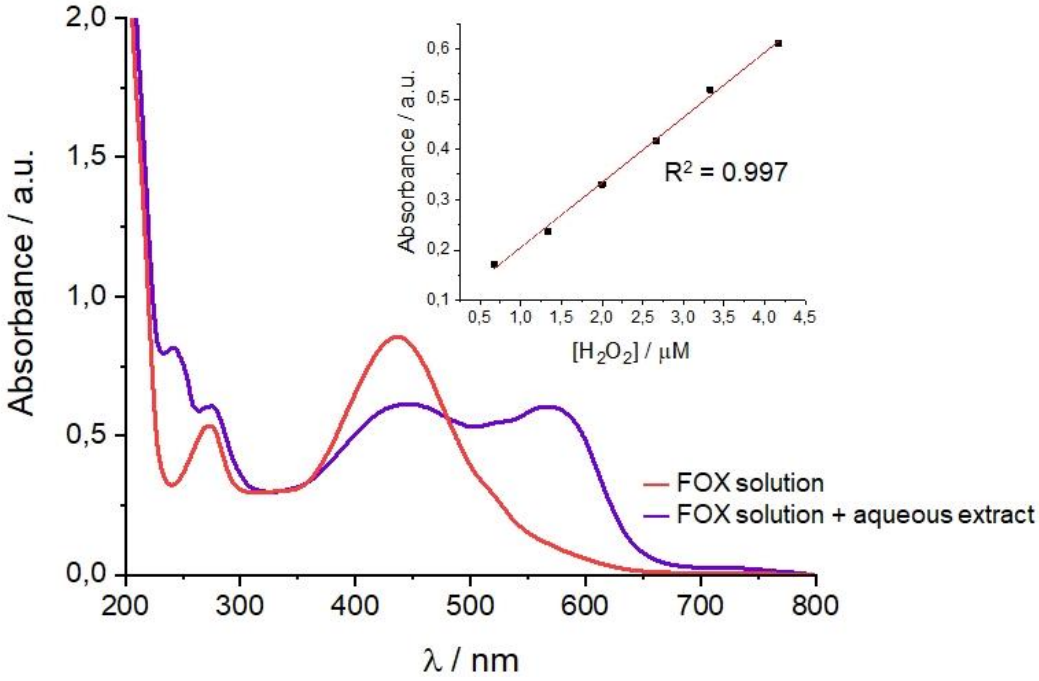

Figure 21. UV-Vis spectra of the FOX-reagent solution before (red line) and after (purple line) addition of the aqueous extract from the oxidation of **4**. The additional absorption at 270 nm is due to the parallel extraction of DMF from the pores. On the top right, the calibration curve used for the quantification of H_2O_2. Absorbance values were read at λ = 560 nm.

Based on the intrinsic redox character of the ligand, the possibility of post-synthetic cycling between redox states in **4** was attempted. The full oxidation of the material was achieved by heating the crystals at 100 °C under aerobic conditions for 3 hours. Very interestingly, the crystals turned again dark red when soaked in a DMF/H_2O mixture in presence of $AlCl_3$ for 24 h, suggesting the presence of the reduced anthrahydroquinone. This was supported by IR spectroscopy (Figure S21), which revealed the reappearance of the absorption bands related to the hydroxy groups and thus indicated possible reversibility. The re-reduction was also supported via solid-state UV-Vis (Figure S22). PXRD analysis shows retention of crystallinity with some structural recombination. (Figure S23). For a quantitative study of the reversibility, an alternating sequence of thermal-oxidative treatment and reductive soaking was carried out and monitored. For this, a material sample was taken after every half-cycle (oxidation or reduction), digested, and analyzed by solution ^{1}H NMR spectroscopy (Figures 22A and 22B). The cycling experiments show that full oxidation of the material is repeatedly possible after thermal treatment under aerobic conditions, supporting the greater stability of the quinone form. In contrast, the reduction via soaking in DMF/H_2O was not quantitative within a reasonable amount of time, probably caused by diffusion limitations of the processes in the solid state. Nevertheless, the framework material could be reproducibly reduced to an oxidation grade of about 20 %, which demonstrates the reversible conversion of the anthraquinone/anthrahydroquinone redox pair.

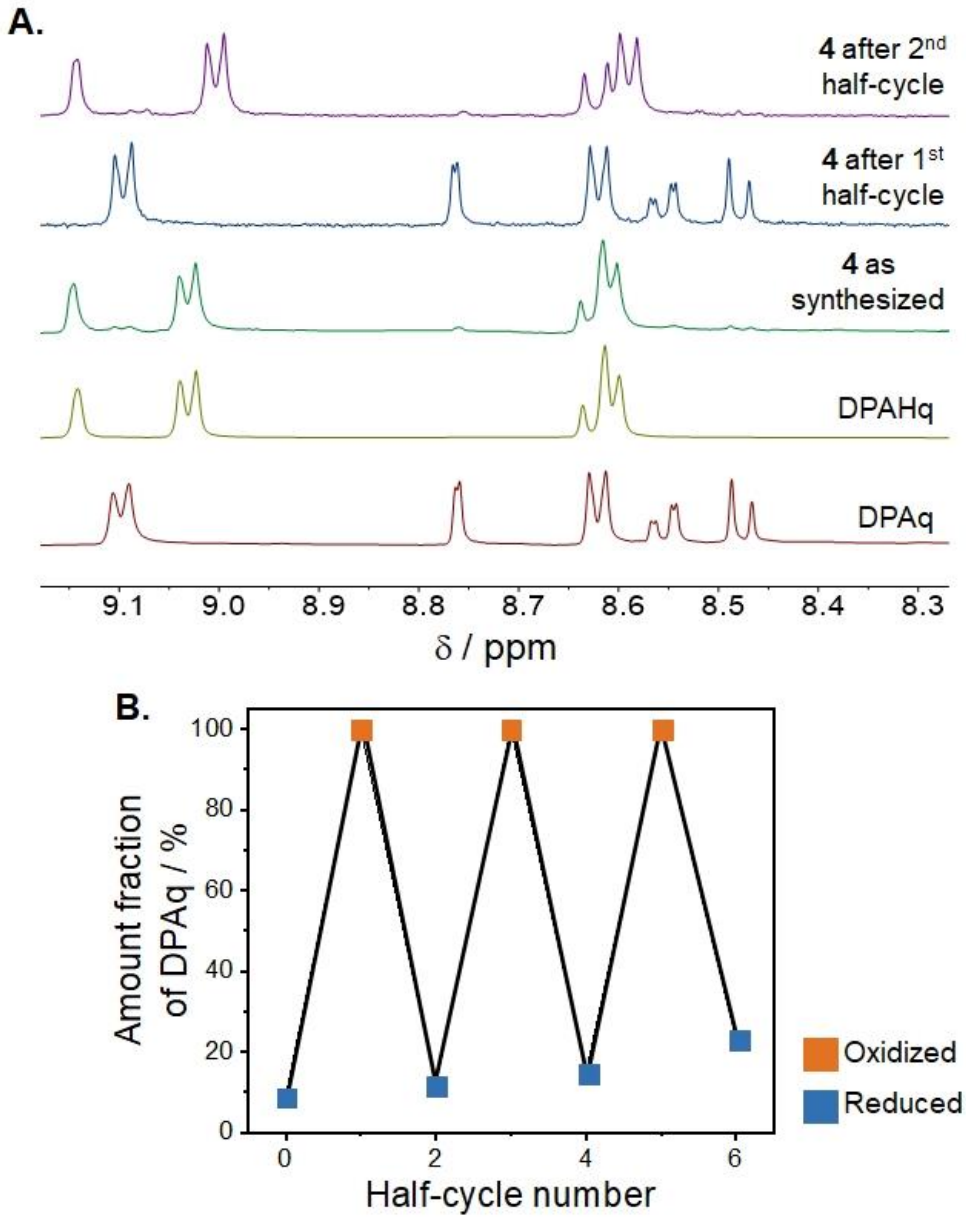

Figure 22. A. ^{1}H NMR spectra illustrating the composition of **4** after synthesis (green spectrum) and after thermal and soaking treatments (blue and purple spectra, respectively); **B.** Ratio of oxidized to the reduced linker (DPAq/DPAHq) over 3 redox cycles monitored by solution ^{1}H NMR (dissolved material samples). Half cycles: aerobic thermal treatment (blue to orange) and reductive soaking (orange to blue). All spectra are shown in Figure S24.

2.1.4. Prospective ideas on mixed-valence and quinhydrone systems

Although both fully oxidized and reduced states of anthraquinone have been isolated in this thesis, no radical intermediate or mixed-valence compositions were investigated. During my thesis, I stumbled on a crystal structure, which exemplifies the possibility of generating a mixture of oxidation states in the same framework. After heating $Cd(NO_3)_2$ and DPAq at 100 °C for one month in a DMF/H_2O mixture, distinct unknown phases could be observed under the microscope, including very few small pink plates. A plate was manually isolated and mounted for SCXRD analysis, yielding, possibly, $[Cd_2(BDC)_2(DPAq)(DPAHq)]_n \cdot DMF$. The structure was analogous to **4**, including the spatial arrangement of the ligands to each other. The model is not as reliable as for the previously presented structures due to weak diffraction and the higher number of restraints applied for refinement; however, the C–O bond of one linker molecule is longer, suggesting the presence of both oxidation states. This is also supported by the hydrogen bonding acceptors close to one of the molecules (DPAHq), whereas the second does not seem to take part in any intermolecular interactions (DPAq). Unfortunately, phase isolation and further characterization were not possible. Nevertheless, it validates fruitful thoughts on post-synthetic modifications and possible through-space intervalence charge transfer (IVCT) studies in **4**–**6**, since 2,5-bis(4-(pyridin-4-yl)phenyl)thiazolo[5,4-d]thiazole-based pillar-layered MOFs with similar cofacial ligand arrangement have shown IVCT upon electrochemical reduction.[97] Additionally, spectroelectrochemical measurements should be conducted, as now being developed at the Chair of Inorganic and Metal-Organic Chemistry, to further understand the electrochemical behavior of DPAq/DPAHq in the distinct crystalline frameworks.

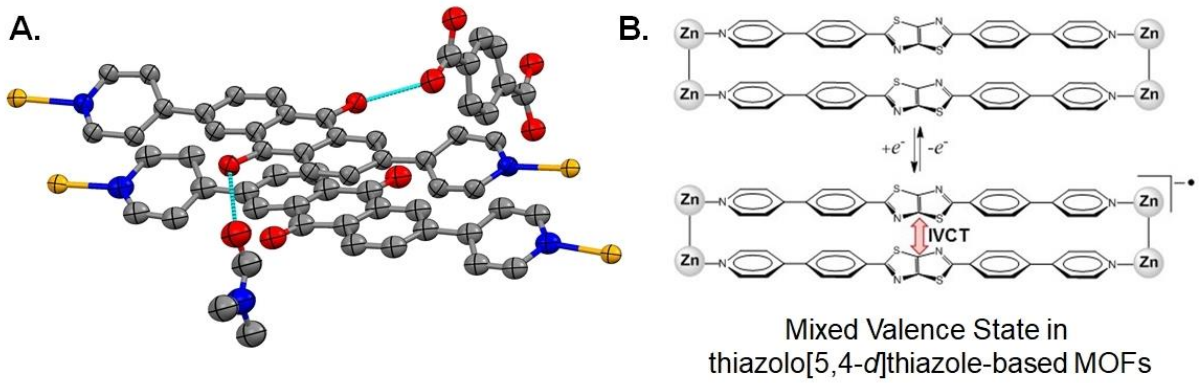

Figure 23. A. Molecular representation of a stacked DPAq/DPAHq pair in the mixed-valence compound $[Cd_2(BDC)_2(DPAq)(DPAHq)]_n \cdot DMF$. **B.** Depiction of the electrochemical reduction of 2,5-bis(4-(pyridin-4-yl)phenyl)thiazolo[5,4-d]thiazole units leading to IVCT in MOFs.[97] Figure 23B adapted and reproduced with permission of the American Chemical Society.

2.2. Solid-State Chemistry and Properties of Diphenylamine-Anthraquinone-Based Metal-Organic Frameworks

The manuscript “Alkaline Earth Metal-Organic Frameworks based on Tetratopic Anthraquinone-based Linkers: Synthesis, Characterization, and Photochemical Applications” was based on this chapter.

de Carvalho, J.G.M., Geißer, K., Weishäupl S., Fischer, R.A., Pöthig A., *Inorg. Chem.* (submitted)

2.2.1. Ligand design, synthesis, and characterization

Metal-organic frameworks (MOFs) could possess advantages compared to solution and exciplex OLEDs. These frameworks are usually mechanically and chemically stable and their structure can be designed and determined by crystallographic methods, allowing a direct structure-effect correlation. Furthermore, coordination of organic chromophores to inorganic metal-nodes and their insertion into a rigid crystalline structure could reduce non-radiative pathways and lead to an enhancement of the optical features compared to the free ligands Additionally, a higher concentration of linker is achieved with MOFs without concentration quenching due to aggregation.[11,98,99] A Zr-MOF containing a diphenylamine-terphenyl-based linker was the first example of green TADF in MOFs;[100] however, the reports are very limited. In this chapter, the solid-state coordination chemistry of a red-emitting diphenylamine-anthraquinone chromophore is explored together with alkaline earth metals as inorganic connecting units.

Most organic TADF chromophores comprise electron-deficient and rich units, which are typically spatially separated by large dihedral angles. Such features reduce HOMO-LUMO orbital overlap and consequently the energy gap between the lowest singlet and triplet states.[26] The H_4L, **9**, linker consists of a central anthraquinone acceptor, a class of molecules with a high-lying triplet state and strong electron-withdrawing properties, and two diphenylamine side wings, acting as donor units. The tetratopic linker molecule was synthesized via a four-step procedure (Scheme 8). First, 2,6-diaminonanthraquinone underwent a Sandmeyer reaction in acetonitrile with tert-butylnitrite and cupric bromide to 2,6-dibromoanthraquinone. Then, a Buchwald-Hartwig palladium-catalyzed coupling reaction was carried out for the synthesis of diethyl 4,4'-azanediyldibenzoate, **7**. The third step involved another Buchwald-Hartwig coupling reaction for the amination of the anthraquinone core. The obtained ester, **8**, was then hydrolyzed under basic conditions. Subsequently, protonation of the carboxylate groups led to the precipitation of **9** as a deep red solid.

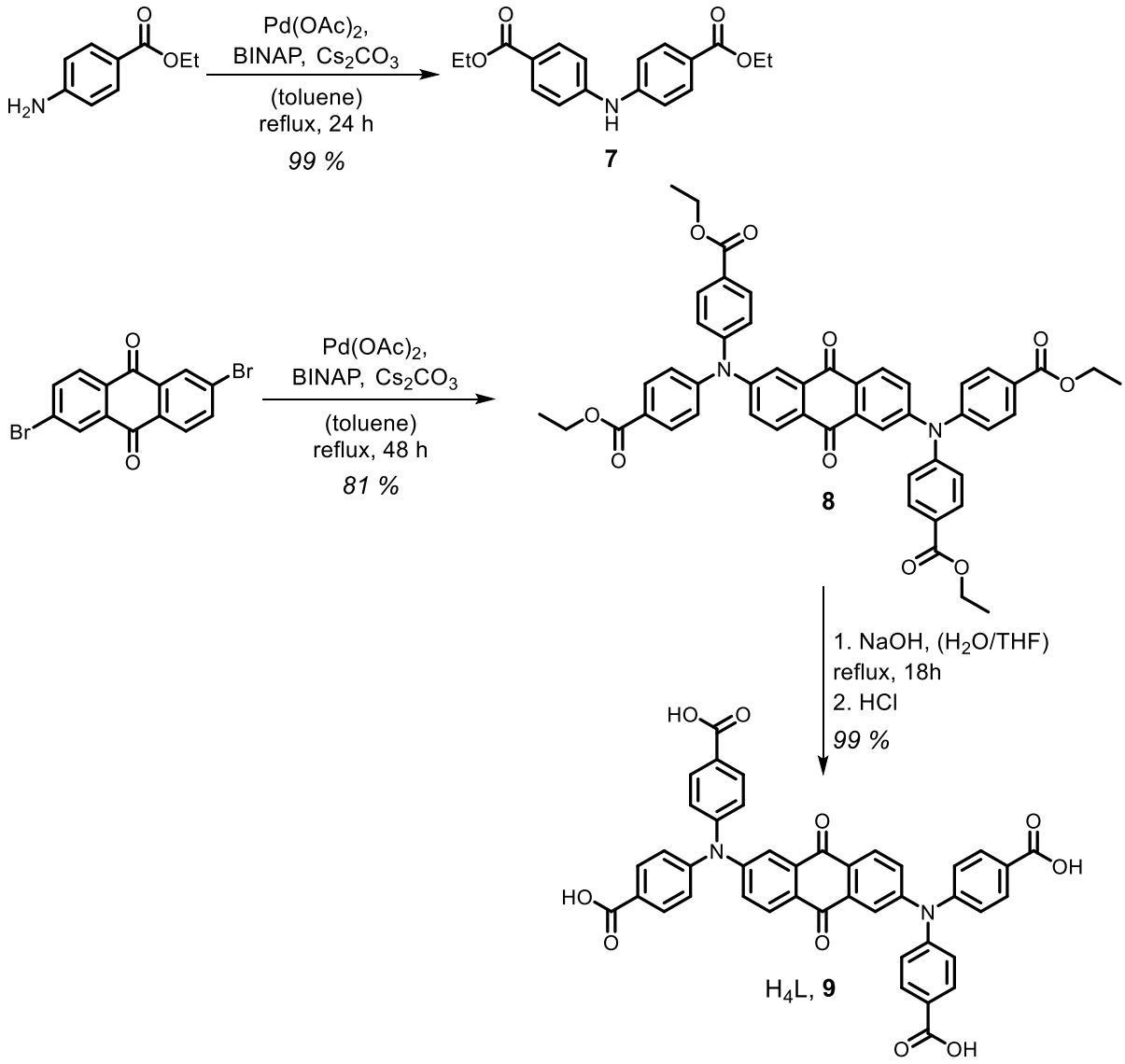

Scheme 8. Illustration of the synthetic approach carried out for the synthesis of the tetratopic ligand H_4L, **9**.

The synthesis of 4,4'-azanediyldibenzoate (**7**) was carried out according to a modified literature procedure (for the ^1H NMR spectrum, see Figure S25).[101] The method developed in this thesis does not require column chromatography and enhanced the yield to be nearly quantitative. Suitable crystals for SCXRD were obtained by slow evaporation of a solution of **7** in $CHCl_3$. The structure was solved and refined in the monoclinic space group $P\,2_1/c$ and the asymmetric unit comprises half a molecule. The N–C and the aromatic C–C bonds are 1.39 Å long and in the expected range (Figure 24A). The geometry around the nitrogen atom is closer to trigonal planar, probably due to the participation of the electron pair in the aromatic system. The substituents are, however, not coplanar and point to opposite directions of the nitrogen atom plane. The packing orientation is defined by hydrogen bonding interactions between the free N–H protons and one C=O acceptor of the ester groups (Figure 24B). The donor-acceptor is 2.9 Å and the N-H-O angle is 166 °, characterizing the interaction as mostly electrostatic.

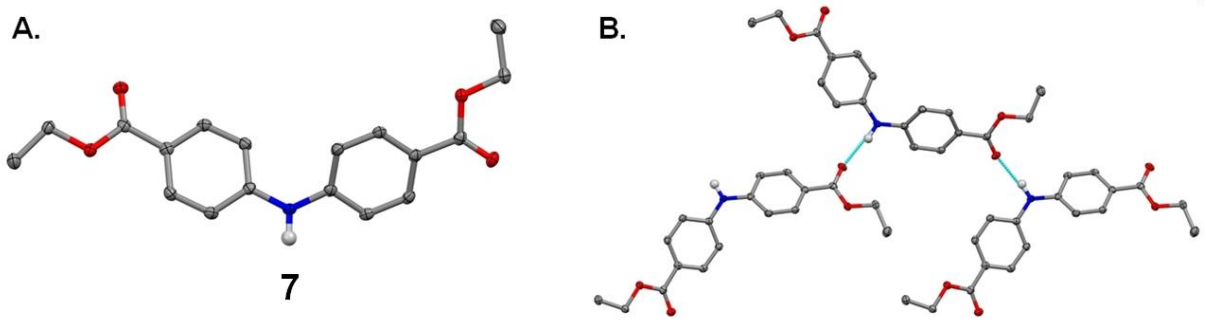

Figure 24. Depiction of the **A.** molecular structure of **7**; **B.** the solid-state hydrogen bonds between **7** molecules. Hydrogen atoms, except for the N–H proton, were omitted for clarity. All ellipsoids are shown at the 50% probability level. Atom colors are grey (C), red (O), blue (N), white (H).

Although several crystallization attempts were carried out with both **8** and **9**, nearly all of them were unsuccessful. The formation of needle-like crystals was observed from a concentrated DMSO solution of **9** when left in an open vessel over several days. Unfortunately, the crystals were too tiny and did not diffract enough within a preliminary SCXRD experiment to yield satisfactory data. Nevertheless, one measurement was performed to get an overview of the packing properties of the tetraacid. The structure was solved and refined in the triclinic space group *P*-1 (Figure 25A). The C=O bond length amounts to about 1.23 Å, as expected for a quinone. Further bond distances are not discussed due to model imprecision. The ligand stacks along the *a*-axis in an eclipsed fashion with a 3.4 Å distance between two molecules (Figure 25B). The carboxylic acid functionalities are stabilized via hydrogen bonding to DMSO molecules.

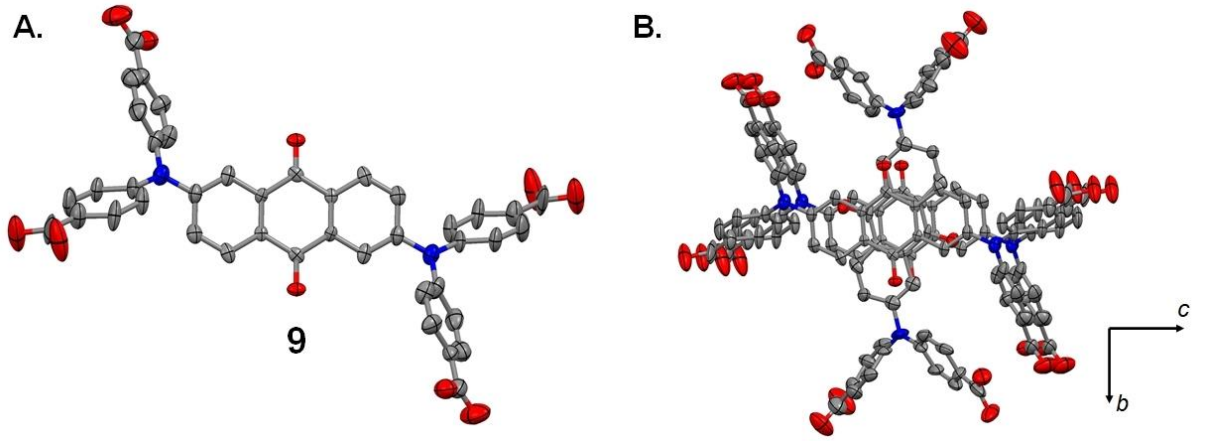

Figure 25. Depiction of the **A.** molecular structure of **9**; **B.** the solid-state eclipsed packing along the *a*-axis. Hydrogen atoms were omitted for clarity. All ellipsoids are shown at the 50% probability level. Atom colors are grey (C), red (O), blue (N).

All organic molecules were characterized via common spectroscopic methods (for details, see appendix, Figures S26–33). A section of the ^{1}H NMR spectrum of **9** is illustrated in Figure 26 and the assignment was made based on integration, chemical shifts, the

multiplicity of the signals, and coupling constants. The protons of the two phenyl rings are assigned to the signals at 7.97 and 7.26 ppm. The anthraquinone core shows the typical splitting for the 2,6-substitution pattern and was attributed to the signals at 8.07, 7.62, and 7.42 ppm. The carboxylic acid proton signal can be seen at 12.94 ppm. In the IR spectrum of **8**, the C=O quinone stretch can be observed at 1665 cm^{-1} and the ester at 1709 cm^{-1}. In the spectrum of **9**, the quinone stretch overlaps with the carboxylic acid stretching modes causing a broad absorption centered at 1690 cm^{-1}. Nevertheless, it is possible to see that the quinone vibration is not shifted (Figure 27A).

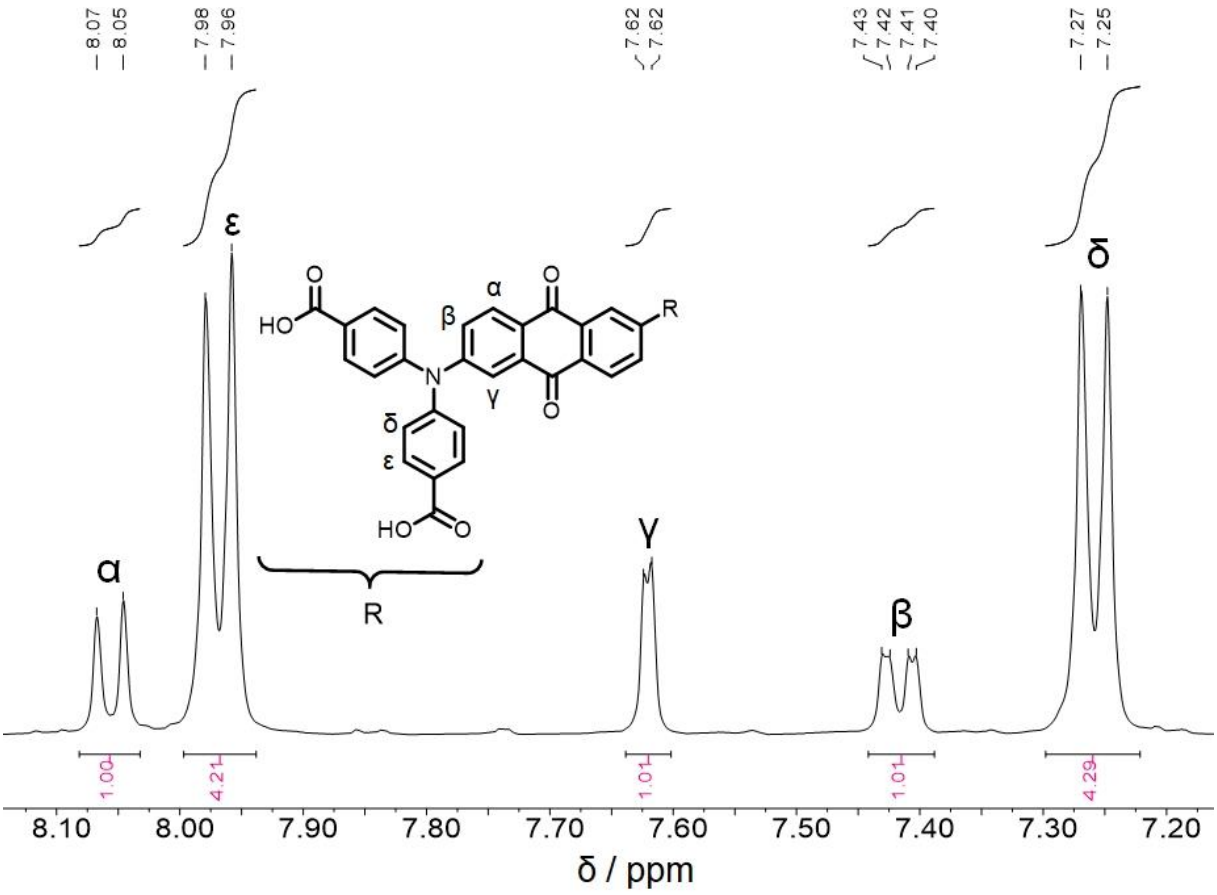

Figure 26. Section of the ^{1}H NMR spectrum of **9** in DMSO-d_6 highlighting the aromatic region.

The photophysical properties of the ligand were investigated in both solution and solid states. The acid (50 µM in DMF) was less emissive than the ester (50 µM in DCM) in solution (Φ = 4 and 14 %, respectively), which might have arisen from hydrogen bonding interactions between chromophores or to the solvent. These may have led to a larger number of non-radiative relaxation pathways. The absorption and emission spectra of dilute solutions (10 µM) of **8** in toluene (orange emission, λ = 580 nm) and of **9** in DMF (red emission, λ = 700 nm) are depicted in Figures 27B and 27C, respectively. The absorption spectra show very similar features and the least energetic absorption band centered at 440 nm can be assigned to a HOMO-1/LUMO (Figure S34) transition with charge transfer character as supported by DFT

calculations. The remaining bands are tentatively assigned to π-π* and n-π* transitions. There are no relevant changes in the absorption spectra of the ligand in different solvents. In contrast, the emission character of the chromophores is strongly dependent on the solvent polarity. **8** becomes less emissive and shows red-shifted emissions in polar solvents as shown in Figure 27D. When a dilute solution of **8** was saturated with argon, the quantum yield was significantly enhanced to 29 %, which might be a consequence of long-lived triplet states. Transient decay spectra were recorded for the determination of the fast decay component, which was determined to be 8.2 ns for **8** in toluene and 5.5 ns for **9** in DMF (Figure S35).

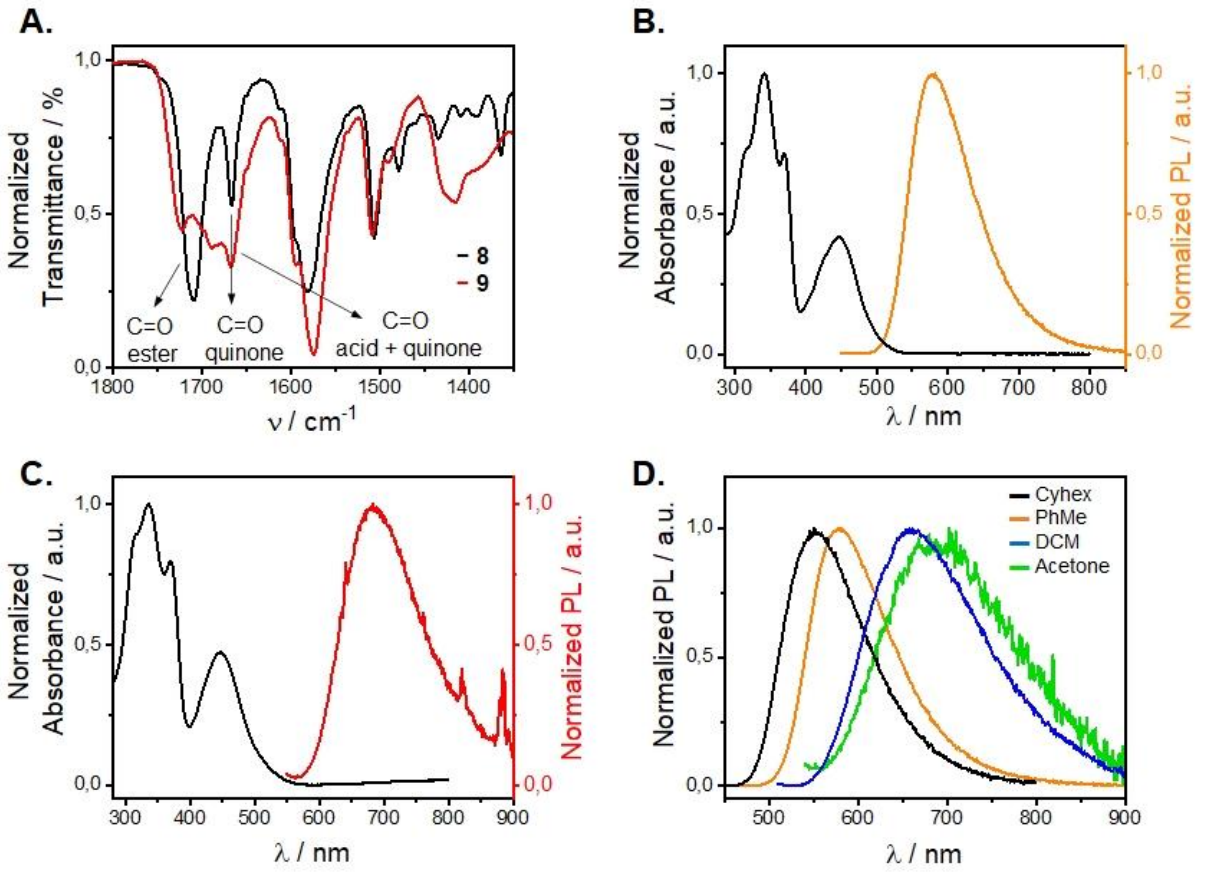

Figure 27. Depiction of the **A.** IR spectra of **8** (black line) and **9** (red line) highlighting the C=O absorptions bands; **B.** absorption (black line) and emission (orange line) spectra of **8** (10^{-5} M) in toluene; **C.** absorption (black line) and emission (red line) spectra of **9** (10^{-5} M) in DMF; **D.** solvent-dependent emission of **8** in cyclohexane (Cyhex, black line), toluene (PhMe, orange line), dichloromethane (DCM, blue line), and acetone (green line).

To get an insight into the emission properties in the solid-state, measurements using the neat materials and PMMA films of different concentrations were performed. The solid-state UV-Vis spectrum of **8** is consistent with the spectrum recorded in solution (Figure 28A). The emission spectrum of the neat powder is shifted to 700 nm (120 nm red shift) when compared to the emission in toluene. When diluted in PMMA, the emission is blue-shifted and, interestingly, the 1% PMMA film shows emission at 580 nm, like in solution (Figure 28B). The same behavior is noticeable when measuring the lifetime decays. The neat powder has the

shortest lifetime (τ = 5.5 ns), whereas the 1% PMMA film has a decay comparable to the dilute solution (τ = 8.0 ns) (Figure 28C). Additionally, the quantum yield of the different films was measured, and it could be observed that aggregation strongly diminished/quenched emissive processes (Figure 28D). Equivalent behavior was observed for **9**.

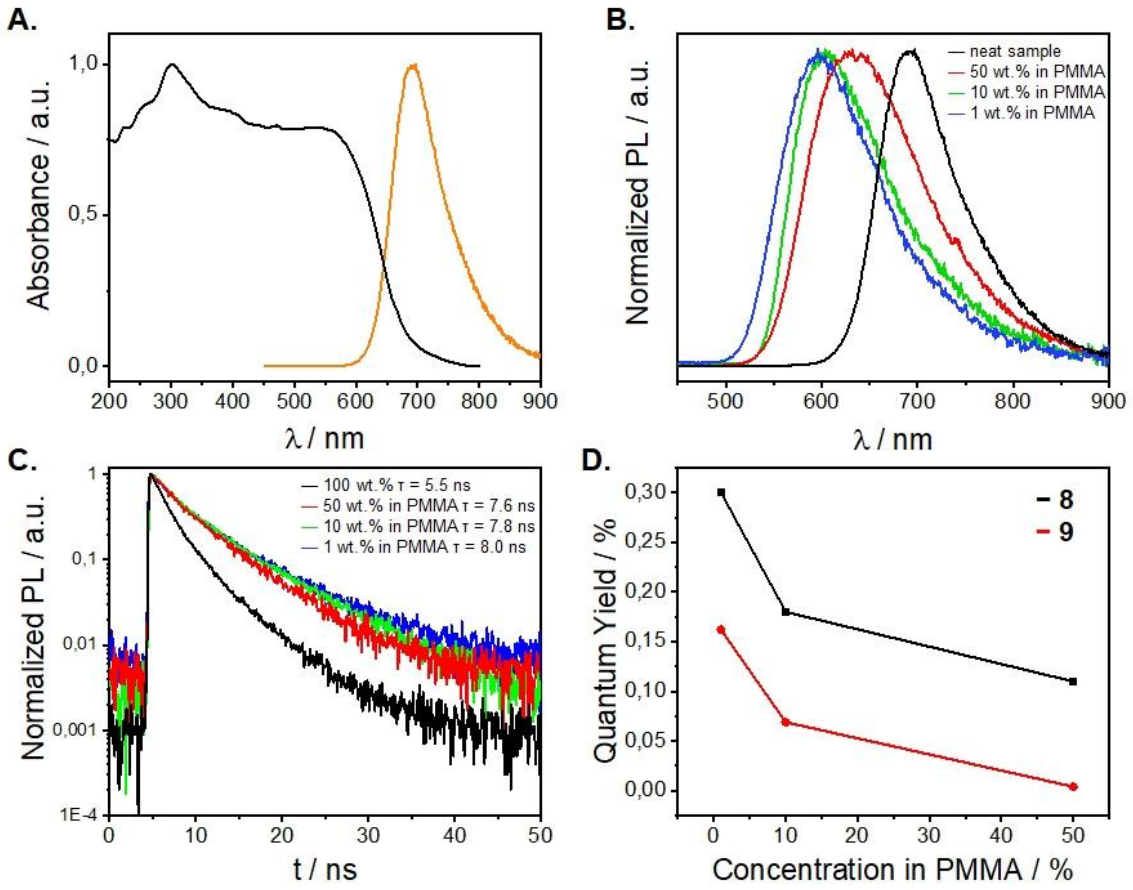

Figure 28. Depiction of the **A.** solid-state absorption (black line) and emission (orange line) spectra of **8**; **B.** solid-state emission spectra of **8** in different concentrations; **C.** time-resolved emission of **8** in different concentrations with associated lifetimes; **D.** concentration/aggregation effect on the quantum yield in the solid state.

2.2.2. Synthesis and Structural Characterization of Alkaline Earth Metal-Based Metal-Organic Frameworks

Four novel alkaline earth metal-based MOFs, namely, Mg-MOF (**10**), Ca-MOF (**11**), Sr-MOF (**12**), Ba-MOF (**13**) were synthesized upon heating **9** and the corresponding metal nitrate at 80 °C in different solvent mixtures for four days as depicted in Scheme 9.

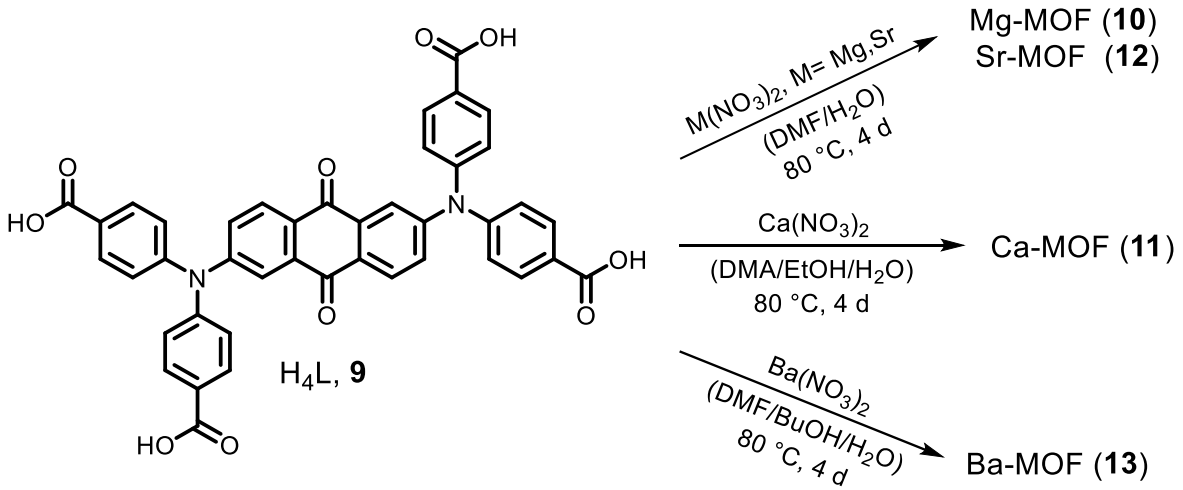

Scheme 9. Schematic illustration of the synthesis of the MOFs **10**–**13**.

The structure of the Mg-MOF, **10**, was solved and refined in the space group *P* $2_1/m$ and displays two distinct pore environments (Figure 29A). There are six crystallographic unique magnesium centers, which are all octahedrally coordinated. The Mg–O bond distances fluctuate between 1.95 and 2.15 Å, depending on the type of ligand and coordination mode. These values are in good agreement with the values observed for different magnesium acetate hydrated phases.[102] Besides linker carboxylates, DMF, aquo/hydroxo, and one formate (from DMF decomposition) ligands fulfill the coordination sphere of the magnesium sites. Two of the Mg-atoms are found in single-sited, slightly distorted octahedral environments, [MgO_6], whilst the other four build up to two distinct dimeric structures, [Mg_2O_{11}]. The single sites are comparable to those observed in the crystal structure of $Mg(OAc)_2{\cdot}4H_2O$, which consist of four terminal equatorial O-donors and two carboxylates *trans* to each other (Figure 29B).[103] The dimers have as bridge two carboxylates and an aquo/hydroxo ligand. Further three O-donors fulfill the coordination sphere of each metal (Figure 29C). There are also two different kinds of ligand molecules in the framework, which are stacked with a 3.5 Å distance. One coordinates via three carboxylates, interpreted as HL^{3-}, and the other via two carboxylates, HL^{2-}. Non-coordinated water molecules sit in the proximity of the free carboxylic functionalities and aquo ligands, stabilizing the inorganic SBUs and the framework through hydrogen bonding. The Mg:linker ratio in **10** is 7:4 and, considering all aquo ligand as neutral, the framework can be

described as $[Mg_7(H_2L)_2(HL)_2(H_2O)_{20}(DMF)_2(HCOO)]^{3+}$. In the pores, several disordered solvent molecules can be seen, including a trigonal planar residue. Considering the possible alternatives, it could be either a nitrate ion or a disordered bent ion, such as formate or dimethylamine/ammonium. Digestion studies revealed the absence of dimethylamine derivatives and two equivalents of formate. Based on the expected overall neutrality of the compound and further elemental and thermogravimetric analyses, the composition of **10** was proposed as $[Mg_7(H_2L)_2(HL)_2(H_2O)_{18}(OH)_2(DMF)_2(HCOO)][HCOO]\cdot 10H_2O\cdot 6DMF$. It is important to highlight the ambiguity of this formula due to the difficulty of attributing the proton distribution throughout the structure. The phase purity of the isolated phase was confirmed using powder X-ray diffraction (Figure 29D). The IR spectrum of the Mg-MOF is also consistent with coordination since the asymmetric vibration of the carboxylates is visible at 1400 cm^{-1}. The quinone stretch is slightly shifted to lower wavenumbers, which might be related to the increased negative charge in the deprotonated ligand (Figure 29E).

The activation, *i.e.,* pore solvent removal, of **10** was performed by solvent exchange with acetone followed by heating the sample at 65 °C under high vacuum. Powder X-ray diffraction shows a reduction of crystallinity after activation, but retention of the framework structure. A shift of the peaks to higher 2θ angles suggests contraction of the unit cell, which might be related to a narrower pore structure (Figure S36). Nevertheless, a BET adsorption experiment of **10** shows porosity towards CO_2 with a surface area of approximately 312 $m^2.g^{-1}$ (Figure S37). No adsorption/uptake of N_2 was observed. Digestion studies show successful removal of encapsulated and coordinated DMF molecules and one equivalent of formate, supporting the assumption in the crystallographic model. Thermogravimetric analysis of **10** (Figure 29F) possibly shows loss of water molecules up to 500 °C, before the organic strut is combusted. These water molecules may be coordinated or involved in hydrogen bonding and structural stabilization. As the mass loss events cannot be undoubtedly defined, elemental analysis was carried out and the activated MOF was formulated as $[Mg_7(H_2L)_2(HL)_2(H_2O)_{19}(OH)_3(HCOO)]$. This formula is in good agreement with the MgO residue observed (9%) in the thermogravimetric curve and the expected value (8.2 %). An emission spectrum of a neat, activated sample of **10** (Figure 29G) was recorded and showed red emission with maximum at 685 nm, which resembles closely the behavior of the acid, **9**. Moreover, the lifetime decay was likewise determined to be 5 ns as expected for the linker. The quantum yield was determined using a neat sample and was 1.7 %. This value is four times higher than the one recorded for a neat sample of ligand **9** (0.4 %). Even so, the low quantum yield could result from the sample preparation and structural features such as stacking between anthraquinone moieties. Production of PMMA films could improve the emission via suppression of physical contact between grains as observed for the pure organic molecules.

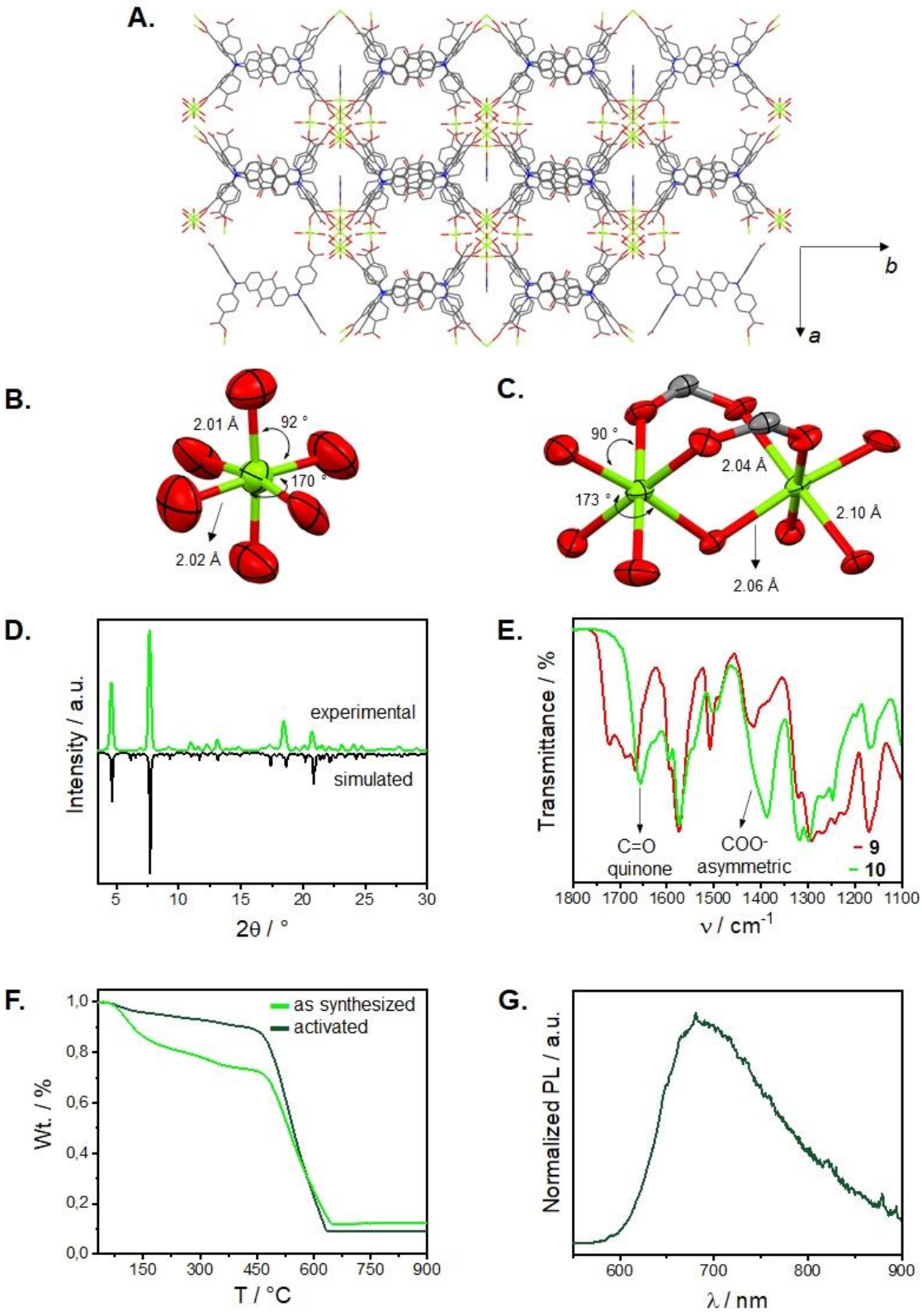

Figure 29. Depiction of **A.** the overall structure of **10**. Hydrogen atoms and encapsulated species were omitted for clarity reasons; **B.** a single-sited magnesium cation, highlighting selected bond distances and angles; **C.** a magnesium dimeric site, highlighting selected bond distances and angles. Atom colors are grey (C), blue (N), red (O), green (Mg). **D.** Simulated (from SCXRD, black line) and experimental (green line) powder diffractograms of **10**. **E.** IR spectra of **9** (red line) and **10** (green line) with selected bands. **F.** Thermogravimetric curves of **10** as-synthesized (green line) and activated (dark green line). **G.** Emission spectrum of an activated sample of **10**.

The Ca-MOF, **11**, could not be obtained from DMF/H_2O mixtures, even when alcohols were added as modulators. However, changing the amide solvent to dimethylacetamide (DMA), large, strong diffracting block-like crystals were obtained. Even though many crystals were measured, twinning could not be avoided. Thus, the structure of the **11** (Figure 30A) was solved and refined in the space group *P* $2_1/m$ (second twin-component factor: 0.09, twin law 1 0 0.168 0 -1 0 0 0 -1). There are seven crystallographic distinct calcium centers in special positions (0.5 occupancy), six of those located in the framework and one in the pores. The former builds up to three unique SBUs in which the coordination numbers range from six to eight. The overall metal:linker ratio is 6:4 in **11**. Three linker molecules are found in the fully deprotonated form, L^{4-}, whereas one molecule is interpreted as H_2L^{2-}, resulting in a negatively charged framework, $[Ca_6(H_2L)L_3(H_2O)_{13}(DMA)_2]^{2-}$. Interestingly, a pentacoordinated calcium ion, $[Ca(H_2O)_2(DMA)_3]^{2+}$, sits in the bigger-sized pores, balancing the negative charge. The Ca–O bond length ranges from 2.22 to 2.53 Å, depending on the ligand and coordination mode. Three of the cations build up together with O-donor ligands a $[Ca_3O_{17}]$ polyhedron (Figure 30C). Ca1 and Ca3 are found in capped trigonal prismatic environments, which share an edge and a trigonal face, respectively, with the bicapped trigonal prism around Ca2. The trigonal prismatic coordination spheres around Ca1 and Ca2 are constituted of carboxylate ligands of **9**. The capping ligands are either water or dimethylacetamide molecules. The second SBU is a $[Ca_2O_{13}]$ dimer comprising two eight coordinated calcium centers. The polyhedron around the Ca4 atom is best described as a bicapped trigonal prism, which shares a trigonal face with the square antiprism around Ca5. The last calcium atom, Ca6, is octahedrally coordinated (Figure 30B). As in the Mg-MOF, the inorganic sites are not isolated but connected via hydrogen bonding over water molecules. As expected, the amount of pore solvent could not be determined exclusively via SCXRD and digestion studies, elemental and thermogravimetric analyses were carried out, leading to the formula $[Ca(H_2O)_2(DMA)_3][Ca_6(H_2L)L_3(H_2O)_{13}(DMA)_2]\cdot 14H_2O\cdot 3DMA$. Phase identity and purity of the as synthesized material were checked via PXRD (Figure 30D). The IR spectrum of **12** is also consistent with coordination since the asymmetric vibration of the carboxylates is visible at 1400 cm^{-1}. The quinone stretch is slightly shifted to lower wavenumbers, which might be related to the increased negative charge in the deprotonated ligand (Figure 30E).

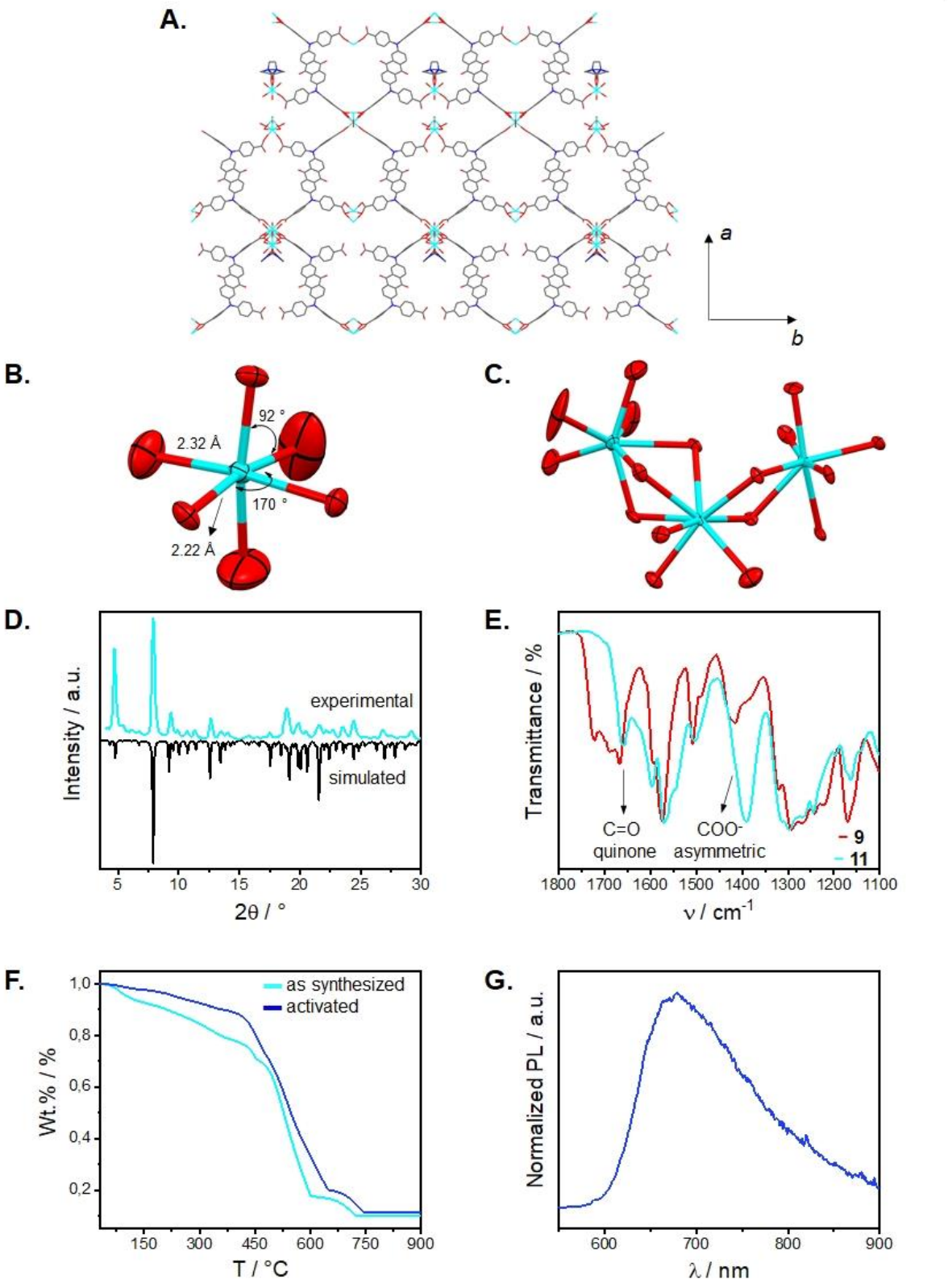

Figure 30. Depiction of **A.** of the overall structure of **11**. Hydrogen atoms and encapsulated species were omitted for clarity reasons; **B.** a single-sited calcium cation, highlighting selected bond distances and angles; **C.** a calcium trimeric site, highlighting selected bond distances and angles. Atom colors are grey (C), blue (N), red (O), cyan (Ca). **D.** Simulated (from SCXRD, black line) and experimental (cyan line) powder diffractograms of **11**. **E.** IR spectra of **9** (red line) and **11** (cyan line) with selected bands. **F.** Thermogravimetric curves of **11** as synthesized (cyan line) and activated (blue line). **G.** Emission spectrum of an activated sample of **11**.

The activation of **11** was performed by solvent exchange with acetone followed by heating the sample at 65 °C under high vacuum. Powder X-ray diffraction shows a reduction of crystallinity after activation, but retention of the framework structure. A shift of the peaks to higher 2θ angles suggests contraction of the unit cell, which might be related to a narrower pore structure (Figure S38). Adsorption/uptake was not observed either for CO_2 or N_2, which could be related to the bulky calcium cation in the pores. Thermogravimetric analysis of **11** (Figure 30F) is consistent with the activation process and possibly shows loss of water molecules up to 500 °C, before the organic strut is combusted. These water molecules may be coordinated or involved in hydrogen bonding and structural stabilization. The last event occurring between 600 and 750 °C is the decomposition of $CaCO_3$ into CaO. As the mass loss events cannot be undoubtedly defined, the activated MOF was formulated as $[Ca(H_2O)_2(DMA)_3][Ca_6(H_2L)L_3(H_2O)_{13}(DMA)_2]$. This formula is in good agreement with the CaO residue observed (11.1%) in the thermogravimetric curve and the expected value (10.6 %). An emission spectrum of a neat, activated sample of **11** (Figure 30G) was recorded and showed red emission with maximum at 678 nm and short lifetime decay of 5 ns, as observed for the analog Mg-MOF. The quantum yield was determined using a neat sample and was 1.4 %. This value was three and a half times higher than the one observed for a neat sample of ligand **9** (0.4 %).

The Sr-MOF, **12**, was obtained also from a DMF/H_2O mixture. However, its synthesis was not as reproducible at first as for the Mg-MOF. Nonetheless, the obtained needle-shaped crystals showed strong diffraction when mounted. Unfortunately, like **11**, twinning in **12** was always observed, which was assumed to be intrinsic to its crystallization process. To investigate the growth of the complex over two weeks, eight different identical reactions were heated up at 80 °C and every 24 h a reaction was stopped and a powder diffractogram of the isolated solid was recorded (Figure 31). The last sample was left to react for fourteen days. In the diffractograms, it is possible to see that an unknown crystalline phase is already present after 24 hours. Over five days, a phase transition into another crystalline phase is observed, which was confirmed to be **12**. Longer reaction times (six to seven days) led to a reduction of crystallinity and after two weeks a mixture of both phases was detected again.

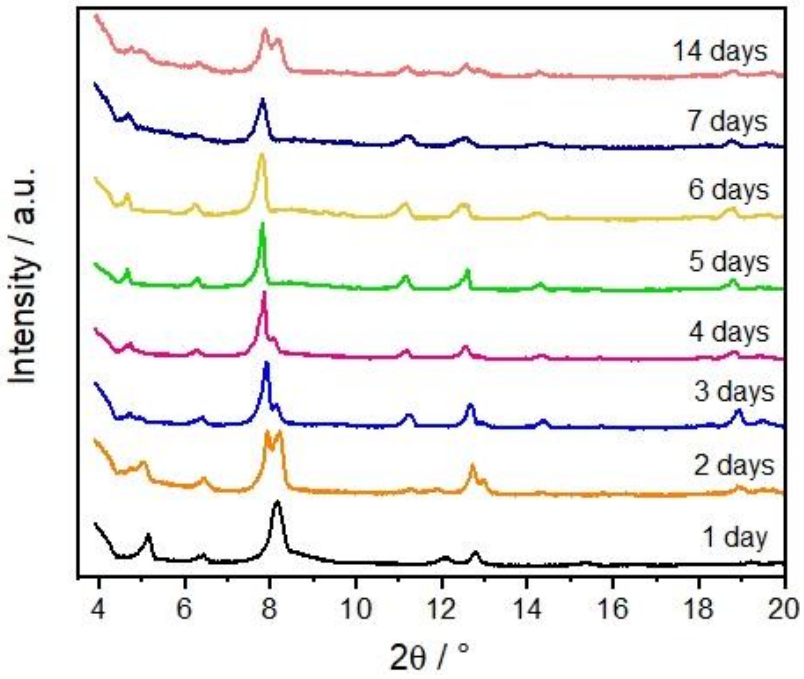

Figure 31. Time-resolved study of the crystallization process of **12**. The phase pure compound is obtained with the best crystallinity after five days (green line).

The structure of **12** was solved and refined with a twinning component (second twin-component factor: 0.31, twin law -1 0 0 0 -1 0 0.741 0 1) in the space group C 2/m. The overall structure displays two distinct pore environments as the previous compounds (Figure 32A). There are two crystallographic unique strontium centers, which build up a trimeric SBU of the formula [Sr_3O_{20}] (Figure 32B). The oxygen donors are either from carboxylates of **9** or from aquo/hydroxo ligands. The central strontium atom, Sr1, is ten-fold coordinated and is best described as a bicapped square prism, in which four carboxylates build up the prism and two water molecules do the capping of two opposite squared faces. The Sr–O bond distances are very similar and found between 2.66 and 2.76 Å. The second strontium cation, Sr2, is octacoordinated and is best described as a square antiprism. Similarly, a water molecule occupies a capping position, whereas carboxylates build up the prism around the metal. The Sr–O bond distances are found between 2.35 and 2.68 Å. Interestingly, Sr2 is found also in a second position, in which one carboxylate moves away from Sr2 and acts then only as a monodentate ligand. Concurrently, one water molecule occupies one available coordination site, leading to a heptacoordinated geometry. Hydrogen bonding between water ligands is observed.[104] The geometry can be described as a distorted pentagonal bipyramid. In this positioning, the Sr–O bond distances are found between 2.38 and 2.81 Å. The long bond distance is found to a water molecule, which can be assumed to be only weakly coordinated to Sr2.

The ligand coordinates via all carboxylates and is best interpreted as fully deprotonated, L^{4-}. The anthraquinone moieties stack in an eclipsed manner with the smallest

distance between two atoms being 2.45 Å. The Sr:linker ratio in **12** is 3:2 and, considering all aquo ligand as neutral, the framework can be described as $[Sr_3(L)_2(H_2O)_6]^{2-}$. Digestion studies, elemental and thermogravimetric analyses were carried out to determine the number of encapsulated molecules, yielding the suggested composition $[H_3O]_2[Sr_3(L)_2(H_2O)_6]\cdot[HCOOH]_{0.3}\cdot 4H_2O\cdot 4DMF$. This formula is in good agreement with the SrO residue observed (17 %) in the thermogravimetric curve and the expected value (16.2 %). The phase purity of the isolated phase was confirmed using powder X-ray diffraction (Figure 32C). The IR spectrum of **12** is also consistent with coordination since the asymmetric vibration of the carboxylates is visible at 1400 cm^{-1}. The quinone stretch is slightly shifted to lower wavenumbers, which might be related to the increased negative charge in the deprotonated ligand (Figure 32D).

The activation of **12** was performed by solvent exchange with acetone followed by heating the sample at 65 °C under high vacuum. Powder X-ray diffraction shows a reduction of crystallinity after activation, but retention of the framework structure. A shift of the peaks to higher 2θ angles suggests contraction of the unit cell, which might be related to a narrower pore structure (Figure S39). Nevertheless, a BET adsorption experiment of **12** shows porosity towards CO_2 with a surface area of approximately 274 $m^2.g^{-1}$ (Figure S37). Very small porosity was observed towards N_2 (79 $m^2.g^{-1}$). Digestion studies show successful removal of encapsulated most DMF molecules. Thermogravimetric analysis of **12** (Figure 32E) is consistent with the activation process and possibly shows loss of water molecules up to 500 °C, before the organic strut is combusted. These water molecules may be coordinated or involved in hydrogen bonding and structural stabilization. The last event occurring between 850 and 1000 °C is the decomposition of $SrCO_3$ into SrO. As the mass loss events cannot be undoubtedly defined, elemental analysis was carried out and the activated MOF was formulated as $[H_3O]_2[Sr_3(L)_2(H_2O)_6]$ $[HCOOH]_{0.3}\cdot H_2O\cdot 0.33DMF$. An emission spectrum of a neat, activated sample of **12** (Figure 32F) was recorded and showed red emission with maximum at 680 nm and short lifetime decay of 5 ns, as observed for the analog Mg and Ca-MOFs. The quantum yield was determined using a neat sample and was 2.8 %. This value was the highest between all MOFs and seven times higher than the one observed for a neat sample of ligand **9** (0.4 %).

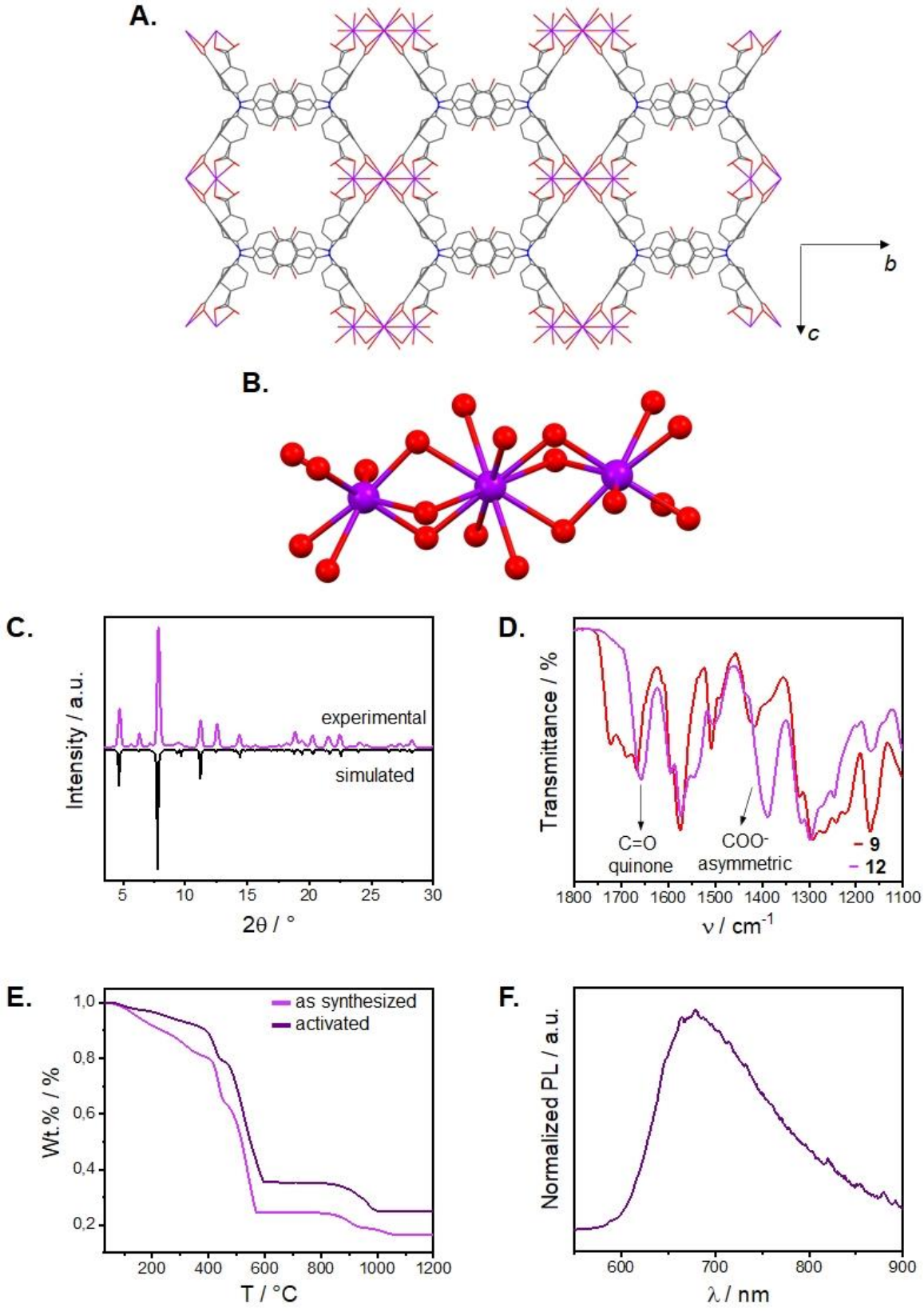

Figure 32. Illustration of **A.** of the overall structure of **12**. Hydrogen atoms and encapsulated species were omitted for clarity reasons; **B.** the trimeric [Sr_3O_{20}] SBU. Atom colors are grey (C), blue (N), red (O), purple (Sr) **C.** Simulated (from SCXRD, black line) and experimental (purple line) powder diffractograms of **12**. **D.** IR spectra of **9** (red line) and **12** (purple line), highlighting selected bands. **E.** Thermogravimetric curves of **12** as synthesized (purple line) and activated (deep purple line). **F.** Emission spectrum of an activated sample of **12**.

The Ba-MOF, **13**, was initially obtained also from a DMF/H_2O mixture. However, the crystallinity of the bulk material was comparatively low. Nonetheless, it could be increased by using butanol as the modulator. Strong diffracting needle-shaped crystals were obtained, which were intrinsically twins like the previous cases. The structure of **13** was solved and refined with a twinning component (second twin-component factor: 0.30, twin law -1 0 0 0 -1 0 0.735 0 1) in the space group C 2/m. The overall structure displays likewise two distinct pore environments (Figure 33A) and is analog to **12**. However, in **13** the trimeric structures are connected building an infinite 1D chain along the *a* axis. There are two crystallographic unique barium centers. The oxygen donors are either from carboxylates of **9** or from aquo/hydroxo ligands. The central strontium atom, Ba1, is ten-fold coordinated and is best described as a bicapped square prism, in which four carboxylates build up the prism and two water molecules do the capping of two opposite squared faces. The Ba–O bond distances are very similar and found between 2.40 and 2.78 Å. The second strontium cation, Ba2, is octacoordinated and is best described as a square antiprism. Similarly, a water molecule does the capping while carboxylates build up the prism around the metal. The Ba–O bond distances are found between 2.30 and 2.70 Å. Interestingly, in the structure of **13,** the same phenomenon involving the displacement of the carboxylate is observed. The ligand coordinates via all carboxylates and is best described as fully deprotonated, L^{4-}. The anthraquinone moieties stack in an eclipsed manner with the smallest distance between two atoms being 2.45 Å. The Ba:linker ratio in **13** is 3:2 and, considering all aquo ligand as neutral, the framework can be described as $[Ba_3(L)_2(H_2O)_6]^{2-}$. Digestion studies, elemental and thermogravimetric analyses were carried out to determine the number of encapsulated molecules, yielding the suggested composition $[H_3O]_2[Ba_3(L)_2(H_2O)_6]\cdot[HCOOH]_{0.3}\cdot 8H_2O\cdot 2.7DMF$. The phase purity of the isolated phase was confirmed through powder X-ray diffraction (Figure 33B). The IR spectrum of **13** is also consistent with coordination since the asymmetric vibration of the carboxylates is visible at 1400 cm^{-1}. The quinone stretch is slightly shifted to lower wavenumbers, which might be related to the increased negative charge in the deprotonated ligand (Figure 3C).

The activation of **13** was performed by solvent exchange with acetone followed by heating the sample at 65 °C under high vacuum. Powder X-ray diffraction shows a reduction of crystallinity after activation, but retention of the framework structure. A shift of the peaks to higher 2θ angles suggests contraction of the unit cell, which might be related to a narrower pore structure (Figure S40). A BET adsorption experiment of **13** shows porosity towards CO_2 with a surface area of approximately 282 $m^2.g^{-1}$ (Figure S37). Very small porosity was observed towards N_2 (30 $m^2.g^{-1}$). Digestion studies show the removal of most solvent molecules. Thermogravimetric analysis of **13** (Figure 33D) is consistent with the activation process. The last event occurring between 1000 and 1200 °C is the decomposition of $BaCO_3$ into BaO. As the mass loss events cannot be undoubtedly defined, elemental analysis was carried out and

the activated MOF was formulated as $[H_3O]_2[Ba_3(L)_2(H_2O)_6]\cdot[HCOOH]_{0.3}\cdot 3H_2O \cdot 0.3DMF$. An emission spectrum of a neat, activated sample of **13** (Figure 33E) was recorded and showed red emission with maximum at 680 nm and short lifetime decay of 5 ns. The quantum yield was determined using a neat sample and was 0.7 %. This value was the lowest among the MOFs close to the one observed for a neat sample of ligand **9** (0.4 %).

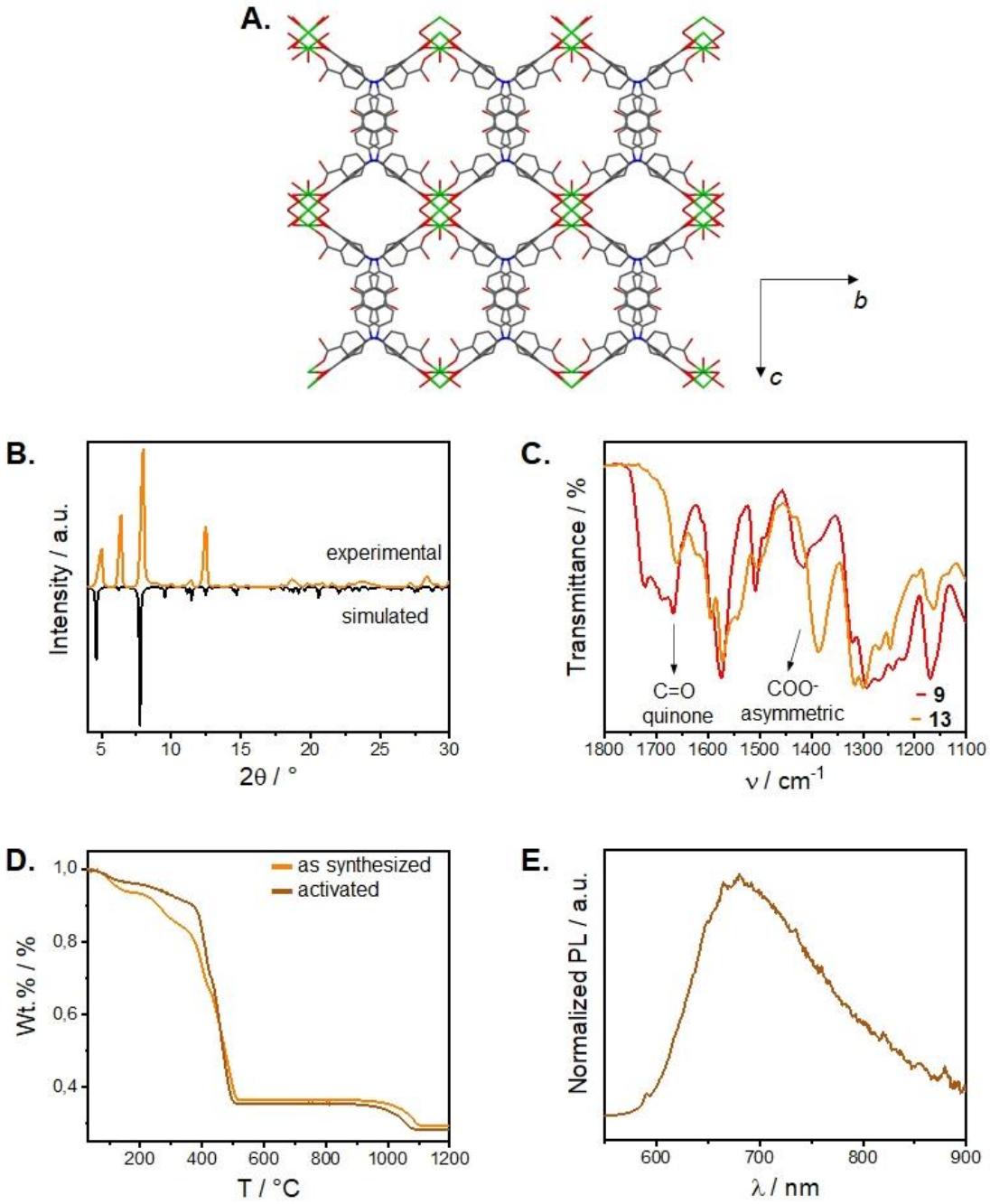

Figure 33. Illustration of **A.** of the overall structure of **13**. Hydrogen atoms and encapsulated species were omitted for clarity reasons. Atom colors are grey (C), blue (N), red (O), dark green (Ba). **D.** Simulated (from SCXRD, black line) and experimental (orange line) powder diffractograms of **13**. **E.** IR spectra of **9** (red line) and **13** (orange line), highlighting selected bands. **F.** Thermogravimetric curves of **13** as synthesized (orange line) and activated (brown line). **G.** Emission spectrum of an activated sample of **13**.

2.2.3. Light-driven Heterogeneous Photooxidation of Sulfides to Sulfoxides

Anthraquinones have been used as catalysts for different reactions, including photocatalysis under visible light. Specifically, they can be used for photooxidation reactions of different substrates via activation of molecular oxygen.[42-45] Inspired by that, the photocatalytic properties of **9** and the corresponding MOFs were studied using the oxidation reaction of sulfides into sulfoxides as a model. The photooxidation of tetrahydrothiophene (THT) with **9** was attempted in acetonitrile (acn) under an O_2 atmosphere and irradiation of a purple LED, λ = 420 nm. Acetonitrile was chosen due to the insolubility of the linker, which allowed its separation by filtration, and compatibility with GC-MS analysis. The linker was able to fully oxidize the sulfide (> 99 conversion) to the corresponding sulfoxide in 2.5 hours with 98 % selectivity (Figure 34, for GC, see Figure S42). The sulfone was observed as a minor side product. All the initial performed experiments are summarized in Table 1. First, the concentration of catalyst was optimized (entries 1–3) and determined to be ideally 5 mol% maintaining the remaining variables constant (see Table 1 footnotes). Then, to ensure that the reaction was being promoted by **9** a catalyst-free reaction was carried out and indeed no oxidation products were detected (entry 4). Similarly, no oxidation was possible in the absence of light and dioxygen (entries 5 and 6). When the reaction was performed under air (entry 7), the conversion was smaller in the same reaction time. This would be expected due to the lower dioxygen concentration available. Longer reaction times did not lead to considerable further oxidation of the sulfoxide (entry 8).

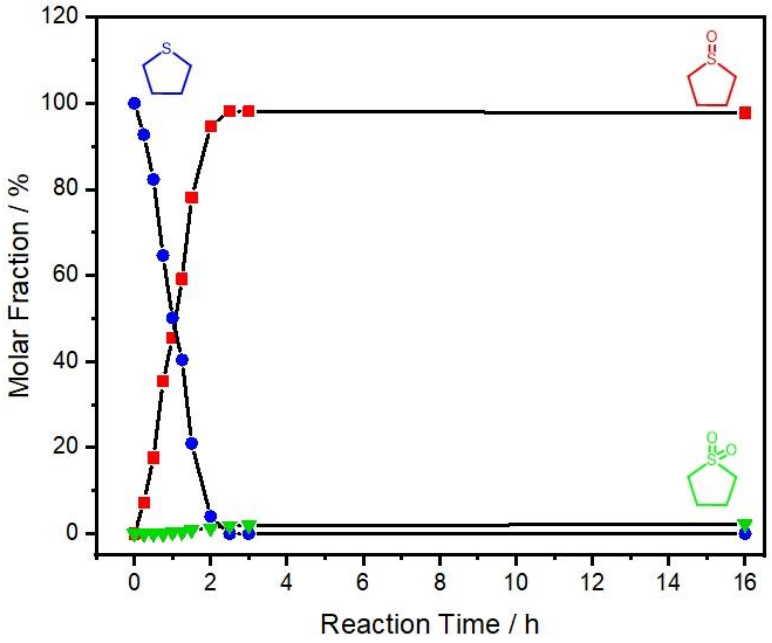

Figure 34. Catalytic profile of the photooxidation of THT over **9** under visible light. Reaction conditions: THT (0.125 mmol), **9** (5 mol%), CH_3CN (5.0 mL), O_2 (1 atm), purple LED (λ = 420 nm), room temperature.

Table 1. Catalytic visible-light-driven selective aerobic oxidation of THT over **9** in acetonitrile.

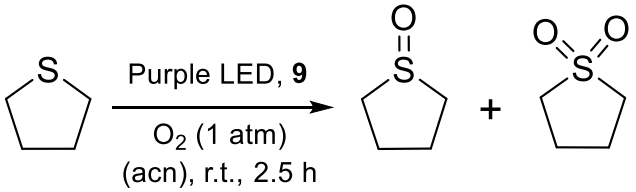

Entry[a,b]	Catalyst (mol%)	Conversion	Selectivity
1	10	>99	98
2	5	>99	98
3	3	84	99
4[c]	5	n.d.	----------
5[d]	5	n.d.	----------
6[e]	5	n.d.	----------
7[f]	5	25	100
8[g]	5	99	97

[a] Reaction conditions: THT (0.125 mmol), **9** (x mol%), CH_3CN (5.0 mL), O_2 (1 atm), purple LED (λ = 420 nm), room temperature, 2.5 hours. [b] Determined by GC and GC-MS. [c] No catalyst. [d] In darkness. [e] In argon atmosphere. [f] In air. [g] 16 h reaction time.

Following the optimization of the conditions, further experiments were conducted to gain insights into the mechanism of photocatalytic oxidation (Scheme 10). For that, a series of trapping studies were performed using distinct scavengers. All scavengers had a negative effect on the conversion (Figure 35), suggesting quenching of several reactive species. When using hydroquinone, it acts as a free radical scavenger and, therefore, sustains a radical pathway for the oxidation. As expected, the light-induced electron-hole separation was suppressed when $CuSO_4$ (electron scavenger) and KI (hole scavenger) were used. When using KI, no conversion was observed. The formation of the $\cdot O_2^-$ radical species was strongly hindered when using *p*-benzoquinone (*p*-Bzq). This radical reacts with the sulfide radical cation to a zwitterionic intermediate. The diradical intermediate is formed when a sulfide molecule reacts with a singlet dioxygen molecule, $^1O_2$. The formation of the latter was quenched when TEMPO was added to the reaction mixture. Both intermediates may react with another sulfide molecule to generate the sulfoxide. Lastly, the use of ^{t}BuOH did not lead to a strong suppression of the conversion, suggesting hydroxyl radicals do not play a decisive role in the mechanism.

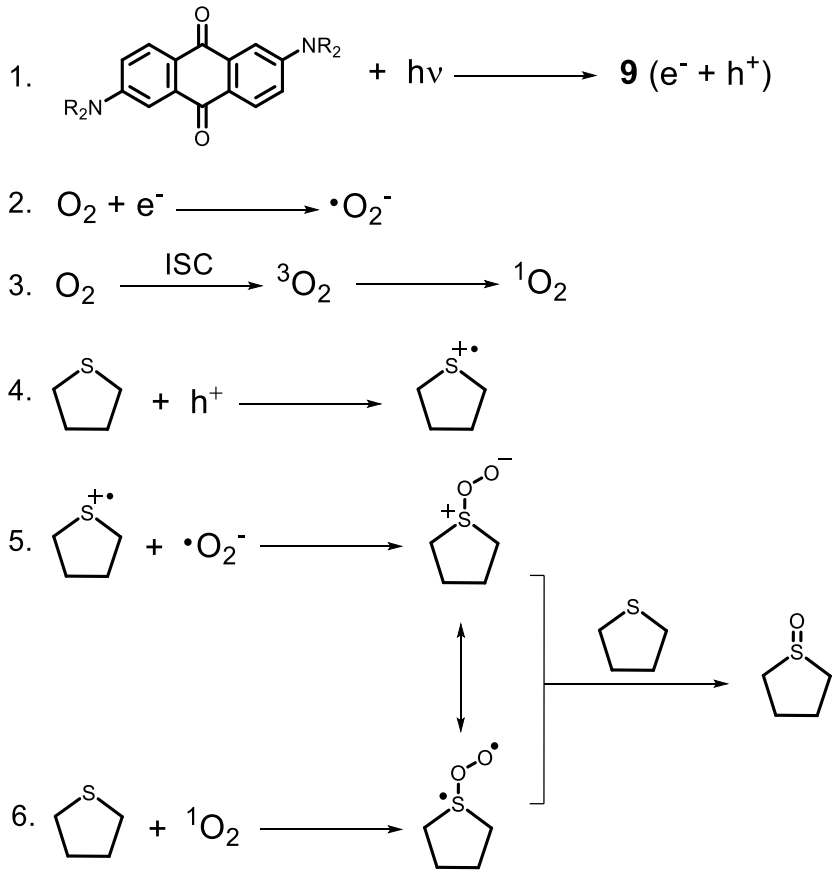

Scheme 10. Schematic illustration of the possible reaction mechanisms[45] for the photooxidation of THT under visible light.

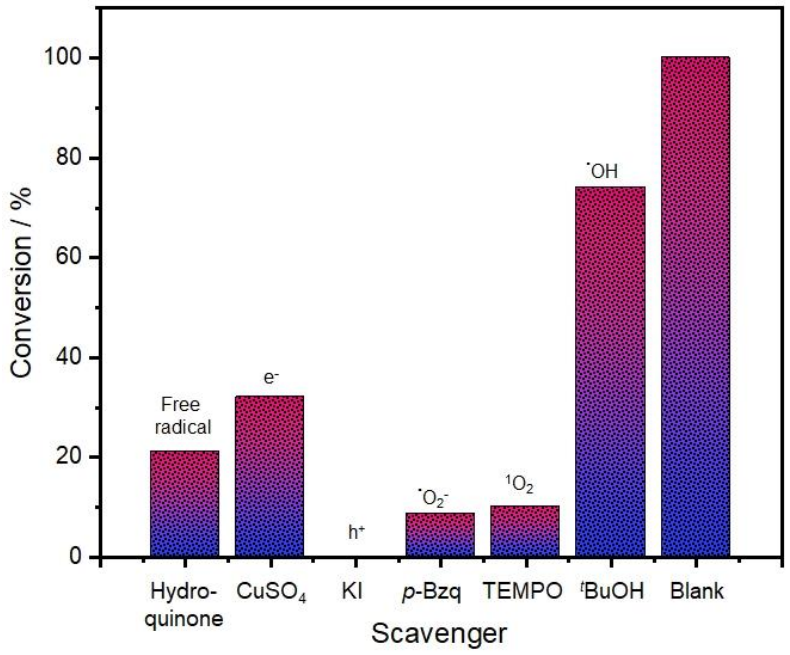

Figure 35. The influence of scavengers in the photooxidation of THT. The quenched reaction species by each scavenger is presented on top of the corresponding conversion bar. Reaction conditions: THT (0.125 mmol), **9** (5 mol%), scavenger, CH_3CN (5.0 mL), O_2 (1 atm), purple LED (λ = 420 nm), room temperature, 2.5 hours.

After confirming the photocatalytic activity of **9**, the Mg-MOF, **10**, which has the greatest porosity between the materials, was selected for studying the aerobic oxidation of sulfides over coordination frameworks. The amount of MOF used was 10 mg, which, considering the suggested formula, would correspond to roughly 9 mol %. All other conditions were maintained unchanged and a reaction profile over time was then constructed (Figure 36). As it is possible to see, the reaction over the MOF was much slower than over organic linker. This might have been a consequence of slow substrate diffusion into the MOF pores. The reaction time was defined as 16 hours based on the obtained data. Additionally, it is possible to see that the reaction was also less selective to the sulfoxide, meaning the pore environment of the MOF may play a role in the overall reaction mechanism.

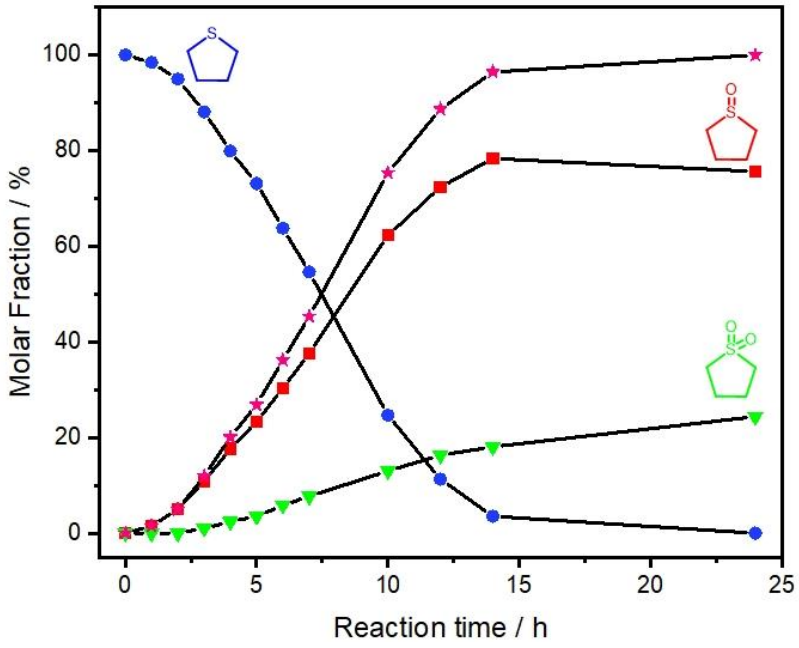

Figure 36. Catalytic profile of the photooxidation of THT over **10** under visible light. Reaction conditions: THT (0.125 mmol), **10** (10 mg), CH_3CN (5.0 mL), O_2 (1 atm), purple LED (λ = 420 nm), room temperature. The pink star-marked line corresponds to the overall conversion (sulfoxide + sulfone).

To test the influence of the polarity of the milieu, four different solvents were chosen, and the conversion and selectivity were determined (Figure 37). The reaction was complete in acetonitrile and methanol after 16 h (for GCs see Figure S43), whereas the conversion was not as high in acetone and dichloromethane (roughly 70 %) after the same reaction time. Acetonitrile, however, led to the highest rate of overoxidation and, thus, to the lowest selectivity (88 %) towards the sulfoxide. Methanol, on the other hand, increased the selectivity to 97 %. To investigate if the catalysis was happening in the pores or in the surface of the MOF, sulfide substrates with different sizes were tested (Figure 38). Interestingly, small sulfides like THT and diethyl sulfide reacted completely, whereas bulky aromatic substrates (thioanisole and diphenyl sulfide) almost did not show any conversion (< 2%). Dipropyl sulfide was partially

oxidized (60 % conversion), which might show that the longer alkyl chains reduced the diffusion rate into the MOF. In the oxidation of alkyl sulfides, it was also observed that acetonitrile would lead to a lower selectivity, mainly due to the formation of disulfide subproducts. This reaction could be suppressed when using methanol. Lastly, the analog MOFs **11-13** were tested on the photooxidation of THT. These materials did not perform as well as the Mg-MOF. The Ca-MOF did not show any activity, which is compatible with the lack of porosity. Even though the Sr and Ba-MOFs show porosity close to the Mg-MOF, only roughly 30 % conversion was observed.

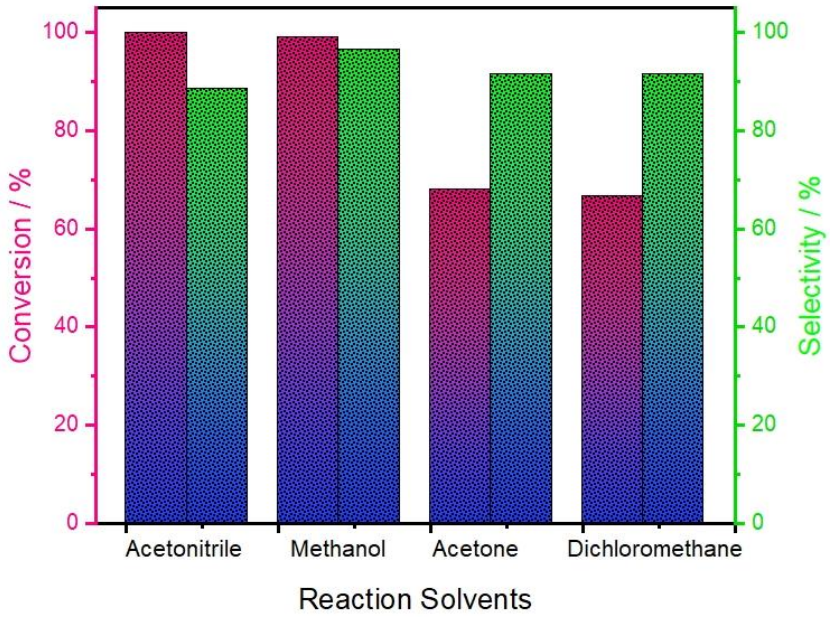

Figure 37. Conversion and selectivity of the photooxidation of THT over **10** under visible light in different solvents. Reaction conditions: THT (0.125 mmol), **10** (10 mg), solvent (5.0 mL), O_2 (1 atm), purple LED (λ = 420 nm), room temperature.

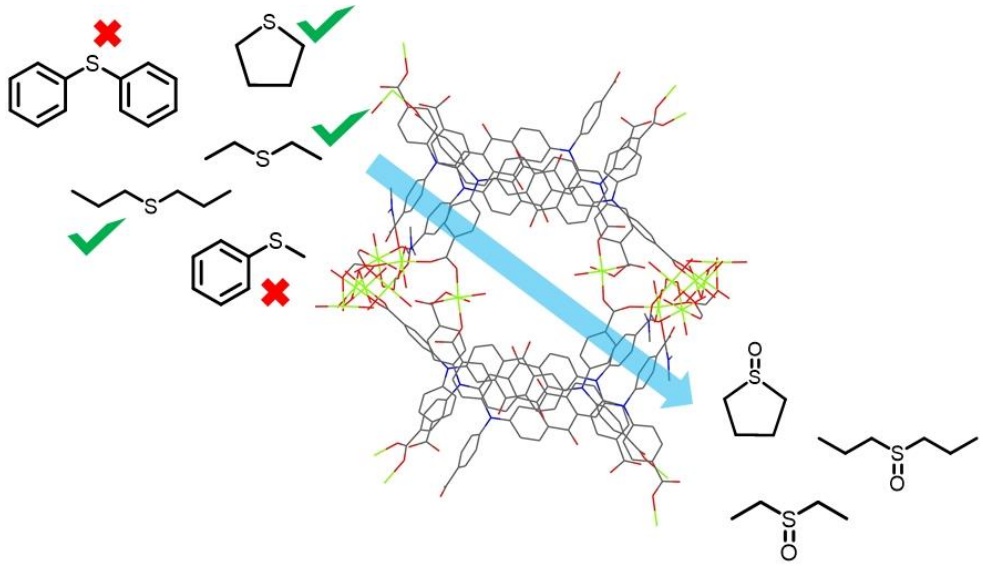

Figure 38. Figurative illustration of the substrate scope of **10** studied in this thesis. The material is capable of oxidizing small sulfide molecules, while bulkier molecules remain unchanged.

When compared to the reported COF, the Mg-MOF underperforms, especially when it comes to the substrate range. Due to the smaller voids and associated porosity, the scope of synthetic applicability is limited. Additionally, the Mg-MOF is sensitive to the pH value of the medium, which would difficult reactions in presence of acids and bases. To circumvent such drawbacks, a zirconium-based material could be promising, since this class of MOFs is very robust and has wide-pore structures.

2.3. Incorporation of Established Synthetic Dyes into Metal-Organic Frameworks

2.3.1. Synthesis of soluble anthanthrone-derived linkers from commercial vat dyes

As presented in chapter two, π-stacking can lead to dense-packed structures and smaller pore environments, which were not favorable features for photocatalysis. Therefore, linker design can be applied to circumvent such hindrances maintaining the main functional groups, quinone, and electron-donating amines. For this analysis, it is important to consider how the anthraquinones are packed in the solid state. They were eclipsed with approximately 90 ° rotation as depicted in Figure 39, left. To destabilize such interactions, the repulsion in the quinone core should be enhanced, which could be possibly achieved by using a larger aromatic system, for example, anthanthrone (Figure 39, right). In this chapter, attempts to synthesize a non-interpenetrated MOF with larger accessible pores using a novel anthanthrone-linker are described.

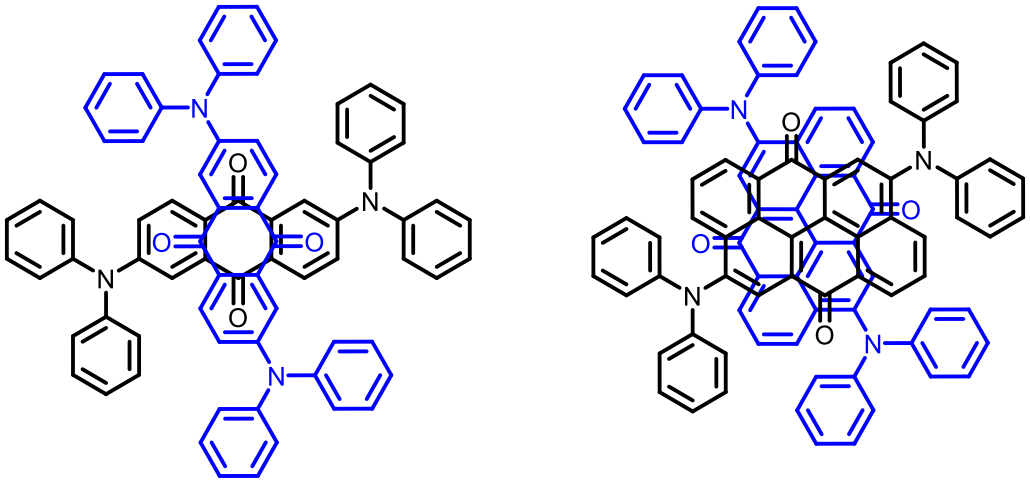

Figure 39. Depiction of the 90 ° eclipsed π-stacking of two molecules of bis(diphenylamino)anthraquinone (left) and bis(diphenylamino)anthanthrone (right).

The coordination chemistry of anthanthrone in MOFs has not been explored so far. One major difficulty is the low solubility of the available precursors; however, the larger aromatic core might hinder π-interactions and lead to materials with higher porosity and possibly enhanced photocatalytic performance compared to the presented MOFs in the previous chapter. Thus, a new tetratopic anthanthrone-based linker was synthetically accessible within a two-step procedure. First, 4,10-dibromoanthanthrone underwent a palladium-catalyzed *Buchwald-Hartwig* amination in toluene to yield the ester **14**. The second step involved the alkaline saponification of the ester functionalities followed by acidification to obtain the desired linker molecule **15** (Scheme 11). Both functionalized dye molecules display enhanced solubility compared to the original brominated vat dye. The tetraacid is very soluble in high-boiling amide-based solvents, facilitating its use in MOF synthesis. Additionally, it is reasonably soluble in other common solvents, such as alcohols, acetone, and ethyl acetate.

Attempts to crystallize the ester were not successful and always led to amorphous precipitates. However, suitable crystals for SCXRD of **15** could be grown by slow evaporation of either DMF, DMA or DMSO solutions. The crystal growth in DMSO was considerably faster and led to very weak diffracting crystals. The slower crystallization in DMF and DMA yielded larger units, which enabled its structural analysis. The structure from DMA was solved and refined in the monoclinic space group $P\,2_1/c$ and the asymmetric unit comprises half a molecule. The C=O bond length is 1.23 Å, compatible with a quinone core. The nitrogen atoms are in the same plane as the anthanthrone core. π-Stacking, as desired, is not observed directly between two anthanthrone moieties, but between the polyaromatic cores and intercalated phenyl rings of the amines with a 3.48 Å stacking distance (Figure 40).

The linker **15** was obtained as a dark blue brittle powder and its purity was checked through ^{1}H NMR spectroscopy (Figure 41). The proton assignment was carried out based on chemical shifts and multiplicity of the signals. The isolated proton H_α is found as a singlet at 8.16 ppm. The ortho protons H_β and H_δ couple with H_γ with constants $^{ortho}J$ = 7 and 8 Hz and were respectively assigned to the signals at 8.65 8.31 and 7.94 ppm. The diphenylamine protons were attributed considering the stronger shielding effect of the N-atom on the α and γ positions. Thus, the signals at 7.20 and 7.90 ppm were assigned to H_ε and H_ζ, respectively. The carboxylic acid protons can be seen as a broad signal at 12.78 ppm (for the full spectrum, see Figure S45). The ^{1}H NMR spectrum of **14** and the assignment of the protons can be found in Figure S44.

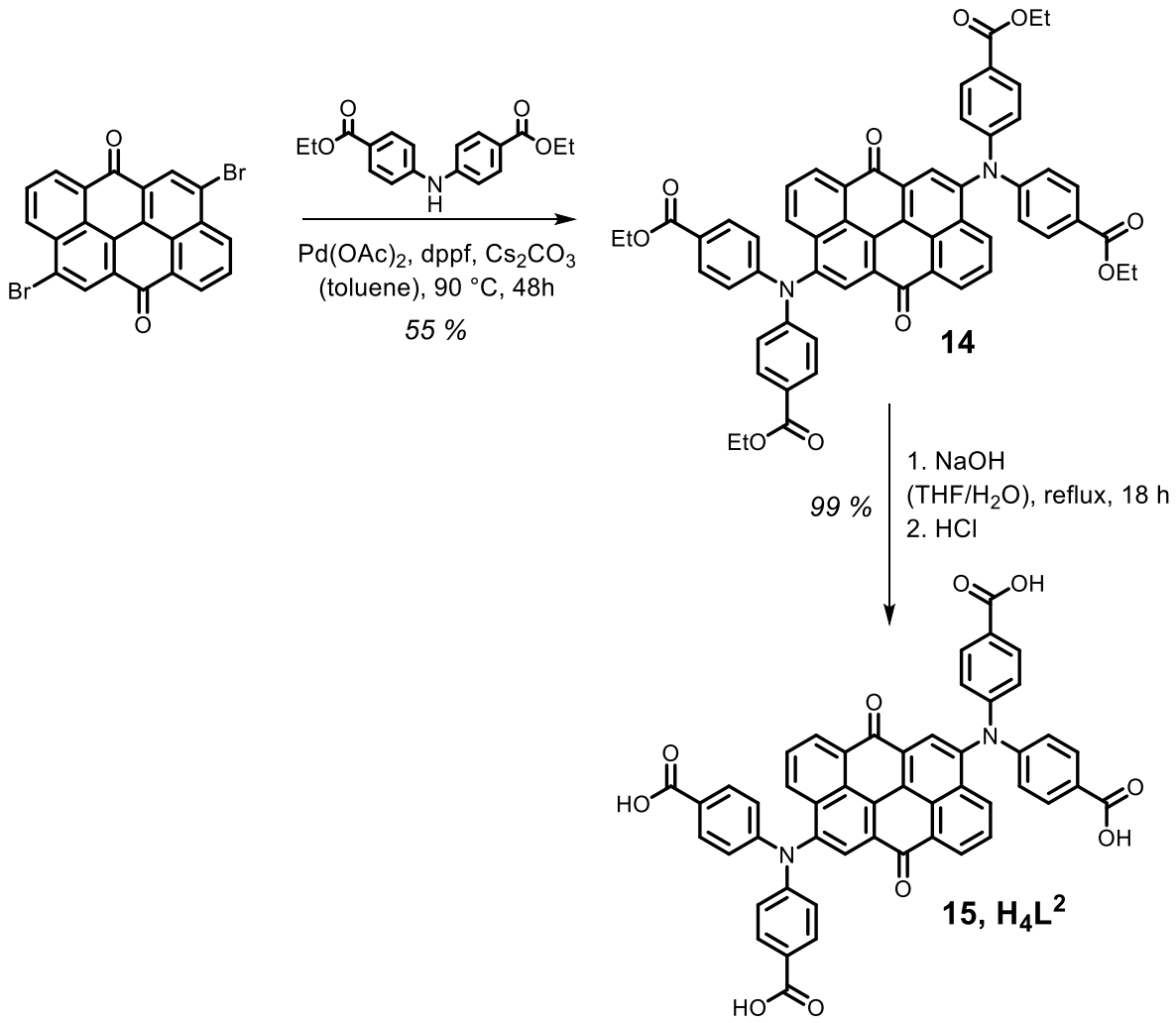

Scheme 11. The synthetic approach of a soluble anthanthrone-based ligand from commercial vat orange 3.

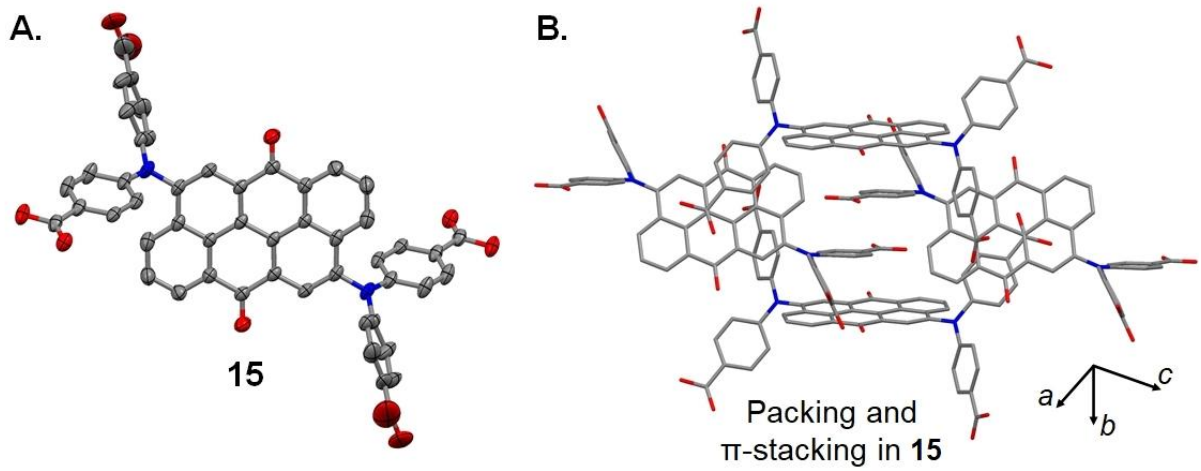

Figure 40. A. Molecular structure of **15** as determined by SCXRD. **B.** Solid-state structure of DPAq along the *a* axis and depiction of the π-stacking between molecules. Aromatic hydrogen atoms and solvent molecules were omitted for clarity reasons. All ellipsoids, if shown, are at the 50% probability level. Atom colors are grey (C), blue (N), red (O).

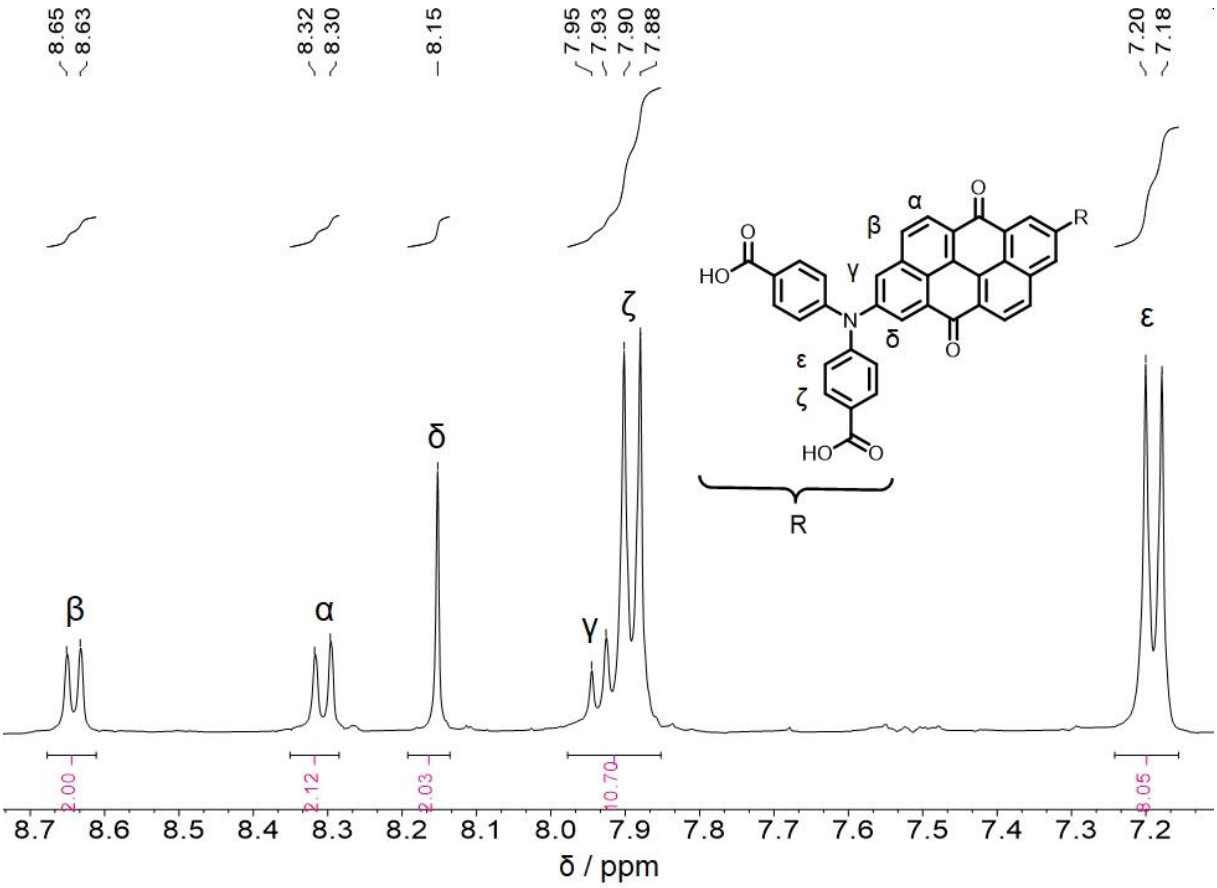

Figure 41. Section of the ^{1}H NMR spectrum of **15** with the assignment of aromatic protons.

Further spectroscopic characterization of the linker was carried out. In the IR spectrum of **14** (Figure 42A, green line), there are two carbonyl stretches, which can be assigned to the ester (ν = 1703 cm^{-1}) and quinone (ν = 1655 cm^{-1}) functionalities. In the spectrum of the tetraacid, **15** (Figure 3.4A, red line), an overly broad absorption centered at 3000 cm^{-1} is observed, which is attributed to O–H stretching modes. The carbonyl stretch of the carboxylic acids is found at 1680 cm^{-1}. The quinone stretch absorption band is somewhat broader than in the spectrum of the ester but is not considerably shifted. The solution-state absorption and emission spectra of **15** were recorded in DMF (Figure 42B). The absorptions at 290 and 350 nm were attributed to π→π* and n→π* transitions, whereas the broad and less intense band at 600 nm is assigned to a charge transfer transition from the amino groups to the quinone. The emission is observed as a broad band centered at 660 nm. The solution-state photoluminescence of **15** is solvent-dependent as depicted in Figure 42C, ranging from 645 nm in THF to 760 nm in acetone. Such behavior was also observed for **14** (Figure S46). The decay lifetime was determined to be 13 ns for the ester in toluene and 7.5 ns for the acid in DMF (Figure S47). In the solid state, the emission band of **14** is found centered at 700 nm and the decay lifetime was determined to be 11 ns (Figures S48).

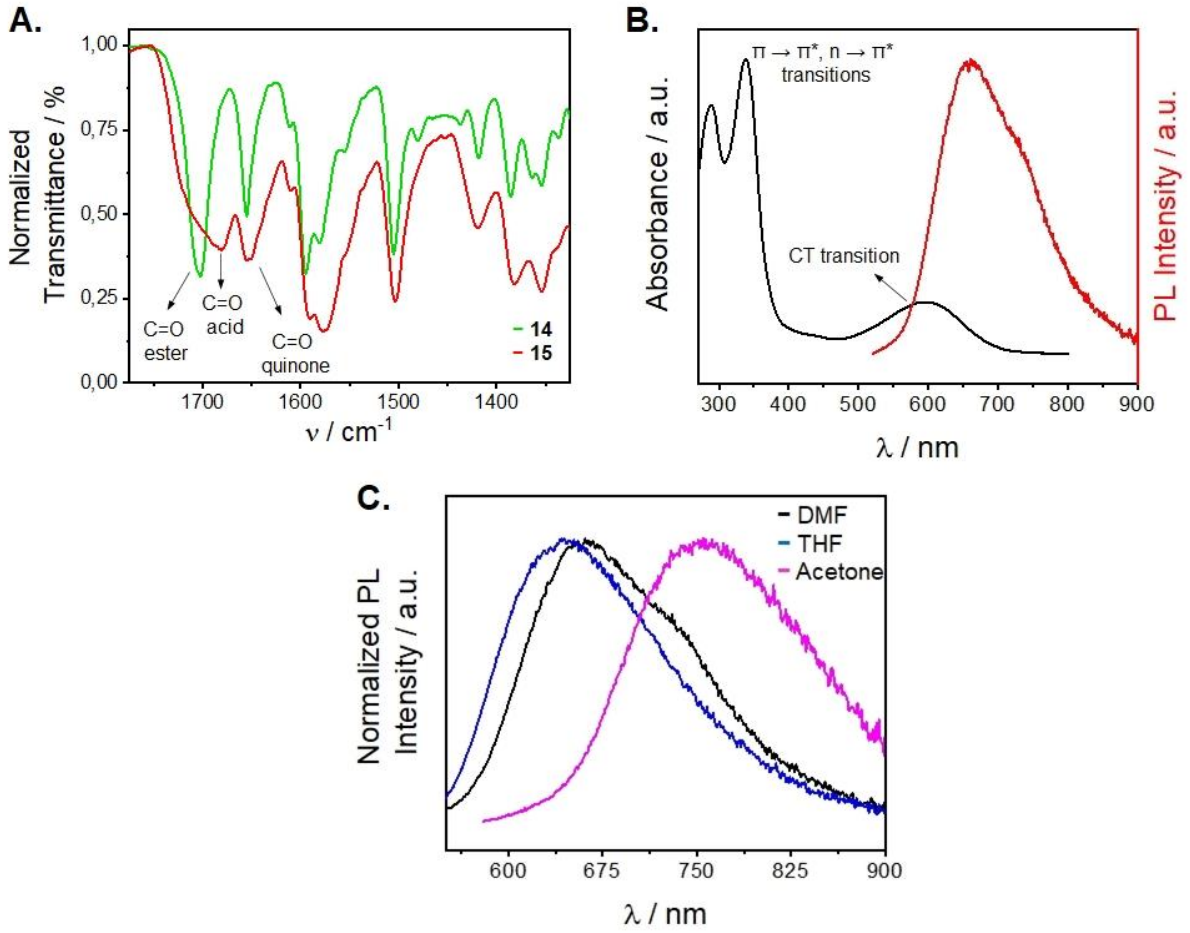

Figure 42. A. Section of the IR spectra of **14** and **15** highlighting carbonyl bands. **B.** Electronic absorption (black line) and emission (red line) spectra of **15** in DMF (10 µM). **C.** Emission spectra of **15** in different solvents (10µM).

2.3.2. Construction of polymeric anthanthrone-derived coordination frameworks

Having a soluble anthanthrone ligand attempts to obtain coordination polymers were carried out. Even though **15** is structurally related to the diphenylamine anthraquinone ligand, **9**, the reactivity was considerably distinct. No precipitation was observed with alkaline earth metals under distinct conditions. Nevertheless, a novel Zn(II) MOF, $[Zn_2(H_2O)_2(L^2)]_n$ (**16**), was synthesized upon heating **15** and zinc(II) nitrate at 80 °C in NMP as depicted in Scheme 12. This is, to the best of my knowledge, the first example of a MOF comprising an anthanthrone core.

Blue plates were obtained after 24 h and subjected to structural analysis. It is important to remind that such space-demanding ligands lead to less diffracting crystals and, therefore, to a crystallographic model with a greater number of constraints and rigid parameters. For that reason, bond lengths will not be discussed to avoid any misinterpretation of data. The crystal structure of **16** was solved and refined in the orthorhombic space group *Imma* (Figure 43A).

The ligand is fully deprotonated and acts as a four-connecting node. Each carboxylate bridges two equivalent zinc(II) atoms, building up paddle-wheel-like SBUs. The axial position is occupied by a water molecule. The coordination process can be followed and supported via infrared spectroscopy. In the spectrum of **16**, a broad absorption centered roughly at 3200 cm^{-1} appears, which is attributed to the O–H stretching of the coordinated water molecules. The characteristic absorption of carboxylic acids at 1680 cm^{-1} is completely absent, whereas the signal referring to the asymmetric vibration of the carboxylate rises as a shoulder band at 1550 cm^{-1}. The symmetric mode overlaps with other bands between 1450 – 1300 cm^{-1} yielding a broad, intense absorption. In contrast, the C=O stretching of the quinone is not shifted (Figure 43B).

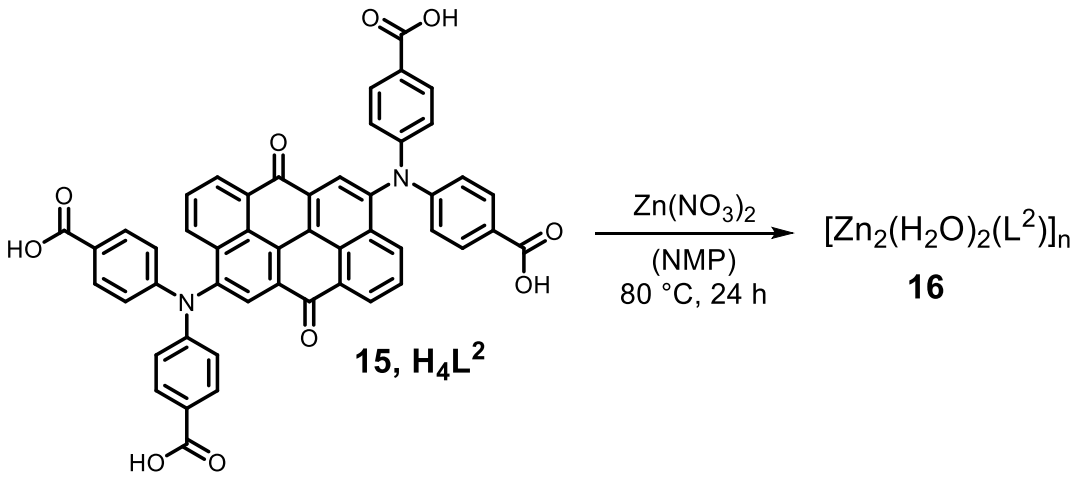

Scheme 12. The synthetic route towards **16**.

Fortunately, the structure is not interpenetrated, and no π-stacking is observed between ligands, leading to potential large accessible voids. Pore solvent removal was performed by solvent exchange with acetone for two days followed by heating at 65 °C under high vacuum. Phase purity and crystallinity after activation were confirmed via PXRD analysis (Figure 43C). The activation process was controlled via thermogravimetric analysis (Figure 43D). The recorded TGA curve for the non-activated MOF (black line) shows three distinguishable events. The first mass loss (T < 150 °C, 3 %) was attributed to the release of encapsulated and coordinated water molecules. The second mass loss (150 °C < T < 350 °C, 17 %) was attributed to the release of encapsulated NMP molecules. Decomposition and combustion of the framework were observed between 360 – 500 °C. The recorded curve for the activated MOF (blue line) shows only two events, showing successful activation since NMR release is no longer observed. Considering the “molar mass” of a $[Zn_2(H_2O)_2(L^2)]$ unit, 978.8 g mol^{-1}, the final ZnO content (19 %) is in good accordance with the expected value (17 %). A sample of **16** excited at 350 nm showed emission compatible with the ligand at 730 nm (Figure S49).

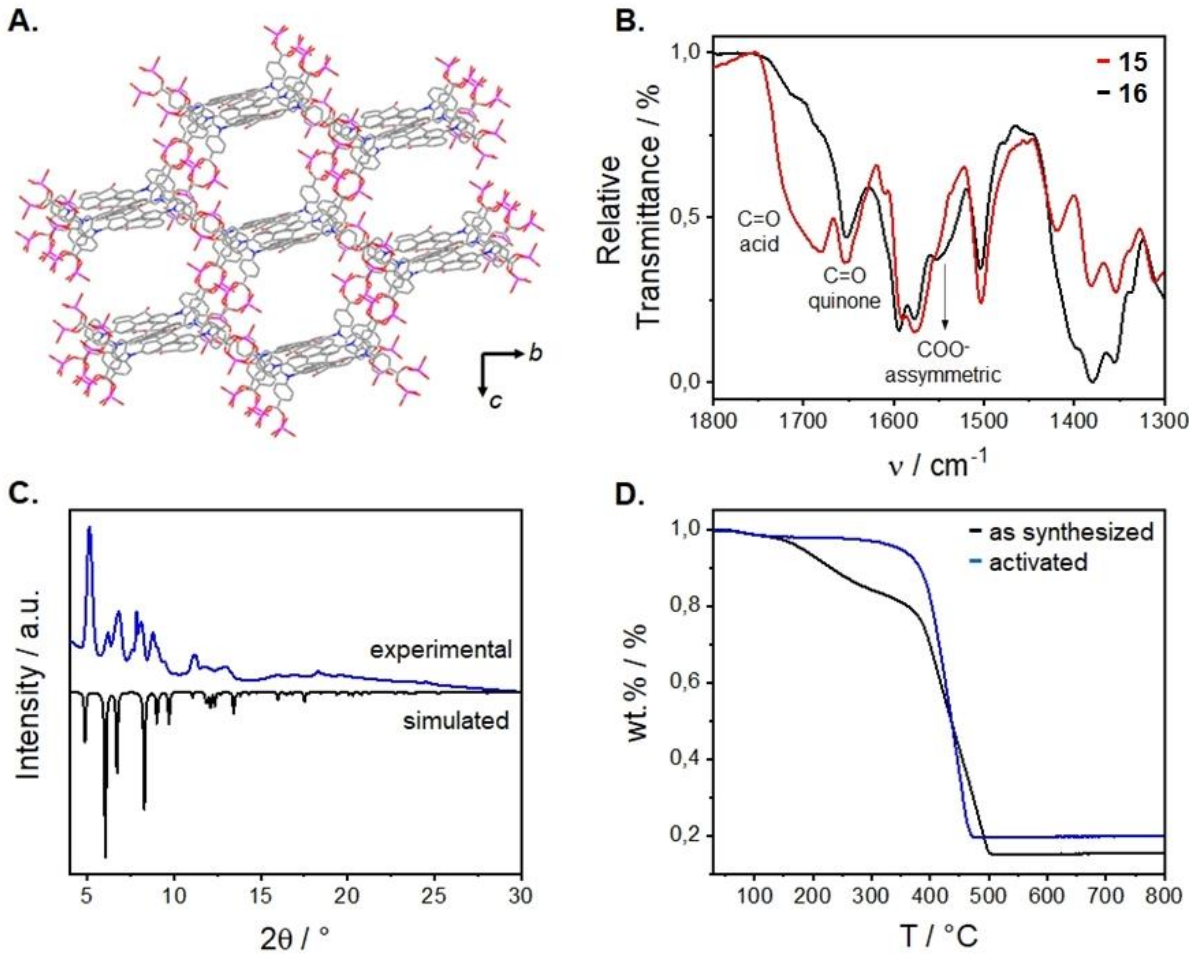

Figure 43. A. Representation of the crystal structure of **16**. Hydrogen atoms and disordered solvent molecules were omitted for clarity reasons. Atom colors are grey (C), blue (N), red (O), pink (Zn). **B.** IR spectra of **15** (red line) and **16** (black line), highlighting relevant bands. **C.** Simulated (from SCXRD, black line) and experimental (activated, blue line) powder diffractograms of **16**. **D.** Thermogravimetric curves of **16** as synthesized (black line) and after activation (blue line).

2.3.3. Appraisal of Hydroxyquinones as Building Blocks for Metal-Organic Frameworks

Quinizarin (1,4-dihydroxyanthraquinone, H_2Quinz) is a bright orange solid, which has been used for the complexation of several metal cations. Some existing species in metal-quinizarin solution are known to be highly fluorescent[105,106], which allow quinizarin to be used as a probe for spectrophotometric quantification metals in low concentrations.[107] Preparative synthesis of solid polymeric complexes has also been reported; however, most examples in the literature are not fully structurally characterized due to the fast precipitation and difficulty of growing larger crystals for SCXRD analysis.[108,109]

To investigate the formation of coordination frameworks with optically inert metals, quinizarin was reacted under different conditions with d^0 (Mg^{2+}, Ca^{2+}, Sr^{2+}, Ba^{2+}, Al^{3+}) and d^{10}

(Zn^{2+}, Cd^{2+}) metal nitrates. In general, no precipitate was obtained in neither alcoholic nor aqueous conditions at solvent boiling temperature and partial recrystallization of the ligand or metal nitrate (Ca^{2+}, $Sr^{2+,}$ and Ba^{2+}) was observed upon cooling. High-boiling solvents such as DMF and DMA also did not lead to precipitation, except with aluminum, which yielded a deep-purple amorphous precipitate. Reactions conducted in 1:1 ethanol/water mixtures at 150 °C led to somewhat crystalline precipitate formation (Mg^{2+}, Al^{3+}, Cd^{2+} and Ti^{4+}, Figure 44); however, particle size was not large enough for SCXRD analysis. Even though titanium(IV) is not photo/redox-inert, one attempt was conducted due to its d^0 shell and fondness for octahedral geometry. From the powder diffractograms, magnesium, aluminum, and titanium seem to generate structurally comparable complexes, which is probably due to preference for an octahedral coordination sphere. To promote reactivity, deprotonation of the phenolic groups was carried out using aqueous sodium hydroxide. Unfortunately, some reaction mixtures yielded purple-colored amorphous precipitates after a few minutes (Mg^{2+}, $Al^{3+,}$ and Cd^{2+}) and some did not react even after three days at solvothermal conditions (Ca^{2+}, Sr^{2+}, Ba^{2+}). Possibly the formation of the metal hydroxides hinders any reactivity of the heavier alkaline earth metals. Although most attempts under basic conditions were unsuccessful, the addition of zinc nitrate to an alkaline methanolic quinizarin solution led to a bright red mixture and no direct precipitation. This stable solution was monitored at 60°C; however, no relevant precipitation was observed after heating it for an extended period (> 1 week). Because of that, different bipyridines were added as co-ligands to assist the crystallization. The attempted conditions are presented in Table 2.

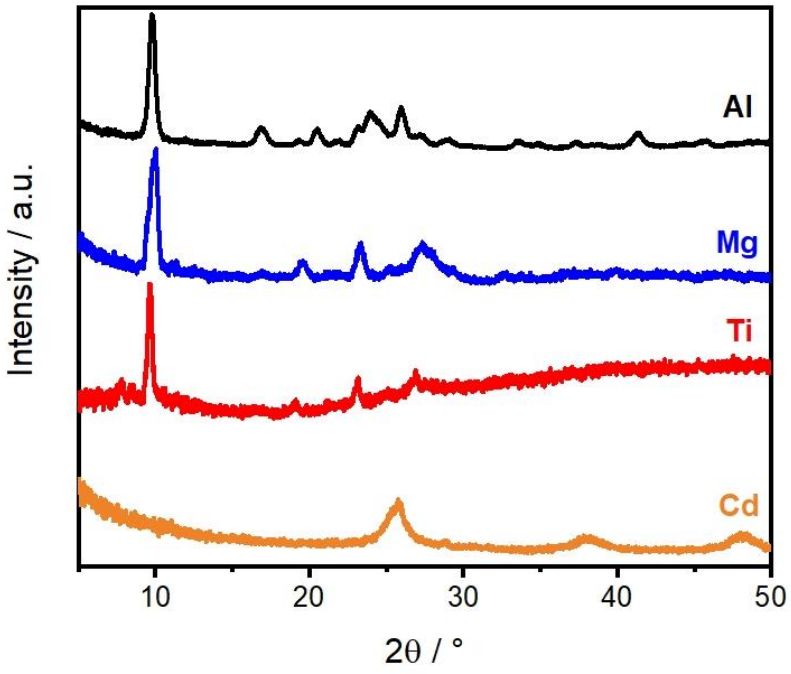

Figure 44. Powder diffractograms of the isolated products from the reactions of quinizarin with different metals in EtOH/H_2O mixtures.

Table 2. Attempted reaction mixtures for the synthesis of coordination polymers with quinizarin and different bipyridines as coligands.

	E1	E2	E3	E4
Quinizarin (sat. in MeOH) [a] / mL	2	2	2	2
NaOH (aq., 0.1 M) / µL	10	10	10	10
$Zn(NO_3)_2 \cdot 6H_2O$ / mg	20	20	20	20
2,2-Bipyridine / mg	5	–	–	–
4,4-Bipyridine / mg	–	5	–	–
4,4-Azopyridine / mg	–	–	5	–
1,2-bis(4'-pyridyl)ethane / mg	–	–	–	5
Crystalline precipitate	no	yes	no	yes[c]

[a]A saturated solution was prepared via sonication of a methanolic suspension of quinizarin followed by filtration through a 0.2 µm PTFE syringe filter.

[b]All reaction mixtures were heated at 60 °C for 18 hours in 4 mL sealable glass vials.

[c]Crystallization could already be observed after 10 min at 60 °C.

The reaction in presence of 4,4-bipyridine (4,4-bpy) yielded glittering purple crystals, which were suitable for SCXRD. The structure was solved and refined in the monoclinic space group *C*2/*c* and revealed a novel metal-organic framework with formula $[Zn_2(NO_3)_2(Quinz)(4,4\text{-bpy})_2]_n$ (**17**). The overall structure can be described as a two-fold interpenetrated network built up from concurrent zigzag strands (Figure 45B). The quinizarin ligand is found in its dianionic form and coordinates as an acac-like bidentate ligand. All four C–O bonds are virtually equidistant (~1.28 Å), supporting delocalization of the negative charge. Small deviations of the ideal valence angles of the oxygenated groups are observed, probably for more effective orbital overlap. The zinc(II) atoms are coordinated in a distorted octahedral fashion (Figure 45A). The quinizarin ligand occupies one equatorial and one axial position of each coordination polyhedron. The average $Zn–O_{Quinz}$ bond distance is 2.0 Å. Likewise, one equatorial and the remaining axial position are filled by two distinct 4,4-bipyridine molecules. The $Zn–N_{bpy}$ bond distances are slightly longer, on average 2.1 Å. The coordination sphere is fulfilled by a bidentate nitrate ligand, with $Zn–O_{nitrate}$ around 2.2 Å.

Phase identification and purity were checked using PXRD (Figure 45C). The complex is very soluble in polar coordinating solvents such as DMF and DMSO and labile in presence of mineral acids and bases. A ^{1}H NMR spectrum of a digested sample of **17** was in good accordance with the expected ratios from the structural model and was used to determine the amount of pore solvent, suggesting the formula $[Zn_2(NO_3)_2(Quinz)(4,4\text{-bpy})_2]_n \cdot CH_3OH$. Thermogravimetric analysis of **17** (Figure 45D) is also consistent with the structural model. The curve shows multiple events and suggests stability of the framework up to 250 °C. The initial

mass loss (2 %) is attributed to the desolvation of the network and corresponds to 0.5 equivalents of methanol per $[Zn_2(NO_3)_2(Quinz)(4,4\text{-bpy})_2]$ unit. The lower amount of methanol might arise from the gradual loss of the volatile pore solvent. The MOF decomposition and combustion represent the greatest mass loss (77 %) and comprise distinct sequential events. The remaining solid after MOF combustion is assumed to be zinc oxide (21 %) and is in good agreement with the expected value (20 %). A powder sample excited at 350 nm showed emission at 670 nm (Figure 45E).

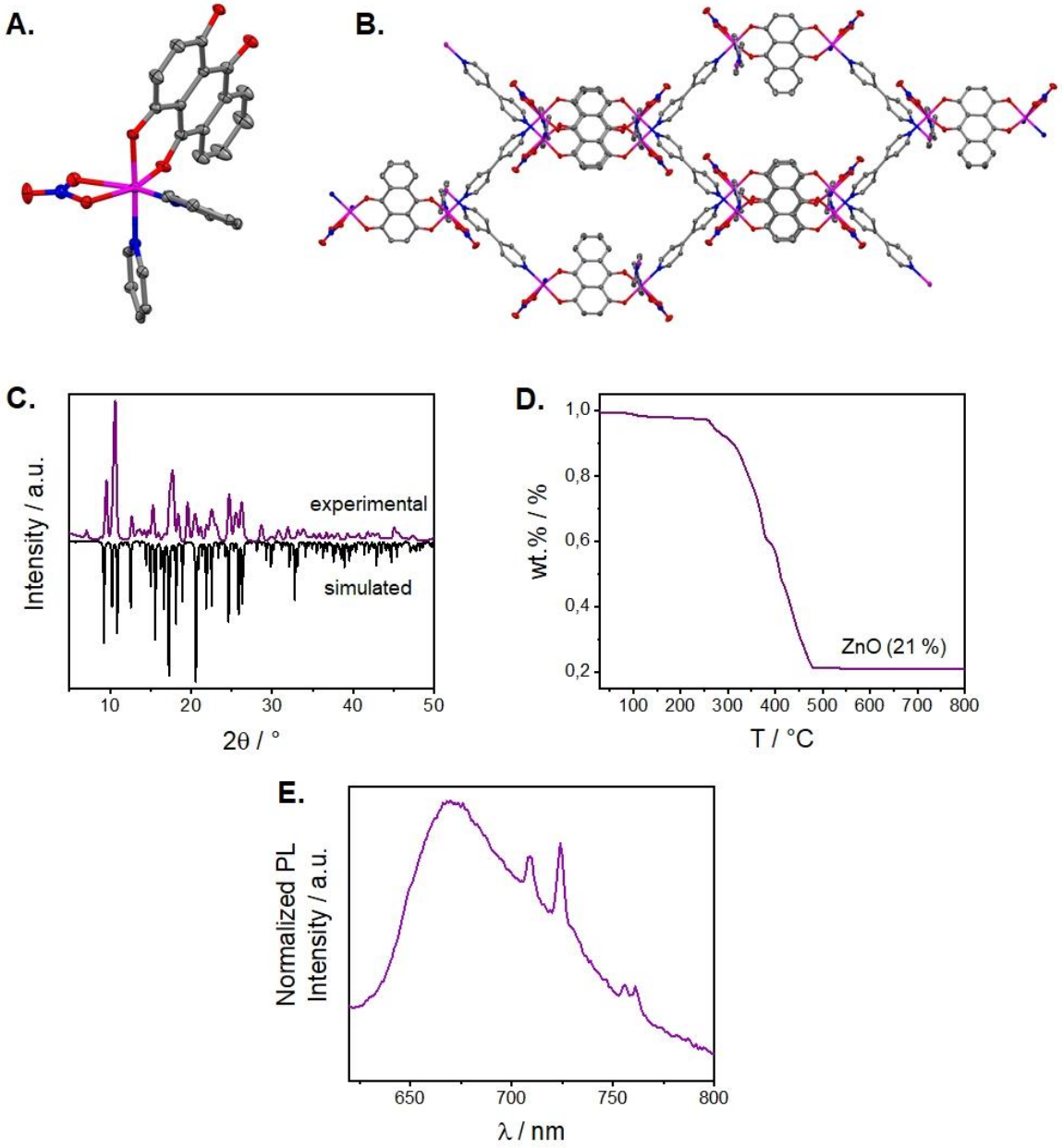

Figure 45. Representation of the crystal structure of **17** displaying **A.** the octahedral coordination of the Zn(II) centers and **B.** the overall structure built up from overlapping 1D zigzag chains. **C.** Simulated (from SCXRD data, black line) and experimental (purple line) PXRD data. **D.** Thermogravimetric curve of **17**. All ellipsoids are shown at the 50% probability level. Atom colors are grey (C), blue (N), red (O), pink (Zn). **E.** Emission spectrum of a powder sample of **17**.

The reaction in presence of 1,2-bis(4'-pyridyl)ethane (Et-bpy) yielded seeming purple crystals, also suitable for SCXRD. The structure was solved and refined in the triclinic space group *P* -1 and comprises zigzag 1D strands with formula $[Zn(NO_3)_2(Et\text{-}bpy)]_n$ (**18**). In this case, no quinone ligand was incorporated. The synthesis was reproduced without quinizarin and yielded as expected a white crystalline powder. The zinc(II) atoms are pentacoordinated and the geometry is best described as distorted square pyramidal. The polyhedron base is built up from one pyridine nitrogen and three oxygen atoms of two distinct nitrate ligands. The apical position is occupied by a different pyridine molecule, which connects it to the top of the next coordination site (Figures 46A and 46B).

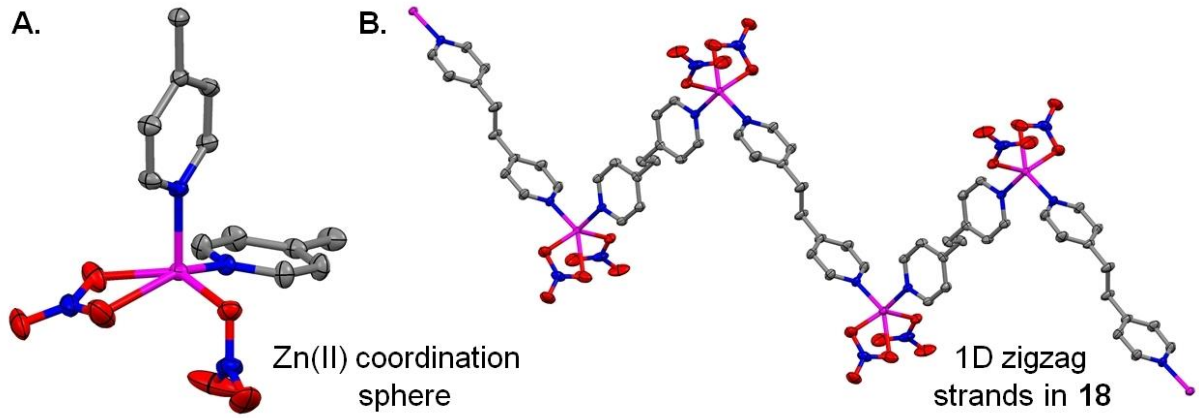

Figure 46. Representation of the crystal structure of **18** displaying the **A.** coordination of the Zn(II) centers; and **B.** 1D zig-zag chain structure. Aromatic hydrogen atoms were omitted for clarity reasons. All ellipsoids are shown at the 50% probability level. Atom colors are grey (C), blue (N), red (O), pink (Zn).

2.3.4. Prospective ideas on applications of anthanthrone and quinizarin-derived MOFs

The first part of this chapter was mainly synthetic and aimed at the incorporation of a novel building block into MOFs, namely anthanthrone. This was achieved by using a bis(diphenylamino)anthanthrone ligand and zinc(II) paddle-wheels as inorganic nodes. Because of the bulkier core, the ligands are not able to stack in the solid state as observed when using the smaller parent compound anthraquinone. This allowed the synthesis of a non-interpenetrated MOF, which could potentially overcome the diffusion hindrances observed in the anthraquinone-based compounds presented in chapter two. This could eventually lead to more active systems and the photooxidation of larger sulfides, such as thioanisole (methyl phenyl sulfide) derivatives, and relatable functional groups, like benzylic alcohols.

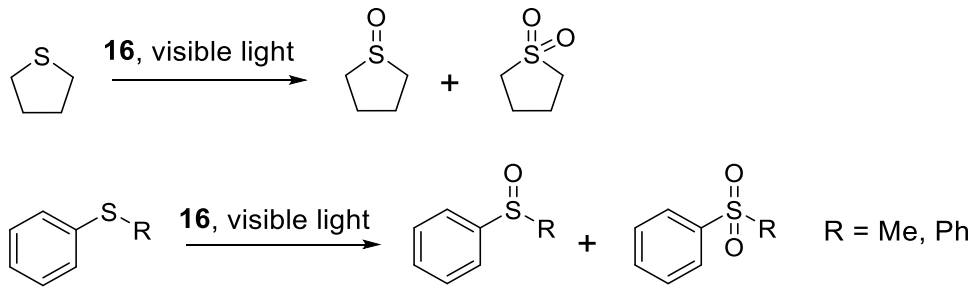

Scheme 13. Possible test photooxidation reactions to evaluate the photocatalytic properties of **16**.

In the second part, the reactivity of quinizarin towards different closed-shell metals (d^0 or d^{10}) was studied. Unfortunately, most of the experiments did not lead to any relevant result or only to microcrystalline powders, which could not be used for SCXRD structure determination. Nevertheless, one zinc(II) MOF was obtained, but the lability in presence of coordinating solvents and lack of strong photoluminescence would probably hinder its further application. Based on that, I would suggest the exploration of non-innocent metals with hydroxyquinones. Many examples are showing their relevance on conductive and magnetic coordination polymers (see 'The Ouverture' for further details).

The reported Fe-quinizarin MOF, named FeQ, is claimed to be a semiconducting material.[70] Nonetheless, there are a few gaps in the publication, which could allow further steps to be taken towards mixed-valence systems. The authors do not discuss profoundly the oxidation state of the metal, which one could assume is Fe(III) (Fe(II) acetate is used as the iron source) due to the metal:ligand ratio in the crystal structure and the aerobic synthetic conditions. However, the authors removed all electron density from the pores (SQUEEZE routine), which puzzles the interpretation of oxidation states of non-innocent motives. The authors also do not provide a powder diffractogram to show the phase purity of the material before appraising its properties. Considering my attempts to reproduce this MOF, I do believe its synthesis is not as trivial as reported. Nevertheless, the existence of FeQ opens a few possibilities for synthetic exploration. The reported MOF could be, for example, activated and post-synthetically reduced in different degrees. Alternatively, reduced states could be obtained directly from synthesis under inert conditions. The conductive and magnetic properties should then be measured. As stated, I failed to reproduce FeQ. In fact, all different attempted conditions led to completely amorphous products. For comparison, I tried the reported conditions with the vicinal metals, vanadium, and cobalt. Interestingly, the reaction with $VO(SO)_4$ led to a very crystalline precipitate, whereas with cobalt to a nearly amorphous product. Unfortunately, SCXRD structure determination was not doable considering the particle size.

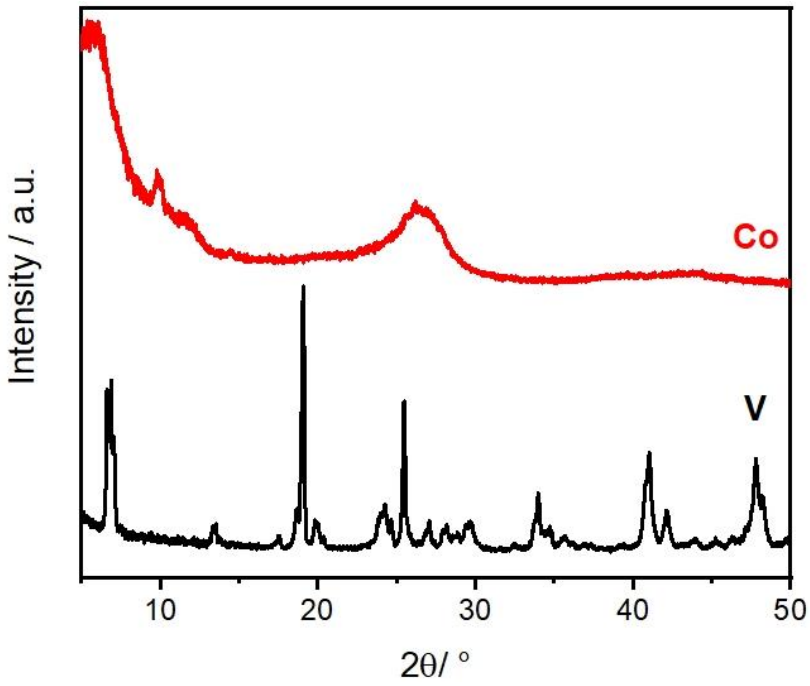

Figure 47. Powder diffractograms of the isolated products from the reactions of quinizarin with $VO(SO_4)$ (black line) and $Co(OAc)_2$ (red line) in $EtOH/H_2O$ mixtures.

The semiconducting character of FeQ was attributed to the mobility of electrons between aromatic rings through space (π-stacking). Based on that, it would be reasonable to assume that increasing the aromatic surface could potentially lead to higher conductivity. Therefore, I synthesized 5,7,12,14-tetrahydroxypentacene-6,13-dione as a potential ligand. The compound, as many quinone dyes, is quite insoluble in common organic solvents but is soluble enough to generate fluorescent pink solutions. The crystal structure was determined by slow recrystallization in argon saturated DMSO. It was observed that the solutions would fade within a few days if exposed to air. I believe that the hydroxy groups are active enough to reduce dioxygen and generate a polyketone. The fading is not observed when the solvents are previously bubbled with argon. When exposed to metal cations (Li^+, Zn^{2+}), the DMF and DMSO solutions immediately turned blue, indicating possibly a proton dislocation reaction. However, these solutions were stable and did not lead to any precipitate when heated at 100 °C. When iron(II/III) and copper(II) salts were used, the formation of black and purple precipitates, respectively, was observed. Even though some initial experiments show that the linker might react with late transition metals, further experiments were not conducted in the timeframe of this thesis and are encouraged in future projects.

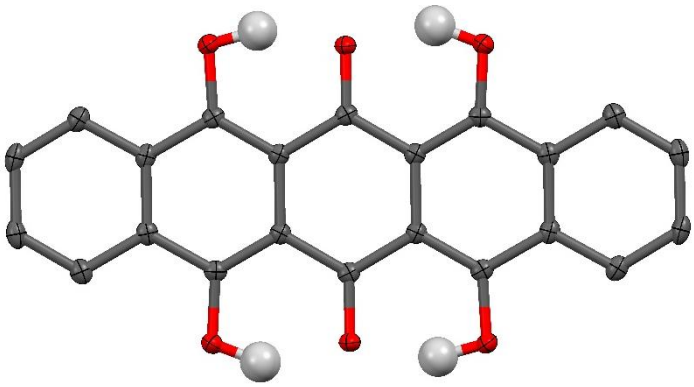

Figure 48. A. Molecular structure of 5,7,12,14-tetrahydroxypentacene-6,13-dione as determined by SCXRD. Aromatic hydrogen atoms. All ellipsoids, if shown, are at the 50% probability level. Atom colors are grey (C), red (O), white (H).

3. CONCLUSION

This thesis comprises contributions to the coordination and solid-state chemistry of anthraquinones. Distinct anthraquinone-based linkers have been synthesized and incorporated into metal-organic frameworks. The reticular structures were determined and analyzed via single-crystal X-ray diffraction. The physical properties of the materials and potential applications were then investigated.

In the first part, a dipyridyl-substituted anthraquinone (2,6-di(pyridin-4-yl)-9,10-anthraquinone, DPAq) was synthesized to be incorporated as a redox-active linker into crystalline frameworks. The reduced anthrahydroquinone form, DPAHq, was accessible by using dimethylformamide as a mild reducing agent under solvothermal conditions and was isolated as a hydrogen-bonded framework, which was surprisingly stable under aerobic conditions. No oxidation was observed during weeks when kept in the solid state; however, almost instant oxidation occurred when exposed to dioxygen in solution. This supports hydrogen bonding as a substantial stabilization factor. The oxidation state of the organic linker could also be selectively controlled when constructing metal-organic architectures. When dimethylformamide was used as the reaction solvent, a coordination network containing the reduced ligand was obtained. In contrast, the non-reducing analog dimethylacetamide led to frameworks comprising the linker in its oxidized form. Additionally, it was shown that the anthraquinone-anthrahydroquinone redox pair could be switched reversibly even after the incorporation in the solid state by a thermal treatment/soaking procedure – going along with the formation of hydrogen peroxide from dioxygen during the oxidation process.

In the second part, a novel bis(diphenylamino)anthraquinone tetratopic linker was synthesized and characterized. Both ester and acid were orange/red-emissive and their emission was solvent polarity-dependent. Four novel alkaline earth metal-based metal-organic frameworks could be synthesized and structurally characterized. The emissive properties of the ligands in the coordination networks were comparable to those of the free linker. Nevertheless, neat samples of all metal-organic frameworks showed higher quantum yield than a neat sample of the uncoordinated ligand. After activation, three materials showed accessible porosity and, therefore, potential application for photocatalysis. The free linker was able to selectively oxidize tetrahydrothiophene to its sulfoxide heterogeneously under visible light. The Mg-based material showed also relatable catalytic properties; however, diffusion of the substrate into the pores was determined to be a relevant limiting factor. Small alkyl sulfides could be oxidized, whereas bulkier aromatic derivatives remained unreacted.

In the last part, the design of quinone-based architectures with potential greater porosity was attempted. For this purpose, the quinone core was expanded to a six-condensed system, namely, anthanthrone. The novel bis(diphenylamino)anthranthrone tetratopic linker in presence of zinc(II) generated a non-interpenetrated metal-organic framework, in which the ligands also do not stack and a higher diffusion rate is conceivable. Additionally, the utilization of a known pigment, quinizarin, for the construction of new metalorganic materials has been investigated. The hydroxyquinone did not show strong reactivity in a neutral medium. The fast precipitation in presence of bases led to amorphous precipitates. Nonetheless, a polymer could be characterized with zinc(II) using 4,4-bypyridine as coligand. The ligand is fully deprotonated and showed red fluorescence emission.

These results exemplify how the electrochemistry and photochemistry of anthraquinones could be explored in metal-organic frameworks. The reversible quinone/hydroquinone reaction was exploited for the development of switchable materials and hydrogen peroxide synthesis. The design of charge transfer chromophores led to red-emitting photocatalytic active materials in sulfide oxidation reactions. Lastly, the incorporation of unexplored anthanthrone dyes into coordination polymers could potentially lead to more active catalysts. The contributions presented in this thesis should motivate further work on quinone-based materials and their applications.

4. EXPERIMENTAL

4.1. General Procedures

All reagents were obtained from commercial sources and used as received unless otherwise stated. Deuterated solvents were purchased from Sigma Aldrich. Solution state ^{1}H NMR spectra of ligands and digested MOFs were recorded on a Bruker UltraShield 400 MHz spectrometer at 298 K. Residual solvent peaks ($CDCl_3$: δ = 7.26 ppm, DMSO-d_6: δ = 2.50 ppm) were used as internal references for chemical shifts. Elemental analysis was performed in the Microanalytical Laboratory of the Catalysis Research Center – Technical University of Munich. PXRD data were collected on a PANanalytical Empyrean X-ray diffractometer (Cu-K_α λ = 1.5406 Å) or on a Rigaku MiniFlex benchtop X-ray diffractometer. TGA measurements were performed on a Mettler Toledo TGA/DSC 3+ at a 5 K min^{-1} heating rate, under a constant stream of synthetic air. Solution-state UV-Vis spectra were recorded on an Agilent Cary 60 UV-Vis spectrometer. FTIR data were collected on an Elmer Perkin Frontier FT-IR in the 400 – 650 cm^{-1} range. Electrochemical measurements were recorded on a Metrohm Autolab PGSTAT302N potentiostat using a standard electrode configuration: a glassy carbon working electrode, a Pt mesh as the counter electrode, and a saturated Ag/AgCl reference electrode. Tetrabutylammonium hexafluorophosphate was used as the supporting electrolyte. Photophysical measurements were performed by M.Sc. Sebastian Weishäupl at the chair of Prof. Dr. Jürgen Hauer, Technical University of Munich on an FS5 spectrofluorometer from Edinburgh Instruments. Quantum yield measurements in solution were performed in a Quantaurus-QY device. Quantum yield of neat solid samples and PMMA films were partially carried by B.Sc. Korbinian Geißer. Data treatment and analysis by myself.

Single crystal X-ray diffraction data were collected at 100(2)K using a Bruker D8 Venture diffractometer equipped with a PHOTON100 CMOS detector, a TXS rotating anode with MoK_α radiation (λ = 0.71073 Å) and the APEX3 software package[110] or a Bruker D8 Venture diffractometer with a PHOTON2 CPAD detector, an IμS 2 microsource with MoK_α radiation (λ= 0.71073 Å), using the APEX3 software package. The data collection was performed on single crystals coated with perfluorinated ether. The crystals were fixed on top of a kapton micro sampler and frozen under a stream of cold nitrogen. A matrix scan was used to determine the initial lattice parameters. The raw area detector data frames were reduced and corrected for absorption effects using the SAINT[111] and SADABS[112] programs with multiscan absorption correction. Final unit cell parameters were determined by least-squares refinement of independent reflections taken from the data sets. The structure was solved by intrinsic phasing with SHELXT.[113] Difference Fourier calculations and full-matrix least-squares refinement against F^2 were performed by SHELXL-2014/7 together with SHELXLE.[114,115] The

SQUEEZE routine was implemented in PLATON[116] and was used to remove the contribution of the disordered electron density of solvent molecules in the void spaces. Hydrogen atoms on carbon atoms could not be located in the Fourier difference maps and were calculated in ideal positions using a riding model (d(C-H) = 0.95 Å, Uiso(H) = 1.2Ueq(C)) or a rotating model for methyl groups (d(C-H) = 0.98 Å, Uiso(H) = 1.5Ueq(C)). Hydrogen atoms on hetero atoms (DPAHQ) could be found in the Fourier difference maps and were refined freely. Hydrogen atoms on hetero atoms that could be found in the Fourier difference maps were calculated in ideal positions using a rotating model ((d(O-H) = 0.82 Å, Uiso(H) = 1.5Ueq(C)) for stable refinement. Non-hydrogen atoms were refined with anisotropic displacement parameters. Disordered structure refinement (DSR)[117,118] was implemented for the split layer refinement. Images of the crystal structures were generated with Mercury.[119]

4.2. Synthetic Part

2,6-dibromoanthraquinone (1). 2,6-dibromoanthraquinone was synthesized according to a previously reported literature procedure.[85] $CuBr_2$ (1.77 g, 7.92 mmol) was added to a 50 mL round-bottom flask and dissolved in 12 mL acetonitrile to yield a deep green solution. *t*-Butyl nitrite (0.97 g, 9.10 mmol) was slowly given (5 min) to the stirring mixture. 2,6-Diaminoanthraquinone (0.73 g, 3.06 mmol) was then added in small portions (10 min). The resulting brownish mixture was left to stir and heat for 4 h at 60 °C. Once the flask reached room temperature, 40 mL 6 M HCl was poured, causing immediate precipitation of a brown solid. The crude product was vacuum filtered, thoroughly washed with H_2O and EtOH, until the alcoholic washing was colorless. Finally, the solid was dried at 100 °C overnight to yield 1.052 g of **2.1** (2.87 mmol, 91% yield) as a pale brown powder. ^{1}H NMR (400 MHz, $CDCl_3$): δ 8.44 (d, ^4J = 1.6 Hz, 2H), 8.17 (d, ^3J = 8.1 Hz, 2H), 7.94 (d, ^3J = 9.8 Hz, 2H) ppm. Elemental analysis: *expected* C 45.94, H 1.65 *found* C 45.63, H 1.53

2,6-Di(pyridin-4-yl)-9,10-anthraquinone (DPAq, 2). 2,6-Dibromoanthraquinone (366 mg, 1.0 mmol), K_3PO_4 (638 mg, 3.0 mmol), and 4-pyridinylboronic acid (271 mg, 2.2 mmol) were weighed out in a Schlenk pressure tube. The flask was evacuated (residual pressure ~10^{-3} mbar) and backfilled with argon 3 times. 20 mL 1,4-dioxane were then added and the suspension was saturated with argon for at least 45 min. $Pd(OAc)_2$ (22.5 mg, 0.1 mmol) and dppf (110 mg, 0.2 mmol) were thereafter added in one portion under positive argon pressure and the mixture was heated to reflux for 2 days. After completion of the reaction, the resulting brown suspension was left to cool down and was diluted with EtOAc (30 mL). The precipitate was separated by vacuum filtration and washed with EtOAc (50 mL) and excess of water. The desired product was recrystallized from DMF and obtained as pale beige needles. For elemental analysis, a small sample was dried on high vacuum. (225 mg, 62 % yield). ^{1}H NMR (400 MHz, $CDCl_3$): δ 8.79 (d, 4H, $^3J_{H–H}$ = 6 Hz) 8.63 (d, 2H, $^4J_{H–H}$ = 1.6 Hz) 8.49 (d, 2H,

$^{3}J_{H\text{-}H}$ = 8 Hz) 8.11 (dd, 2H, $^{3,4}J_{H–H}$ = 8, 1.6 Hz) 7.67 (d, 4H, $^{3}J_{H–H}$ = 6 Hz) ppm. Selected IR bands: v 1672, 1590, 1396, 1314, 1273, 1244, 1170, 957, 814 cm^{-1}. UV-Vis (CH_2Cl_2): λ 276, 341 nm. Elemental analysis *expected* C 79.55 H 3.89 N 7.73 *found* C 79.73 H 3.83 N 7.70.

2,6-Di(pyridine-4-yl)-9,10-anthrahydroquinone (DPAHq, 3). DPAq (110 mg, 0.3 mmol) was suspended in 10 mL of a 4:1 DMF/H_2O mixture. $AlCl_3$ (0.4 mg, 0.003 mmol) was added, and the resulting mixture was heated to 100 °C for 18 h. The precipitate was collected by filtration, washed with DMF, water, and EtOH, then air-dried and isolated as a glittering dark wine-red solid (95 mg, 87 % yield). For elemental analysis, a small sample was dried on high vacuum. ^{1}H NMR (400 MHz, DMSO-d_6, F_3CCOOH): δ 9.15 (d, 2H, $^{4}J_{H–H}$ = 1.6 Hz) 9.03 (d, 4H, $J_{H–H}$ = 6.8 Hz) 8.62 (m, 6H) 8.07 (dd, 2H, $^{3,4}J_{H\text{-}H}$ = 9.2, 1.6 Hz) ppm. IR: v 3000 (broad), 1617, 1597, 1418, 1385, 1308, 1207, 1147, 1060, 841, 806 cm^{-1}. Elemental analysis: *expected* C 79.11 H 4.43 N 7.69 *found* C 79.34 H 4.35 N 7.65.

$[Zn_2(BDC)_2(DPAHq)_2]_n$·4DMF (4). $Zn(NO_3)_2·6H_2O$ (36.0 mg, 0.12 mmol), 1,4-benzenedicarboxylic acid (9.6 mg, 0.06 mmol) and DPAq (10.8 mg, 0.03 mmol) were suspended in 7.5 mL of a 4:1 DMF/H_2O mixture and heated at 100 °C for 18 h. The precipitate was separated by filtration while hot to prevent recrystallization of the linker and was washed with DMF and EtOH. The desired phase was separated from colorless impurities by flotation using a $CHCl_3$/$CHBr_3$ mixture and washed again with EtOH. The phase was obtained as dark wine-red crystals and was stored under a saturated DMF atmosphere. Elemental analysis: *expected* C 61.67 H 4.63 N 7.57 *found* C 60.88 H 4.86 N 7.81.

$[Zn_2(BDC)_2(DPAq)]_n$·DMA (5). $Zn(NO_3)_2·6H_2O$ (12.0 mg, 0.04 mmol), 1,4-benzenedicarboxylic acid (3.2 mg, 0.02 mmol) and DPAq (3.6 mg, 0.01 mmol) were suspended in 2.0 mL DMA and heated at 100 °C for 18 h. The precipitate was separated by filtration while hot to prevent recrystallization of the linker and was washed with DMA and EtOH. The phase was isolated as a glittering tan yellow powder. Elemental analysis: *expected* C 58.15 H 3.41 N 4.62 *found* C 53.94 H 4.02 N 5.07.

$[Cd_2(BDC)_2(DPAq)_2]_n$·DMA (6). $Cd(NO_3)_2·4H_2O$ (12.0 mg, 0.04 mmol), 1,4-benzenedicarboxylic acid (3.2 mg, 0.02 mmol) and DPAq (3.6 mg, 0.01 mmol) suspended in 2.5 mL of a 4:1 DMA/H_2O mixture and heated at 100 °C for 18 h. The precipitate was separated by filtration while hot to prevent recrystallization of the linker and was washed with DMA and EtOH. The phase was isolated as dark yellow crystals. Elemental analysis: *expected* C 59.83 H 3.30 N 5.13 *found* C 57.51 H 3.67 N 5.47.

Redox Switching of 4. For the thermal oxidation, **4** was heated to 100 °C in an oven for 3 hours. The dark-red powder turned yellow. A solution ^{1}H NMR of the sample in degassed TFA solution in DMSO-d_6 was recorded. For the reduction procedure, a 4:1 DMF/H_2O solution with

a catalytic amount of $AlCl_3$ was prepared. The obtained yellow solid was then soaked in the solution and heated at 90 °C for 24 hours to yield a dark-colored powder. A ^1H NMR spectrum was recorded as described previously. PXRDs were recorded after each half cycle. The procedure was repeated for three consecutive cycles.

Qualitative Peroxide Detection. A spatula tip of **4** was heated at 100 °C for 3 hours in a sealed vial. Afterward, 0.1 mL distilled water was added via syringe. The mixture was left to sit for 15 min and then a low concentration peroxide stripe was immersed into the aqueous phase. A color change to blue was immediate.

Quantitative Peroxide Detection. 5.0 mg of **4** were heated at 100 °C for 4 hours in a sealed vial. Afterward, 0.5 mL distilled water was added via syringe. The mixture was left to sit for 1 hour and further diluted to 2.0 mL with water. The aqueous phase was separated by filtration and 10 µL were given to 3.0 mL of a modified FOX reagent solution[26] (50 µM xylenol orange, 125 µM $FeSO_4$, 12.5 µM H_2SO_4, 50 mM D-glucose). A UV-Vis spectrum of the resulting mixture was recorded after 30 min and the H_2O_2 concentration was calculated based on a calibration curve. Absorbance values were read at λ = 560 nm.

Diethyl 4,4'-azanediyldibenzoate (7). 7 was synthesized according to a modified literature procedure.[101] A Schlenk-flask was evacuated (residual pressure ~10^{-3} mbar) and backfilled with argon 3 times before use. 200 mL toluene were then added and saturated with argon for at least 45 min. Ethyl 4-bromobenzoate (4.6 g, 20.0 mmol), ethyl 4-aminobenzoate (4.0 g, 24.0 mmol), Cs_2CO_3 (9.8 g, 30.0 mmol), $Pd(OAc)_2$ (224.5 mg, 1.0 mmol), and BINAP (1.2 g, 2.0 mmol) were thereafter added in one portion under positive argon pressure and the mixture was heated to reflux for 18 h. After completion of the reaction, the resulting suspension was left to cool down, diluted with EtOAc, and filtered. The solvent was completely removed under reduced pressure. The residual solid was then dissolved in EtOAc, washed with 2M HCl, and dried over $MgSO_4$. Filtration over silica (DCM:EtOAc 10:1 as eluent) yielded the desired product as a yellow solid (6.2 g, 99 % yield). ^1H NMR (400 MHz, $CDCl_3$): δ 8.01 (d, 4H, $^3J_{H–H}$ = 8.7 Hz) 7.15 (d, 4H, $^3J_{H-H}$ = 8.7 Hz) 6.35 (s, 1H, broad) 4.38 (q, 4H, $^3J_{H–H}$ = 7.1 Hz) 1.41 (t, 6H, $^3J_{H–H}$ = 7.1 Hz) ppm. Elemental analysis *expected* C 69.00 H 6.11 N 4.47 *found* C 69.11 H 6.33 N 4.03.

Tetraethyl 4,4',4'',4'''-((9,10-dioxo-9,10-dihydroanthracene-2,6-diyl)bis(azanetriyl))tetrabenzoate (8, Et_4L). A Schlenk-flask was evacuated (residual pressure ~10^{-3} mbar) and backfilled with argon 3 times prior to use. 60 mL toluene were then added and saturated with argon for at least 45 min. 2,6-Dibromoanthraquinone (1.1 g, 3.0 mmol), **7** (2.1 g, 6.6 mmol), Cs_2CO_3 (2.9 g, 9.0 mmol), $Pd(OAc)_2$ (67.5 mg, 0.3 mmol) and BINAP (372.0 mg, 0.6 mmol) were thereafter added in one portion under positive argon pressure and the mixture was heated to reflux for 2 days. After completion of the reaction, the resulting red-brown suspension was

left to cool down and the solvent was removed under reduced pressure. The residual solid was washed with EtOAc and filtered over silica (DCM:EtOAc 10:1 as eluent) to yield the desired product as a neon orange solid (1.9 g, 76 % yield). ^{1}H NMR (400 MHz, $CDCl_3$): δ 8.14 (d, 2H, $^{3}J_{H–H}$ = 8.6 Hz) 8.02 (d, 8H, $^{3}J_{H–H}$ = 8.8 Hz) 7.90 (d, 2H, $^{4}J_{H-H}$ = 2.4 Hz) 7.37 (dd, 2H, $^{3,4}J_{H–H}$ = 8.6, 2.4 Hz) 7.18 (d, 8H, $^{3}J_{H–H}$ = 8.8 Hz) 4.39 (q, 8H, $^{3}J_{H–H}$ = 7.1 Hz) 1.40 (t, 12H, $^{3}J_{H-H}$ = 7.1 Hz) ppm. ^{13}C NMR (101 MHz, $CDCl_3$): δ 181.88, 166.27, 152.25, 150.06, 135.88, 131.91, 129.83, 128.59, 127.42, 127.37, 125.07, 120.55, 61.51, 14.83 ppm. ESI-MS (m/z): 831 $[M+H]^+$ UV-Vis (CH_2Cl_2): λ 314, 341, 370, 448 nm. Elemental analysis *expected* C 72.28 H 5.10 N 3.37 *found* C 72.43 H 5.12 N 3.42.

4,4',4'',4'''-((9,10-dioxo-9,10-dihydroanthracene-2,6-diyl)bis-(azanetriyl))tetrabenzoic acid (9, H_4L). 8 (1.5 g, 1.8 mmol) and NaOH (372.0 mg, 9.3 mmol) were suspended in 200 mL of a THF/H_2O mixture and heated to reflux for 18 h. After completion of the reaction, the resulting mixture was left to cool down and the organic phase was removed under reduced pressure. The aqueous phase was acidified to pH = 1 and the precipitate was filtered. The solid was washed with an excess of water and dried at 100 °C. The product was isolated as a deep dark red solid (1.3 g, 100 % yield). ^{1}H NMR (400 MHz, DMSO-d_6): δ 8.05 (d, 2H, $^{3}J_{H-H}$ = 8.6 Hz) 7.97 (d, 8H, $^{3}J_{H–H}$ = 8.6 Hz) 7.62 (d, 2H, $^{4}J_{H-H}$ = 2.6 Hz) 7.42 (dd, 2H, $^{3,4}J_{H–H}$ = 8.6, 2.6 Hz) 7.26 (d, 8H, $^{3}J_{H-H}$ = 8.6 Hz) ppm. ^{13}C NMR (101 MHz, DMSO-d_6): δ 180.79, 166.80, 151.46, 149.15, 134.85, 131.50, 129.39, 127.32, 127.22, 126.54, 125.09, 118.52 ppm. MS (m/z): 717 $[M–H]^–$, 718 $[M]^–$, 739 $[M–2H+Na]^–$. UV-Vis (DMF): λ 315, 336, 370, 448 nm. Elemental analysis *expected* C 70.19 H 3.65 N 3.90 *found* C 69.00 H 4.08 N 3.81.

Mg-MOF (10). 9 (35.0 mg, 0.05 mmol) was fully dissolved in 10 mL DMF in a sealable glass vial to yield an orange solution. 5 mL of an aqueous solution of $Mg(NO_3)_2{\cdot}9H_2O$ (90.0 mg, 0.3 mmol) was then added. The obtained mixture was heated at 80 °C for four days. The needle-shaped crystals were separated by filtration, washed with DMF and acetone, and then dried under a stream of argon. The MOF was isolated as glittering red needles and was stored under an inert atmosphere.

Ca-MOF (11). 9 (35.0 mg, 0.05 mmol) was fully dissolved in 10 mL DMA in a sealable glass vial to yield an orange solution. 5 mL of an aqueous solution of $Ca(NO_3)_2{\cdot}4H_2O$ (70.0 mg, 0.3 mmol) was then added together with 5 mL ethanol. The obtained mixture was heated at 80 °C for four days. The needle-shaped crystals were separated by filtration, washed with DMA and acetone, and then dried under a stream of argon. The MOF was isolated as glittering red needles and was stored under an inert atmosphere.

Sr-MOF (12). 9 (35.0 mg, 0.05 mmol) was fully dissolved in 10 mL DMF in a sealable glass vial to yield an orange solution. 5 mL of an aqueous solution of $Sr(NO_3)_2$ (63.0 mg, 0.3 mmol) was then added. The obtained mixture was heated at 80 °C for four days. The needle-shaped

crystals were separated by filtration, washed with DMF and acetone, and then dried under a stream of argon. The MOF was isolated as glittering red needles and was stored under an inert atmosphere.

Ba-MOF (13). 9 (35.0 mg, 0.05 mmol) was fully dissolved in 10 mL DMF in a sealable glass vial to yield an orange solution. 2.5 mL of an aqueous solution of $Ba(NO_3)_2$ (78.0 mg, 0.3 mmol) was then added together with 2.5 mL butanol. The obtained mixture was heated at 80 °C for four days. The brick-orange precipitate was separated by filtration, washed with DMF and acetone, and then dried under a stream of argon. The MOF was isolated as a glittering brick-orange solid and was stored under an inert atmosphere.

General MOF activation. For pore solvent removal, the MOFs were soaked in dry acetone (exchange for fresh acetone every 24 hours, three cycles) for 4 days. Afterward, the solid samples were dried under a high vacuum at 65 °C for 24 h.

Tetraethyl 4,4',4'',4'''-((6,12-dioxo-6,12-dihydronaphtho[7,8,1,2,3-*nopqr*]tetraphene-4,10-diyl)bis(azanetriyl))tetrabenzoate (14, Et_4L^2). A Schlenk-flask was evacuated (residual pressure ~10^{-3} mbar) and backfilled with argon 3 times prior to use. 60 mL toluene were then added and saturated with argon for at least 45 min. 4,10-Dibromoanthanthrone (1.4 g, 3.0 mmol), diethyl 4,4'-azanediyldibenzoate (2.1 g, 6.6 mmol), Cs_2CO_3 (2.9 g, 9.0 mmol), $Pd(OAc)_2$ (67.5 mg, 0.3 mmol) and dppf (332.0 mg, 0.6 mmol) were thereafter added in one portion under positive argon pressure and the mixture was heated at 90 °C for 2 days. After completion of the reaction, the resulting purple suspension was left to cool down and the solvent was removed under reduced pressure. The residual solid was washed with MeOH and filtered over silica (DCM:EtOAc 10:1 as eluent) to yield the desired product as a deep blue solid (1.5 g, 55 % yield). ^{1}H NMR (400 MHz, $CDCl_3$): δ 8.73 (dd, 2H, $^3J_{H–H}$ = 7.4 Hz, $^4J_{H–H}$ = 1.2 Hz) 8.34 (s, 2H) 8.24 (dd, 2H, $^3J_{H–H}$ = 7.4 Hz, $^4J_{H–H}$ = 1.2 Hz) 7.95 (d, 8H, $^3J_{H–H}$ = 8.8 Hz) 7.73 (t, 2H, $^3J_{H–H}$ = 7.2 Hz) 7.13 (d, 8H, $^3J_{H–H}$ = 8.8 Hz) 4.36 (q, 8H, $^3J_{H–H}$ = 7.1 Hz) 1.38 (t, 12H, $^3J_{H-H}$ = 7.1 Hz) ppm. ^{13}C NMR (101 MHz, $CDCl_3$): δ 165.97 153.98 151.06 145.40 131.35 126.62 125.23 125.16 121.91 121.86 60.91 14.39 ppm. UV-Vis (CH_2Cl_2): λ 290, 340, 590 nm. Elemental analysis *expected* C 74.99 H 4.77 N 3.02 *found* C 74.62 H 4.84 N 3.31.

4,4',4'',4'''-((6,12-dioxo-6,12-dihydronaphtho[7,8,1,2,3-*nopqr*]tetraphene-4,10-diyl)bis-(azanetriyl))tetrabenzoic acid (15, H_4L^2). 14 (1.4 g, 1.5 mmol) and NaOH (312.0 mg, 7.8 mmol) were suspended in 200 mL of a THF/H_2O mixture and heated to reflux for 18 h. After completion of the reaction, the resulting mixture was left to cool down and the organic phase was removed under reduced pressure. The aqueous phase was acidified to pH = 1 and the precipitate was filtered. The solid was washed with an excess of water and dried at 100 °C. The product was isolated as a deep dark blue solid (1.2 g, 99 % yield). ^{1}H NMR (400 MHz, DMSO-d_6): δ 12.17 (s, 4H) 8.64 (d, 2H, $^3J_{H–H}$ = 7.4 Hz) 8.31 (d, 2H, $^3J_{H–H}$ = 7.4 Hz) 8.15 (s, 2H)

7.91 (m, 10H) 7.19 (d, 8H, $^3J_{H-H}$ = 8.8 Hz) ppm. UV-Vis (DMF): λ 290, 350, 600 nm. Elemental analysis *expected* C 73.53 H 3.46 N 3.43 *found* C 72.54 H 4.08 N 3.22.

Zn-MOF (16). 15 (8.0 mg, 0.01 mmol) was fully dissolved in 2 mL NMP in a sealable glass vial to yield a deep blue solution. $Zn(NO_3)_2 \cdot 6H_2O$ (18.0 mg, 0.06 mmol) was then added. The obtained mixture was heated at 80 °C for 24 hours. The needle-shaped crystals were separated by filtration, washed with NMP and acetone, and then dried under a stream of argon. The MOF was isolated as glittering blue needles.

$[Zn_2(NO_3)_2(Quinz)(4,4\text{-bpy})_2]_n$ (17). 100 µL of a 0.1 M NaOH solution was added to a saturated solution of quinizarin in methanol in a 20 mL sealable glass vial, yielding a deep purple solution. $Zn(NO_3)_2 \cdot 6H_2O$ (90.0 mg, 0.3 mmol) and 4,4-bpy (32.0 mg, 0.2 mmol) were added in one portion and fully dissolved, yielding a bright red mixture. The mixture was heated at 60 °C for 24 h. The purple crystals were separated by filtration while hot and washed with DCM. The product was dried on air and isolated as a dark purple glittering solid.

$[Zn(NO_3)_2(Et\text{-bpy})]_n$ (18). $Zn(NO_3)_2 \cdot 6H_2O$ (90.0 mg, 0.3 mmol) and Et-bpy (32.0 mg, 0.2 mmol) were dissolved in 5 mL MeOH. After a few minutes, a fine white precipitate could be observed. The mixture was heated at 60 °C for 4 h. The white crystals were separated by filtration while hot and washed with MeOH. The product was dried on air and isolated as a white glittering solid.

4.3. Crystallographic Refinement Data and Tables

Table S1. Selected crystallographic data of organic reactants **1** and **7**.

Compound	**1**	**7**
Formula	$C_{14}H_2O_2Br_2$	$C_{18}H_{18}NO_4$
FW ($g.mol^{-1}$)	366.0	312.33
Space group (no)	$P2_1/c$ (14)	$P2_1/c$ (14)
a (Å)	10.0208(5)	8.4198(3)
b (Å)	3.8433(2)	27.154(1)
c (Å)	14.8116(7)	7.4482(2)
α (deg)	90	90
β (deg)	97.277(2)	111.401(1)
γ (deg)	90	90
V ($Å^3$)	565.84(5)	1585.47(9)
Z	4	4
T (K)	100(2)	100(2)
λ (nm)	0.71373	0.71373
Collected reflections	14431	40151

Independent reflections	993	3250
Parameters/restraints	82/0	210/0
R_1	0.0188	0.0420
wR_2	0.0981	0.1075
Goodness of fit	0.993	1.039

Table S2. Selected crystallographic data of the organic linkers DPAq and DPAHq.

Compound	**DPAq, 2**	**DPAHq, 3**
Formula	$C_{24}H_{12}N_2O_2$	$C_{12}H_8NO$
FW (g.mol^{-1})	362.37	182.19
Space group (no)	*Pn* (7)	*P*2$_1$/c (14)
a (Å)	3.7283(5)	8.2499(6)
b (Å)	17.490(2)	7.2903(8)
c (Å)	25.231(3)	14.348(1)
α (deg)	90	90
β (deg)	91.793(4)	98.689(3)
γ (deg)	90	90
V (Å^3)	1664.5(4)	853.1(1)
Z	4	4
T (K)	100(2)	100(2)
λ (nm)	0.71373	0.71373
Collected reflections	6045	1563
Independent reflections	5325	1451
Parameters/restraints	505/2	131/0
R_1	0.0409	0.0338
wR_2	0.0987	0.0855
Goodness of fit	1.055	1.045

Table S3. Selected crystallographic data of the organic linkers **9** and **14**.

Compound	**9·DMSO**	**14·2DMA**
Formula	$C_{42}H_{22}N_2O_{10}{\cdot}C_2H_6SO$	$C_{54}H_{33}N_2O_{10}{\cdot}2C_4H_9NO$
FW (g.mol^{-1})	792.74	986.95
Space group (no)	$P\bar{1}$ (2)	*P*2$_1$/c (14)
a (Å)	6.757(3)	18.304(5)
b (Å)	20.964(8)	12.645(4)
c (Å)	20.972(8)	14.918(4)
α (deg)	109.385(11)	90
β (deg)	96.891(12)	103.288(9)

γ (deg)	94.456(12)	90
V (Å^3)	2760.3(18)	3360.3(2)
Z	2	4
T (K)	100(2)	100(2)
λ (nm)	0.71373	0.71373
Collected reflections	121188	63361
Independent reflections	11345	5957
Parameters/restraints	525/0	337/0
R_1	0.1743	0.0877
wR_2	0.4357	0.2590
Goodness of fit	2.513	1.052

Table S4. Selected crystallographic data for the MOFs **4**–**6**.

Compound	**4**	**5**	**6**
Formula	$C_{76}H_{40}N_4O_{12}Zn_2$	$C_{40}H_{22}N_2O_{10}Zn_2$	$C_{32}H_{18}N_2O_6Cd$
FW (g.mol^{-1})	1480.17	821.01	638.88
Space group (no)	*Pca*2$_1$ (29)	$P\bar{1}$ (2)	*Ibca* (73)
a (Å)	16.395(3)	10.869(5)	15.409(4)
b (Å)	20.218(3)	10.879(5)	20.472(6)
c (Å)	19.111(3)	22.84(1)	40.36(1)
α (deg)	90	91.96(2)	90
β (deg)	90	95.38(1)	90
γ (deg)	90	104.14(2)	90
V (Å^3)	6336(2)	2603(2)	12733(6)
Z	4	2	16
T (K)	100(2)	100(2)	100(2)
λ (nm)	0.71373	0.71373	0.71373
Collected reflections	12458	9505	5829
Independent reflections	11648	7803	4780
Parameters/restraints	930/65	970/2344	370/0
R_1	0.474	0.0474	0.0367
wR_2	0.1243	0.1228	0.0980
Goodness of fit	1.093	1.060	1.043

Table S5. Selected crystallographic data for the MOFs **10** and **11**.

Compound	**Mg-MOF (10)**	**Ca-MOF (11)**
Formula	$C_{43.75}H_{26.75}N_{2.5}O_{16}Mg_{1.75}$	$C_{102}H_{84.5}N_{8.5}O_{39}Ca_3$
FW (g.mol^{-1})	885.97	2193.56
Space group (no)	*P*2$_1$/m (11)	*P*2$_1$/m (11)
a (Å)	14.9364(6)	18.60(2)
b (Å)	38.0282(16)	28.11(3)
c (Å)	20.6102(9)	20.53(2)
α (deg)	90	90
β (deg)	105.7990(10)	95.31(4)
γ (deg)	90	90
V (Å^3)	11264.4(8)	10691(21)
Z	8	4
T (K)	100(2)	100(2)
λ (nm)	0.71373	0.71373
Collected reflections	105908	19502
Independent reflections	20930	15540
Parameters/restraints	1199/0	1671/1107
R_1	0.0991	0.1077
wR_2	0.2621	0.3344
Goodness of fit	0.997	2.731

Table S6. Selected crystallographic data for the MOFs **12** and **13**.

Compound	**Sr-MOF (12)**	**Ba-MOF (13)**
Formula	$C_{42}H_{22}N_2O_{14}Sr_{1.5}$	$C_{21}H_{11}NO_{9.5}Ba_{0.75}$
FW (g.mol^{-1})	910.04	532.32
Space group (no)	*C*2/m (12)	*C*2/m (12)
a (Å)	10.187(4)	10.183(11)
b (Å)	28.387(12)	28.36(3)
c (Å)	19.333(9)	19.73(2)
α (deg)	90	90
β (deg)	101.259(8)	104.10(4)
γ (deg)	90	90
V (Å^3)	5483(4)	5527(10)
Z	4	8
T (K)	100(2)	100(2)
λ (nm)	0.71373	0.71373
Collected reflections	5143	5821

Independent reflections	4388	5053
Parameters/restraints	316/0	338/259
R_1	0.0902	0.1690
wR_2	0.2798	0.5090
Goodness of fit	2.281	4.868

Table S7. Selected crystallographic data for the MOFs **16**-**18**.

Compound	**Zn-MOF (16)**	**17**	**18**
Formula	$C_{25}H_{14}NO_6Zn$	$C_{36}H_{28}N_6O_{12}Zn_2$	$C_{12}H_{12}N_4O_6Zn$
FW ($g.mol^{-1}$)	489.74	867.38	373.63
Space group (no)	*Imma* (74)	*C*2/*c* (15)	$P\bar{1}$ (2)
a (Å)	23.308(4)	32.432(3)	7.011(5)
b (Å)	36.325(7)	17.2227(15)	7.652(5)
c (Å)	15.980(3)	12.2466(11)	14.143(9)
α (deg)	90	90	76.61(3)
β (deg)	90	90	89.18(3)
γ (deg)	90	90	88.42(2)
V ($Å^3$)	13529(4)	6840.5(11)	737.8(8)
Z	8	8	2
T (K)	100(2)	100(2)	100(2)
λ (nm)	0.71373	0.71373	0.71373
Collected reflections	47948	6365	43438
Independent reflections	3762	4993	3034
Parameters/restraints	315/496	508/330	208/0
R_1	0.0852	0.0490	0.0279
wR_2	0.2859	0.1198	0.0719
Goodness of fit	2.303	1.077	1.053

5. REFERENCES

1. Nelson, D. L, Cox, M. M., *Lehninger Principles of Biochemistry*, **2017**, 7th Edition, W.H. Freeman,

2. Lippard, S. J., Berg, J. M., *Principles of Bioinorganic Chemistry*, **1994**, University Science Books.

3. Bertini, I., Gray, H. B., Lippard, S. J., Valentine, J. S., *Bioinorganic Chemistry*, **1994**, University Science Books.

4. Blankenship, R. E., *Molecular Mechanisms of Photosynthesis*, **2014**, 2nd Edition, John Wiley & Sons.

5. Zhou, H., Long, J. R., Yaghi, O. M., *Chem. Rev.*, **2012**, 112, 2, 673–674.

6. Wang, Q., Astruc, D., *Chem. Rev.*, **2020**, 120, 2, 1438–1511.

7. Calbo, J., Golomb, M. J., Walsh, A., *J. Mater. Chem. A*, **2019**, 7, 16571–16597.

8. Li, L., Wang, K., Sun, Y., Lollar, C, T., Li. J., Zhou, H., *Mater. Today*, **2018**, 21, 2, 108–121.

9. Ma, S., Zhou, H., *Chem. Commun.*, **2010**, 46, 44-53.

10. Baumann, A. E., Burns, D. A., Liu, B., Thoi, V. S., *Commun. Chem.*, **2019**, 2, 86.

11. Medishetty, R., Zaręba, J. K., Mayer, D., Samoć, Marek, Fischer, R. A., *Chem. Soc. Rev.*, **2017**, 46, 4976–5004.

12. Yang, L., Xu, C., Ye, W., Liu, W., *Sens. Actuators, B*, **2015**, 215, 489–496.

13. Yue, D., Zhao, D., Zhang, J., Zhang, L., Jiang, K., Zhang, X., Cui, Y., Yang, Y., Chen, B. Qian, G., *Chem. Commun.*, **2017**, 53, 11221–11224.

14. Wang, X., Liu, X., Rong, H., Song, Y., Wen, H., Liu, Q., *RSC Adv.*, **2017**, 7, 29611–29617.

15. Dan-Hardi, M., Serre, C., Frot, T., Rozes, L., Maurin, G., Sanchez, C., Férey, G., Maurín, G., *J. Am. Chem. Soc.*, **2009**, 131, 10857–10859.

16. Zhang, Z., Yoshikawa, H., Awaga, K., *J. Am. Chem. Soc.*, **2014**, 136, 16112–16115.

17. Darago, L. E., Aubrey, M. L., Yu, C. J., Gonzalez, M. I., Long, J. R., *J. Am. Chem. Soc.*, **2015**, 137, 15703–15711.

18. Ahrenholtz, S. R., Epley, C. C., Morris, A. J., *J. Am. Chem. Soc.*, **2014**, 136, 2464–2472.

19. Ward, D. E., Shen, J., *Org. Lett.*, **2007**, 9, 2843–2846.

20. Osyezka, A., Moser, C. C., Daldal, F., Dutton, P. L., *Nature*, **2004**, 427, 607–612.

21. Cramer, W. A., Zhang, H., Yan, J., Kurisu, G., Smith, J. L., *Biochemistry*, **2004**, 43, 5921–5929.

22. Tiede, D. M., Vazquez, J., Cordova, J., Marone, P. A., *Biochemistry*, **1996**, 35, 10763–10775.

23. Kivala, M., Boudon, C., Gisselbrecht, J. P., Seiler, P., Gross, M., Diederich, F., *Chem. Commun.*, **2007**, 4731–4733.

24. Arimura, T., Ide, S., Sugihara, H., Murata, S., Sessler, J. L., *New J. Chem.*, **1999**, 23, 977–979.

25. Bitenc, J., Lindahl, N., Vizintin, A., Abdelhamid, M. E., Dominko, R., Johansson, P., *Energy Storage Mater.*, **2020**, 24, 379–383.

26. Zhang, Q., Kuwabara, H., Potscavage, W. J., Huang, S., Hatae, Y., Shibata, T., Adachi, C., *J. Am. Chem. Soc.*, **2014**, 136, 52, 18070–18081.

27. Chiba, K., Jinno, M., Nozaki, A., Tada, M., *Chem. Commun.*, **1997**, 1403–1404.

28. Fujita, S., Sano, K., *J. Org. Chem.*, **1979**, 44, 15, 2647–2651.

29. Ensafi, A. A., Jamei, H. R., Heydari-Bafrooei, E., Rezaei, B., *Bioelectrochemistry*, **2016**, 111, 15–22.

30. Guin, P. S., Das, S., Mandal, P. C., *Int. J. Electrochem.*, **2011**, 1–22.

31. Campos-Martin, J. M., Blanco-Brieva, G., Fierro, J. L. G., *Angew. Chem. Int. Ed.*, **2006**, 45, 6962–6984.

32. Murata, T., Kotsuki, K., Murayama, H., Ryotaro, T., Morita, Y., *Comun. Chem.*, **2019**, 2, 46.

33. Wang, W., Xu, W., Cosimbescu, L., Choi, D., Li, L., Yang, Z., *Chem. Commun.*, **2012**, 48, 6669–6671.

34. Gao, C., Li, J., Yin, S., Sun, J., Wang, C., *Nat. Commun.*, **2020**, 11, 4919.

35. Deviprasad, G. R., D'Souza, F., *J. Org. Chem.*, **2001**, 66, 13, 4601–4609.

36. Payne, D. T., Webre, W. A., Matsushita, Y., Zhu, N., Futera, Z., Labuta, J., Jevasuwan, W., Fukata, N., Fossey, J. S., D'Souza, F., Ariga, K., Schmitt, W., Hill, J. P., *Nat. Commun.*, **2019**, 10, 1007.

37. Fuks-Janczarek, I., Luc, J., Sahraoui, B., Dumur, F., Hudhomme, P., Berdowski, J., Kityk, I. V., *J. Phys. Chem. B*, **2005**, 109, 20, 10179–10183.

38. Iyoda, T., Saika, T., Honda, K., Shimidzu, T., *Tetrahedron Lett.*, **1989**, 30, 5429–5432.

39. De Santis, G., Fabbrizzi, L., Licchelli, M., Sardone, N., Velders, A. H., *Chem. Eur. J.*, **1996**, 2, 1243–1250.

40. Bergonzi, R., Fabbrizzi, L., Licchelli, N., Mangano, C., *Coord. Chem. Rev.*, **1998**, 170, 31–46.

41. Illos, R. A., Harlev, E., Bittner, S., *Tetrahedron Lett.*, **2005**, 46, 8427–8430.

42. Cervantes-González, J., Vosburg, D. A., Mora-Rodriguez, S. E., Vázquez, M. A., Zepeda, L. G., Gómez, C. V., Lagunas-Rivera, S., *Chem. Cat. Chem.*, **2020**, 12, 3811–3827.

43. Bardagi, J. I., Ghosh, I., Schmalzbauer, M., Ghosh, T., König, B., *Eur. J. Org. Chem.*, **2018**, 1, 34–40.

44. Petzold, D., König, B., *Adv. Synth. Catal.*, **2018**, 4, 626–630.

45. Li, Q., Lan, X., An, G., Ricardez-Sandoval, L., Wang, Z., Bai, G.*, ACS Catal.*, **2020**, 10, 12, 6664–6675.

46. Morin, J.-F., *J. Mater. Chem. C*, **2017**, 5, 12298–12307.

47. Pham, H. D., Hayasake, K., Kim, J., Do, T. T., Matsui, H., Manzhos, S., Feron, K., Tokito, S., Watson, T., Tsoi, W. C., Motta, N., Durrant, J. R., Jain, S. M., Sonar, P., J. Mater. Chem. C, **2018**, 6, 3699–3708.

48. Sytnyk, M., Glowacki, E. D., Yakunin, S., Voss, G., Schöfberger, W., Kriegner, D., Stangl, J., Trotta, R., Gollner, C., Tollabimazraehno, S., Romanazzi, G., Bozkurt, Z., Havlicek, M., Sariciftci, N. S., J. Am. Chem. Soc., **2014**, 136, 16522–16532.

49. Kotwica, K., Bujak, P., Wamil, D., Materna, M., Skorka, L., Gunka, P. A., Nowakowski, R., Golec, B., Luszczynska, B., Zagorska, M. Pron, A., *Chem. Commun.*, **2014**, 50, 11543–11546.

50. Winkler, M., Houk, K. N.., *J. Am. Chem. Soc.*, **2007**, 129, 1805–1815.

51. Fogel, Y., Kastler, M., Wang, Z. H., Andrienko, D., Bodwell, G. J., Müllen, K., *J. Am. Chem. Soc.*, **2007**, 129, 11743–11749.

52. Kotwica, K., Bujak, P., Wamil, D., Pieczonk, A., Wiosna-Salyga, G., Gunka, P. A., Jaroch, T., Nowakowski, R., Luszczynska, B., Witkowska, E., Glowacki, I., Ulanski, J., Zagorska, M., Pron, A., *J. Phys. Chem. C*, **2015**, 119, 10700.

53. Zhang, L., Fonari, A., Zhang, Y., Zhao, G., Coropceanu, V., Hu, W., Parkin, S., Brédas, J.-L., Briseno, A. L., Chem. Eur. J., **2013**, 19, 17907–17916.

54. Kaim, W., Schwederski, B., *Coord. Chem. Rev.*, **2010**, 254,1580–1588.

55. Raymond, K. N., Dertz, E. A., Kim, S. S., *PNAS*, **2003**, 100, 3584–3588.

56. Oh, M., Carpenter, G. B., Sweigart, D. A., *Angew. Chem. Int. Ed.*, **2002**, 41, 3650–3653.

57. Oh, M., Carpenter, G. B., Sweigart, D. A., *Angew. Chem. Int. Ed.*, **2003**, 42, 2026–2028.

58. Oh, M., Carpenter, G. B., Sweigart, D. A., *Organometallics.*, **2003**, 22, 2364–2366.

59. Moussa, J., Guyard-Duhayon, C., Herson, P., Amouri, H., Rager, M. N., Jutand, A., *Organometallics*, **2004**, 23, 26, 6231–6238.

60. Oh, M., Carpenter, G. B., Sweigart, D. A., *Organometallics.*, **2002**, 21, 1290–1295.

61. Oh, M., Carpenter, G. B., Sweigart, D. A., *Angew. Chem. Int. Ed.*, **2001**, 40, 3191–3194.

62. Attia, A. S., Pierpont, C. G., *Inorg. Chem.*, **1997**, 36, 6184–6187.

63. Buchanan, R. M., Pierpont, C. G., *Inorg. Chem.*, **1979**, 18, 3439–3444.

64. Buchanan, R. M., Pierpont, C. G., J. Am. Chem. Soc., **1980**, 102, 4951–4957.

65. Chakarawet, K., Harris, T. D., Long, J. R., *Chem. Sci.*, **2020**, 11, 8196-8203.

66. Darago, L. E., Aubrey, M. L., Yu C. J., Gonzalez, M. I., Long, J. R., *J. Am. Chem. Soc.*, **2015**, 137, 50, 15703–15711.

67. DeGayner, J. A., Jeon, I.-R., Sun, L., Dincă, M., Harris, T. D., *J. Am. Chem. Soc.*, **2017**, 139, 11, 4175–4184.

68. Jin, Y., Jiang, H., Tang, X., Zhang, W., Lin, Y., Cui, Y., *Dalton Trans.*, **2021**, 50, 8533–8539.

69. Pullen, S., Tessarolo, J., Clever, G. H., *Chem. Sci.*, **2021**, 12, 7269–7393.

70. Agrawal, S., Clarke, S. M., Vitorica-Yrezabal, I. J., Liu, C., Fang, W., Wood, P. T., Wright, D., *Mol. Phys.*, **2019**, 117, 22, 3424-3433.

71. Li, W.-H., Deng, W.-H., Wang, G.-E., Xu, G., *EnergyChem*, **2020**, 2, 100029.

72. Jiang, Y., Oh, I., Joo, S. H., Buyukcakir, O., Chen, X., Lee, S., H., Huang, M., Seong, W. K., Kwak, S. K., Yoo, J.-W., Ruoff, R. S., *J. Am. Chem. Soc.*, **2019**, 141, 42, 16884–16893.

73. Sheberla, D., Sun, L., Blood-Forsythe, M. A., Er, E., Wade, C. R., Brozek, C. K., Aspuru-Guzik, A., Dincă, M., *J. Am. Chem. Soc.*, **2014**, 136, 25, 8859–8862.

74. Nguyen, N. T. T., Furukawa, H., Gándara, F., Trickett, C. A., Jeong, H. M., Cordova, K. E., Yaghi, O. M., *J. Am. Chem. Soc.*, **2015**, 137, 49, 15394–15397.

75. Skorupskii, G., Dincă, M., *J. Am. Chem. Soc.*, **2020**, 142, 15, 6920–6924.

76. Leubner, S., Bengtsson, V. E. G., Inge, A. K., Wahiduzzaman, M., Steinke, F., Jaworski, A., Xu, H., Halis, S., Rönfeldt, P., Reinsch, H., Maurin, G., Zou, X., Stock, N., *Dalton Trans.*, **2020**, 49, 3088–3092.

77. Gui, B., Meng, X., Chen, Y., Tian, J., Liu, G., Shen, C., Zeller, M., Yuan, D., Wang, C., *Chem. Mater.*, **2015**, 27, 18, 6426–6431.

78. Maka, V. K., Mukhopadhyay, A., Jindal, S., Moorthy, J. N., *Chem. Eur. J.*, **2019**, 25, 12, 3835-3842.

79. Celis-Salazar, P., Epley, C. C., Ahrenholtz, S. R., Maza, W. A., Usov, P. M., Morris, A. J., *Inorg. Chem.*, **2017**, 56, 22, 13741-13747.

80. Furman, J. D., Burwood, R. P., Tang, M., Mikhailovsky, A. A., Cheetham, A. K., *J. Mater. Chem.*, **2011**, 21, 6595-6601.

81. Zhang, G., Fei, H., *Top. Curr. Chem.*, **2019**, 377, 32.

82. Gándara, F., Sneijko, N., de Andrés, A., Fernandez, J. R., Gómez-Sal, J. C., Gutierrez-Puebla, E., Monge, A., *RSC Adv.*, **2012**, 2, 949-955.

83. Konarev, D. V., Andronov, M. G., Batov, M. S., Kuzmin, A. V., Khasanov, S. S., Shestakov, A. F., Otsuka, A., Yamochi, H., Kitagawa, H., Lyubovskaya, R. N., *New J. Chem.*, **2020**, 44, 10849-10858.

84. Coudret, C., Mazenc, V., *Tetrahedron Lett.*, **1997**, 38, 5293-5296.

85. Skalamera D., Veljkovic J., Pticek L., Sambol M., Mlinaric-Majerski K., Basaric N., *Tetrahedron*, **2017**, 73, 5892-5899.

86. Prakash, A., *Acta Cryst.*, **1967**, 22, 439-440.

87. Pastoriza-Santos, I., Liz-Marzán, L., *Langmuir*, **1999**, 15, 948-951.

88. Yu, J. Y., Schreiner, S., Vaska, L., *Inorg. Chim. Acta*, **1990**, 170, 145-147.

89. As resulted from a survey on the Cambridge Crystallographic Data Centre (CCDC), December 7th, **2020**.

90. Watson, H.C., Hargreaves, A., *Acta Cryst.*, **1958**, 11, 556-562.

91. Steiner T., *Angew. Chem. Int. Ed.*, **2002**, 41(1), 49-76.

92. Cook, D., Can. J. Chem., **1961**, 39, 2009.

93. Ishii, Y., Tashiro, K., Hosoe, K., Al-zubaidi, A., Kawasaki, S., Phys. Chem. Chem. Phys. **2016**, 18, 10411–10418.

94. Anouar, E.A, Osman C. P., Weber J.-F., Ismail, N.H., SpringerPlus, **2014**, 3, 233.

95. Ajloo, D., Yoonesi, B., Soleymanpour, A., *Int. J. Electrochem. Sci.*, **2010**, 5, 459 – 477.

96. Wolff, S. P., *Methods Enzymol.*, **1994**, 233, 182-189.

97. Hua, C., Doheny, P. W., Ding, B., Chan, B., Yu M., Kepert, C.J., D'Alessandro, D. M., *J. Am. Chem. Soc.*, **2018**, 140, 21, 6622-6630.

98. Mingabudinova, L. R., Vinogradov, V. V., Milichko, V. A., Hey-Hawkins, E., Vinogradov, A. V., Chem. Soc. Rev., 2016, 45, 5408–5431.

99. Nguyen, T. N., Ebrahim, F. M., Stylianou, K. C., *Coord. Chem. Rev.*, 2018, 377, 259–306.

100. Mieno, H., Kabe, R., Allendorf, M. D., Adachi, C., *Chem. Commun.*, **2018**, 54, 631–634.

101. Vo, G. D., Hartwig, J. F., *J. Am. Chem. Soc.*, **2009**, 131, 31, 11049–11061.

102. Scheurell, K., König, R., Troyanov, S. I., Kemnitz, E., *Z. anorg. allg. Chem.*, **2012**, 9, 1265–1273.

103. Irish, D. E., Semmler, J., Taylor, N. J., Toogood, G. E., *Acta Cryst*., **1991**, 47, 2322–2324.

104. Steiner, T., *Acta Cryst.*, **1998**, B54, 456–463.

105. Allen, N. S., Hayes, G., Riley, P. N. K., Richards, A. M., *Journal of Photochemistry*, 1987, 38, 365–373.

106. Quinti, L., Allen, N. S., Edge, M., Murphy, B. P., Perotti, A., *J. Photochem. Photobiol. A*, **2003**, 155, 1–3, 79–91.

107. Gracia, L. G., Rodríguez, L. C., Ceba, M. R., *Talanta*, **1997**, 44, 1, 75–83.

108. Fain, V. Ya., Zaitsev, B. E., Ryabov, M. A., *Koord. Khim.*, **2003**, 29, 5, 395–398.

109. Fain, V. Ya., Zaitsev, B. E., Ryabov, M. A., *Russ. J. Coord. Chem.*, **2007**, 33, 621–629.

110. *APEX suite of crystallographic software*, APEX 3, Version 2015.52, Bruker AXS Inc., Madison, Wisconsin, USA, 2015.

111. *SAINT*, Version 8.38A, Bruker AXS Inc., Madison, Wisconsin, USA, 2017.

112. *SADABS*, Version 2016/2, Bruker AXS Inc., Madison, Wisconsin, USA, 2016.

113. G. M. Sheldrick, *Acta Crystallogr. Sect. A* **2015**, *71*, 3–8.

114. G. M. Sheldrick, *Acta Crystallogr. Sect. C* **2015**, *71*, 3–8.

115. C. B. Hübschle, G. M. Sheldrick, B. Dittrich, *J. Appl. Cryst.* **2011**, *44*, 1281–1284.

116. A. L. Spek, *Acta Crystallogr. Sect. C* **2015**, *71*, 9–18.

117. D. Kratzert, I. Krossing, *J. Appl. Cryst.*, **2018**, *51*, 928-934.

118. D. Kratzert, J.J. Holstein, I. Krossing, *J. Appl. Cryst.*, **2015**, *48*, 933-938.

119. C. F. Macrae, I. J. Bruno, J. A. Chisholm, P. R. Edgington, P. McCabe, E. Pidcock, L. Rodriguez-Monge, R. Taylor, J. van de Streek, P. A. Wood, *J. Appl. Cryst.* **2008**, *41*, 466–470.

6. APPENDIX

2.1. Exploiting the Anthraquinone/Anthrahydroquinone Chemistry in Metal-Organic Frameworks: Immobilized Redox Switches for Molecular Oxygen Activation

2.2.1. Design of anthraquinone-based linkers for redox-active architectures

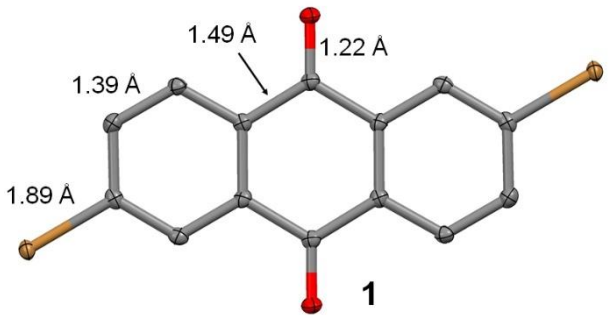

Figure S1. Molecular structure of DBAq. Aromatic hydrogen atoms were omitted for clarity reasons. All ellipsoids are shown at the 50% probability level. Atom colors are grey (C), red (O), brown (Br).

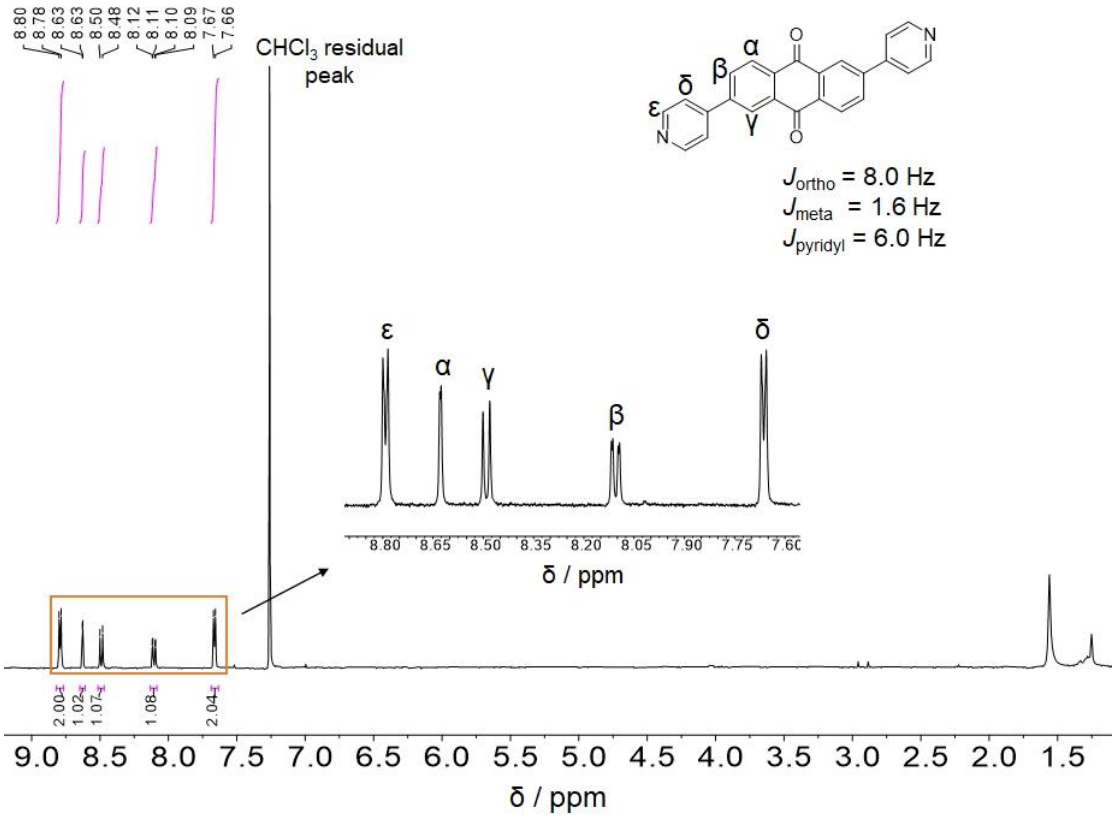

Figure S2. ^{1}H NMR spectrum of DPAq in $CDCl_3$.

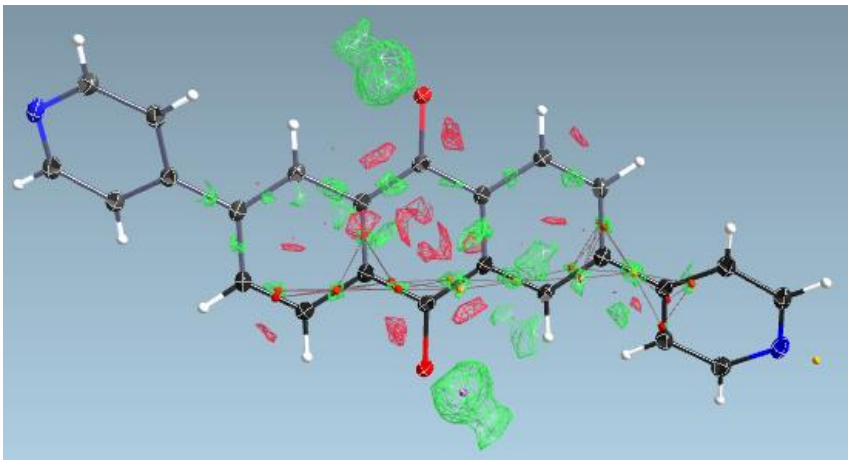

Figure S3. Difference Fourier maps showing the residual electronic density assigned to the protons of the phenolic groups of DPAHq.

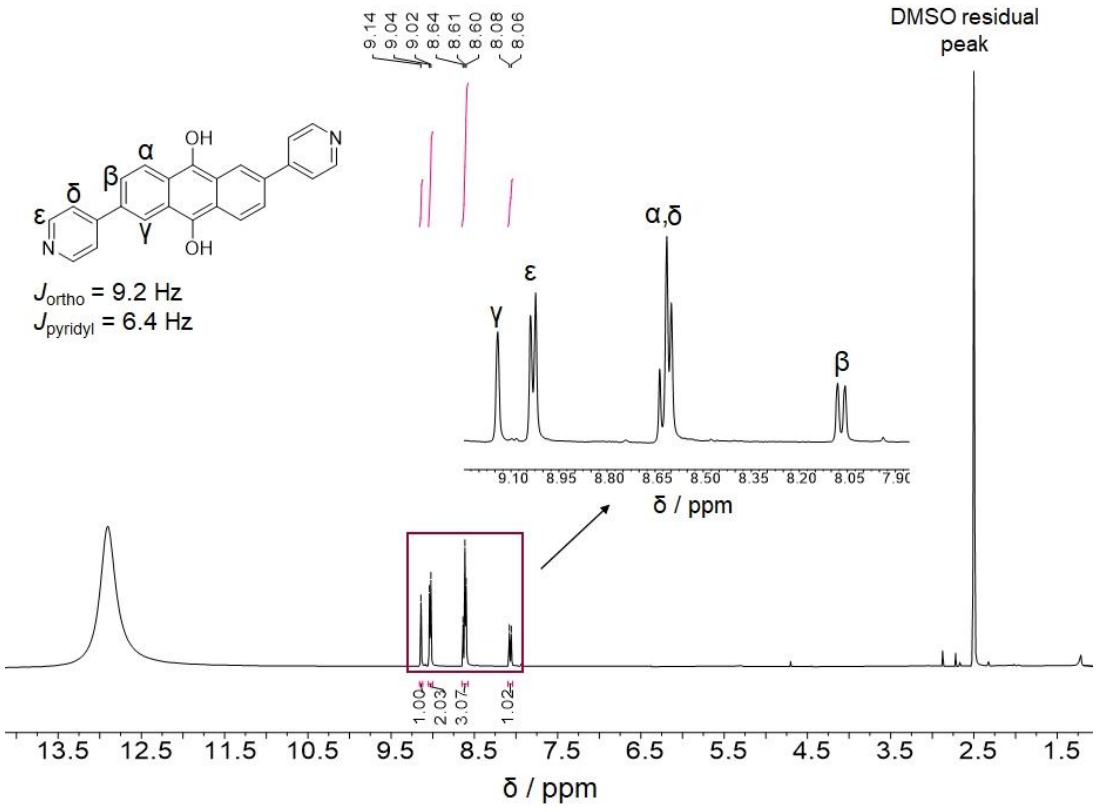

Figure S4. ^{1}H NMR spectrum of DPAHq in degassed TFA/DMSO-d_6.

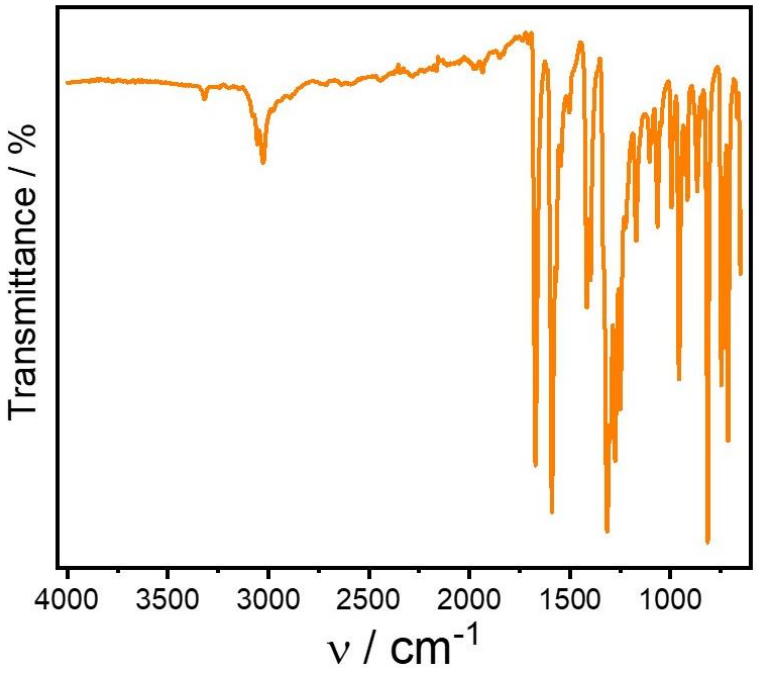

Figure S5. FTIR spectrum of DPAq.

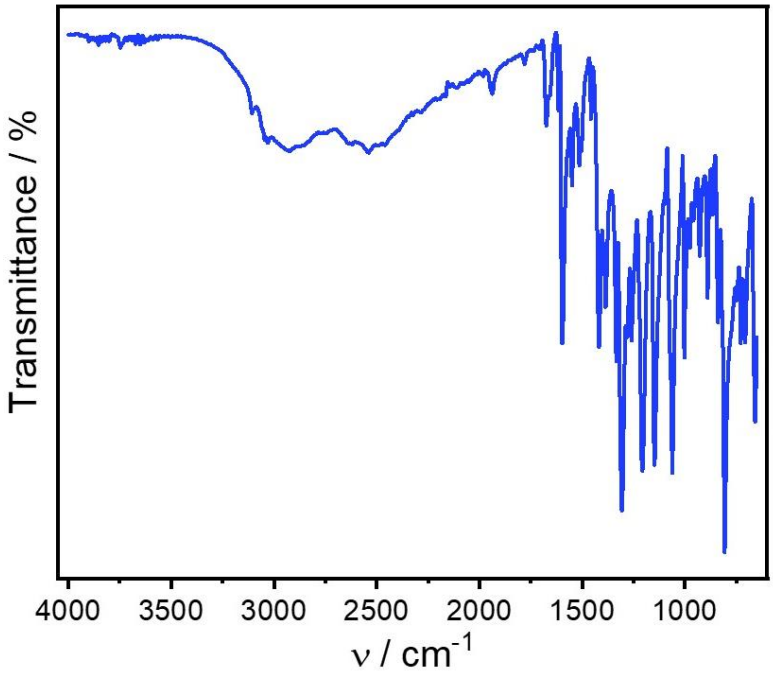

Figure S6. FTIR spectrum of DPAHq.

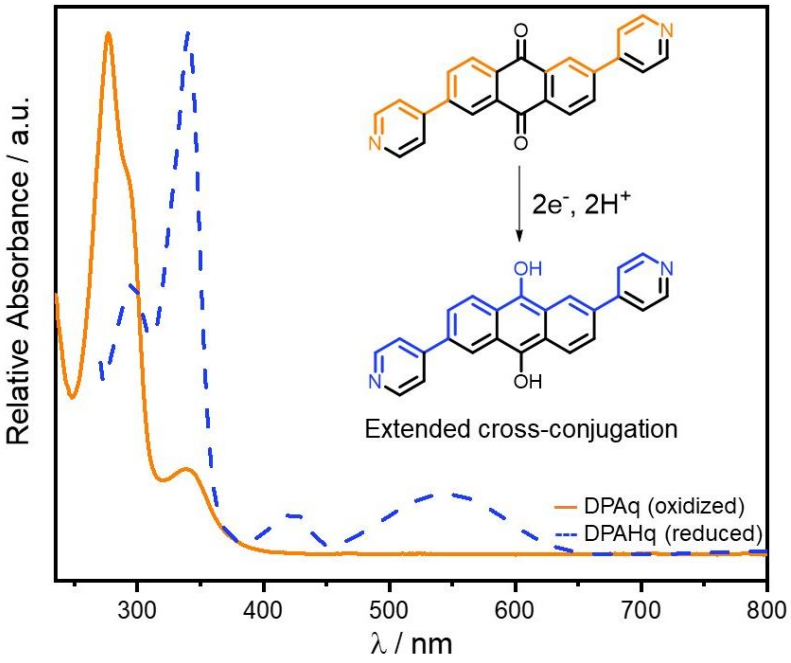

Figure S7. UV-Vis electronic spectra of DPAq (orange line, in CH_2Cl_2) and DPAHq (blue line, in degassed TFA/DMF solution).

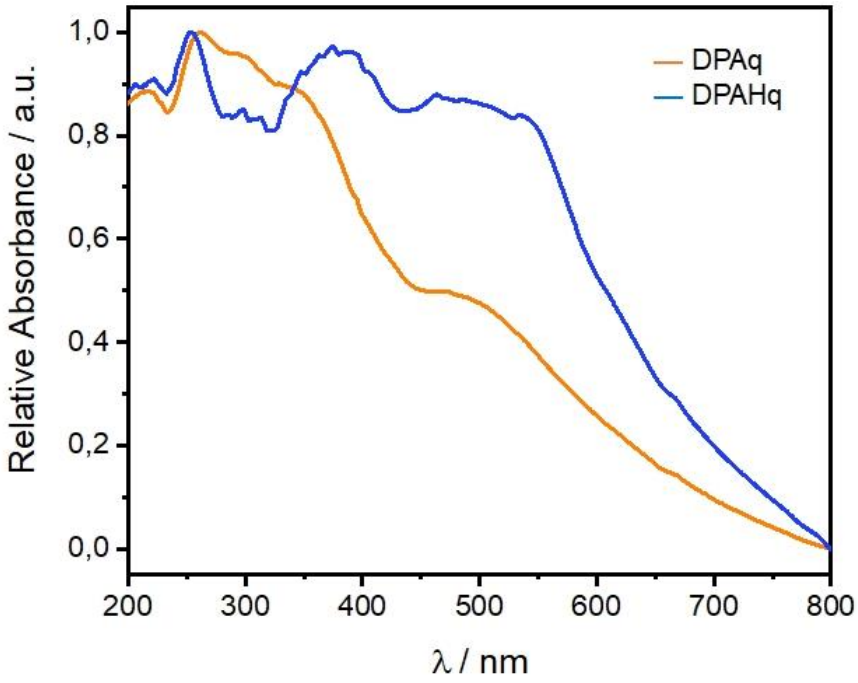

Figure S8. Solid-state UV-Vis electronic spectra of DPAq (orange line) and DPAHq (blue line).

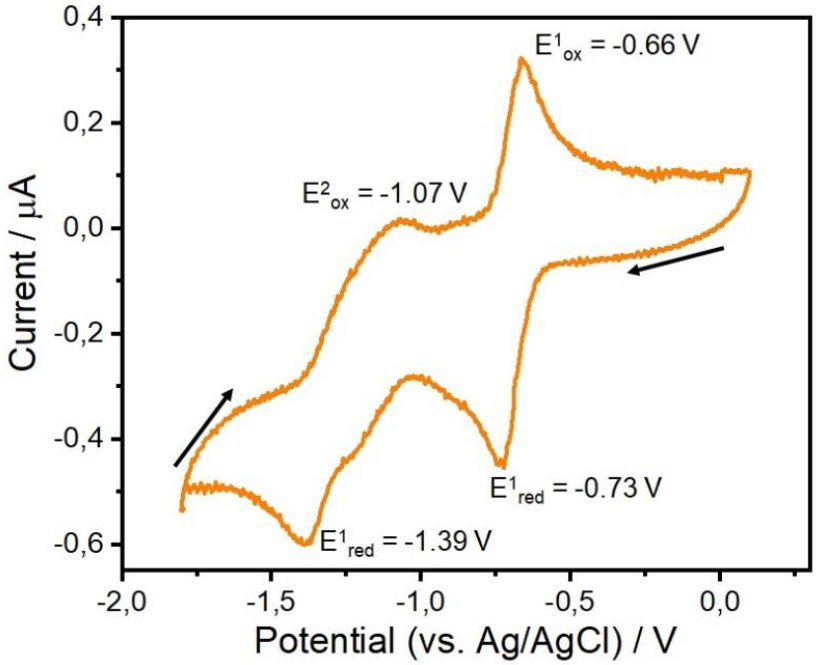

Figure S9. Cyclic voltammogram of DPAq (0.1 mM, orange line) in DMF at a 20 $mV.s^{-1}$ with $[NBu_4][PF_6]$ (100 mM) as supporting electrolyte.

2.2.2. Controlling the incorporation of distinct oxidation states into metal-organic frameworks

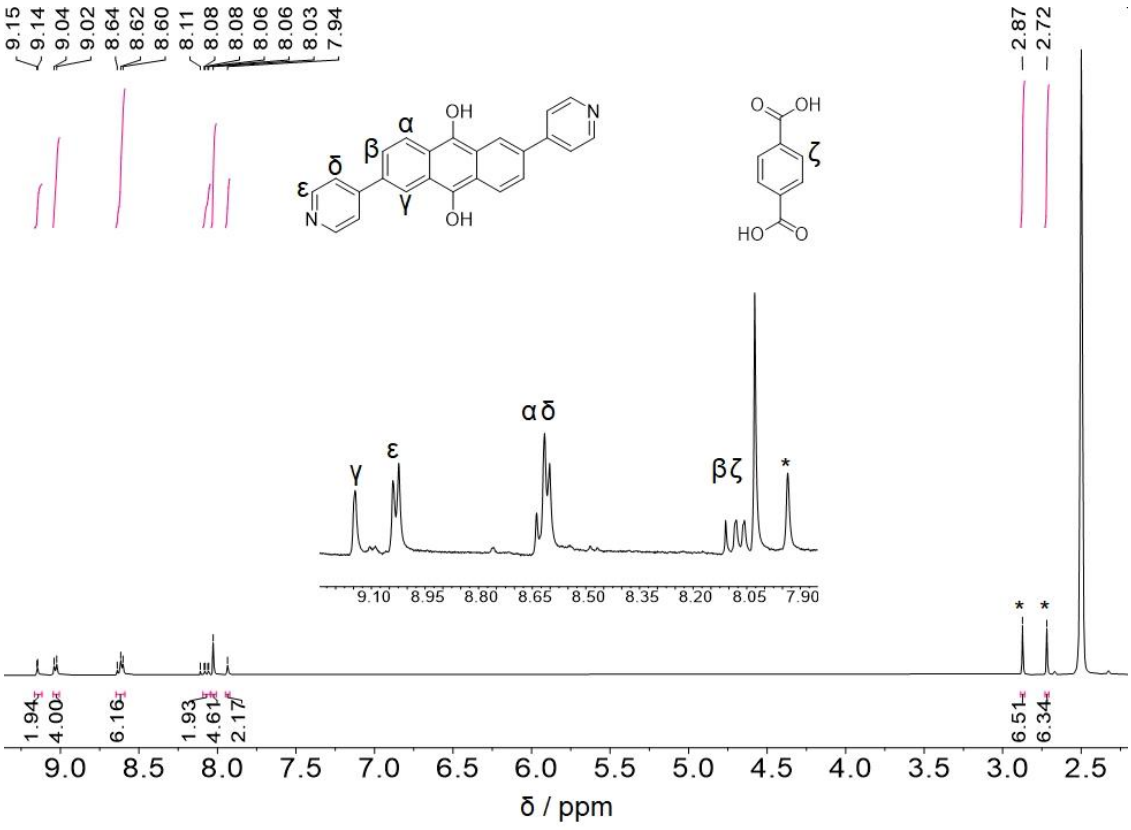

Figure S10. Section of the ^1H NMR spectrum of digested crystals of **4** in degassed TFA/DMSO-d_6. The water peak shifted downfield was omitted for clarity.

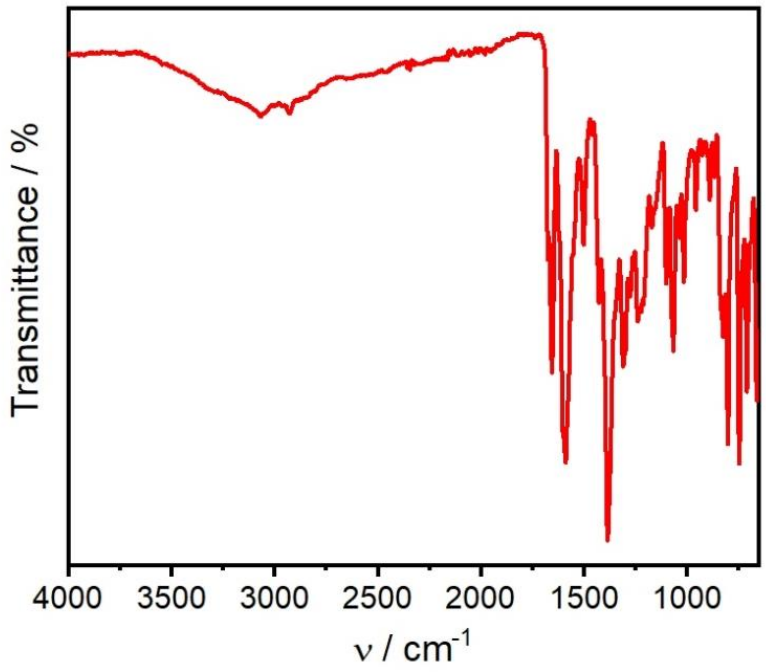

Figure S11. FTIR spectrum of **4**.

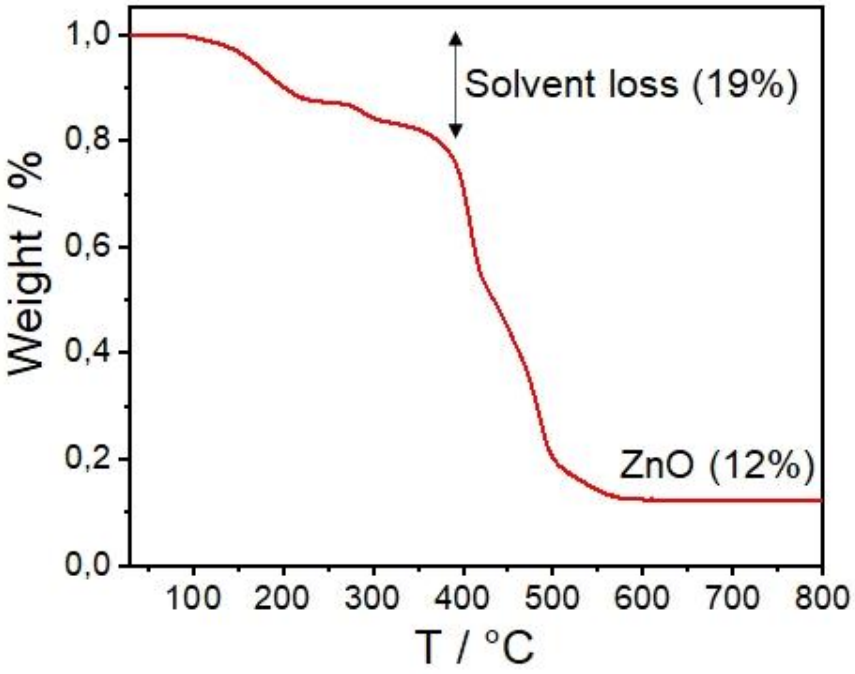

Figure S12. Thermogravimetric curve of **4**.

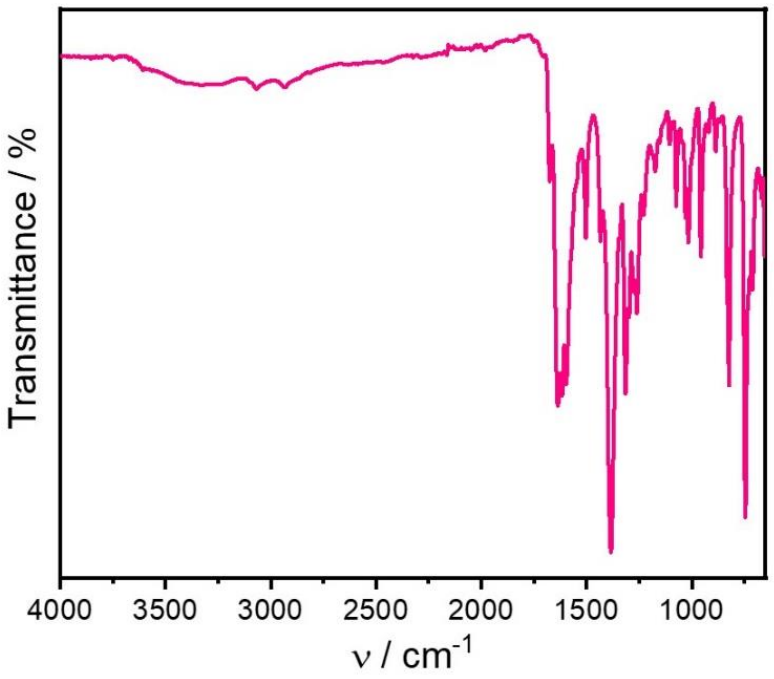

Figure S13. FTIR spectrum of **5**.

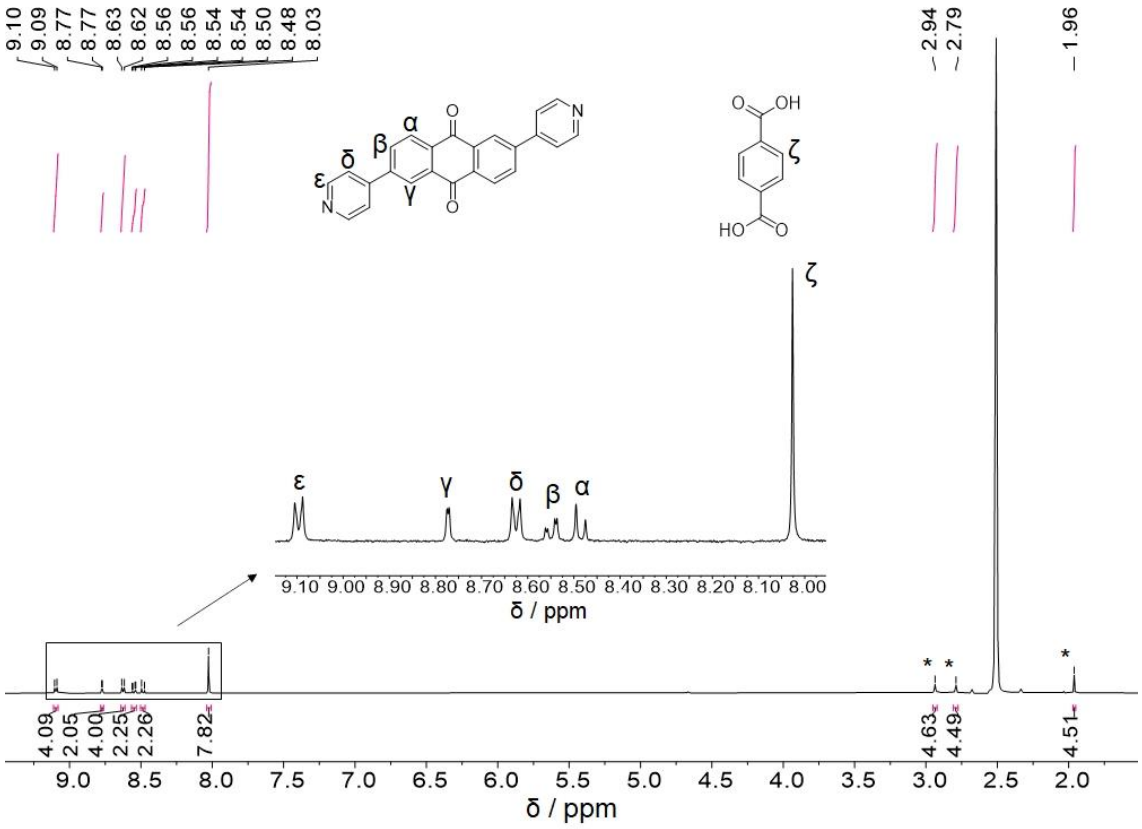

Figure S14. Section of the ^{1}H NMR spectrum of digested crystals of **5** in TFA/DMSO-d_6. The water peak shifted downfield was omitted for clarity.

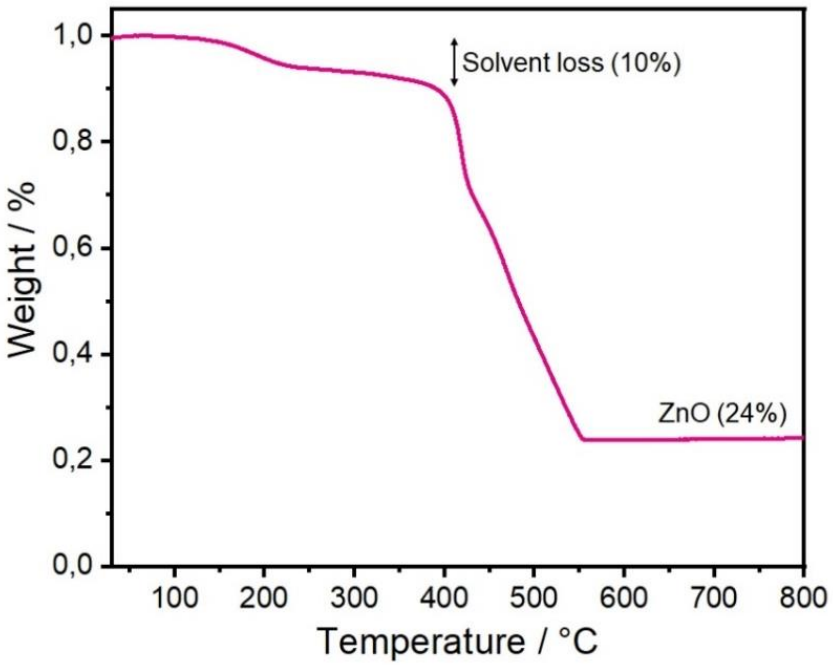

Figure S15. Thermogravimetric curve of **5**.

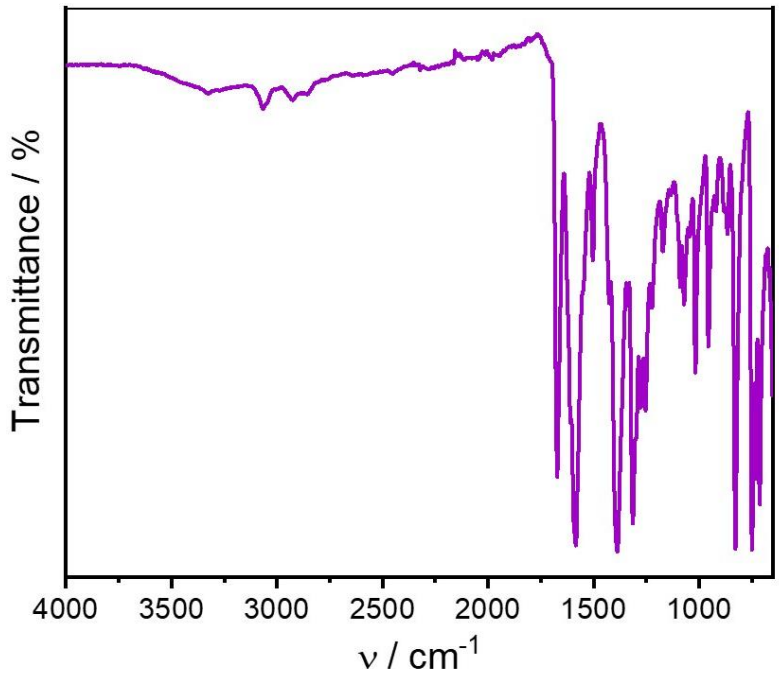

Figure S16. FTIR spectrum of **6**.

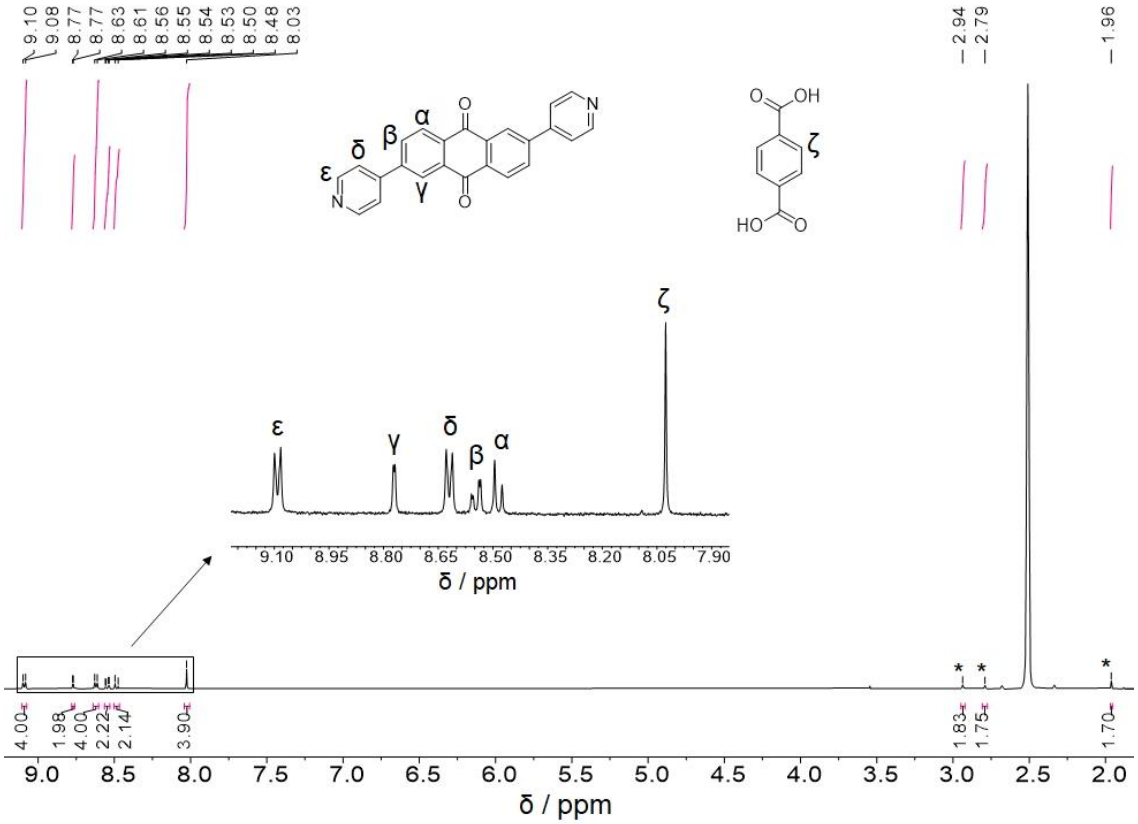

Figure S17. Section of the ^{1}H NMR spectrum of digested crystals of **6** in TFA/DMSO-d_6. The water peak shifted downfield was omitted for clarity.

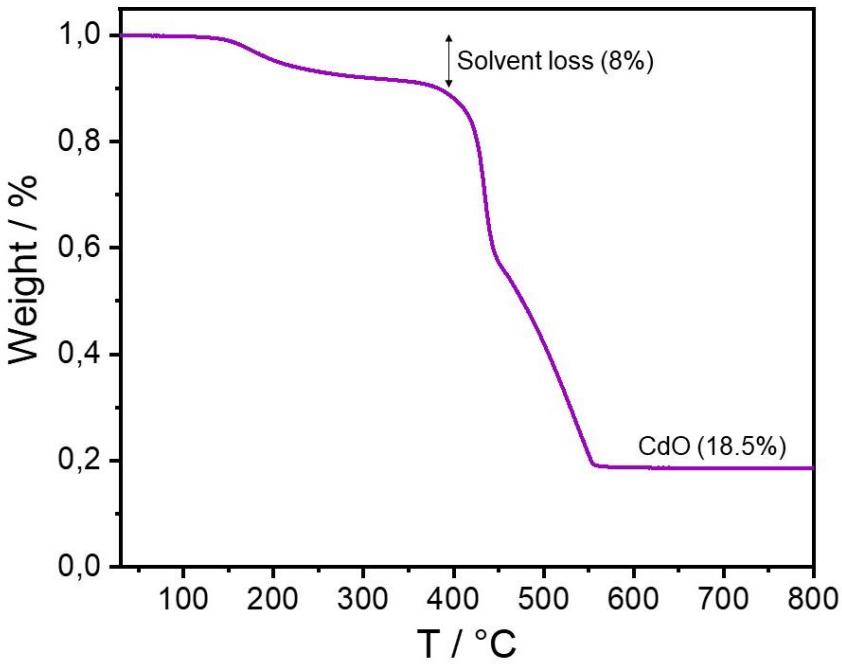

Figure S18. Thermogravimetric curve of **6**.

2.2.3. Anthraquinone-based redox-switches: following new perspectives on heterogeneous systems for dioxygen activation and hydrogen peroxide synthesis

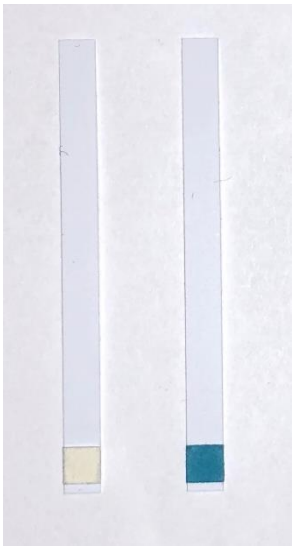

Figure S19. Low concentration peroxide stripes for the qualitative detection of H_2O_2 after oxidation of **4**. Left: negative control. Right: positive result after immersion in the aqueous extract.

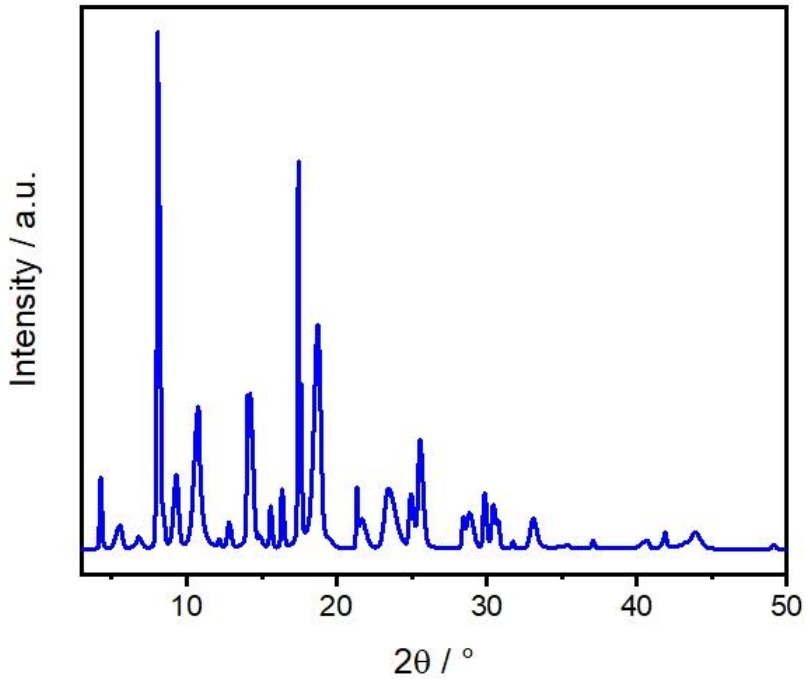

Figure S20. Powder diffractogram of **4** after thermal oxidation and aqueous extraction.

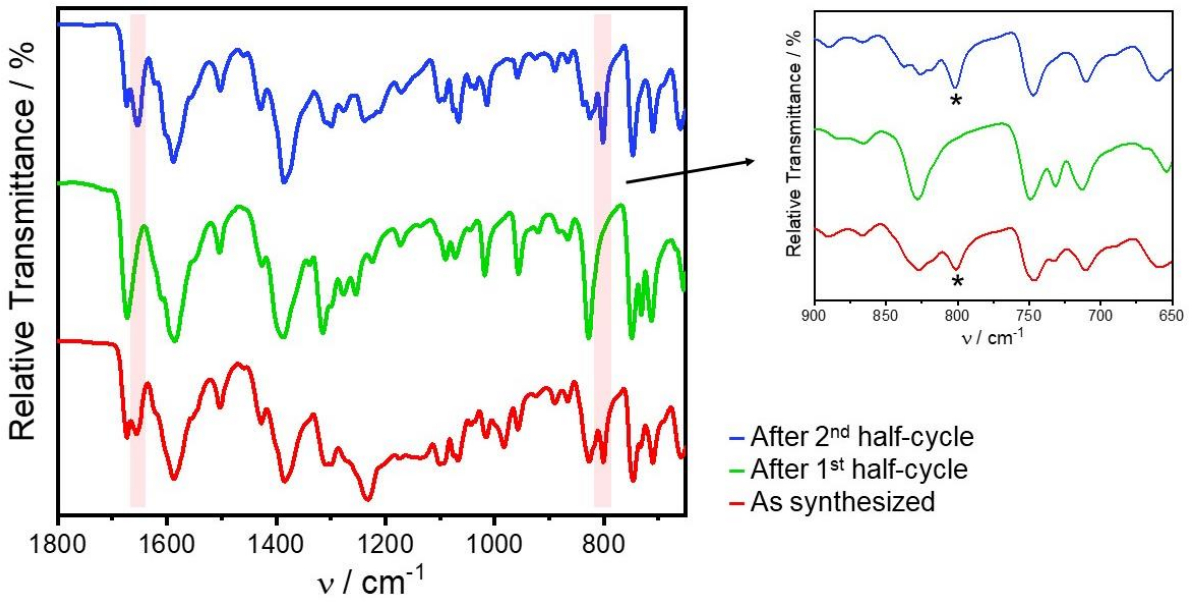

Figure S21. Infrared spectra of **4** as synthesized, after 1st half-cycle (aerobic thermal treatment) and after the 2nd half-cycle (reductive soaking procedure).

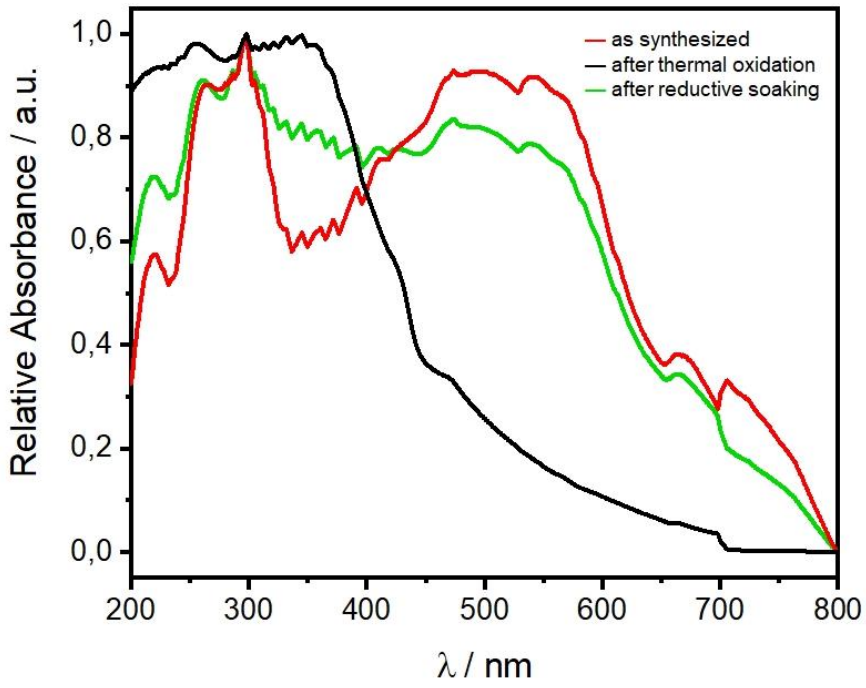

Figure S22. Solid-state UV-Vis electronic spectra of **4** as synthesized (red line), after oxidation (black line), and after reduction (green line).

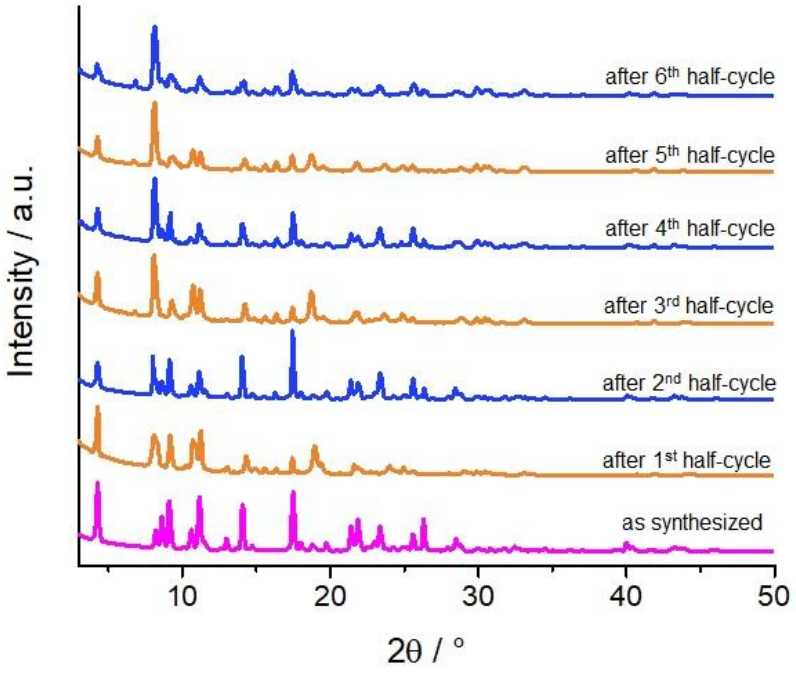

Figure S23. PXRDs of **4** as synthesized and after the respective number of half-cycles.

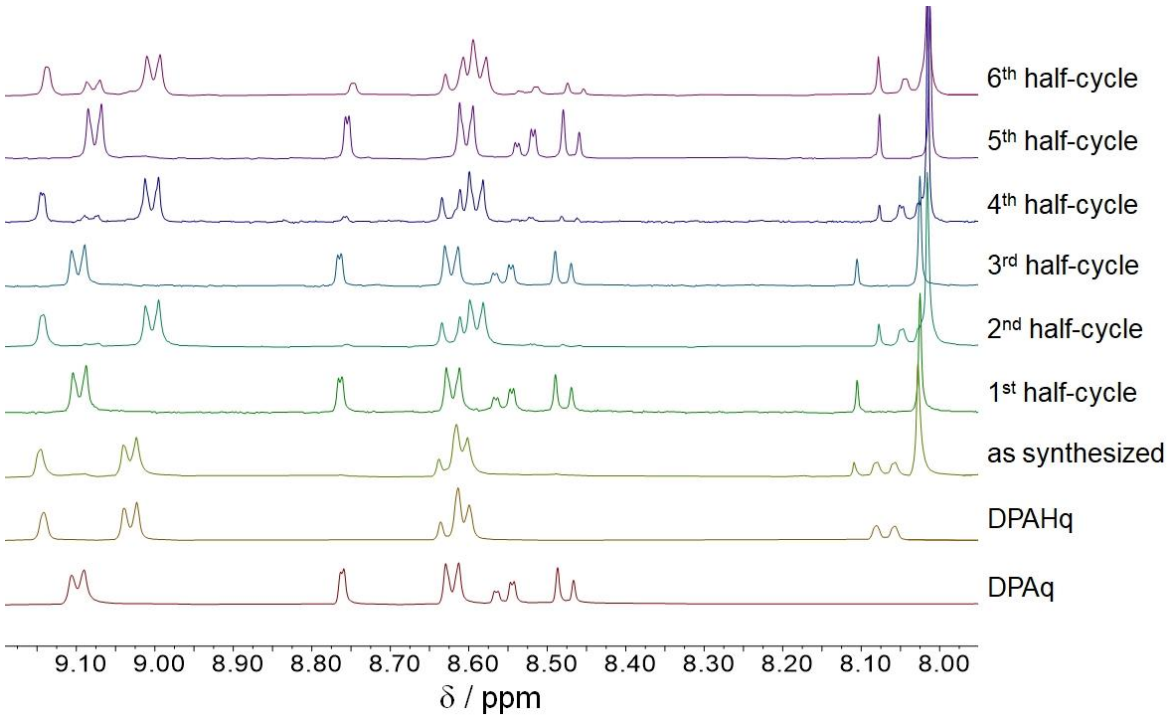

Figure S24. ^{1}H NMR spectra of pure linkers and **4** as synthesized and after the respective number of cycles.

2.2. Solid-State Chemistry and Properties of Diphenylamine-Anthraquinone-Based Metal-Organic Frameworks

2.2.1. Ligand design, synthesis, and characterization

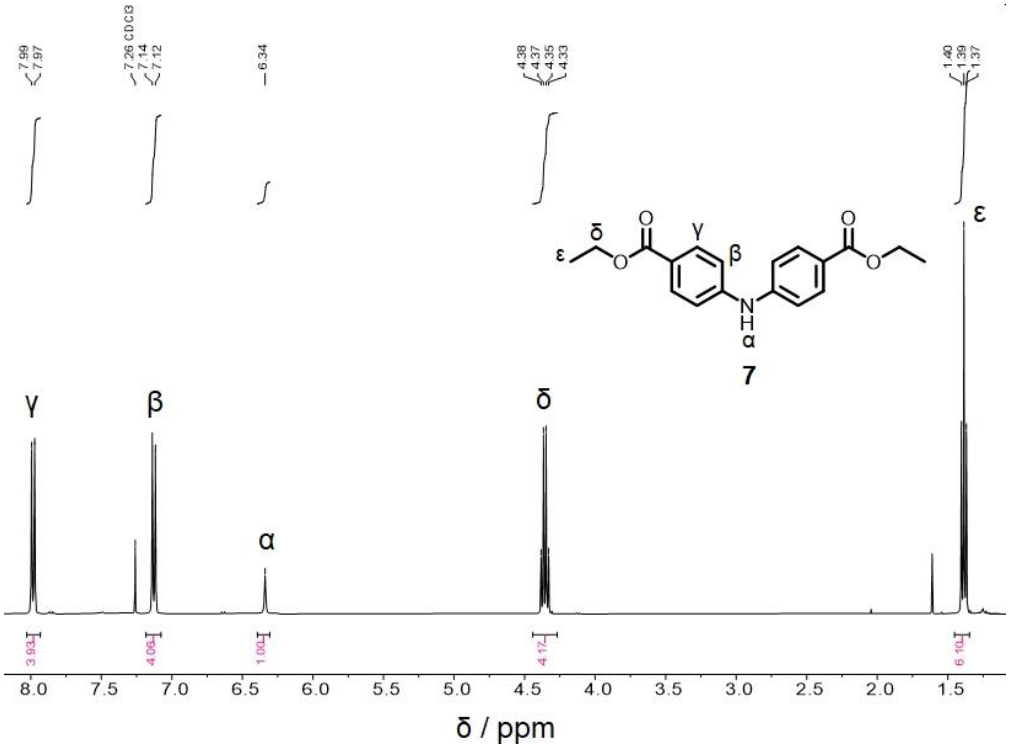

Figure S25. ^{1}H NMR spectrum of **7** in $CDCl_3$.

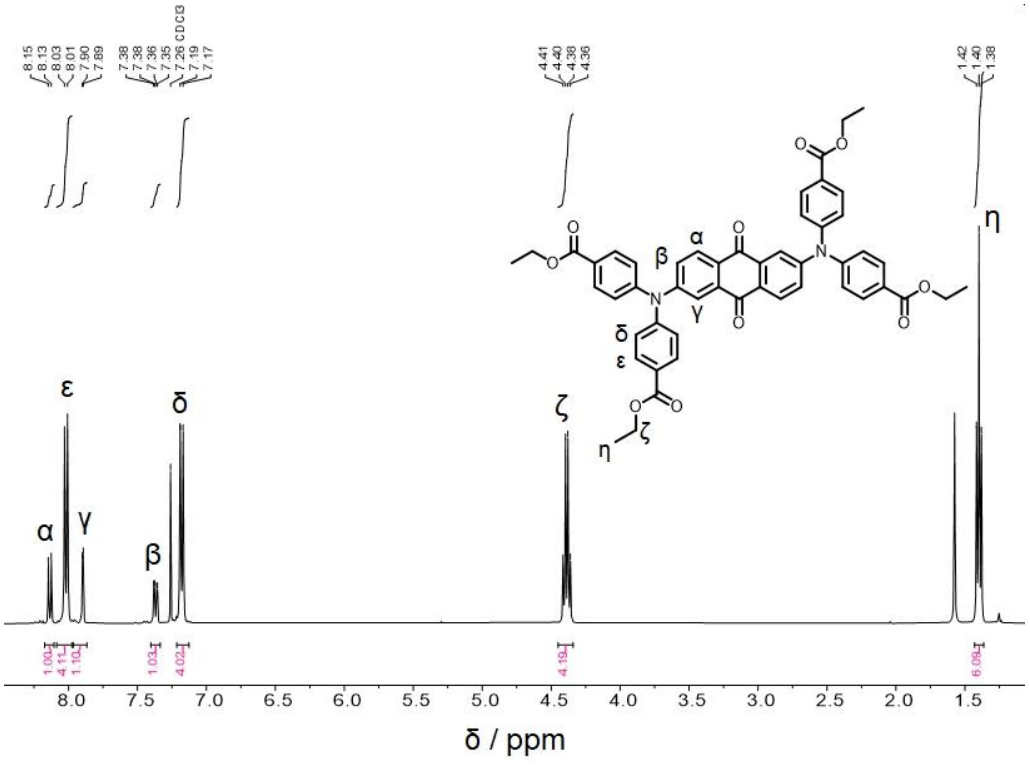

Figure S26. ^{1}H NMR spectrum of **8** in $CDCl_3$.

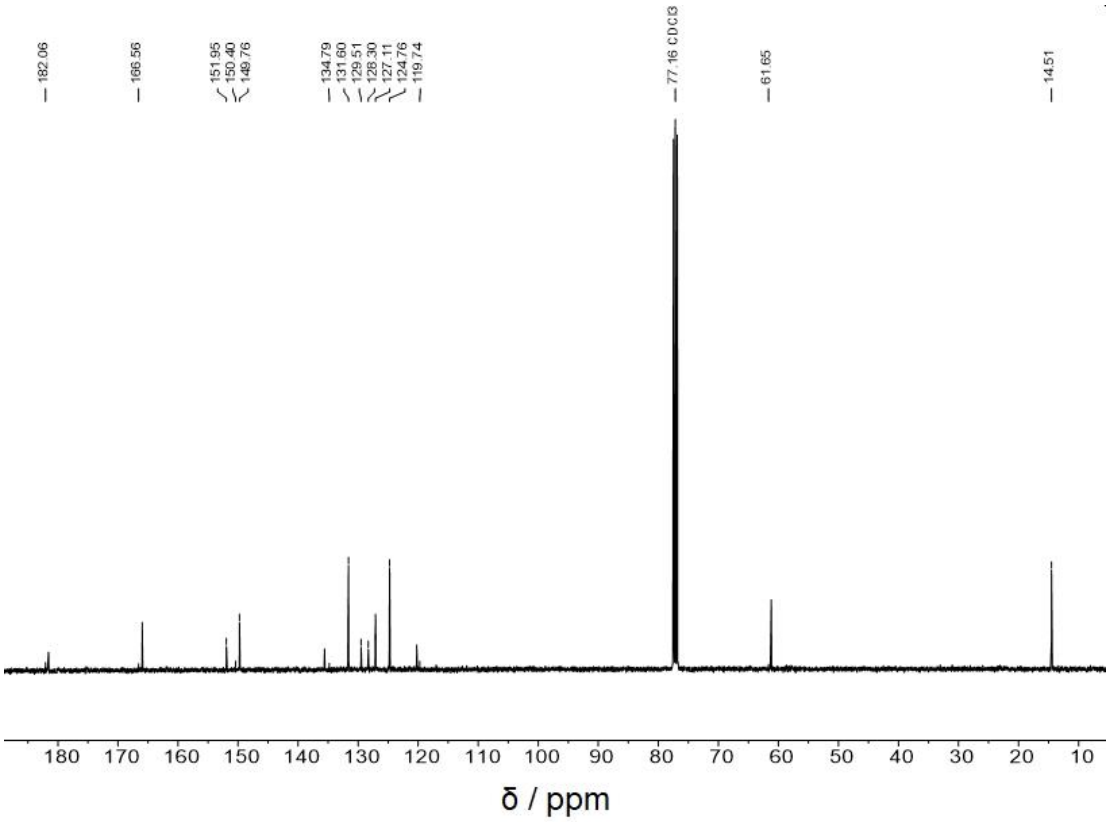

Figure S27. ^{13}C NMR spectrum of **8** in $CDCl_3$.

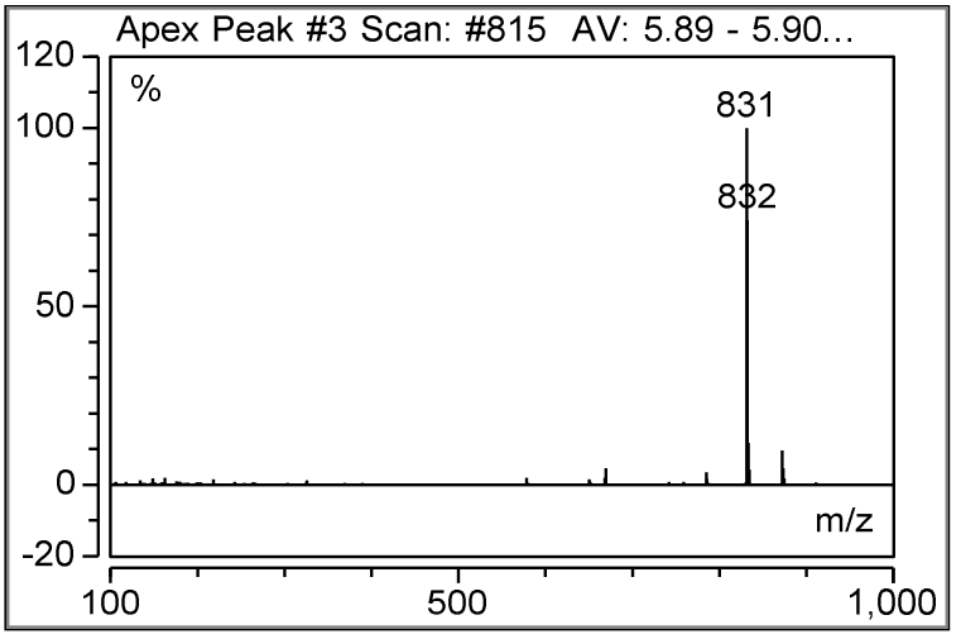

Figure S28. Mass spectrum of **8** showing $[M+H]^+$, m/z = 831.

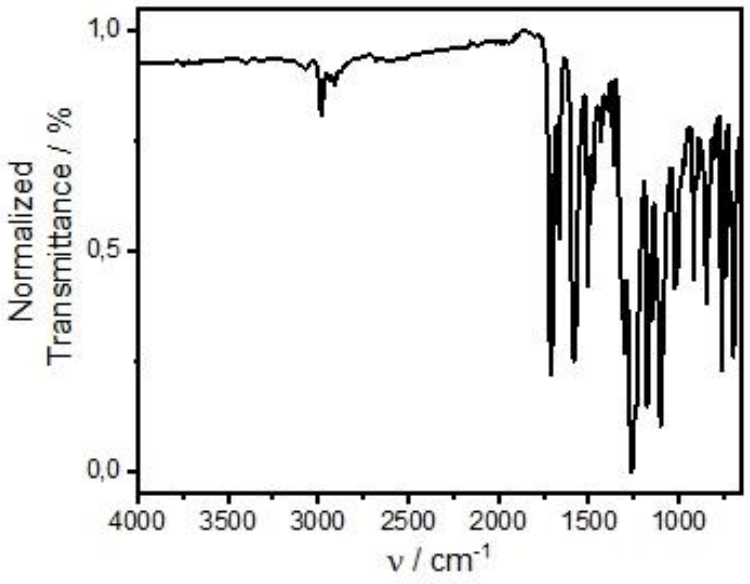

Figure S29. FTIR spectrum of **8**.

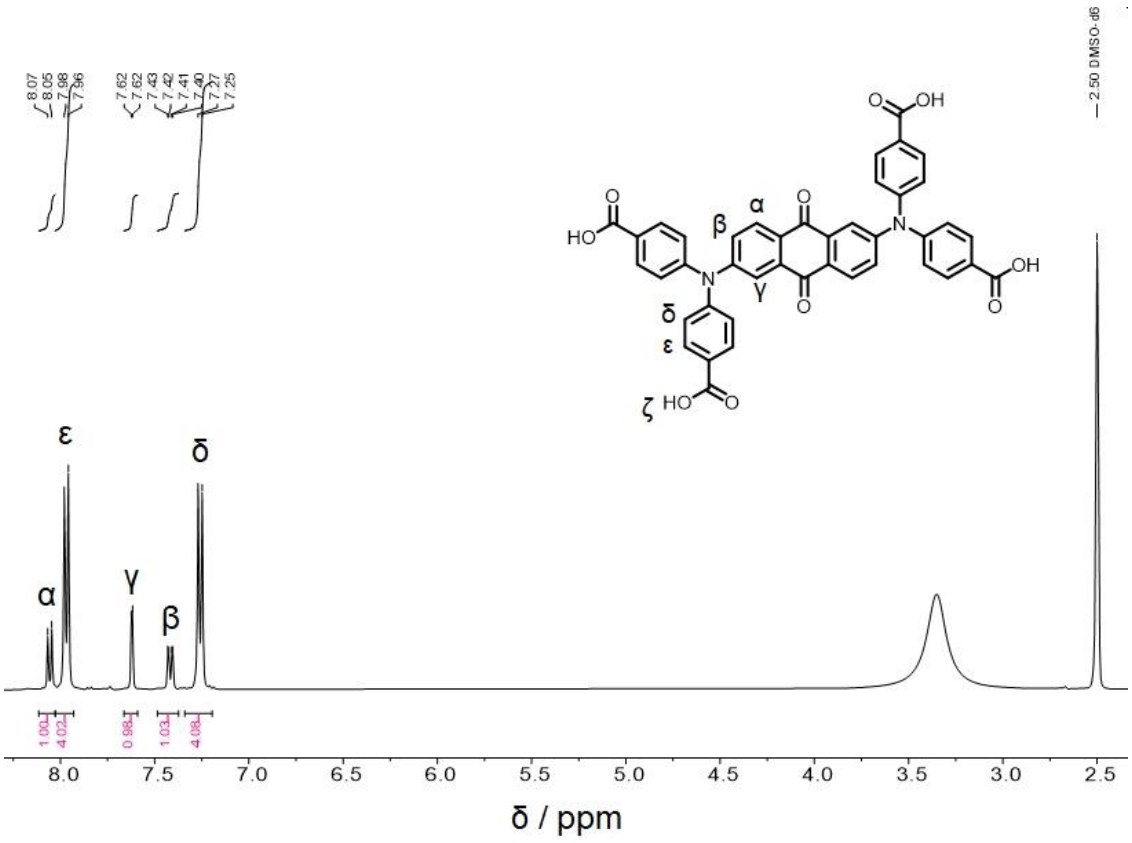

Figure S30. ^{1}H NMR spectrum of **9** in DMSO-d_6. The carboxylic acid proton was omitted for clarity.

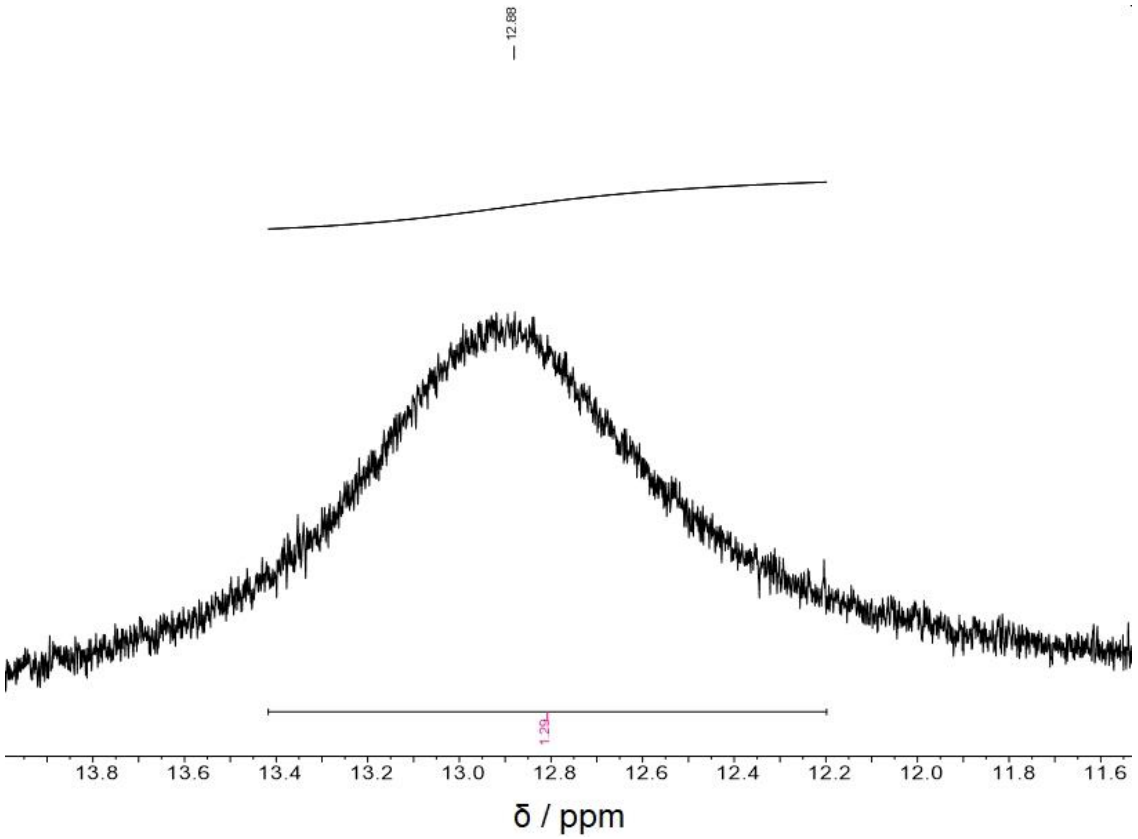

Figure S31. Section of the ^{1}H NMR spectrum of **9** in DMSO-d_6 highlighting the carboxylic acid proton (ζ).

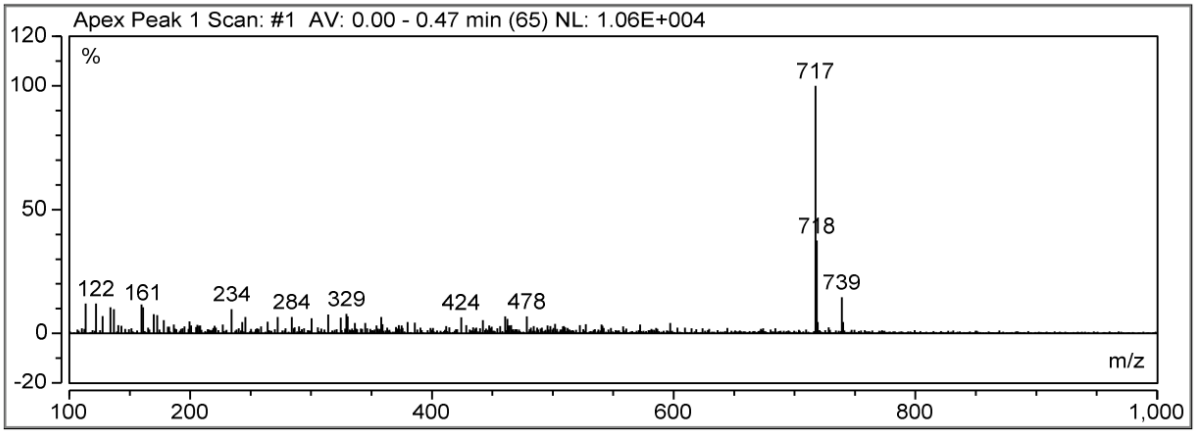

Figure S32. Mass spectrum of **9** showing $[M-H]^-$, m/z = 717 and $[M-2H+Na]^-$, m/z = 739.

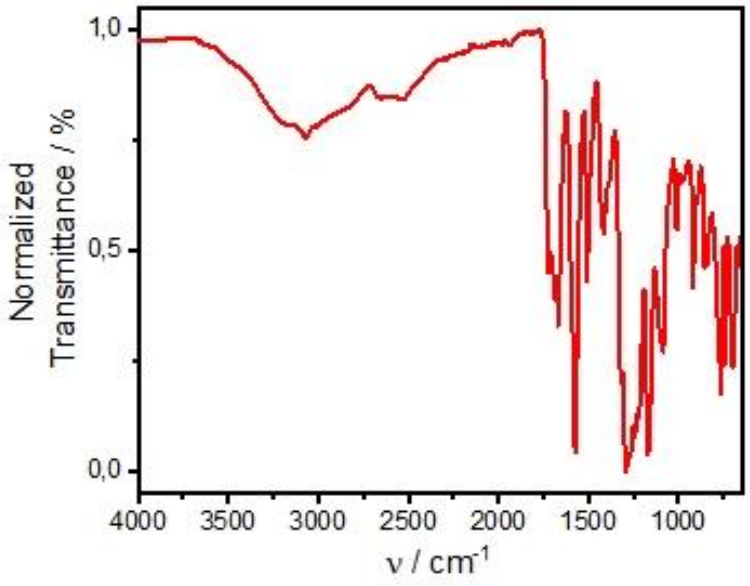

Figure S33. FTIR spectrum of **9**.

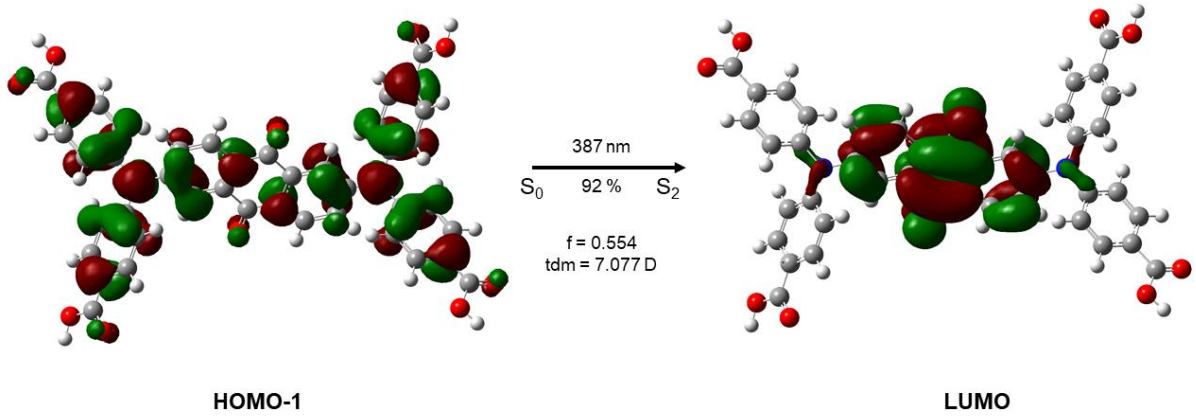

Figure S34. Representation of the molecular orbitals involved in the CT transition (HOMO-1/LUMO) in **9**.

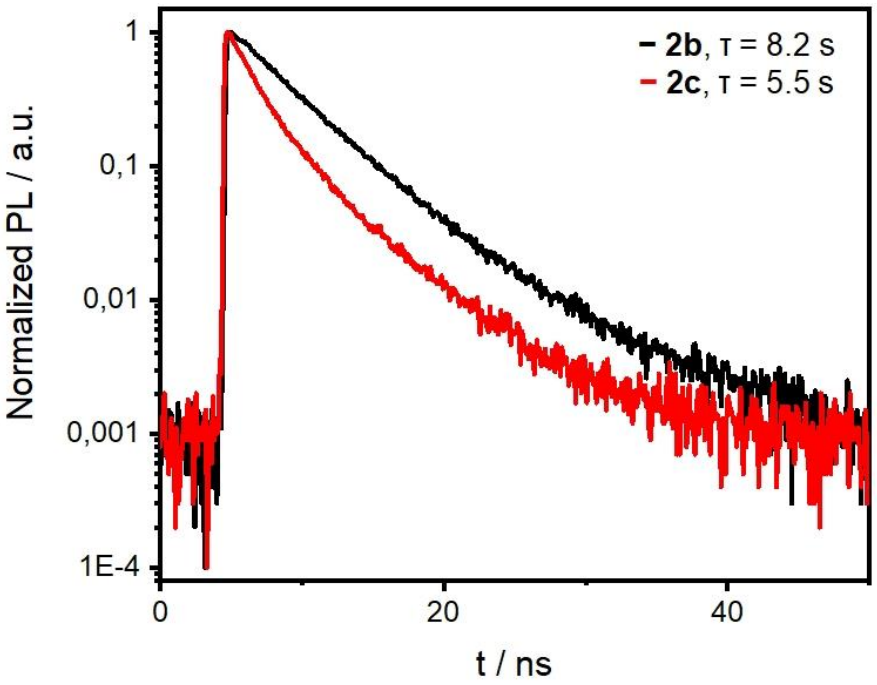

Figure S35. Time-resolved emission of **8** (in toluene, black line) and **9** (in DMF, red line) with associated lifetimes.

2.2.2. Synthesis and Structural Characterization of Alkaline Earth Metal-Based Metal-Organic Frameworks

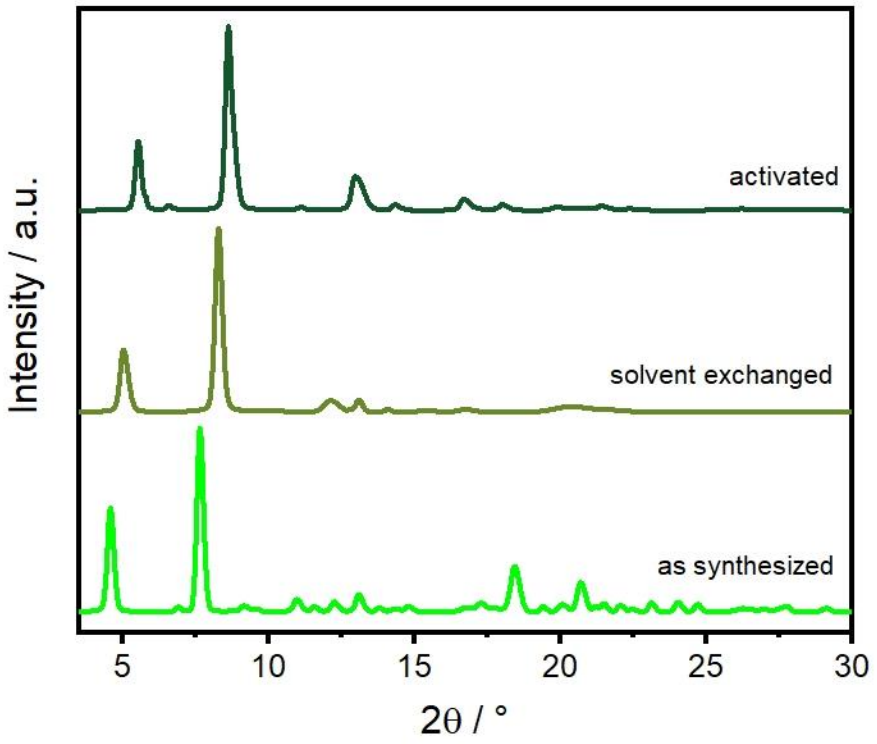

Figure S36. Powder diffractogram of **10** as synthesized (light green line) and after activation (dark green line).

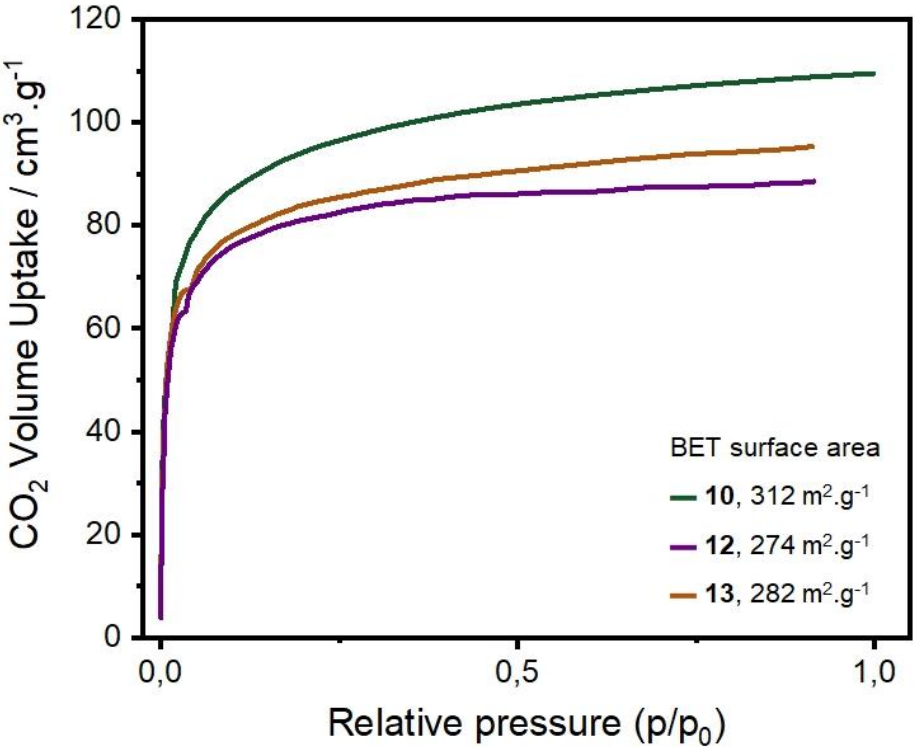

Figure S37. BET CO_2 adsorption curves of **10** (green line), **12** (blue line), and **13** (brown line).

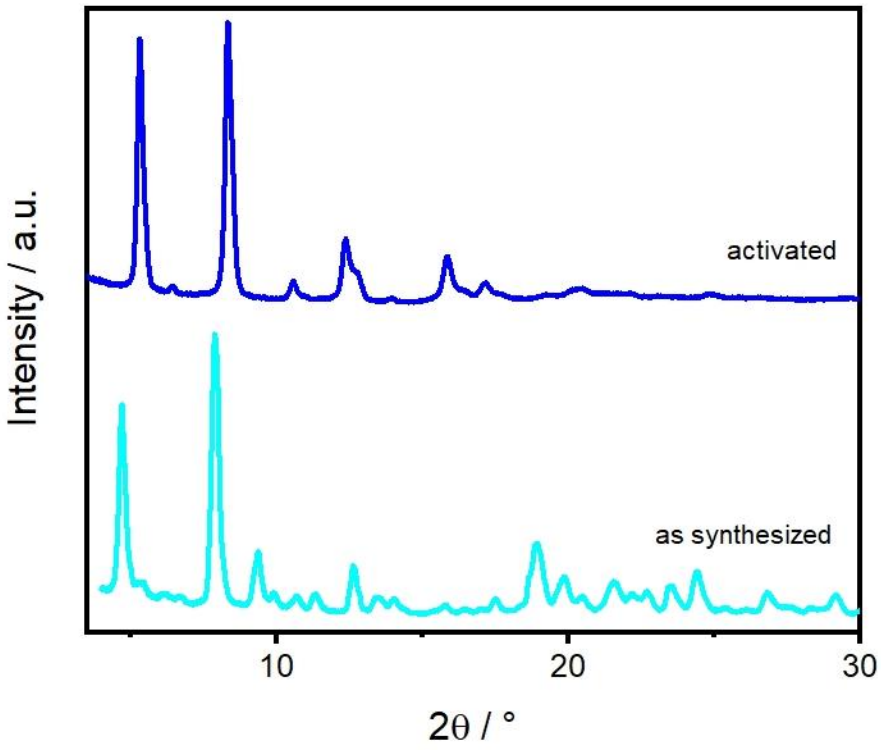

Figure S38. Powder diffractogram of **11** as synthesized (cyan line) and after activation (blue line).

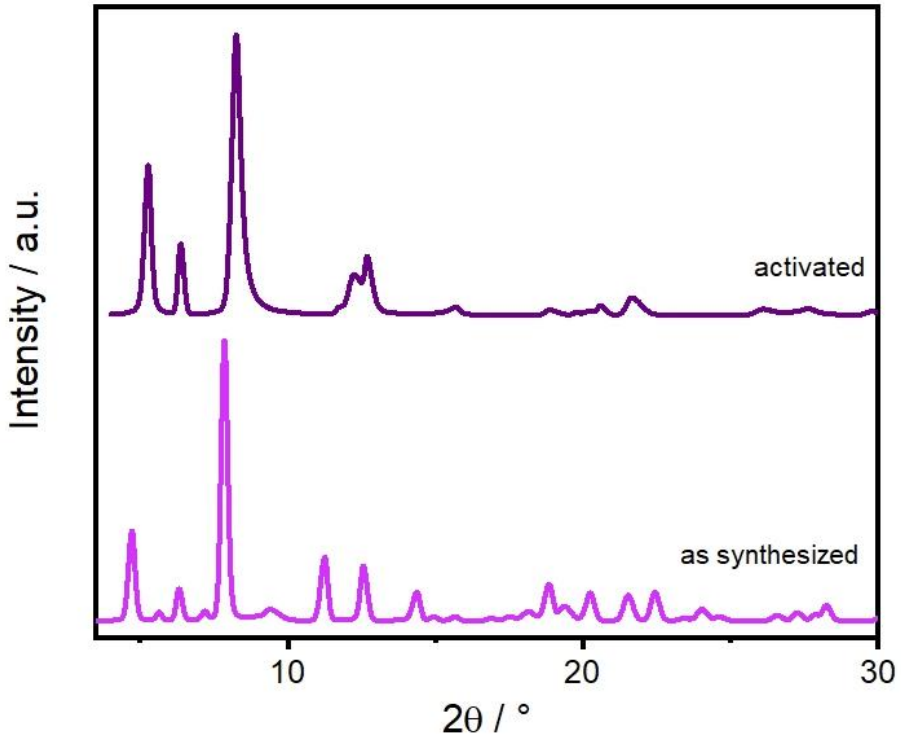

Figure S39. Powder diffractogram of **12** as synthesized (purple line) and after activation (dark purple line).

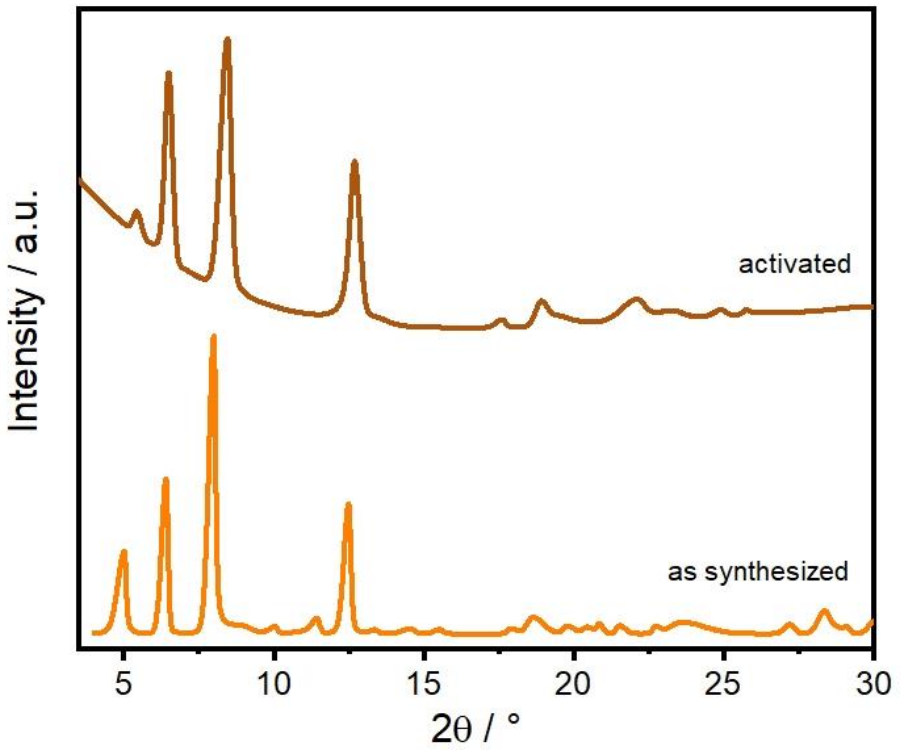

Figure S40. Powder diffractogram of **13** as synthesized (orange line) and after activation (brown line).

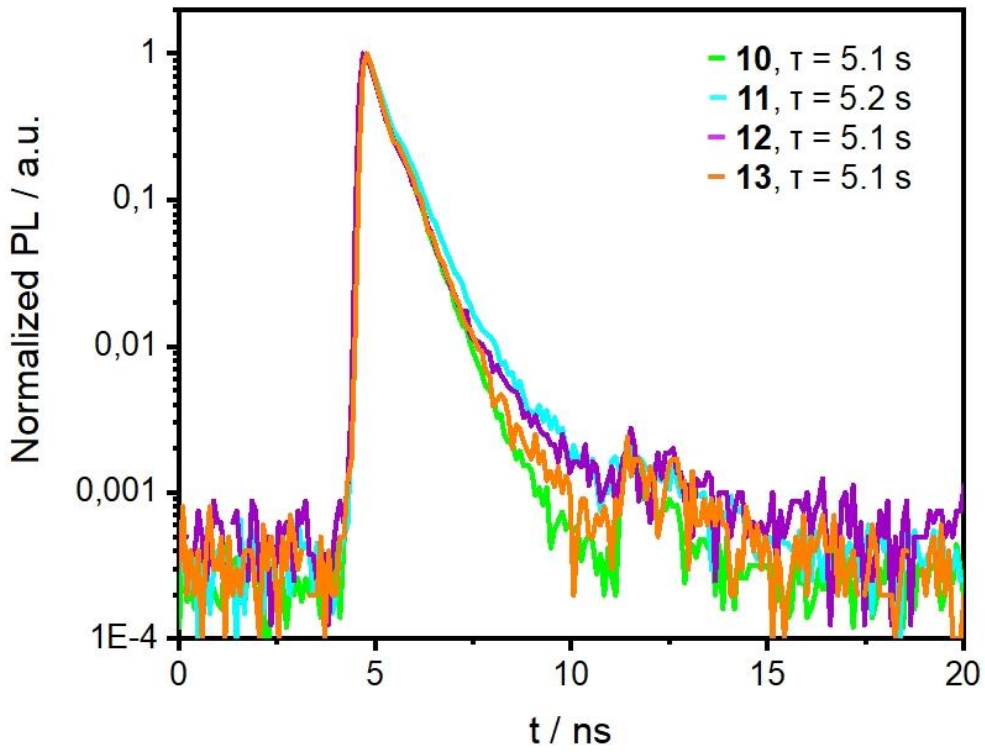

Figure S41. Time-resolved emission of **10** (green line)**, 11** (cyan line), **12** (purple line), and **13** (orange line) with associated lifetimes.

2.2.3. Light-driven Heterogeneous Photooxidation of Sulfides to Sulfoxides

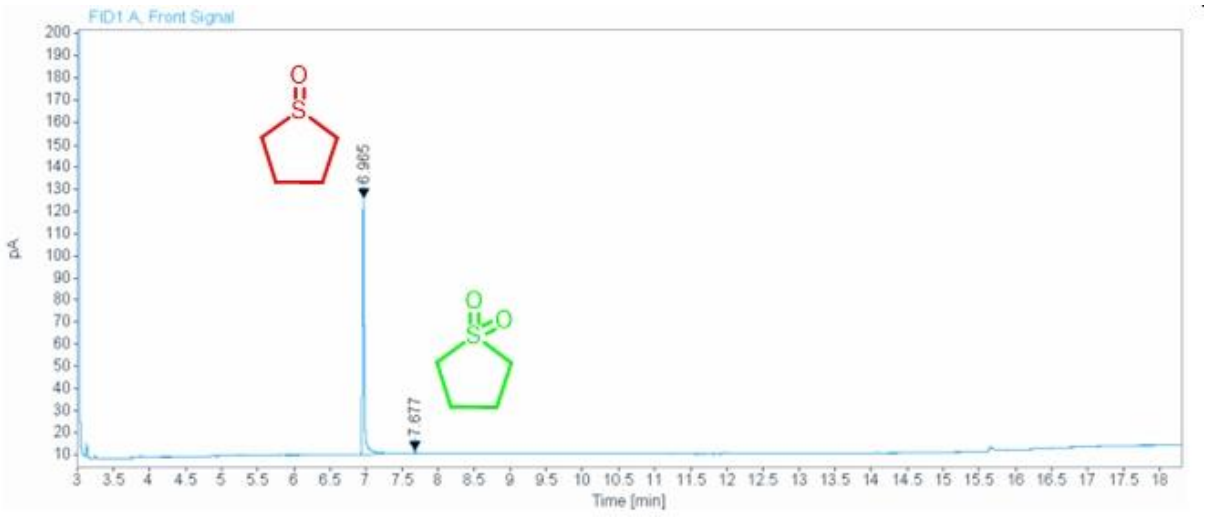

Figure S42. Chromatogram of the resulting mixture after the photooxidation of THT over **9**. Reaction conditions: THT (0.125 mmol), **9** (5 mol%), CH_3CN (5.0 mL), O_2 (1 atm), purple LED (λ = 420 nm), room temperature.

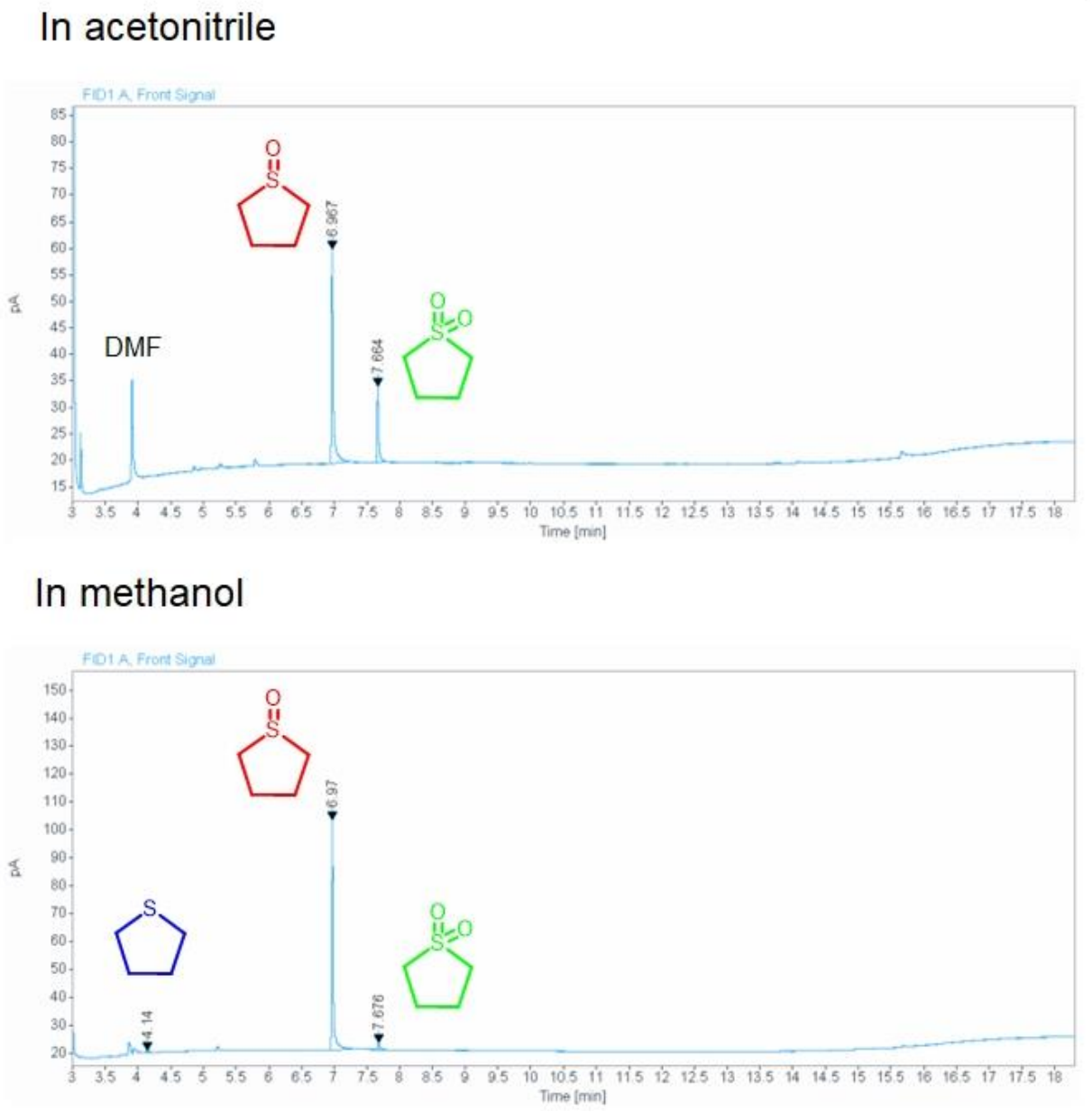

Figure S43. Chromatogram of the resulting mixture after the photooxidation of THT over **10**. Reaction conditions: THT (0.125 mmol), **10** (10 mg), solvent (5.0 mL), O_2 (1 atm), purple LED (λ = 420 nm), room temperature.

2.3. Incorporation of Established Synthetic Dyes into Metal-Organic Frameworks

2.3.1. Synthesis of soluble anthanthrone-derived linkers from commercial vat dyes

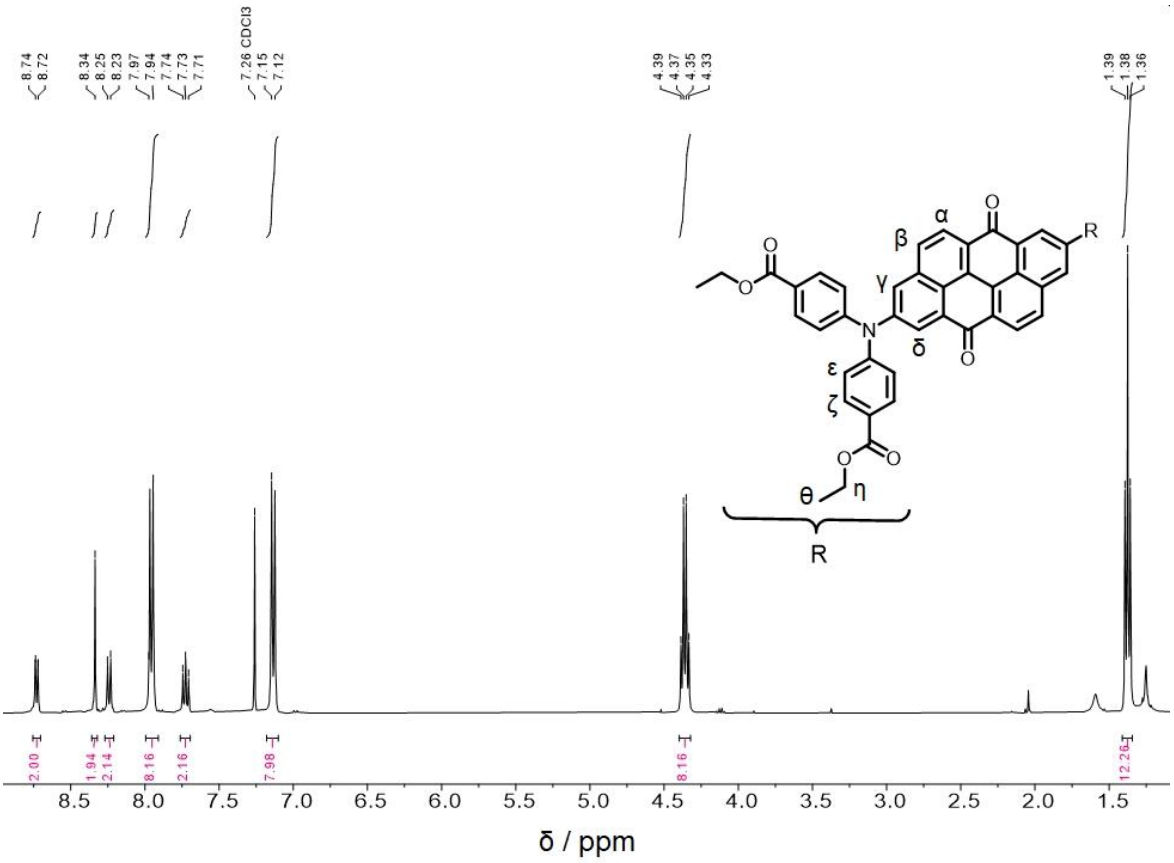

Figure S44. ^{1}H NMR spectrum of **14** in $CDCl_3$.

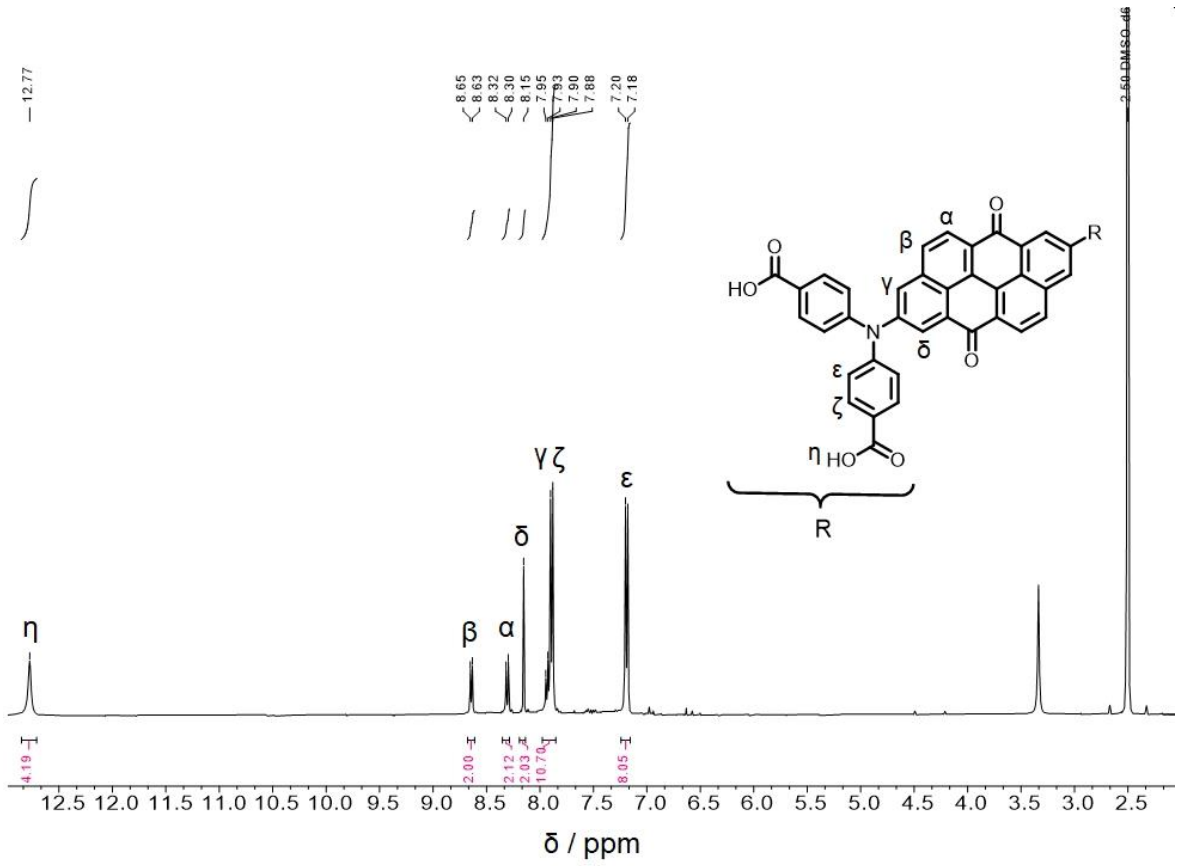

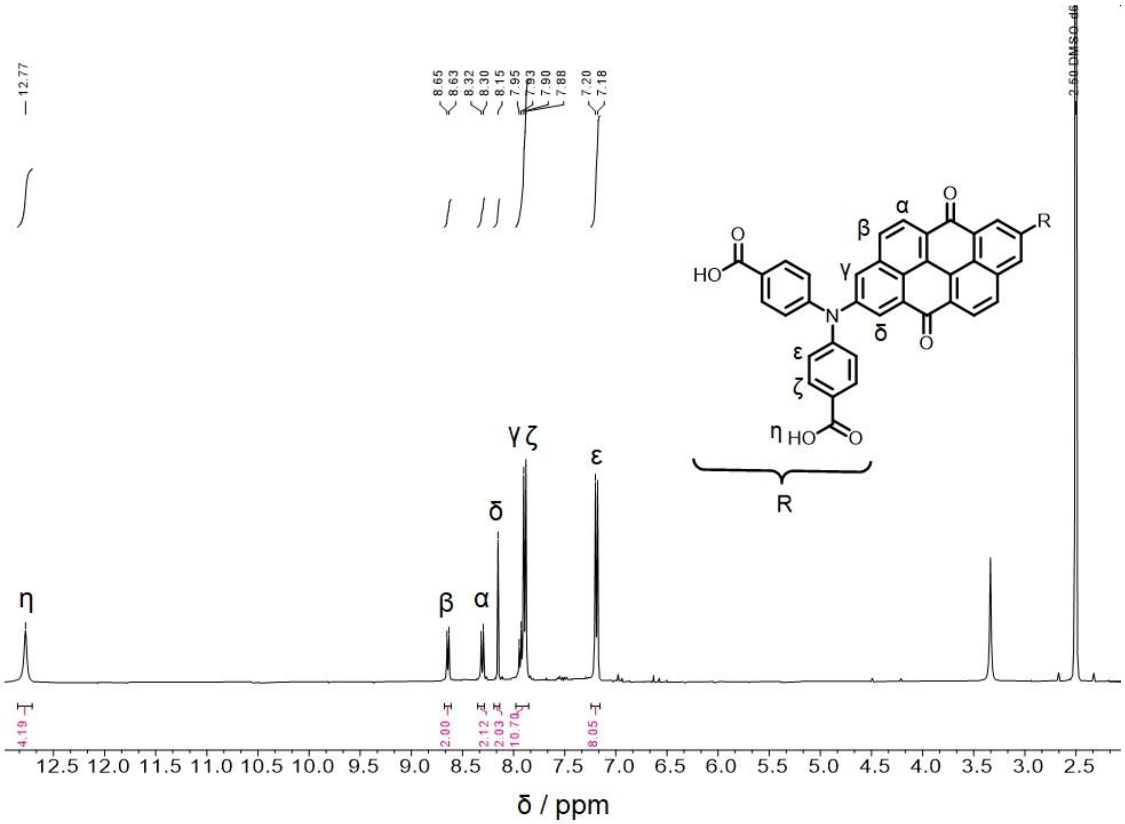

Figure S45. ^{1}H NMR spectrum of **15** in /DMSO-d_6.

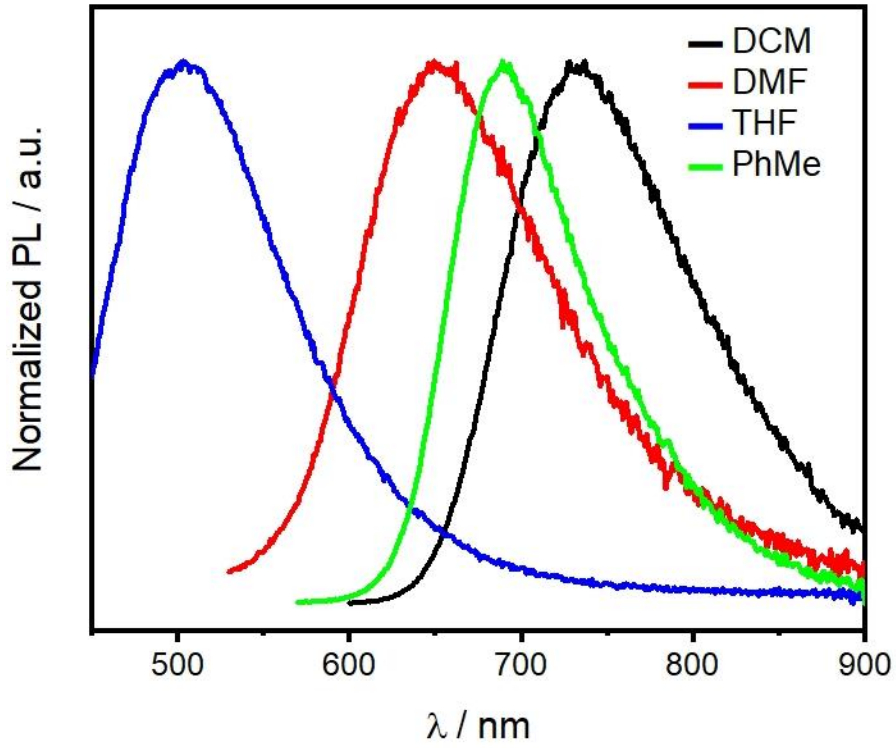

Figure S46. Depiction of the solvent dependance of the emission of **14**.

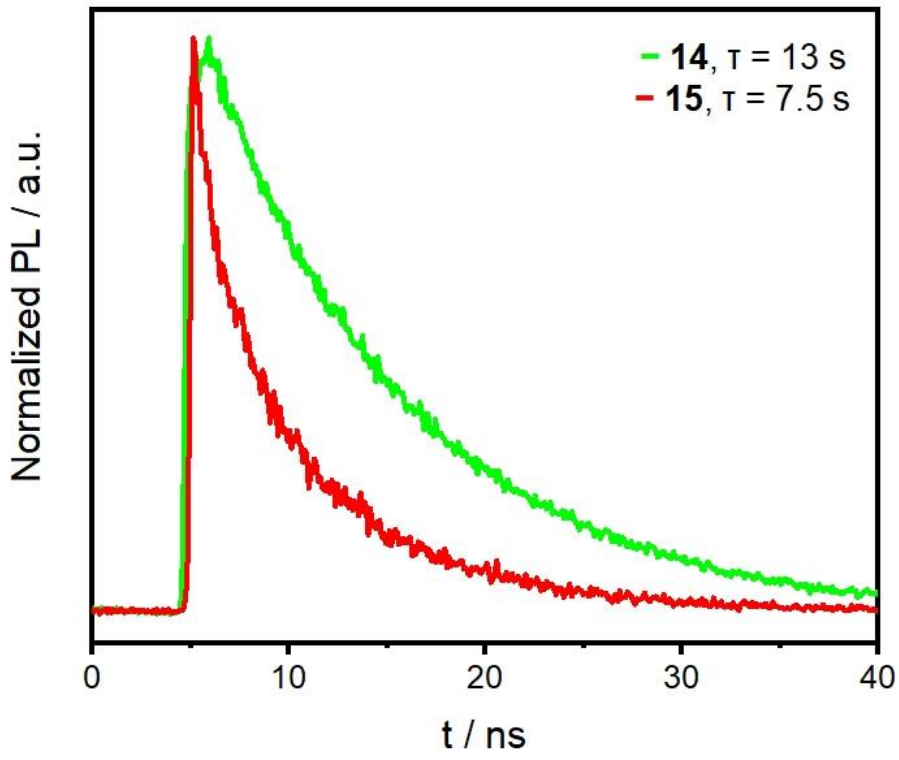

Figure S47. Time-resolved emission of **14** (green line) and **15** (red line) with associated lifetimes.

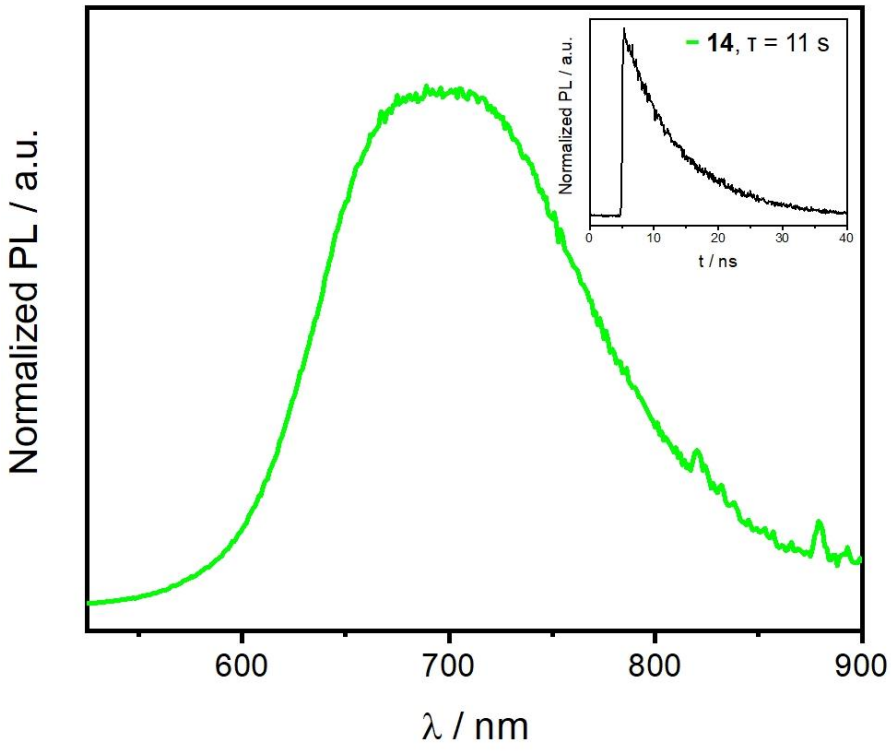

Figure S48. Solid-state emission spectrum of **14** and the associated lifetime/decay.

2.3.2. Construction of polymeric anthanthrone-derived coordination frameworks

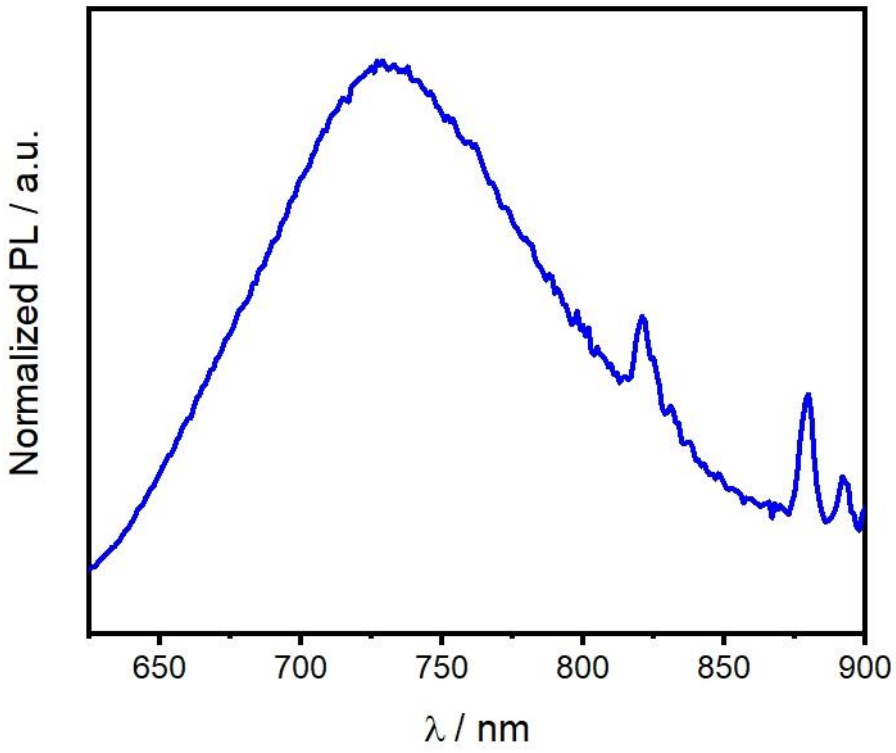

Figure S49. Emission spectrum of the anthanthrone-based Zn-MOF, 16.

7. REPRINT PERMISSIONS

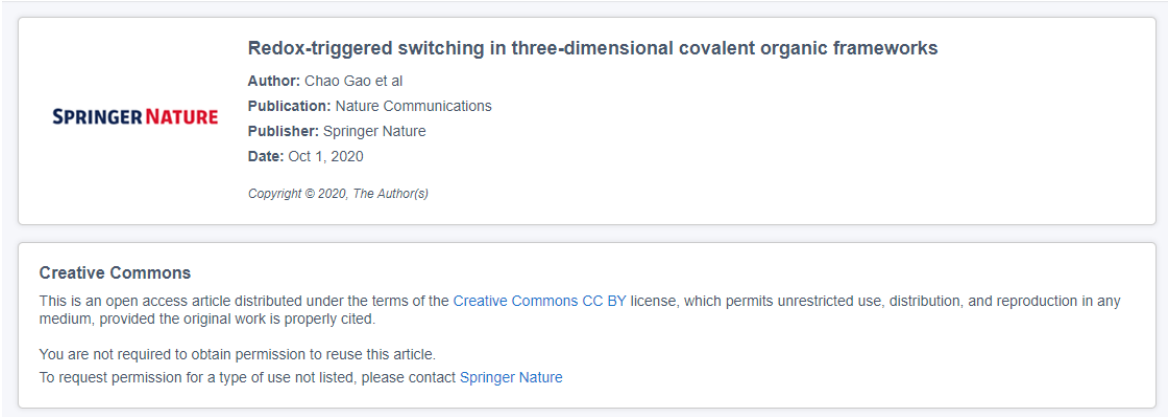

SPRINGER NATURE

Redox-triggered switching in three-dimensional covalent organic frameworks

Author: Chao Gao et al
Publication: Nature Communications
Publisher: Springer Nature
Date: Oct 1, 2020

Copyright © 2020, The Author(s)

Creative Commons

This is an open access article distributed under the terms of the Creative Commons CC BY license, which permits unrestricted use, distribution, and reproduction in any medium, provided the original work is properly cited.

You are not required to obtain permission to reuse this article.
To request permission for a type of use not listed, please contact Springer Nature

Link to license: http://creativecommons.org/licenses/by/4.0/.

SPRINGER NATURE

Multimodal switching of a redox-active macrocycle

Author: Daniel T. Payne et al
Publication: Nature Communications
Publisher: Springer Nature
Date: Mar 1, 2019

Copyright © 2019, The Author(s)

Creative Commons

This is an open access article distributed under the terms of the Creative Commons CC BY license, which permits unrestricted use, distribution, and reproduction in any medium, provided the original work is properly cited.

You are not required to obtain permission to reuse this article.
To request permission for a type of use not listed, please contact Springer Nature

Link to license: http://creativecommons.org/licenses/by/4.0/.

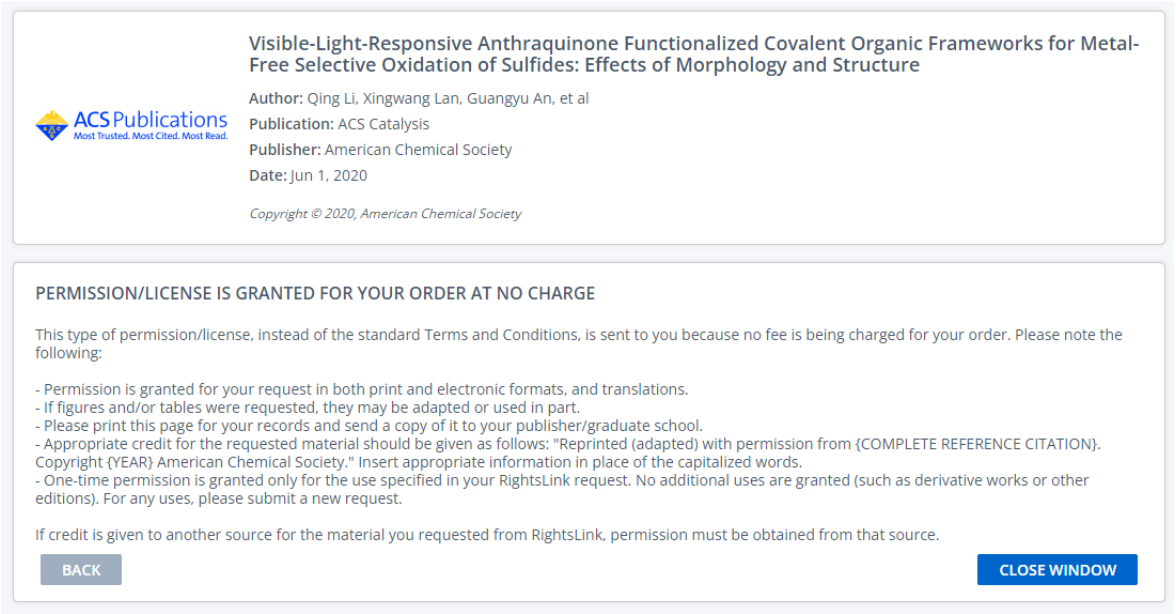

ACS Publications
Most Trusted. Most Cited. Most Read.

Visible-Light-Responsive Anthraquinone Functionalized Covalent Organic Frameworks for Metal-Free Selective Oxidation of Sulfides: Effects of Morphology and Structure

Author: Qing Li, Xingwang Lan, Guangyu An, et al
Publication: ACS Catalysis
Publisher: American Chemical Society
Date: Jun 1, 2020

Copyright © 2020, American Chemical Society

PERMISSION/LICENSE IS GRANTED FOR YOUR ORDER AT NO CHARGE

This type of permission/license, instead of the standard Terms and Conditions, is sent to you because no fee is being charged for your order. Please note the following:

- Permission is granted for your request in both print and electronic formats, and translations.
- If figures and/or tables were requested, they may be adapted or used in part.
- Please print this page for your records and send a copy of it to your publisher/graduate school.
- Appropriate credit for the requested material should be given as follows: "Reprinted (adapted) with permission from {COMPLETE REFERENCE CITATION}. Copyright {YEAR} American Chemical Society." Insert appropriate information in place of the capitalized words.
- One-time permission is granted only for the use specified in your RightsLink request. No additional uses are granted (such as derivative works or other editions). For any uses, please submit a new request.

If credit is given to another source for the material you requested from RightsLink, permission must be obtained from that source.

BACK CLOSE WINDOW

CCC Marketplace™

This is a License Agreement between João Guilherme Machado de Carvalho ("User") and Copyright Clearance Center, Inc. ("CCC") on behalf of the Rightsholder identified in the order details below. The license consists of the order details, the CCC Terms and Conditions below, and any Rightsholder Terms and Conditions which are included below.

All payments must be made in full to CCC in accordance with the CCC Terms and Conditions below.

Order Date	26-Nov-2021	Type of Use	Republish in a thesis/dissertation
Order License ID	1164372-1		
ISSN	2050-7496	Publisher	Royal Society of Chemistry
		Portion	Image/photo/illustration

LICENSED CONTENT

Publication Title	Journal of materials chemistry. A, Materials for energy and sustainability	Publication Type	e-Journal
		Start Page	16571
Article Title	Redox-active metal-organic frameworks for energy conversion and storage	End Page	16597
		Issue	28
		Volume	7
		URL	http://pubs.rsc.org/en/journals/journalissues/ta
Author/Editor	Royal Society of Chemistry (Great Britain)		
Date	01/01/2013		
Language	English		
Country	United Kingdom of Great Britain and Northern Ireland		
Rightsholder	Royal Society of Chemistry		

REQUEST DETAILS

Portion Type	Image/photo/illustration	Distribution	Worldwide
Number of images / photos / illustrations	1	Translation	Original language of publication
Format (select all that apply)	Print, Electronic	Copies for the disabled?	No
		Minor editing privileges?	Yes
Who will republish the content?	Academic institution	Incidental promotional use?	No
Duration of Use	Life of current edition	Currency	EUR
Lifetime Unit Quantity	Up to 499		
Rights Requested	Main product		

NEW WORK DETAILS

Title	Investigations of Physical Properties of Metal-Organic Frameworks with Functional Ligands	Institution name	Technical University of Munich
		Expected presentation date	2022-03-01
Instructor name	Roland A. Fischer		

ADDITIONAL DETAILS

Order reference number	N/A

The requesting person / organization to appear on the license	João Guilherme Machado de Carvalho

REUSE CONTENT DETAILS

Title, description or numeric reference of the portion(s)	Figure 1	Title of the article/chapter the portion is from	Redox-active metal-organic frameworks for energy conversion and storage
Editor of portion(s)	Calbo, Joaquín; Golomb, Matthias Johannes; Walsh, Aron	Author of portion(s)	Calbo, Joaquín; Golomb, Matthias Johannes; Walsh, Aron
Volume of serial or monograph	7	Issue, if republishing an article from a serial	28
Page or page range of portion	16571-16597	Publication date of portion	2019-01-01

CCC Terms and Conditions

1. Description of Service; Defined Terms. This Republication License enables the User to obtain licenses for republication of one or more copyrighted works as described in detail on the relevant Order Confirmation (the "Work(s)"). Copyright Clearance Center, Inc. ("CCC") grants licenses through the Service on behalf of the rightsholder identified on the Order Confirmation (the "Rightsholder"). "Republication", as used herein, generally means the inclusion of a Work, in whole or in part, in a new work or works, also as described on the Order Confirmation. "User", as used herein, means the person or entity making such republication.

2. The terms set forth in the relevant Order Confirmation, and any terms set by the Rightsholder with respect to a particular Work, govern the terms of use of Works in connection with the Service. By using the Service, the person transacting for a republication license on behalf of the User represents and warrants that he/she/it (a) has been duly authorized by the User to accept, and hereby does accept, all such terms and conditions on behalf of User, and (b) shall inform User of all such terms and conditions. In the event such person is a "freelancer" or other third party independent of User and CCC, such party shall be deemed jointly a "User" for purposes of these terms and conditions. In any event, User shall be deemed to have accepted and agreed to all such terms and conditions if User republishes the Work in any fashion.

3. Scope of License; Limitations and Obligations.

   3.1. All Works and all rights therein, including copyright rights, remain the sole and exclusive property of the Rightsholder. The license created by the exchange of an Order Confirmation (and/or any invoice) and payment by User of the full amount set forth on that document includes only those rights expressly set forth in the Order Confirmation and in these terms and conditions, and conveys no other rights in the Work(s) to User. All rights not expressly granted are hereby reserved.

   3.2. General Payment Terms: You may pay by credit card or through an account with us payable at the end of the month. If you and we agree that you may establish a standing account with CCC, then the following terms apply: Remit Payment to: Copyright Clearance Center, 29118 Network Place, Chicago, IL 60673-1291. Payments Due: Invoices are payable upon their delivery to you (or upon our notice to you that they are available to you for downloading). After 30 days, outstanding amounts will be subject to a service charge of 1-1/2% per month or, if less, the maximum rate allowed by applicable law. Unless otherwise specifically set forth in the Order Confirmation or in a separate written agreement signed by CCC, invoices are due and payable on "net 30" terms. While User may exercise the rights licensed immediately upon issuance of the Order Confirmation, the license is automatically revoked and is null and void, as if it had never been issued, if complete payment for the license is not received on a timely basis either from User directly or through a payment agent, such as a credit card company.

   3.3. Unless otherwise provided in the Order Confirmation, any grant of rights to User (i) is "one-time" (including the editions and product family specified in the license), (ii) is non-exclusive and non-transferable and (iii) is subject to any and all limitations and restrictions (such as, but not limited to, limitations on duration of use or circulation) included in the Order Confirmation or invoice and/or in these terms and conditions. Upon completion of the licensed use, User shall either secure a new permission for further use of the

Work(s) or immediately cease any new use of the Work(s) and shall render inaccessible (such as by deleting or by removing or severing links or other locators) any further copies of the Work (except for copies printed on paper in accordance with this license and still in User's stock at the end of such period).

3.4. In the event that the material for which a republication license is sought includes third party materials (such as photographs, illustrations, graphs, inserts and similar materials) which are identified in such material as having been used by permission, User is responsible for identifying, and seeking separate licenses (under this Service or otherwise) for, any of such third party materials; without a separate license, such third party materials may not be used.

3.5. Use of proper copyright notice for a Work is required as a condition of any license granted under the Service. Unless otherwise provided in the Order Confirmation, a proper copyright notice will read substantially as follows: "Republished with permission of [Rightsholder's name], from [Work's title, author, volume, edition number and year of copyright]; permission conveyed through Copyright Clearance Center, Inc. " Such notice must be provided in a reasonably legible font size and must be placed either immediately adjacent to the Work as used (for example, as part of a by-line or footnote but not as a separate electronic link) or in the place where substantially all other credits or notices for the new work containing the republished Work are located. Failure to include the required notice results in loss to the Rightsholder and CCC, and the User shall be liable to pay liquidated damages for each such failure equal to twice the use fee specified in the Order Confirmation, in addition to the use fee itself and any other fees and charges specified.

3.6. User may only make alterations to the Work if and as expressly set forth in the Order Confirmation. No Work may be used in any way that is defamatory, violates the rights of third parties (including such third parties' rights of copyright, privacy, publicity, or other tangible or intangible property), or is otherwise illegal, sexually explicit or obscene. In addition, User may not conjoin a Work with any other material that may result in damage to the reputation of the Rightsholder. User agrees to inform CCC if it becomes aware of any infringement of any rights in a Work and to cooperate with any reasonable request of CCC or the Rightsholder in connection therewith.

4. Indemnity. User hereby indemnifies and agrees to defend the Rightsholder and CCC, and their respective employees and directors, against all claims, liability, damages, costs and expenses, including legal fees and expenses, arising out of any use of a Work beyond the scope of the rights granted herein, or any use of a Work which has been altered in any unauthorized way by User, including claims of defamation or infringement of rights of copyright, publicity, privacy or other tangible or intangible property.

5. Limitation of Liability. UNDER NO CIRCUMSTANCES WILL CCC OR THE RIGHTSHOLDER BE LIABLE FOR ANY DIRECT, INDIRECT, CONSEQUENTIAL OR INCIDENTAL DAMAGES (INCLUDING WITHOUT LIMITATION DAMAGES FOR LOSS OF BUSINESS PROFITS OR INFORMATION, OR FOR BUSINESS INTERRUPTION) ARISING OUT OF THE USE OR INABILITY TO USE A WORK, EVEN IF ONE OF THEM HAS BEEN ADVISED OF THE POSSIBILITY OF SUCH DAMAGES. In any event, the total liability of the Rightsholder and CCC (including their respective employees and directors) shall not exceed the total amount actually paid by User for this license. User assumes full liability for the actions and omissions of its principals, employees, agents, affiliates, successors and assigns.

6. Limited Warranties. THE WORK(S) AND RIGHT(S) ARE PROVIDED "AS IS". CCC HAS THE RIGHT TO GRANT TO USER THE RIGHTS GRANTED IN THE ORDER CONFIRMATION DOCUMENT. CCC AND THE RIGHTSHOLDER DISCLAIM ALL OTHER WARRANTIES RELATING TO THE WORK(S) AND RIGHT(S), EITHER EXPRESS OR IMPLIED, INCLUDING WITHOUT LIMITATION IMPLIED WARRANTIES OF MERCHANTABILITY OR FITNESS FOR A PARTICULAR PURPOSE. ADDITIONAL RIGHTS MAY BE REQUIRED TO USE ILLUSTRATIONS, GRAPHS, PHOTOGRAPHS, ABSTRACTS, INSERTS OR OTHER PORTIONS OF THE WORK (AS OPPOSED TO THE ENTIRE WORK) IN A MANNER CONTEMPLATED BY USER; USER UNDERSTANDS AND AGREES THAT NEITHER CCC NOR THE RIGHTSHOLDER MAY HAVE SUCH ADDITIONAL RIGHTS TO GRANT.

7. Effect of Breach. Any failure by User to pay any amount when due, or any use by User of a Work beyond the scope of the license set forth in the Order Confirmation and/or these terms and conditions, shall be a material breach of the license created by the Order Confirmation and these terms and conditions. Any breach not cured within 30 days of written notice thereof shall result in immediate termination of such license without further notice. Any unauthorized (but licensable) use of a Work that is terminated immediately upon notice thereof may be liquidated by payment of the Rightsholder's ordinary license price therefor; any unauthorized (and unlicensable) use that is not terminated immediately for any reason (including, for example, because materials containing the Work cannot reasonably be recalled) will be subject to all remedies available at law or in equity, but in no event to a payment of

less than three times the Rightsholder's ordinary license price for the most closely analogous licensable use plus Rightsholder's and/or CCC's costs and expenses incurred in collecting such payment.

8. Miscellaneous.

8.1. User acknowledges that CCC may, from time to time, make changes or additions to the Service or to these terms and conditions, and CCC reserves the right to send notice to the User by electronic mail or otherwise for the purposes of notifying User of such changes or additions; provided that any such changes or additions shall not apply to permissions already secured and paid for.

8.2. Use of User-related information collected through the Service is governed by CCC's privacy policy, available online here:https://marketplace.copyright.com/rs-ui-web/mp/privacy-policy

8.3. The licensing transaction described in the Order Confirmation is personal to User. Therefore, User may not assign or transfer to any other person (whether a natural person or an organization of any kind) the license created by the Order Confirmation and these terms and conditions or any rights granted hereunder; provided, however, that User may assign such license in its entirety on written notice to CCC in the event of a transfer of all or substantially all of User's rights in the new material which includes the Work(s) licensed under this Service.

8.4. No amendment or waiver of any terms is binding unless set forth in writing and signed by the parties. The Rightsholder and CCC hereby object to any terms contained in any writing prepared by the User or its principals, employees, agents or affiliates and purporting to govern or otherwise relate to the licensing transaction described in the Order Confirmation, which terms are in any way inconsistent with any terms set forth in the Order Confirmation and/or in these terms and conditions or CCC's standard operating procedures, whether such writing is prepared prior to, simultaneously with or subsequent to the Order Confirmation, and whether such writing appears on a copy of the Order Confirmation or in a separate instrument.

8.5. The licensing transaction described in the Order Confirmation document shall be governed by and construed under the law of the State of New York, USA, without regard to the principles thereof of conflicts of law. Any case, controversy, suit, action, or proceeding arising out of, in connection with, or related to such licensing transaction shall be brought, at CCC's sole discretion, in any federal or state court located in the County of New York, State of New York, USA, or in any federal or state court whose geographical jurisdiction covers the location of the Rightsholder set forth in the Order Confirmation. The parties expressly submit to the personal jurisdiction and venue of each such federal or state court.If you have any comments or questions about the Service or Copyright Clearance Center, please contact us at 978-750-8400 or send an e-mail to support@copyright.com.

v 1.1

CCC Marketplace™

Order Date	26-Nov-2021	Type of Use	Republish in a thesis/dissertation
Order License ID	1164373-1		
ISSN	2050-7534	Publisher	Royal Society of Chemistry
		Portion	Image/photo/illustration

LICENSED CONTENT

Publication Title	Journal of materials chemistry. C, Materials for optical and electronic devices	Publication Type	e-Journal
		Start Page	12298
		End Page	12307
Article Title	Recent advances in the chemistry of vat dyes for organic electronics	Issue	47
		Volume	5
		URL	http://pubs.rsc.org/en/journals/journalissues/tc
Author/Editor	Royal Society of Chemistry (Great Britain)		
Date	01/01/2013		
Language	English		
Country	United Kingdom of Great Britain and Northern Ireland		
Rightsholder	Royal Society of Chemistry		

REQUEST DETAILS

Portion Type	Image/photo/illustration	Distribution	Worldwide
Number of images / photos / illustrations	1	Translation	Original language of publication
Format (select all that apply)	Print, Electronic	Copies for the disabled?	No
		Minor editing privileges?	Yes
Who will republish the content?	Academic institution	Incidental promotional use?	No
Duration of Use	Life of current edition	Currency	EUR
Lifetime Unit Quantity	Up to 499		
Rights Requested	Main product		

NEW WORK DETAILS

Title	Investigations of Physical Properties of Metal-Organic Frameworks with Functional Ligands	Institution name	Technical University of Munich
		Expected presentation date	2022-03-01
Instructor name	Roland A. Fischer		

ADDITIONAL DETAILS

Order reference number	N/A

The requesting person / organization to appear on the license	João Guilherme Machado de Carvalho

REUSE CONTENT DETAILS

Title, description or numeric reference of the portion(s)	Figure 13	**Title of the article/chapter the portion is from**	Recent advances in the chemistry of vat dyes for organic electronics
Editor of portion(s)	Morin, Jean-François	**Author of portion(s)**	Morin, Jean-François
Volume of serial or monograph	5	**Issue, if republishing an article from a serial**	47
Page or page range of portion	12298-12307	**Publication date of portion**	2017-12-21

CCC Terms and Conditions

1. Description of Service; Defined Terms. This Republication License enables the User to obtain licenses for republication of one or more copyrighted works as described in detail on the relevant Order Confirmation (the "Work(s)"). Copyright Clearance Center, Inc. ("CCC") grants licenses through the Service on behalf of the rightsholder identified on the Order Confirmation (the "Rightsholder"). "Republication", as used herein, generally means the inclusion of a Work, in whole or in part, in a new work or works, also as described on the Order Confirmation. "User", as used herein, means the person or entity making such republication.

2. The terms set forth in the relevant Order Confirmation, and any terms set by the Rightsholder with respect to a particular Work, govern the terms of use of Works in connection with the Service. By using the Service, the person transacting for a republication license on behalf of the User represents and warrants that he/she/it (a) has been duly authorized by the User to accept, and hereby does accept, all such terms and conditions on behalf of User, and (b) shall inform User of all such terms and conditions. In the event such person is a "freelancer" or other third party independent of User and CCC, such party shall be deemed jointly a "User" for purposes of these terms and conditions. In any event, User shall be deemed to have accepted and agreed to all such terms and conditions if User republishes the Work in any fashion.

3. Scope of License; Limitations and Obligations.

   3.1. All Works and all rights therein, including copyright rights, remain the sole and exclusive property of the Rightsholder. The license created by the exchange of an Order Confirmation (and/or any invoice) and payment by User of the full amount set forth on that document includes only those rights expressly set forth in the Order Confirmation and in these terms and conditions, and conveys no other rights in the Work(s) to User. All rights not expressly granted are hereby reserved.

   3.2. General Payment Terms: You may pay by credit card or through an account with us payable at the end of the month. If you and we agree that you may establish a standing account with CCC, then the following terms apply: Remit Payment to: Copyright Clearance Center, 29118 Network Place, Chicago, IL 60673-1291. Payments Due: Invoices are payable upon their delivery to you (or upon our notice to you that they are available to you for downloading). After 30 days, outstanding amounts will be subject to a service charge of 1-1/2% per month or, if less, the maximum rate allowed by applicable law. Unless otherwise specifically set forth in the Order Confirmation or in a separate written agreement signed by CCC, invoices are due and payable on "net 30" terms. While User may exercise the rights licensed immediately upon issuance of the Order Confirmation, the license is automatically revoked and is null and void, as if it had never been issued, if complete payment for the license is not received on a timely basis either from User directly or through a payment agent, such as a credit card company.

   3.3. Unless otherwise provided in the Order Confirmation, any grant of rights to User (i) is "one-time" (including the editions and product family specified in the license), (ii) is non-exclusive and non-transferable and (iii) is subject to any and all limitations and restrictions (such as, but not limited to, limitations on duration of use or circulation) included in the Order Confirmation or invoice and/or in these terms and conditions. Upon completion of the licensed use, User shall either secure a new permission for further use of the Work(s) or immediately cease any new use of the Work(s) and shall render inaccessible (such as by deleting or by removing or severing links or other locators) any further copies of the Work (except for copies printed on paper in accordance with this license and still in User's stock at the end of such period).

3.4. In the event that the material for which a republication license is sought includes third party materials (such as photographs, illustrations, graphs, inserts and similar materials) which are identified in such material as having been used by permission, User is responsible for identifying, and seeking separate licenses (under this Service or otherwise) for, any of such third party materials; without a separate license, such third party materials may not be used.

3.5. Use of proper copyright notice for a Work is required as a condition of any license granted under the Service. Unless otherwise provided in the Order Confirmation, a proper copyright notice will read substantially as follows: "Republished with permission of [Rightsholder's name], from [Work's title, author, volume, edition number and year of copyright]; permission conveyed through Copyright Clearance Center, Inc. " Such notice must be provided in a reasonably legible font size and must be placed either immediately adjacent to the Work as used (for example, as part of a by-line or footnote but not as a separate electronic link) or in the place where substantially all other credits or notices for the new work containing the republished Work are located. Failure to include the required notice results in loss to the Rightsholder and CCC, and the User shall be liable to pay liquidated damages for each such failure equal to twice the use fee specified in the Order Confirmation, in addition to the use fee itself and any other fees and charges specified.

3.6. User may only make alterations to the Work if and as expressly set forth in the Order Confirmation. No Work may be used in any way that is defamatory, violates the rights of third parties (including such third parties' rights of copyright, privacy, publicity, or other tangible or intangible property), or is otherwise illegal, sexually explicit or obscene. In addition, User may not conjoin a Work with any other material that may result in damage to the reputation of the Rightsholder. User agrees to inform CCC if it becomes aware of any infringement of any rights in a Work and to cooperate with any reasonable request of CCC or the Rightsholder in connection therewith.

4. Indemnity. User hereby indemnifies and agrees to defend the Rightsholder and CCC, and their respective employees and directors, against all claims, liability, damages, costs and expenses, including legal fees and expenses, arising out of any use of a Work beyond the scope of the rights granted herein, or any use of a Work which has been altered in any unauthorized way by User, including claims of defamation or infringement of rights of copyright, publicity, privacy or other tangible or intangible property.

5. Limitation of Liability. UNDER NO CIRCUMSTANCES WILL CCC OR THE RIGHTSHOLDER BE LIABLE FOR ANY DIRECT, INDIRECT, CONSEQUENTIAL OR INCIDENTAL DAMAGES (INCLUDING WITHOUT LIMITATION DAMAGES FOR LOSS OF BUSINESS PROFITS OR INFORMATION, OR FOR BUSINESS INTERRUPTION) ARISING OUT OF THE USE OR INABILITY TO USE A WORK, EVEN IF ONE OF THEM HAS BEEN ADVISED OF THE POSSIBILITY OF SUCH DAMAGES. In any event, the total liability of the Rightsholder and CCC (including their respective employees and directors) shall not exceed the total amount actually paid by User for this license. User assumes full liability for the actions and omissions of its principals, employees, agents, affiliates, successors and assigns.

6. Limited Warranties. THE WORK(S) AND RIGHT(S) ARE PROVIDED "AS IS". CCC HAS THE RIGHT TO GRANT TO USER THE RIGHTS GRANTED IN THE ORDER CONFIRMATION DOCUMENT. CCC AND THE RIGHTSHOLDER DISCLAIM ALL OTHER WARRANTIES RELATING TO THE WORK(S) AND RIGHT(S), EITHER EXPRESS OR IMPLIED, INCLUDING WITHOUT LIMITATION IMPLIED WARRANTIES OF MERCHANTABILITY OR FITNESS FOR A PARTICULAR PURPOSE. ADDITIONAL RIGHTS MAY BE REQUIRED TO USE ILLUSTRATIONS, GRAPHS, PHOTOGRAPHS, ABSTRACTS, INSERTS OR OTHER PORTIONS OF THE WORK (AS OPPOSED TO THE ENTIRE WORK) IN A MANNER CONTEMPLATED BY USER; USER UNDERSTANDS AND AGREES THAT NEITHER CCC NOR THE RIGHTSHOLDER MAY HAVE SUCH ADDITIONAL RIGHTS TO GRANT.

7. Effect of Breach. Any failure by User to pay any amount when due, or any use by User of a Work beyond the scope of the license set forth in the Order Confirmation and/or these terms and conditions, shall be a material breach of the license created by the Order Confirmation and these terms and conditions. Any breach not cured within 30 days of written notice thereof shall result in immediate termination of such license without further notice. Any unauthorized (but licensable) use of a Work that is terminated immediately upon notice thereof may be liquidated by payment of the Rightsholder's ordinary license price therefor; any unauthorized (and unlicensable) use that is not terminated immediately for any reason (including, for example, because materials containing the Work cannot reasonably be recalled) will be subject to all remedies available at law or in equity, but in no event to a payment of less than three times the Rightsholder's ordinary license price for the most closely analogous licensable use plus Rightsholder's and/or CCC's costs and expenses incurred in collecting such payment.

8. Miscellaneous.

8.1. User acknowledges that CCC may, from time to time, make changes or additions to the Service or to these terms and conditions, and CCC reserves the right to send notice to the User by electronic mail or otherwise for the purposes of notifying User of such changes or additions; provided that any such changes or additions shall not apply to permissions already secured and paid for.

8.2. Use of User-related information collected through the Service is governed by CCC's privacy policy, available online here:https://marketplace.copyright.com/rs-ui-web/mp/privacy-policy

8.3. The licensing transaction described in the Order Confirmation is personal to User. Therefore, User may not assign or transfer to any other person (whether a natural person or an organization of any kind) the license created by the Order Confirmation and these terms and conditions or any rights granted hereunder; provided, however, that User may assign such license in its entirety on written notice to CCC in the event of a transfer of all or substantially all of User's rights in the new material which includes the Work(s) licensed under this Service.

8.4. No amendment or waiver of any terms is binding unless set forth in writing and signed by the parties. The Rightsholder and CCC hereby object to any terms contained in any writing prepared by the User or its principals, employees, agents or affiliates and purporting to govern or otherwise relate to the licensing transaction described in the Order Confirmation, which terms are in any way inconsistent with any terms set forth in the Order Confirmation and/or in these terms and conditions or CCC's standard operating procedures, whether such writing is prepared prior to, simultaneously with or subsequent to the Order Confirmation, and whether such writing appears on a copy of the Order Confirmation or in a separate instrument.

8.5. The licensing transaction described in the Order Confirmation document shall be governed by and construed under the law of the State of New York, USA, without regard to the principles thereof of conflicts of law. Any case, controversy, suit, action, or proceeding arising out of, in connection with, or related to such licensing transaction shall be brought, at CCC's sole discretion, in any federal or state court located in the County of New York, State of New York, USA, or in any federal or state court whose geographical jurisdiction covers the location of the Rightsholder set forth in the Order Confirmation. The parties expressly submit to the personal jurisdiction and venue of each such federal or state court.If you have any comments or questions about the Service or Copyright Clearance Center, please contact us at 978-750-8400 or send an e-mail to support@copyright.com.

v 1.1

CCC Marketplace™

This is a License Agreement between Joao Guilherme Machado de Carvalho ("User") and Copyright Clearance Center, Inc. ("CCC") on behalf of the Rightsholder identified in the order details below. The license consists of the order details, the CCC Terms and Conditions below, and any Rightsholder Terms and Conditions which are included below.

All payments must be made in full to CCC in accordance with the CCC Terms and Conditions below.

Order Date	26-Nov-2021	**Type of Use**	Republish in a thesis/dissertation
Order License ID	1164377-1		
ISSN	0959-9428	**Publisher**	ROYAL SOCIETY OF CHEMISTRY,
		Portion	Image/photo/illustration

LICENSED CONTENT

Publication Title	Journal of materials chemistry	**Rightsholder**	Royal Society of Chemistry
		Publication Type	Journal
Article Title	Understanding ligand-centred photoluminescence through flexibility and bonding of anthraquinone inorganic–organic frameworks	**Start Page**	6595
		Issue	18
		Volume	21
Author/Editor	ROYAL SOCIETY OF CHEMISTRY (GREAT BRITAIN)		
Date	01/01/1991		
Language	English		
Country	United Kingdom of Great Britain and Northern Ireland		

REQUEST DETAILS

Portion Type	Image/photo/illustration	**Distribution**	Worldwide
Number of images / photos / illustrations	3	**Translation**	Original language of publication
Format (select all that apply)	Print, Electronic	**Copies for the disabled?**	No
		Minor editing privileges?	Yes
Who will republish the content?	Academic institution	**Incidental promotional use?**	No
Duration of Use	Life of current edition	**Currency**	USD
Lifetime Unit Quantity	Up to 499		
Rights Requested	Main product		

NEW WORK DETAILS

Title	Investigations of Physical Properties of Metal-Organic Frameworks with Functional Ligands	**Institution name**	Technical University of Munich
		Expected presentation date	2022-03-01
Instructor name	Roland A. Fischer		

ADDITIONAL DETAILS

Order reference number	N/A	**The requesting person / organization to appear on the license**	Joao Guilherme Machado de Carvalho

REUSE CONTENT DETAILS

Title, description or numeric reference of the portion(s)	Figures 3,7,8	**Title of the article/chapter the portion is from**	Understanding ligand-centred photoluminescence through flexibility and bonding of anthraquinone inorganic–organic frameworks
Editor of portion(s)	Furman, Joshua D.; Burwood, Ryan P.; Tang, Min; Mikhailovsky, Alexander A.; Cheetham, Anthony K.	**Author of portion(s)**	Furman, Joshua D.; Burwood, Ryan P.; Tang, Min; Mikhailovsky, Alexander A.; Cheetham, Anthony K.
Volume of serial or monograph	21		
Page or page range of portion	6595	**Issue, if republishing an article from a serial**	18
		Publication date of portion	2011-01-01

CCC Terms and Conditions

1. Description of Service; Defined Terms. This Republication License enables the User to obtain licenses for republication of one or more copyrighted works as described in detail on the relevant Order Confirmation (the "Work(s)"). Copyright Clearance Center, Inc. ("CCC") grants licenses through the Service on behalf of the rightsholder identified on the Order Confirmation (the "Rightsholder"). "Republication", as used herein, generally means the inclusion of a Work, in whole or in part, in a new work or works, also as described on the Order Confirmation. "User", as used herein, means the person or entity making such republication.

2. The terms set forth in the relevant Order Confirmation, and any terms set by the Rightsholder with respect to a particular Work, govern the terms of use of Works in connection with the Service. By using the Service, the person transacting for a republication license on behalf of the User represents and warrants that he/she/it (a) has been duly authorized by the User to accept, and hereby does accept, all such terms and conditions on behalf of User, and (b) shall inform User of all such terms and conditions. In the event such person is a "freelancer" or other third party independent of User and CCC, such party shall be deemed jointly a "User" for purposes of these terms and conditions. In any event, User shall be deemed to have accepted and agreed to all such terms and conditions if User republishes the Work in any fashion.

3. Scope of License; Limitations and Obligations.

    3.1. All Works and all rights therein, including copyright rights, remain the sole and exclusive property of the Rightsholder. The license created by the exchange of an Order Confirmation (and/or any invoice) and payment by User of the full amount set forth on that document includes only those rights expressly set forth in the Order Confirmation and in these terms and conditions, and conveys no other rights in the Work(s) to User. All rights not expressly granted are hereby reserved.

    3.2. General Payment Terms: You may pay by credit card or through an account with us payable at the end of the month. If you and we agree that you may establish a standing account with CCC, then the following terms apply: Remit Payment to: Copyright Clearance Center, 29118 Network Place, Chicago, IL 60673-1291. Payments Due: Invoices are payable upon their delivery to you (or upon our notice to you that they are available to you for downloading). After 30 days, outstanding amounts will be subject to a service charge of 1-1/2% per month or, if less, the maximum rate allowed by applicable law. Unless otherwise specifically set forth in the Order Confirmation or in a separate written agreement signed by CCC, invoices are due and payable on "net 30" terms. While User may exercise the rights licensed immediately upon issuance of the Order Confirmation, the license is automatically revoked and is null and void, as if it had never been issued, if complete payment for the license is not received on a timely basis either from User directly or through a payment agent, such as a credit card company.

    3.3. Unless otherwise provided in the Order Confirmation, any grant of rights to User (i) is "one-time" (including

the editions and product family specified in the license), (ii) is non-exclusive and non-transferable and (iii) is subject to any and all limitations and restrictions (such as, but not limited to, limitations on duration of use or circulation) included in the Order Confirmation or invoice and/or in these terms and conditions. Upon completion of the licensed use, User shall either secure a new permission for further use of the Work(s) or immediately cease any new use of the Work(s) and shall render inaccessible (such as by deleting or by removing or severing links or other locators) any further copies of the Work (except for copies printed on paper in accordance with this license and still in User's stock at the end of such period).

3.4. In the event that the material for which a republication license is sought includes third party materials (such as photographs, illustrations, graphs, inserts and similar materials) which are identified in such material as having been used by permission, User is responsible for identifying, and seeking separate licenses (under this Service or otherwise) for, any of such third party materials; without a separate license, such third party materials may not be used.

3.5. Use of proper copyright notice for a Work is required as a condition of any license granted under the Service. Unless otherwise provided in the Order Confirmation, a proper copyright notice will read substantially as follows: "Republished with permission of [Rightsholder's name], from [Work's title, author, volume, edition number and year of copyright]; permission conveyed through Copyright Clearance Center, Inc. " Such notice must be provided in a reasonably legible font size and must be placed either immediately adjacent to the Work as used (for example, as part of a by-line or footnote but not as a separate electronic link) or in the place where substantially all other credits or notices for the new work containing the republished Work are located. Failure to include the required notice results in loss to the Rightsholder and CCC, and the User shall be liable to pay liquidated damages for each such failure equal to twice the use fee specified in the Order Confirmation, in addition to the use fee itself and any other fees and charges specified.

3.6. User may only make alterations to the Work if and as expressly set forth in the Order Confirmation. No Work may be used in any way that is defamatory, violates the rights of third parties (including such third parties' rights of copyright, privacy, publicity, or other tangible or intangible property), or is otherwise illegal, sexually explicit or obscene. In addition, User may not conjoin a Work with any other material that may result in damage to the reputation of the Rightsholder. User agrees to inform CCC if it becomes aware of any infringement of any rights in a Work and to cooperate with any reasonable request of CCC or the Rightsholder in connection therewith.

4. Indemnity. User hereby indemnifies and agrees to defend the Rightsholder and CCC, and their respective employees and directors, against all claims, liability, damages, costs and expenses, including legal fees and expenses, arising out of any use of a Work beyond the scope of the rights granted herein, or any use of a Work which has been altered in any unauthorized way by User, including claims of defamation or infringement of rights of copyright, publicity, privacy or other tangible or intangible property.

5. Limitation of Liability. UNDER NO CIRCUMSTANCES WILL CCC OR THE RIGHTSHOLDER BE LIABLE FOR ANY DIRECT, INDIRECT, CONSEQUENTIAL OR INCIDENTAL DAMAGES (INCLUDING WITHOUT LIMITATION DAMAGES FOR LOSS OF BUSINESS PROFITS OR INFORMATION, OR FOR BUSINESS INTERRUPTION) ARISING OUT OF THE USE OR INABILITY TO USE A WORK, EVEN IF ONE OF THEM HAS BEEN ADVISED OF THE POSSIBILITY OF SUCH DAMAGES. In any event, the total liability of the Rightsholder and CCC (including their respective employees and directors) shall not exceed the total amount actually paid by User for this license. User assumes full liability for the actions and omissions of its principals, employees, agents, affiliates, successors and assigns.

6. Limited Warranties. THE WORK(S) AND RIGHT(S) ARE PROVIDED "AS IS". CCC HAS THE RIGHT TO GRANT TO USER THE RIGHTS GRANTED IN THE ORDER CONFIRMATION DOCUMENT. CCC AND THE RIGHTSHOLDER DISCLAIM ALL OTHER WARRANTIES RELATING TO THE WORK(S) AND RIGHT(S), EITHER EXPRESS OR IMPLIED, INCLUDING WITHOUT LIMITATION IMPLIED WARRANTIES OF MERCHANTABILITY OR FITNESS FOR A PARTICULAR PURPOSE. ADDITIONAL RIGHTS MAY BE REQUIRED TO USE ILLUSTRATIONS, GRAPHS, PHOTOGRAPHS, ABSTRACTS, INSERTS OR OTHER PORTIONS OF THE WORK (AS OPPOSED TO THE ENTIRE WORK) IN A MANNER CONTEMPLATED BY USER; USER UNDERSTANDS AND AGREES THAT NEITHER CCC NOR THE RIGHTSHOLDER MAY HAVE SUCH ADDITIONAL RIGHTS TO GRANT.

7. Effect of Breach. Any failure by User to pay any amount when due, or any use by User of a Work beyond the scope of the license set forth in the Order Confirmation and/or these terms and conditions, shall be a material breach of the license created by the Order Confirmation and these terms and conditions. Any breach not cured within 30 days of written notice thereof shall result in immediate termination of such license without further notice. Any

unauthorized (but licensable) use of a Work that is terminated immediately upon notice thereof may be liquidated by payment of the Rightsholder's ordinary license price therefor; any unauthorized (and unlicensable) use that is not terminated immediately for any reason (including, for example, because materials containing the Work cannot reasonably be recalled) will be subject to all remedies available at law or in equity, but in no event to a payment of less than three times the Rightsholder's ordinary license price for the most closely analogous licensable use plus Rightsholder's and/or CCC's costs and expenses incurred in collecting such payment.

8. Miscellaneous.

    8.1. User acknowledges that CCC may, from time to time, make changes or additions to the Service or to these terms and conditions, and CCC reserves the right to send notice to the User by electronic mail or otherwise for the purposes of notifying User of such changes or additions; provided that any such changes or additions shall not apply to permissions already secured and paid for.

    8.2. Use of User-related information collected through the Service is governed by CCC's privacy policy, available online here:https://marketplace.copyright.com/rs-ui-web/mp/privacy-policy

    8.3. The licensing transaction described in the Order Confirmation is personal to User. Therefore, User may not assign or transfer to any other person (whether a natural person or an organization of any kind) the license created by the Order Confirmation and these terms and conditions or any rights granted hereunder; provided, however, that User may assign such license in its entirety on written notice to CCC in the event of a transfer of all or substantially all of User's rights in the new material which includes the Work(s) licensed under this Service.

    8.4. No amendment or waiver of any terms is binding unless set forth in writing and signed by the parties. The Rightsholder and CCC hereby object to any terms contained in any writing prepared by the User or its principals, employees, agents or affiliates and purporting to govern or otherwise relate to the licensing transaction described in the Order Confirmation, which terms are in any way inconsistent with any terms set forth in the Order Confirmation and/or in these terms and conditions or CCC's standard operating procedures, whether such writing is prepared prior to, simultaneously with or subsequent to the Order Confirmation, and whether such writing appears on a copy of the Order Confirmation or in a separate instrument.

    8.5. The licensing transaction described in the Order Confirmation document shall be governed by and construed under the law of the State of New York, USA, without regard to the principles thereof of conflicts of law. Any case, controversy, suit, action, or proceeding arising out of, in connection with, or related to such licensing transaction shall be brought, at CCC's sole discretion, in any federal or state court located in the County of New York, State of New York, USA, or in any federal or state court whose geographical jurisdiction covers the location of the Rightsholder set forth in the Order Confirmation. The parties expressly submit to the personal jurisdiction and venue of each such federal or state court.If you have any comments or questions about the Service or Copyright Clearance Center, please contact us at 978-750-8400 or send an e-mail to support@copyright.com.

v 1.1

CCC Marketplace™

This is a License Agreement between João Guilherme Machado de Carvalho ("User") and Copyright Clearance Center, Inc. ("CCC") on behalf of the Rightsholder identified in the order details below. The license consists of the order details, the CCC Terms and Conditions below, and any Rightsholder Terms and Conditions which are included below.

All payments must be made in full to CCC in accordance with the CCC Terms and Conditions below.

Order Date	26-Nov-2021	**Type of Use**	Republish in a thesis/dissertation
Order License ID	1164379-1		
ISSN	1369-9261	**Publisher**	ROYAL SOCIETY OF CHEMISTRY
		Portion	Image/photo/illustration

LICENSED CONTENT

Publication Title	New journal of chemistry	**Publication Type**	e-Journal
Article Title	Flavanthrone – new ligand with accessible radical anion and dianion states. Preparation of zwitter-ionic {(Cp2V)2(Flavanthrone)} and {(Cp2V)2(Chloranil)} complexes	**Start Page**	10849
		End Page	10858
		Issue	26
		Volume	44
		URL	http://www.rsc.org/njc
Author/Editor	Centre national de la recherche scientifique (France), Royal Society of Chemistry (Great Britain)		
Date	01/01/1987		
Language	English		
Country	United Kingdom of Great Britain and Northern Ireland		
Rightsholder	Royal Society of Chemistry		

REQUEST DETAILS

Portion Type	Image/photo/illustration	**Distribution**	Worldwide
Number of images / photos / illustrations	1	**Translation**	Original language of publication
Format (select all that apply)	Print, Electronic	**Copies for the disabled?**	No
		Minor editing privileges?	Yes
Who will republish the content?	Academic institution	**Incidental promotional use?**	No
Duration of Use	Current edition and up to 5 years	**Currency**	EUR
Lifetime Unit Quantity	Up to 499		
Rights Requested	Main product		

NEW WORK DETAILS

Title	Investigations of Physical Properties of Metal-Organic Frameworks with Functional Ligands	**Institution name**	Technical University of Munich
		Expected presentation date	2022-03-01

Instructor name	Roland A. Fischer

ADDITIONAL DETAILS

Order reference number	N/A	**The requesting person / organization to appear on the license**	João Guilherme Machado de Carvalho

REUSE CONTENT DETAILS

Title, description or numeric reference of the portion(s)	Figure 4	**Title of the article/chapter the portion is from**	Flavanthrone – new ligand with accessible radical anion and dianion states. Preparation of zwitter-ionic {(Cp2V)2(Flavanthrone)} and {(Cp2V)2(Chloranil)} complexes
Editor of portion(s)	Konarev, Dmitri V.; Andronov, Mikhail G.; Batov, Mikhail S.; Kuz`min, Alexey V.; Khasanov, Salavat S.; Shestakov, Alexander F.; Otsuka, Akihiro; Yamochi, Hideki; Kitagawa, Hiroshi; Lyubovskaya, Rimma N.	**Author of portion(s)**	Konarev, Dmitri V.; Andronov, Mikhail G.; Batov, Mikhail S.; Kuz`min, Alexey V.; Khasanov, Salavat S.; Shestakov, Alexander F.; Otsuka, Akihiro; Yamochi, Hideki; Kitagawa, Hiroshi; Lyubovskaya, Rimma N.
Volume of serial or monograph	44	**Issue, if republishing an article from a serial**	26
Page or page range of portion	10849-10858	**Publication date of portion**	2020-01-01

CCC Terms and Conditions

1. Description of Service; Defined Terms. This Republication License enables the User to obtain licenses for republication of one or more copyrighted works as described in detail on the relevant Order Confirmation (the "Work(s)"). Copyright Clearance Center, Inc. ("CCC") grants licenses through the Service on behalf of the rightsholder identified on the Order Confirmation (the "Rightsholder"). "Republication", as used herein, generally means the inclusion of a Work, in whole or in part, in a new work or works, also as described on the Order Confirmation. "User", as used herein, means the person or entity making such republication.

2. The terms set forth in the relevant Order Confirmation, and any terms set by the Rightsholder with respect to a particular Work, govern the terms of use of Works in connection with the Service. By using the Service, the person transacting for a republication license on behalf of the User represents and warrants that he/she/it (a) has been duly authorized by the User to accept, and hereby does accept, all such terms and conditions on behalf of User, and (b) shall inform User of all such terms and conditions. In the event such person is a "freelancer" or other third party independent of User and CCC, such party shall be deemed jointly a "User" for purposes of these terms and conditions. In any event, User shall be deemed to have accepted and agreed to all such terms and conditions if User republishes the Work in any fashion.

3. Scope of License; Limitations and Obligations.

    3.1. All Works and all rights therein, including copyright rights, remain the sole and exclusive property of the Rightsholder. The license created by the exchange of an Order Confirmation (and/or any invoice) and payment by User of the full amount set forth on that document includes only those rights expressly set forth in the Order Confirmation and in these terms and conditions, and conveys no other rights in the Work(s) to User. All rights not expressly granted are hereby reserved.

    3.2. General Payment Terms: You may pay by credit card or through an account with us payable at the end of the month. If you and we agree that you may establish a standing account with CCC, then the following terms apply: Remit Payment to: Copyright Clearance Center, 29118 Network Place, Chicago, IL 60673-1291.

Payments Due: Invoices are payable upon their delivery to you (or upon our notice to you that they are available to you for downloading). After 30 days, outstanding amounts will be subject to a service charge of 1-1/2% per month or, if less, the maximum rate allowed by applicable law. Unless otherwise specifically set forth in the Order Confirmation or in a separate written agreement signed by CCC, invoices are due and payable on "net 30" terms. While User may exercise the rights licensed immediately upon issuance of the Order Confirmation, the license is automatically revoked and is null and void, as if it had never been issued, if complete payment for the license is not received on a timely basis either from User directly or through a payment agent, such as a credit card company.

3.3. Unless otherwise provided in the Order Confirmation, any grant of rights to User (i) is "one-time" (including the editions and product family specified in the license), (ii) is non-exclusive and non-transferable and (iii) is subject to any and all limitations and restrictions (such as, but not limited to, limitations on duration of use or circulation) included in the Order Confirmation or invoice and/or in these terms and conditions. Upon completion of the licensed use, User shall either secure a new permission for further use of the Work(s) or immediately cease any new use of the Work(s) and shall render inaccessible (such as by deleting or by removing or severing links or other locators) any further copies of the Work (except for copies printed on paper in accordance with this license and still in User's stock at the end of such period).

3.4. In the event that the material for which a republication license is sought includes third party materials (such as photographs, illustrations, graphs, inserts and similar materials) which are identified in such material as having been used by permission, User is responsible for identifying, and seeking separate licenses (under this Service or otherwise) for, any of such third party materials; without a separate license, such third party materials may not be used.

3.5. Use of proper copyright notice for a Work is required as a condition of any license granted under the Service. Unless otherwise provided in the Order Confirmation, a proper copyright notice will read substantially as follows: "Republished with permission of [Rightsholder's name], from [Work's title, author, volume, edition number and year of copyright]; permission conveyed through Copyright Clearance Center, Inc. " Such notice must be provided in a reasonably legible font size and must be placed either immediately adjacent to the Work as used (for example, as part of a by-line or footnote but not as a separate electronic link) or in the place where substantially all other credits or notices for the new work containing the republished Work are located. Failure to include the required notice results in loss to the Rightsholder and CCC, and the User shall be liable to pay liquidated damages for each such failure equal to twice the use fee specified in the Order Confirmation, in addition to the use fee itself and any other fees and charges specified.

3.6. User may only make alterations to the Work if and as expressly set forth in the Order Confirmation. No Work may be used in any way that is defamatory, violates the rights of third parties (including such third parties' rights of copyright, privacy, publicity, or other tangible or intangible property), or is otherwise illegal, sexually explicit or obscene. In addition, User may not conjoin a Work with any other material that may result in damage to the reputation of the Rightsholder. User agrees to inform CCC if it becomes aware of any infringement of any rights in a Work and to cooperate with any reasonable request of CCC or the Rightsholder in connection therewith.

4. Indemnity. User hereby indemnifies and agrees to defend the Rightsholder and CCC, and their respective employees and directors, against all claims, liability, damages, costs and expenses, including legal fees and expenses, arising out of any use of a Work beyond the scope of the rights granted herein, or any use of a Work which has been altered in any unauthorized way by User, including claims of defamation or infringement of rights of copyright, publicity, privacy or other tangible or intangible property.

5. Limitation of Liability. UNDER NO CIRCUMSTANCES WILL CCC OR THE RIGHTSHOLDER BE LIABLE FOR ANY DIRECT, INDIRECT, CONSEQUENTIAL OR INCIDENTAL DAMAGES (INCLUDING WITHOUT LIMITATION DAMAGES FOR LOSS OF BUSINESS PROFITS OR INFORMATION, OR FOR BUSINESS INTERRUPTION) ARISING OUT OF THE USE OR INABILITY TO USE A WORK, EVEN IF ONE OF THEM HAS BEEN ADVISED OF THE POSSIBILITY OF SUCH DAMAGES. In any event, the total liability of the Rightsholder and CCC (including their respective employees and directors) shall not exceed the total amount actually paid by User for this license. User assumes full liability for the actions and omissions of its principals, employees, agents, affiliates, successors and assigns.

6. Limited Warranties. THE WORK(S) AND RIGHT(S) ARE PROVIDED "AS IS". CCC HAS THE RIGHT TO GRANT TO USER THE RIGHTS GRANTED IN THE ORDER CONFIRMATION DOCUMENT. CCC AND THE RIGHTSHOLDER DISCLAIM ALL OTHER WARRANTIES RELATING TO THE WORK(S) AND RIGHT(S), EITHER EXPRESS OR IMPLIED, INCLUDING

WITHOUT LIMITATION IMPLIED WARRANTIES OF MERCHANTABILITY OR FITNESS FOR A PARTICULAR PURPOSE. ADDITIONAL RIGHTS MAY BE REQUIRED TO USE ILLUSTRATIONS, GRAPHS, PHOTOGRAPHS, ABSTRACTS, INSERTS OR OTHER PORTIONS OF THE WORK (AS OPPOSED TO THE ENTIRE WORK) IN A MANNER CONTEMPLATED BY USER; USER UNDERSTANDS AND AGREES THAT NEITHER CCC NOR THE RIGHTSHOLDER MAY HAVE SUCH ADDITIONAL RIGHTS TO GRANT.

7. Effect of Breach. Any failure by User to pay any amount when due, or any use by User of a Work beyond the scope of the license set forth in the Order Confirmation and/or these terms and conditions, shall be a material breach of the license created by the Order Confirmation and these terms and conditions. Any breach not cured within 30 days of written notice thereof shall result in immediate termination of such license without further notice. Any unauthorized (but licensable) use of a Work that is terminated immediately upon notice thereof may be liquidated by payment of the Rightsholder's ordinary license price therefor; any unauthorized (and unlicensable) use that is not terminated immediately for any reason (including, for example, because materials containing the Work cannot reasonably be recalled) will be subject to all remedies available at law or in equity, but in no event to a payment of less than three times the Rightsholder's ordinary license price for the most closely analogous licensable use plus Rightsholder's and/or CCC's costs and expenses incurred in collecting such payment.

8. Miscellaneous.

    8.1. User acknowledges that CCC may, from time to time, make changes or additions to the Service or to these terms and conditions, and CCC reserves the right to send notice to the User by electronic mail or otherwise for the purposes of notifying User of such changes or additions; provided that any such changes or additions shall not apply to permissions already secured and paid for.

    8.2. Use of User-related information collected through the Service is governed by CCC's privacy policy, available online here:https://marketplace.copyright.com/rs-ui-web/mp/privacy-policy

    8.3. The licensing transaction described in the Order Confirmation is personal to User. Therefore, User may not assign or transfer to any other person (whether a natural person or an organization of any kind) the license created by the Order Confirmation and these terms and conditions or any rights granted hereunder; provided, however, that User may assign such license in its entirety on written notice to CCC in the event of a transfer of all or substantially all of User's rights in the new material which includes the Work(s) licensed under this Service.

    8.4. No amendment or waiver of any terms is binding unless set forth in writing and signed by the parties. The Rightsholder and CCC hereby object to any terms contained in any writing prepared by the User or its principals, employees, agents or affiliates and purporting to govern or otherwise relate to the licensing transaction described in the Order Confirmation, which terms are in any way inconsistent with any terms set forth in the Order Confirmation and/or in these terms and conditions or CCC's standard operating procedures, whether such writing is prepared prior to, simultaneously with or subsequent to the Order Confirmation, and whether such writing appears on a copy of the Order Confirmation or in a separate instrument.

    8.5. The licensing transaction described in the Order Confirmation document shall be governed by and construed under the law of the State of New York, USA, without regard to the principles thereof of conflicts of law. Any case, controversy, suit, action, or proceeding arising out of, in connection with, or related to such licensing transaction shall be brought, at CCC's sole discretion, in any federal or state court located in the County of New York, State of New York, USA, or in any federal or state court whose geographical jurisdiction covers the location of the Rightsholder set forth in the Order Confirmation. The parties expressly submit to the personal jurisdiction and venue of each such federal or state court.If you have any comments or questions about the Service or Copyright Clearance Center, please contact us at 978-750-8400 or send an e-mail to support@copyright.com.

v 1.1

DOI: 10.1039/D0SC03078C (Edge Article) *Chem. Sci.*, 2020, **11**, 8196-8203

Semiquinone radical-bridged M_2 (M = Fe, Co, Ni) complexes with strong magnetic exchange giving rise to slow magnetic relaxation†

Khetpakorn Chakarawet[a], **T. David Harris**[a] **and Jeffrey R. Long**[*abc]

[a]*Department of Chemistry, University of California Berkeley, Berkeley, California 94720, USA. E-mail: jrlong@berkeley.edu*

[b]*Department of Chemical and Biomolecular Engineering, University of California Berkeley, Berkeley, California 94720, USA*

[c]*Materials Sciences Division, Lawrence Berkeley National Laboratory, Berkeley, California 94720, USA*

Received 1st June 2020 , Accepted 20th July 2020

First published on 21st July 2020

2D Conductive Iron-Quinoid Magnets Ordering up to Tc = 105 K via Heterogenous Redox Chemistry

Author: Jordan A. DeGayner, Ie-Rang Jeon, Lei Sun, et al
Publication: Journal of the American Chemical Society
Publisher: American Chemical Society
Date: Mar 1, 2017

PERMISSION/LICENSE IS GRANTED FOR YOUR ORDER AT NO CHARGE

This type of permission/license, instead of the standard Terms and Conditions, is sent to you because no fee is being charged for your order. Please note the following:

- Permission is granted for your request in both print and electronic formats, and translations.
- If figures and/or tables were requested, they may be adapted or used in part.
- Please print this page for your records and send a copy of it to your publisher/graduate school.
- Appropriate credit for the requested material should be given as follows: "Reprinted (adapted) with permission from {COMPLETE REFERENCE CITATION}. Copyright {YEAR} American Chemical Society." Insert appropriate information in place of the capitalized words.
- One-time permission is granted only for the use specified in your RightsLink request. No additional uses are granted (such as derivative works or other editions). For any uses, please submit a new request.

If credit is given to another source for the material you requested from RightsLink, permission must be obtained from that source.

BACK CLOSE WINDOW

Three-Dimensional Metal-Catecholate Frameworks and Their Ultrahigh Proton Conductivity

Author: Nhung T. T. Nguyen, Hiroyasu Furukawa, Felipe Gándara, et al
Publication: Journal of the American Chemical Society
Publisher: American Chemical Society
Date: Dec 1, 2015

PERMISSION/LICENSE IS GRANTED FOR YOUR ORDER AT NO CHARGE

This type of permission/license, instead of the standard Terms and Conditions, is sent to you because no fee is being charged for your order. Please note the following:

- Permission is granted for your request in both print and electronic formats, and translations.
- If figures and/or tables were requested, they may be adapted or used in part.
- Please print this page for your records and send a copy of it to your publisher/graduate school.
- Appropriate credit for the requested material should be given as follows: "Reprinted (adapted) with permission from {COMPLETE REFERENCE CITATION}. Copyright {YEAR} American Chemical Society." Insert appropriate information in place of the capitalized words.
- One-time permission is granted only for the use specified in your RightsLink request. No additional uses are granted (such as derivative works or other editions). For any uses, please submit a new request.

If credit is given to another source for the material you requested from RightsLink, permission must be obtained from that source.

BACK CLOSE WINDOW

Reversible Tuning Hydroquinone/Quinone Reaction in Metal–Organic Framework: Immobilized Molecular Switches in Solid State

Author: Bo Gui, Xiangshi Meng, Yi Chen, et al
Publication: Chemistry of Materials
Publisher: American Chemical Society
Date: Sep 1, 2015

PERMISSION/LICENSE IS GRANTED FOR YOUR ORDER AT NO CHARGE

This type of permission/license, instead of the standard Terms and Conditions, is sent to you because no fee is being charged for your order. Please note the following:

- Permission is granted for your request in both print and electronic formats, and translations.
- If figures and/or tables were requested, they may be adapted or used in part.
- Please print this page for your records and send a copy of it to your publisher/graduate school.
- Appropriate credit for the requested material should be given as follows: "Reprinted (adapted) with permission from {COMPLETE REFERENCE CITATION}. Copyright {YEAR} American Chemical Society." Insert appropriate information in place of the capitalized words.
- One-time permission is granted only for the use specified in your RightsLink request. No additional uses are granted (such as derivative works or other editions). For any uses, please submit a new request.

If credit is given to another source for the material you requested from RightsLink, permission must be obtained from that source.

BACK CLOSE WINDOW

ACS Publications
Most Trusted. Most Cited. Most Read.

Monitoring the Solid-State Electrochemistry of Cu(2,7-AQDC) (AQDC = Anthraquinone Dicarboxylate) in a Lithium Battery: Coexistence of Metal and Ligand Redox Activities in a Metal–Organic Framework

Author: Zhongyue Zhang, Hirofumi Yoshikawa, Kunio Awaga
Publication: Journal of the American Chemical Society
Publisher: American Chemical Society
Date: Nov 1, 2014

PERMISSION/LICENSE IS GRANTED FOR YOUR ORDER AT NO CHARGE

This type of permission/license, instead of the standard Terms and Conditions, is sent to you because no fee is being charged for your order. Please note the following:

- Permission is granted for your request in both print and electronic formats, and translations.
- If figures and/or tables were requested, they may be adapted or used in part.
- Please print this page for your records and send a copy of it to your publisher/graduate school.
- Appropriate credit for the requested material should be given as follows: "Reprinted (adapted) with permission from {COMPLETE REFERENCE CITATION}. Copyright {YEAR} American Chemical Society." Insert appropriate information in place of the capitalized words.
- One-time permission is granted only for the use specified in your RightsLink request. No additional uses are granted (such as derivative works or other editions). For any uses, please submit a new request.

If credit is given to another source for the material you requested from RightsLink, permission must be obtained from that source.

BACK CLOSE WINDOW

ACS Publications
Most Trusted. Most Cited. Most Read.

η5-Semiquinone Complexes and the Related η4-Benzoquinone of (Pentamethylcyclopentadienyl)rhodium and -iridium: Synthesis, Structures, Hydrogen Bonding, and Electrochemical Behavior

Author: Jamal Moussa, Carine Guyard-Duhayon, Patrick Herson, et al
Publication: Organometallics
Publisher: American Chemical Society
Date: Dec 1, 2004

PERMISSION/LICENSE IS GRANTED FOR YOUR ORDER AT NO CHARGE

This type of permission/license, instead of the standard Terms and Conditions, is sent to you because no fee is being charged for your order. Please note the following:

- Permission is granted for your request in both print and electronic formats, and translations.
- If figures and/or tables were requested, they may be adapted or used in part.
- Please print this page for your records and send a copy of it to your publisher/graduate school.
- Appropriate credit for the requested material should be given as follows: "Reprinted (adapted) with permission from {COMPLETE REFERENCE CITATION}. Copyright {YEAR} American Chemical Society." Insert appropriate information in place of the capitalized words.
- One-time permission is granted only for the use specified in your RightsLink request. No additional uses are granted (such as derivative works or other editions). For any uses, please submit a new request.

If credit is given to another source for the material you requested from RightsLink, permission must be obtained from that source.

BACK CLOSE WINDOW

ACS Publications
Most Trusted. Most Cited. Most Read.

Through-Space Intervalence Charge Transfer as a Mechanism for Charge Delocalization in Metal–Organic Frameworks

Author: Carol Hua, Patrick W. Doheny, Bowen Ding, et al
Publication: Journal of the American Chemical Society
Publisher: American Chemical Society
Date: May 1, 2018

PERMISSION/LICENSE IS GRANTED FOR YOUR ORDER AT NO CHARGE

This type of permission/license, instead of the standard Terms and Conditions, is sent to you because no fee is being charged for your order. Please note the following:

- Permission is granted for your request in both print and electronic formats, and translations.
- If figures and/or tables were requested, they may be adapted or used in part.
- Please print this page for your records and send a copy of it to your publisher/graduate school.
- Appropriate credit for the requested material should be given as follows: "Reprinted (adapted) with permission from {COMPLETE REFERENCE CITATION}. Copyright {YEAR} American Chemical Society." Insert appropriate information in place of the capitalized words.
- One-time permission is granted only for the use specified in your RightsLink request. No additional uses are granted (such as derivative works or other editions). For any uses, please submit a new request.

If credit is given to another source for the material you requested from RightsLink, permission must be obtained from that source.

BACK CLOSE WINDOW

JOHN WILEY AND SONS LICENSE TERMS AND CONDITIONS

Nov 26, 2021

This Agreement between TU Munich -- João Guilherme Machado de Carvalho ("You") and John Wiley and Sons ("John Wiley and Sons") consists of your license details and the terms and conditions provided by John Wiley and Sons and Copyright Clearance Center.

License Number	5196511271444
License date	Nov 26, 2021
Licensed Content Publisher	John Wiley and Sons
Licensed Content Publication	Angewandte Chemie International Edition
Licensed Content Title	Metal-Mediated Self-Assembly of π-Bonded Benzoquinone Complexes into Polymers with Tunable Geometries
Licensed Content Author	Dwight A. Sweigart, Gene B. Carpenter, Moonhyun Oh
Licensed Content Date	Sep 7, 2001
Licensed Content Volume	40
Licensed Content Issue	17
Licensed Content Pages	4
Type of Use	Dissertation/Thesis
Requestor type	University/Academic
Format	Print and electronic
Portion	Figure/table
Number of figures/tables	3
Will you be translating?	No
Title	Investigations of Physical Properties of Metal-Organic Frameworks with Functional Ligands
Institution name	Technical University of Munich
Expected presentation date	Mar 2022
Portions	Illustration of Polymer 4, page 3191 and Figures 3 and 4
Requestor Location	TU Munich Poccistrasse 2 Munich, other 80336 Germany Attn: TU Munich
Publisher Tax ID	EU826007151
Total	**0.00 USD**
Terms and Conditions	

TERMS AND CONDITIONS

- IN NO EVENT SHALL WILEY OR ITS LICENSORS BE LIABLE TO YOU OR ANY OTHER PARTY OR ANY OTHER PERSON OR ENTITY FOR ANY SPECIAL, CONSEQUENTIAL, INCIDENTAL, INDIRECT, EXEMPLARY OR PUNITIVE DAMAGES, HOWEVER CAUSED, ARISING OUT OF OR IN CONNECTION WITH THE DOWNLOADING, PROVISIONING, VIEWING OR USE OF THE MATERIALS REGARDLESS OF THE FORM OF ACTION, WHETHER FOR BREACH OF CONTRACT, BREACH OF WARRANTY, TORT, NEGLIGENCE, INFRINGEMENT OR OTHERWISE (INCLUDING, WITHOUT LIMITATION, DAMAGES BASED ON LOSS OF PROFITS, DATA, FILES, USE, BUSINESS OPPORTUNITY OR CLAIMS OF THIRD PARTIES), AND WHETHER OR NOT THE PARTY HAS BEEN ADVISED OF THE POSSIBILITY OF SUCH DAMAGES. THIS LIMITATION SHALL APPLY NOTWITHSTANDING ANY FAILURE OF ESSENTIAL PURPOSE OF ANY LIMITED REMEDY PROVIDED HEREIN.

- Should any provision of this Agreement be held by a court of competent jurisdiction to be illegal, invalid, or unenforceable, that provision shall be deemed amended to achieve as nearly as possible the same economic effect as the original provision, and the legality, validity and enforceability of the remaining provisions of this Agreement shall not be affected or impaired thereby.

- The failure of either party to enforce any term or condition of this Agreement shall not constitute a waiver of either party's right to enforce each and every term and condition of this Agreement. No breach under this agreement shall be deemed waived or excused by either party unless such waiver or consent is in writing signed by the party granting such waiver or consent. The waiver by or consent of a party to a breach of any provision of this Agreement shall not operate or be construed as a waiver of or consent to any other or subsequent breach by such other party.

- This Agreement may not be assigned (including by operation of law or otherwise) by you without WILEY's prior written consent.

- Any fee required for this permission shall be non-refundable after thirty (30) days from receipt by the CCC.

- These terms and conditions together with CCC's Billing and Payment terms and conditions (which are incorporated herein) form the entire agreement between you and WILEY concerning this licensing transaction and (in the absence of fraud) supersedes all prior agreements and representations of the parties, oral or written. This Agreement may not be amended except in writing signed by both parties. This Agreement shall be binding upon and inure to the benefit of the parties' successors, legal representatives, and authorized assigns.

- In the event of any conflict between your obligations established by these terms and conditions and those established by CCC's Billing and Payment terms and conditions, these terms and conditions shall prevail.

- WILEY expressly reserves all rights not specifically granted in the combination of (i) the license details provided by you and accepted in the course of this licensing transaction, (ii) these terms and conditions and (iii) CCC's Billing and Payment terms and conditions.

- This Agreement will be void if the Type of Use, Format, Circulation, or Requestor Type was misrepresented during the licensing process.

- This Agreement shall be governed by and construed in accordance with the laws of the State of New York, USA, without regards to such state's conflict of law rules. Any legal action, suit or proceeding arising out of or relating to these Terms and Conditions or the breach thereof shall be instituted in a court of competent jurisdiction in New York County in the State of New York in the United States of America and each party hereby consents and submits to the personal jurisdiction of such court, waives any objection to venue in such court and consents to service of process by registered or certified mail, return receipt requested, at the last known address of such party.

WILEY OPEN ACCESS TERMS AND CONDITIONS

Wiley Publishes Open Access Articles in fully Open Access Journals and in Subscription journals offering Online Open. Although most of the fully Open Access journals publish open access articles under the terms of the Creative Commons Attribution (CC BY) License only, the subscription journals and a few of the Open Access Journals offer a choice of Creative Commons Licenses. The license type is clearly identified on the article.

The Creative Commons Attribution License